Analysis of the local site effects on the amplification of seismic ground motion in Croatia

Stanko, Davor

University of Zagreb

FACULTY OF SCIENCE

DEPARTMENT OF GEOPHYSICS

Davor Stanko

ANALYSIS OF THE LOCAL SITE EFFECTS ON THE AMPLIFICATION OF SEISMIC GROUND MOTION IN CROATIA

DOCTORAL THESIS

Zagreb, 2018

University of Zagreb

Faculty of Science
Department of Geophysics

Davor Stanko

ANALYSIS OF THE LOCAL SITE EFFECTS ON THE AMPLIFICATION OF SEISMIC GROUND MOTION IN CROATIA

DOCTORAL THESIS

Supervisors:

Assoc. Prof. Dr. Snježana Markušić
Assoc. Prof. Dr. Zeynep Gülerce

Zagreb, 2018

Sveučilište u Zagrebu

Prirodoslovno-matematički fakultet
Geofizički odsjek

Davor Stanko

ANALIZA UTJECAJA LOKALNIH UVJETA TLA NA AMPLIFIKACIJU SEIZMIČKOGA POVRŠINSKOGA GIBANJA U HRVATSKOJ

DOKTORSKI RAD

Mentori:

Izv. prof. dr. sc. Snježana Markušić
Izv. prof. dr. sc. Zeynep Gülerce

Zagreb, 2018

This thesis was made under the supervision of Assoc. Prof. Dr. Snježana Markušić (Department of Geophysics, Faculty of Science, University of Zagreb) and Assoc. Prof. Dr. Zeynep Gülerce (Middle East Technical University, Civil Engineering Department, Ankara, Turkey) as a part of the doctoral study at the Department of Geophysics, Faculty of Science, University of Zagreb.

Acknowledgments

Abstract

In this dissertation, the analysis of the local site effects on the amplification of seismic ground motions in Croatia was performed using 1-D equivalent–linear (EQL) stochastic Random Vibration Theory (RVT) method. The main reason for choosing the relatively new 1-D EQL site response analysis with RVT-based method is the limited existing strong motion database in Croatia. In the RVT-based method, single theoretical point source Fourier Amplitude Spectrum (FAS) defined by the local and regional seismological parameters is adequate to represent the input ground motion.

First part of thesis covered calculation of the high-frequency attenuation parameter kappa (κ) and its local site-specific component (κ_0) to describe high-frequency decay of FAS. The recordings from earthquakes with local magnitudes $3.0 \leq M_L \leq 5.7$, focal depths less than 30 km and epicentral distances $R_e \leq 150$ km from ten seismological stations were used for the estimation of the κ using Anderson and Hough (1984) method. Local attenuation parameter κ_0 was estimated using the linear κ–R_e dependence by least-square regression for horizontal and vertical ground motion components (κ_{hor} and κ_{ver}) for each station. The use of error-in-variable regression could limit influence of uncertainty in R_e on the final value of κ_0 and slope κ_R. Estimated κ_0 values for Croatian seismological stations are consistent with the global κ_0 for rock sites. Comparison between κ_{hor} and κ_{ver} models was performed to determine local (κ_0) and regional attenuation (slope κ_R) contributions to the κ. Observations from spatial distribution of the κ values indicate that beside isotropic local and regional geology and complex tectonic structure, other effects such as attenuation anisotropy from different causes (e.g., scattering due to heterogeneity, beamforming, fracturing, flow of fluids in rocks) possibly have effect on the κ distribution. Observed discrepancies between the frequency-dependent $Q(f)$ and the frequency-independent $Q_{est}(\kappa_R)$ for the high-frequency range (10–25 Hz) are mostly within the respective confidence limits, and can be attributed mainly to different techniques to estimate $Q(f)$ and κ, and complexity and variability in the whole-path attenuation contributions to κ.

Second part of thesis is focused on 1-D EQL site response analysis using RVT-based method for different local site profiles around Croatia and for different input ground motion levels (peak ground acceleration at the bedrock—PGA_{ROCK}). Seismological parameters (magnitude,

epicentral distance, focal depth, seismic attenuation, near-site attenuation) are varied to define the input rock motion based on the regional FAS. For lower levels ($PGA_{ROCK} < 0.1$ g), the input motion is significantly amplified at the top layers of the profile ($AF@PGA$) and the amplification factor (AF) is most prominent at predominant peak period particularly for the softer soils with lower V_{S30} and thicker alluvium layers overlying bedrock. At higher levels ($PGA_{ROCK} > 0.1$ g), softer soils with lower values of V_{S10}, V_{S20}, and V_{S30} (average shear wave velocity in top 10 m, 20 m and 30 m) shows non-linear behaviour, therefore, $AF@PGA$ decreases significantly below the $AF = 1$ line at shorter spectral periods, and predominant peak period is prolonged (increased) with decreasing $AF@PP$. At different levels PGA_{ROCK}, AF varies significantly with chosen spectral period for different site characteristics parameters ($V_{S10}, V_{S20}, V_{S30}$).

Finally, the third part of thesis presents the empirical nonlinear site amplification model developed for Croatia for a range of local soil profiles ($160 < V_{S30} < 1389$ m/s) as a function of the local site parameter (V_{S30}) and intensity of input rock motion (PGA_{ROCK}). Proposed AF model for Croatia is in good agreement with Sandikkaya et al. (2013) and Kamai et al. (2014) empirical AF models. Observed differences between models may be related to different equivalent linear soil properties utilized in RVT site response methods, developed site amplifications based on empirical database or definition of the soil profiles (real/measured soil profiles in this study vs. generic randomized soil profiles in others). Proposed AF models are strongly nonlinear for soft sites and heavily dependent on the period compared to weakly period-dependent AF given in Eurocode 8. Significant amplifications were observed for stiffer V_{S30} sites compared to EC8–AFs for site classes B and A. Nonlinear site amplification based solely on single "questionable" site parameter V_{S30} can misled to wrong conclusions and needs to be further investigated.

The findings of this study can be used in future to update peak acceleration attenuation relations (GMPEs) for Croatia based on a new data, particularly strong motion accelerograms taking into consideration attenuation effects ($Q(f), \kappa_0$) and proposed nonlinear site amplification model as well as in local earthquake engineering problems.

Keywords: Local site effects, Amplification factor, Seismic ground motion, Fourier amplitude spectrum, High-frequency attenuation parameter, Random Vibration Theory, Nonlinear site amplification model

Table of Contents

1. Introduction

1.1. Research background

The intensity of the earthquake shaking on site in terms of observed or recorded strong ground motion is influenced by a complex system that depends on the source characteristics, attenuation of seismic waves when they propagate through the Earth's crust, and modification by the local site conditions (e.g., Reiter 1990). First evidence about local soil amplification effects and observed variations in building damage during shaking related to local geology was reported by Stur (1871) for the Klana earthquake of 1870. Destructive earthquakes with large moment magnitudes ($M_W \geq 6.0$) that occurred in the last three decades (USGS-Earthquake Cataloque: https://earthquake.usgs.gov/earthquakes/search/) e.g., Italy (L'Aquila 2009, Amatrice and Norcia 2016), Mexico (1985, 2017), New Zealand (Christchurch 2011, Canterbury 2010, Kaikoura 2016), Nepal (2015), Japan (Kobe 1995, Tohoku 2011), Chile (2010, 2015), China (Sichuan 2008), Taiwan (Chi-Chi 1999), Turkey (Kocaeli 1999), USA (Whittier Narrows 1987, Loma Prieta 1989, Northridge 1994), proved that the effects of local soil conditions are the key elements that influence the spatial distribution of the structural damage in earthquake prone regions. The effects of local soil conditions or so-called "site effects" are defined as the modification of the incoming wavefield characteristics (amplitude, frequency content and duration) due to the specific geological site characteristics, geometrical features of the soil deposits and the surface topography (e.g., Reiter 1990; Kramer 1996; Meunier et al. 2008; Aki and Richards 2009; Panzera et al. 2013). The modification is manifested as the amplification or de-amplification of ground motion amplitudes at all frequencies or periods at the surface compared to the bedrock level.

One of the most cited example related to the site amplification is the 1985 Mexico City earthquake whose magnitude was $M_W = 8.0$ with the epicentre approx. 400 km from Mexico City. The devastating destruction in Mexico City (more than 10000 people were lost their lives, and the damage was appraised to approx. six billion dollars) was primarily related to the resonance effects between 6 to 20-storey buildings and long-period ground motions. Mexico City is situated on a plateau surrounded by mountains and volcanoes. Heavily damaged part of

Mexico City is located on alluvial sediments from ancient lakebed zone which significantly amplified certain frequencies of ground motion. Little to none damage was reported on the foothill zone which is located on volcanic rocks of approx. 10 km from the Mexico City. Figure 1.1 shows the ground acceleration recordings and the average response spectra of recorded ground motions at two stations, one on the nearby rock site (UNAM) and the other one on a lakebed zone (SCT). Maximum peak ground acceleration (PGA) recorded at UNAM was about 0.04 g (35 cm/s^2), while it was about 0.17 g (170 cm/s^2) at SCT - amplified up to 5 times. Amplitudes and durations of strong motion were greater at SCT site underlain by alluvium sediments of ancient lakebed than those at nearby rock site (UNAM). Maximum spectral response peak at the SCT site is observed at the period of 2 s (0.5 Hz) with amplification up to 10 times higher compared to the UNAM site. The amplification effects caused significant strong ground motions over the lakebed zone and resonance of long period ground motions with medium-to-high-period buildings, resulting in heavy destruction in this area (e.g., Reiter 1990).
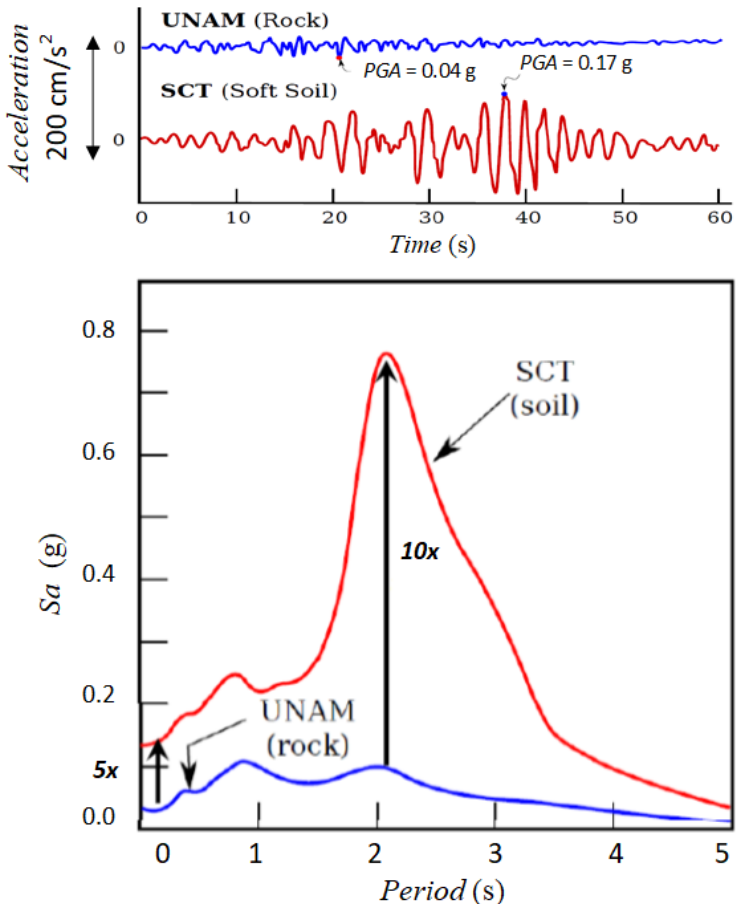
Figure 1.1. Top: recorded EW components of ground motion (acceleration). Bottom: comparison of average response spectra in terms of spectral accelerations at UNAM (rock site) and SCT (lakebed site) from the 1985 Mexico City earthquake with $M_W = 8.0$ (modified after Reiter 1990).

In practice, the effects of the local soil conditions are evaluated through the amplification factor: the ratio of the ground motion at the free surface and the ground motion of nearby rock site (e.g., Schnabel 1972; Reiter 1990; Kramer 1996). Seismic ground motion of the local soil (e.g., soft sediments, rocks) due to an earthquake is represented by the response spectrum: peak response spectral ordinates (Sa—spectral acceleration) of the single degree of freedom oscillator (SDOF) having specific damping (e.g., 5 % of critical damping) for various spectral periods. The site amplification factor (AF) is defined as the ratio of the surface response spectrum (Sa_{SURF}) to the bedrock response spectrum (Sa_{ROCK}) of the same earthquake as a function of period (T):

$$AF(T) = \frac{Sa_{SURF}(T)}{Sa_{ROCK}(T)} \qquad (1.1)$$

The site response analysis is a powerful tool that enables the assessment and estimation of the effects of local soil conditions on the ground shaking, and is based on the one-dimensional wave propagation theory. One-dimensional (1-D) equivalent–linear (EQL) site response analysis that employs recorded or simulated time series (TS-approach) was introduced by Idriss and Seed (1968) and implemented by Schnabel et al. (1972) in the SHAKE software which was later updated by Idriss and Sun (1992) as SHAKE91. Currently, other software (such as DEEPSOIL by Hashash et al. 2012) can perform 1-D EQL site response analysis. In seismically active regions where a large strong motion database exist, the straightforward TS-approach is used to evaluate site amplification factors (e.g., Idriss and Seed 1968; Schnabel et al. 1972; Seed et al. 1984; Idriss and Sun 1992; Kramer 1996; Rathje et al. 2010; Hashash et al. 2012).

Using the 1-D EQL site response analysis with TS-approach is controversial for the low seismicity areas where the strong motion database is sparse or does not exist. For these regions, empirical ground motions from other similar tectonic regions might be utilized after certain modifications or syntetic ground motions might be developed for special structures such as nuclear power plants. An alternative way for estimating the site amplification factors for these regions is the use of stochastic simulations based on simple point source seismological models of the radiated spectra (e.g., Brune 1970; Hanks and McGuire 1981; Boore 1983, 2003). Random Vibration Theory-based (RVT) EQL site response analysis approach is a significant alternative to the TS-approach (e.g., Boore 1983, 2003; Silva and Lee 1987; Silva et al. 1997; Rathje and Ozbey 2006; Kottke and Rathje 2013) since the only required input is the Fourier Amplitude Spectrum (FAS) that represents the input rock motion defined by the seismological

parameters for certain earthquake scenario. In RVT-based method, it is particularly important to define the parameters that affect the high-frequency content of FAS such as the high-frequency attenuation expressed by spectral parameter kappa (κ) and their correlation with regional and local geology (e.g., Anderson and Hough 1984; Ktenidou et al. 2013, 2014). This method and the new software STRATA (Kottke and Rathje 2009) is slowly being adopted among the geotechnical earthquake engineering community because it does not require strong motion records as in the classical time series approach (Kottke and Rathje 2013).

A simplified alternative to site response analysis are the nonlinear site amplification models embedded in ground-motion prediction equations (GMPEs). GMPE presents a statistical model based either on stochastic simulations or empirical data to predict acceleration response spectrum at a site as a function of earthquake magnitude, distance from the source to the site and local site conditions. Nonlinear site amplification models take into account local site conditions and predict the site amplification factors based on the peak intensity of the input rock motion (PGA_{ROCK}—reference rock motion) and general local site characteristics of the site (V_{S30}—the average shear wave velocity in the upper 30 m of soil) (e.g., Choi and Stewart 2005; Walling et al. 2008; Sandikkaya et al. 2013).

1.2. Objective of the research

The main objective of this research is to perform a systematic comparison of the influence of the local site effects on the site amplification factors (AFs) in Croatia, calculated by the RVT-based 1-D EQL site response analysis approach that uses only FAS to represent the input seismic ground motion.

Beyond the magnitude of the earthquake and the source-to-site distance, the most important parameter that describes the high-frequency shape of the FAS is the high-frequency attenuation parameter (κ). The spectral decay parameter kappa (κ) was introduced by Anderson and Hough (1984) in the 1980's to describe the high-frequency attenuation of shear waves (S-waves) from the seismograms. The first part of this research presents the estimation of the spectral parameter κ and its local site-specific component κ_0, calculated for the first time for a selected set of seismological stations in Croatia using classical Anderson and Hough (1984) (AH84) approach. For this purpose, the recordings from earthquakes with local magnitudes $3.0 \leq M_L \leq 5.7$, focal

depths less than 30 km and epicentral distances $R_e \leq 150$ km that were recorded from the time when these stations were deployed until the end of 2016 are collected. Near-site attenuation parameter κ_0 (zero-distance site-specific kappa) related to the local site conditions of the station was determined using a predefined mathematical formulation that treats κ as a function of R_e (Anderson and Hough 1984; Ktenidou et al. 2013). This part of the study was supported by the fieldwork based on geophysical survey method to determine the shear wave velocity (V_S) profiles beneath the seismological stations, as no reliable information of measured V_S profiles at stations had been documented.

Seismological parameters (e.g., magnitude, distance, focal depth, seismic attenuation, near-site attenuation) are varied to define the input rock motion based on the regional FAS. Different combinations of these parameters can be adapted to obtain the FAS that is compatible with the design spectrum for the bedrock conditions (Boore 2003; Rathje and Ozbey 2006). The second part of this research is dealing with the RVT-based 1-D EQL site response analysis approach, carried out for a maximum input rock peak ground acceleration (PGA_{ROCK}) from very weak (0.03 g) to relatively strong (0.37 g) that corresponds to return period of 475-years (Herak et al. 2001, 2011; Markušić et al. 2002). Selected local soil shear wave velocity (V_S) profiles in Croatia are collected from fieldwork (geophysical survey methods and microtremor measurements). Each local soil profile is defined by the geometrical, physical, and mechanical properties of the soil layers. The outcome of the RVT-based 1-D EQL site response analysis approach is the site-specific amplification spectrum defined by Eq. (1.1).

Finally, after the empirical AFs are determined for variety of local V_S profiles for different input rock motions, nonlinear site amplification model for Croatia at a particular spectral period in the functional form of site parameter V_{S30} and input PGA_{ROCK} is developed by the nonlinear regression analysis of the empirical datasets using a reference rock model (e.g. Choi and Stewart 2005; Walling et al. 2008; Sandikkaya et al. 2013; Kamai et al. 2014). Proposed way of estimating the site amplification factors is quite new in the global practice, and no previous studies focusing on this issue for Croatia have been made.

1.3. Outline of Dissertation

This thesis consists of seven chapters. After the *1. Introduction*, theoretical background of Fourier Amplitude Spectrum (FAS) of ground motion and the parameters that describe the effects of source, propagation path and local site conditions on the spectrum is given in Chapter *2. Spectrum of seismic ground motion*.

Chapter *3. Methods to evaluate the local site effects on the site amplification factor of seismic ground motions* provides a theoretical background on the 1-D EQL site response analysis using both TS- and RVT-based approaches. The advantages and disadvantages of both approaches are discussed, particularly in the sense of the evaluation of the amplification factors (AFs) in seismically active regions and low-to-moderate seismicity areas. The alternative to the site response analysis is to use nonlinear site amplification models that have been utilized in the recently proposed ground motion prediction models (GMPEs) for shallow crustal and active tectonic regions (e.g., global NGA-West 1 and West 2 GMPEs, RESOURCE models). The overview of recently developed site AF models as a function of site parameter V_{S30} and input PGA_{ROCK} (e.g., Choi and Stewart 2005; Walling et al. 2008; Sandikkaya et al. 2013; Kamai et al. 2014) is provided in this chapter.

The first part of Chapter *4. Estimation of the high-frequency attenuation parameter kappa* (κ) *in Croatia* presents the background on the Anderson and Hough (1984) method with examples on the calculation of the high-frequency parameter kappa (κ) in Croatia. Details of the seismotectonic and geological characteristics of the study area and stations, findings of the geophysical fieldwork, and properties of the compiled dataset are provided in this chapter. Calculation of κ values and the statistical models of the linear $\kappa - R_e$ dependence for horizontal and vertical ground motion components are summarized, and the empirical κ models are compared to the recent global works. The second part of this chapter compares estimated local site-specific component κ_0 and measured V_{S30} values at seismological stations with the global and regional $\kappa_0 - V_{S30}$ correlations. Correlation between the κ and regional attenuation is presented with the spatial maps of individual κ distributions for each station. Comparison between frequency-dependent quality factor $Q(f)$ from recent attenuation studies of coda waves in the Dinarides (Dasović 2015a; Dasović et al. 2012; 2013, 2015b) and the frequency-independent Q derived from the slope (κ_R) of $\kappa - R_e$ relation in this study is discussed at the end of this chapter.

RVT-based 1-D EQL site response process analysis and the examples of the evaluation on the amplification of seismic ground motion for randomly selected local soil profiles in Croatia are presented in Chapter *5. Analysis of the local site effects on the amplification of seismic ground motion in Croatia using EQL RVT-based method*. Amplification factors at different spectral periods are compared with local site characteristics in terms of V_{S10}, V_{S20} and V_{S30} to identify how surficial soft soil layers strongly influence the site amplification factors for different input PGA_{ROCK}.

Nonlinear site amplification model for Croatia is proposed in a simple functional form as a function of a site parameter V_{S30} and intensity of input rock motion PGA_{ROCK} in Chapter *6. Empirical nonlinear site amplification model for Croatia*. Developed nonlinear site amplification models are compared for different ranges of site V_{S30} intra-categories and for certain values of PGA_{ROCK}. The comparison is performed with Eurocode 8 (EC8) and with recently developed nonlinear site amplification models (e.g., Choi and Stewart 2005; Walling et al. 2008; Sandikkaya et al. 2013; Kamai et al. 2014) and is thoroughly discussed.

Conclusions, summary of each main parts of this dissertation and future recommendations are provided in Chapter *7. Conclusions*.

2. Spectrum of seismic ground motion

When an earthquake occurs, seismic waves travel from the source (fault) through the Earth's interior up to the ground surface. Ground motion at a particular site is influenced by the source parameters, propagation path effects and site effects. The first two features define the size and the nature of the earthquake at its source and how seismic waves attenuate through the Earth's interior. The influence of the local geological features on the ground motions in term of site amplification is known for many years in earthquake engineering. Different damage distribution for various local site conditions were observed in different areas affected by the same earthquake shock (e.g., Idriss and Seed 1968; Reiter 1990; Kramer 1996; Aki and Richards 2009).

The first scientifically explained observation of the local soil amplification effects and variable earthquake damage due to different local geological units during shaking was presented by Stur (1871) by analyzing the Klana (Croatia) earthquake sequence with the mainshock on 1 March 1870 (I_{max} = VIII ° MSK [Medvedev-Sponheuer-Karnik]). Stur (1871) presented detailed report on how houses were built, presented observations of unequal distribution of earthquake damage related to soil conditions with geological sketches, damage locations of objects and map of the shaken area. Herak et al. (2018) presented their macroseismic study of this earthquake sequence, and performed measurements of Horizontal-to-Vertical Spectral Ratios (HVSRs) of ambient noise at six locations to compare estimates of soil response in the epicentral area with observations of site effects during the Klana earthquake. Estimated HVSRs show clear spectral peaks at four places located on younger and softer geological units (Klana on alluvium and Studena on Palaeogene sediments). These observations are similar to the observations of Stur (1871) about local site effects in Klana and Studena.

Figure 2.1 shows the schematic that represents how the morphological and stratigraphic features of the local terrain and their physical and mechanical properties affects the characteristics of the ground motion observed at the site (Panzera et al. 2013). Site effects are the results of several physical processes such as multiple reflections, diffraction, focusing, resonance, wave trapping, etc., when the seismic waves pass through the uppermost several hundred meters of rock and

soil layers. The surface topography and various mechanical properties of the terrain such as water table, slopes, presence of heterogeneities, discontinuities and cavities contribute to the local seismic hazard.
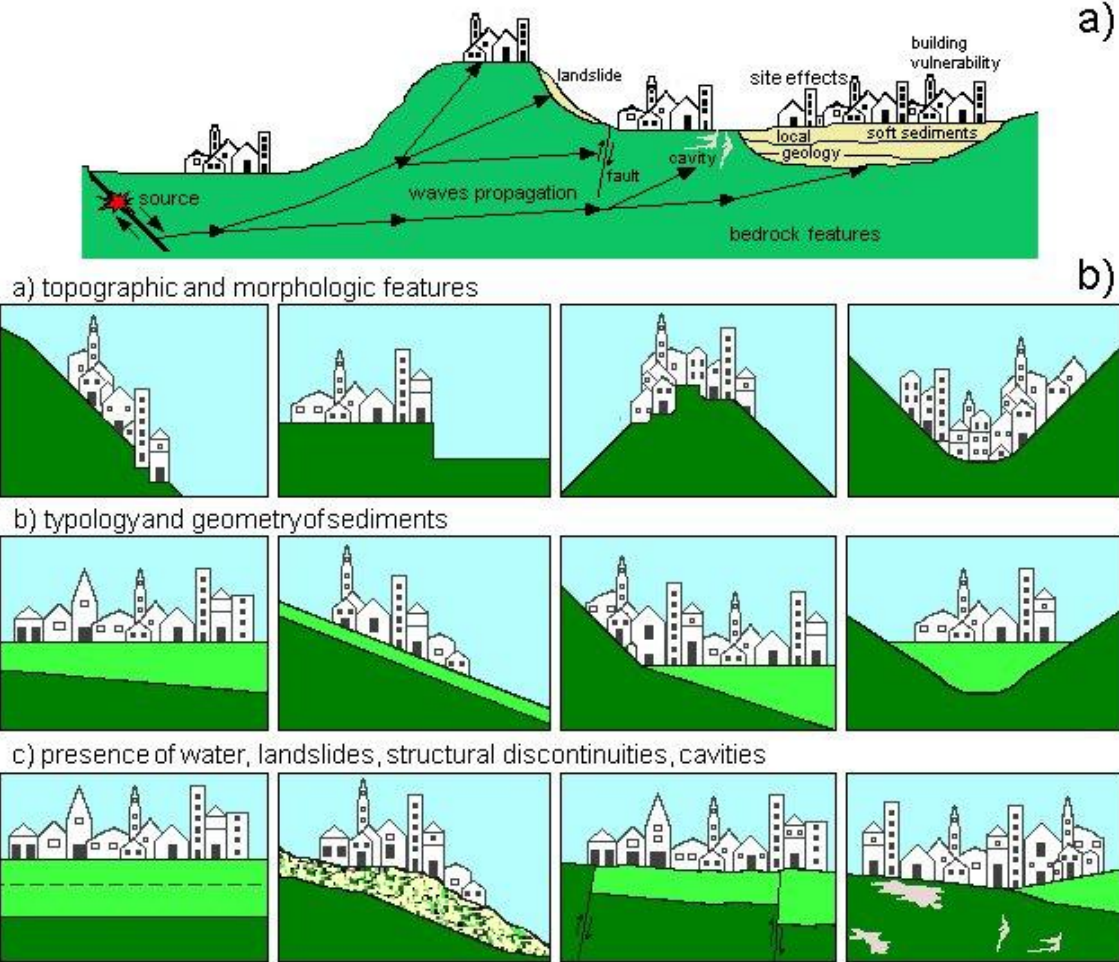
Figure 2.1. Influence of the local site effects on the earthquake ground motion: a) propagation of the seismic waves from the source through the Earth's interior up to the particular local site, b) the morphological and stratigraphic features, and their physical and mechanical properties of the local terrain (taken from Panzera et al. 2013).

Recorded ground motions in terms of acceleration, velocity, and displacement time histories may be presented in different ways for engineering applications. Fourier analysis transforms the ground motion time history into amplitude and phase spectra which depicts the frequency content of the recorded motion (e.g., Silva et al. 1997). Seismologists extensively use the Fourier analysis to evaluate the source and propagation properties of the recorded ground motions (e.g., Reiter 1990; Kramer 1996; Aki and Richards 2009). Fundamental information about the contributions of the earthquake source $E(M_0, f)$, propagation path effects $P(R, f)$,

and site effects $S(f)$ are described by the Fourier Amplitude Spectrum $FAS(M_0, R, f)$ of the certain ground motion $I(f, k)$ (i.e., displacement, velocity or acceleration time series) at the site (e.g., McGuire and Hanks 1980; Boore 1983, 2003; Reiter 1990) as given in Eq. (2.1).

$$FAS(M_0, R, f) = E(M_0, f) \cdot P(R, f) \cdot S(f) \cdot I(f, k) \tag{2.1}$$

M_0 is seismic moment in Nm, R is distance from the source to site (hypocentral) in km, and f is frequency in Hz. The particular type of ground motion in Eq. (2.1) is defined by ground motion function $I(f, k)$ as:

$$I(f, k) = (2\pi f)^k \tag{2.2}$$

In Eq. (2.2), $k = 0$, 1 or 2 for ground displacement, velocity, or acceleration motion, respectively. In seismically active regions, strong motion database generally contains acceleration time histories. In the low seismicity areas, time histories are generally not present, and the lack of recorded ground motions is supported by ground motion simulations. The essential ingredient for the numerical stochastic simulations is the use of Fourier Amplitude Spectrum of the ground acceleration ($k = 2$) (e.g., Hanks and McGuire 1981; Boore 1983, 2003).

2.1. Earthquake source spectrum

In stochastic simulations, the seismic source can be modelled as either a point-source or a propagating stochastic finite-source. In stochastic finite-source models, however, the rupture area is divided into an array of sub-faults each of them treated as a point-source (e.g., Brune 1970; Atkinson and Silva 1997; Yenier and Atkinson 2014). The simplest of the source models for earthquakes is the isotropic point source, where the source is considered as a point from which the seismic waves are propagated with equal amplitudes in all directions. Much of the practical work in seismology is performed in the "far-field conditions", at distances (*r*) of several wavelengths (*λ*) from the source. For a point source, the far-field condition is expressed as *r/λ* >> 1 (e.g., Brune 1970; Stein and Wysession 2003; Udias et al. 2014).

The shape and the amplitude of the source spectrum $E(M_0, f)$ is specified by defining a displacement spectrum as a function of earthquake size:

$$E(M_0, f) = C \cdot B(M_0, f) \tag{2.3}$$

where C is the source constant given below in Eq. (2.9), and $B(M_0, f)$ is the theoretical Brune (1970) point source spectrum expressed by the seismic moment, M_0, and frequency f. Seismic moment M_0 (in Nm) is given by:

$$M_0 = \mu A D \tag{2.4}$$

where μ is the shear modulus (in N/m² or Pa), A is the area of the fault rupture (in m²), and D is the average displacement (slip) over the rupture surface (in m) (e.g., Udias et al. 2014). For the crust, a typical average value of μ is 30 GPa. Seismic moment M_0 is related to the moment magnitude M_W by the following relation (Hanks and Kanamori 1979):

$$M_W = \frac{2}{3}(log M_0 - 10.7) \tag{2.5}$$

The relationship between the slip of an earthquake, fault dimensions (fault rupture) and the seismic moment, are correlated with the value of the magnitude of the stress released by an earthquake—the stress drop $\Delta\sigma$ (e.g., Stein and Wysession 2002). Stress drop is a parameter that describes the change of the stress along the fault during an earthquake. Brune (1970) showed that for a simple circular fault rupture of radius r, the seismic moment M_0 is related to the stress drop $\Delta\sigma$ as shown in Eq. (2.6).

$$M_0 = \frac{16}{7}r^3\Delta\sigma \tag{2.6}$$

The most widely used and qualitatively validated theoretical point source acceleration spectrum (acceleration ground motion function in Eq. (2.2) expressed as $I(f, k = 2) = (2\pi f)^2$) is the ω-square (ω^2) model with a single corner frequency (f_C) and constant stress drop ($\Delta\sigma$) proposed by Brune (1970) as a basis to characterize far-field shear wave motion:

$$B(M_0, f) = 4\pi^2 M_0 \frac{f^2}{1 + \left(\frac{f}{f_C}\right)^2} \tag{2.7}$$

where f_C is the corner frequency where spectrum reaches relatively constant level and is related to stress drop $\Delta\sigma$ and M_0 (e.g., Boore 2003; Udias et al. 2014):

$$\Delta\sigma = 8.47 M_0 \left(\frac{f_C}{\beta_0}\right)^3 \tag{2.8}$$

The source constant C is given as (e.g., Boore 2003):

$$C = \frac{\langle R_{\Theta\Phi}\rangle VF}{4\pi \rho_0 \beta_0^3 R_0} \tag{2.9}$$

where $\langle R_{\Theta\Phi}\rangle$ is the radiation factor of the total shear-wave radiation, V represents the partition of total shear-wave energy into horizontal components, F is the effect of the free surface, ρ_0 is density in kg/m³, β_0 is shear wave velocity in m/s in the vicinity of source, and R_0 is a reference source distance in km. Recommended values of these parameters $\langle R_{\Theta\Phi}\rangle = 0.55$, $V = 1/\sqrt{2}$, $F = 2$, $R_0 = 1$ km are proposed by Boore and Boatwright (1984).

Considering all above stated, theoretical Brune (1970) ω^2 point source spectrum of ground accelerations (acceleration ground motion function for $I(f, k = 2) = I(f)$ and will appear in text in this form) for a single corner frequency f_C given in Eq. (2.3) is simplified into:

$$FAS(M_0, f) = E(M_0, f) \cdot I(f) = \left(0.78 \frac{\pi}{\rho_0 \beta_0^3} M_0 \frac{f^2}{1 + \left(\frac{f}{f_C}\right)^2} \right) \tag{2.10}$$

Figure 2.2 compares theoretical source spectrum of ground acceleration (Eq. 2.10) for different magnitudes and two $\Delta\sigma$ values. In this figure, it is assumed that $\rho_0 = 2800$ kg/m³ and $\beta_0 = 3500$ m/s. According to the idealization of the Brune (1970) ω^2 point source spectrum, far-field shear wave acceleration spectrum should be flat at the frequencies greater than f_C. Figure 2.2 shows that larger magnitude earthquakes have lower corner frequency f_C, while higher $\Delta\sigma$ increase f_C. Change in f_C with magnitude is more significant than its change with $\Delta\sigma$. The seismic moment (or moment magnitude) has influence on the Fourier amplitude spectrum over all frequencies, primarily at low frequencies, whereas the stress drop parameter controls high-frequency spectral amplitudes in terms of change of f_C. With a prescribed constant value of stress drop, the scaling of the Brune (1970) f_C point source spectrum depends only on one source parameter; M_W (or M_0).
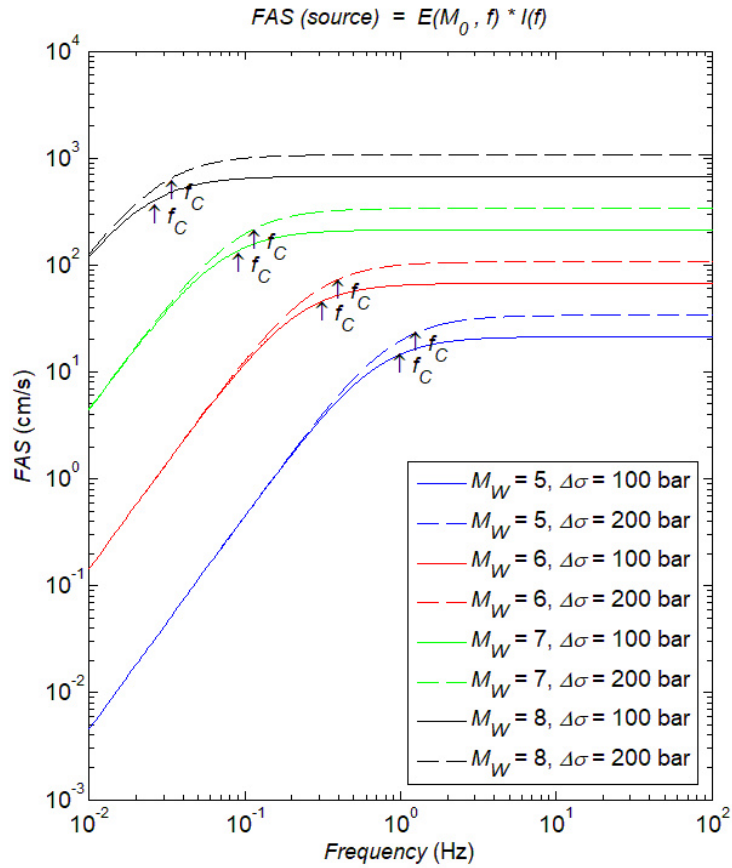
Figure 2.2. Comparison of the acceleration source spectrum $FAS = E(M_0, f) \cdot I(f)$ for different moment magnitudes M_W and stress drops $\Delta\sigma$.

Stress drop is important parameter related to the dynamics of the earthquake rupture. Seismically, the stress drop can be determined using Eg. (2.8) by two measurements: seismic moment and corner frequency from fitting a curve to the Fourier amplitude displacement spectrum or equivalently the acceleration amplitude spectrum. Obtaning stress drop parameter is challenging for a region like Croatia. Firstly, source parameter studies require intermediate and large earthquakes ($M_W > 5.5$) that are rare for Croatian region. Secondly, number of assumptions needs to be made about source model such as shape of the rupture area and the rupture velocity. Thirdly, broad frequency bandwidth is required in the recorded data in order to estimate corner frequencies over large magnitude range (e.g., Allman and Shearer 2009). Corner frequency measurement of small events may suffer from the fact that source and kappa frequencies are near each other for small magnitudes (later shown in more details in Chapter 4). Therefore, for the purposes of this study, prescribed value of stress drop $\Delta\sigma = 100$ bar will be used following the study of Hanks and McGuire (1981). This value is similar to the observed

global stress drop value from Allman and Shearer (2009) for southeastern Europe estimated from Molise (Italy) 2002 and Ston (Croatia) 1996 earthquakes.

Point source model (i.e., circular rupture) is reasonable for small and moderate magnitude earthquakes (e.g., $M_W < 6.0$), but for large earthquakes, finite dimensions of the fault and multiple corner frequencies have been proposed (Atkinson and Silva 1997). Finite-source models can successfully predict the motions from large earthquakes ($M_W > 6.0$), as they explicitly model the causative physical processes of ground-motion distance saturation. Point-source predictions of ground motion amplitudes monotonically increase with decreasing distance, because the total energy is assumed to be released from a single point. For extended faults the observed ground motion amplitudes saturate as they get close to the fault. Recently, Yenier and Atkinson (2014) conclude that *equivalent point-source modelling* can successfully predict the average ground motions from M_W 6+ earthquakes over wide distance range, including close distances (< 20 km). This is achieved by placing virtual point at an equivalent distance $R = \sqrt{(D^2 + h^2)}$ where D is actual distance measure (hypocentral, epicentral or rupture distance) and h is „pseudo-depth" term that accounts for saturation effects. At far distances $R \approx D$ whereas at close distances $R > D$. In finite-source models rupture surface can be divided into a number of sub-faults, each represented as a point-source by using this approach. It is important to recognize that the equivalent point source is this virtual point, not an actual point on the fault rupture. Effectively, by using ground motion attenuation in terms of an effective distance, smaller effective M_W are observed close to a finite fault, while the source contribution to the spectral shape remains the same as the one further away (e.g., Edwards and Fäh 2013; Yenier and Atkinson 2014). There are several advantages to modelling motions by an equivalent point source, rather than invoking more detailed extended-fault models. Firstly, point-source model provides a simple basis to ground motion simulations. Secondly, point-source models are useful tool in seismic hazard analysis for integrating contribution from large events in areas of low seismicity or to incorporate worst-case scenarios in high seismicity areas.

2.2. Propagation path effects

Idealized theoretical Brune (1970) ω^2 source spectrum of the ground acceleration (Eq. 2.10) shown in Figure 2.2 is rarely observed, mainly because of the ground motion attenuation. The attenuation effects on the propagating seismic waves through the Earth's interior are related to the geometrical spreading and mainly to the intrinsic dissipation and scattering attenuation (e.g., Giampiccolo et al. 2004). The simplified crustal attenuation path effects $P(R, f)$ are represented by functions of geometrical spreading $Z(R)$ and frequency dependent quality factor $Q(f)$ (e.g., Boore 2003):

$$P(R, f) = Z(R) \cdot exp\left(-\frac{\pi R f}{Q(f)\beta_0}\right) \tag{2.11}$$

where β_0 is the seismic velocity in m/s used in the determination of quality factor $Q(f)$, and R is hypocentral distance in km. Other distances are also common to use (e.g., epicentral distance R_e, Joyner-Boore distance R_{JB}). The Joyner-Boore distance R_{JB} is defined as the shortest distance from a site to the surface projection of the rupture.

Geometrical spreading refers to the decay of ground motion amplitudes due to spreading of seismic-wave energy over a continuously increasing area as a result of expansion of wave-fronts. If the Earth is assumed to be homogenous and isotropic, ground motions at close distances are dominated by body waves that spread spherically with amplitude decay as R^{-1}, and at far distances by surface waves which decay as $R^{-1/2}$ due to cylindrical spreading (e.g., Reiter 1990). The non-uniform nature of the Earth modifies these factors and the geometrical spreading function $Z(R)$ which describes the loss of seismic energy (wave amplitude) is modelled by a three-linear functional form (Eq. 2.12) with recommended values of reference source distance $R_0 = 1 \text{ km}$, geometrical decay distances $R_1 = 70 \text{ km}, R_2 = 130 \text{ km}$ and coefficients $p_1 = 0.0, p_2 = 0.5$ given by Atkinson and Boore (1995) (Figure 2.3).

$$Z(R) = \begin{cases} \dfrac{R_0}{R}, R \leq R_1 \\[2mm] Z(R_1)\left(\dfrac{R_1}{R}\right)^{p_1}, R_1 \leq R \leq R_2 \\[2mm] Z(R_2)\left(\dfrac{R_2}{R}\right)^{p_2}, R_2 \leq R \end{cases} \tag{2.12}$$
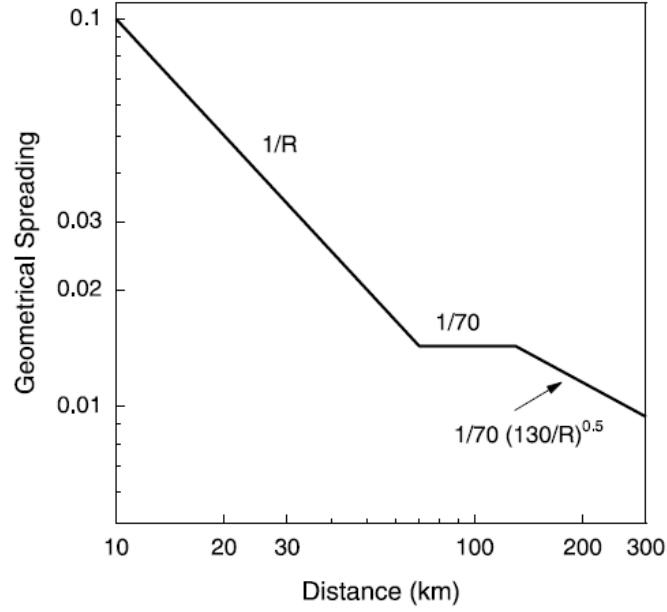
Figure 2.3. Geometrical spreading function $Z(R)$ as a function of distance R recommended by Atkinson and Boore (1995).

The second term in Eq. (2.11) describes the propagation path attenuation as the inverse of the effective quality factor (Q) in the exponential formulation (e.g., Futterman 1962). The most frequently used attenuation model that explains the generation of coda waves and enables the estimation of Q_C is the single backscattering model proposed by Aki and Chouet (1975). Total attenuation (inverse of quality factor) $1/Q_C$ includes the intrinsic absorption $1/Q_i$ (elastic energy converted into heat) and scattering attenuation $1/Q_{sc}$ (energy redistribution of seismic waves scattered on heterogeneities) (e.g., Dainty 1981; Giampiccolo et al. 2004):

$$\frac{1}{Q_C} = \frac{1}{Q_i} + \frac{1}{Q_{sc}} \tag{2.13}$$

Power law of frequency-dependent relationship for $Q(f)$ was used in many studies dealing with seismic attenuation:

$$Q(f) = Q_0 f^n \tag{2.14}$$

where f_0 is reference frequency chosen equal to 1 Hz implying $Q_0 = Q_C(f = f_0 = 1 \text{ Hz})$ for which $Q_C(f) = Q(f) = Q_0 f^n$, and the degree of the frequency dependence of $Q(f)$ is determined with exponent n (Aki and Chouet 1975).

16

If the seismic source spectrum (Eq. 2.10) is combined with propagation path effects (Eq. 2.11), the Fourier Amplitude Spectrum $FAS(M_0, R, f)$ is given by:

$$FAS(M_0, R, f) = E(M_0, f) \cdot P(R, f) \cdot I(f)$$

$$= \left(0.78 \frac{\pi}{\rho_0 \beta_0^3} M_0 \frac{f^2}{1 + \left(\frac{f}{f_c} \right)^2} \right) \left[\frac{1}{R} exp \left(-\frac{\pi R f}{Q(f) \beta_0} \right) \right] \tag{2.15}$$

Figure 2.4 shows the change in $FAS(M_0, R, f)$ for different propagation path effect factors: geometrical spreading term at different distances and frequency-dependent $Q(f)$ for two different values of M_W and $\Delta\sigma$. For near-source geometrical spreading ($R = 1$ km), attenuation effects are very similar (thick colored lines), and the spectrum is practically constant at higher frequencies (similar to the source spectrum in Figure 2.2); therefore, propagation effects can be neglected near the source (e.g., Boore 2003). The clear distinction between the source spectrum ($R = 1$ km) and the spectrum when the propagation path effects are included ($R = 20$ km) is observed at the high-frequency part of the spectrum. Corner frequency f_c does not change and at larger distances ($R = 20$ km), amplitude of $FAS(M_0, R, f)$ is shifted to lower values (dashed colored lines). For $n \approx 1$, the attenuation $Q(f)^{-1}$ is lower (black or green dashed line) and spectrum decays very little to none. For $n \ll 1$, the attenuation $Q(f)^{-1}$ is higher and the spectrum decays up to a certain degree (red and blue dashed lines). The degree of spectrum decay at higher frequencies is related to the factor Q_0; if it is higher, for the same exponent n, $Q(f)^{-1}$ is lower, and the decay is lower (red vs. blue dashed lines). Combination of Q_0 factors and exponents n determine the value of frequency dependent attenuation $Q(f)^{-1}$ and the degree of spectrum decay at higher frequencies.

Recently, single backscattering model was used to estimate attenuation of coda waves of local earthquakes recorded on Croatia seismological stations in the complex area of Pannonian basin and Dinarides by Dasović et al. (2012, 2013, 2015b). These studies estimated values of Q_0 and n of the frequency dependent $Q_C(f)$ model by Eq. (2.14). Estimated values will be discussed in Chapter 4.4 in terms of the comparison between two different attenuation approaches (coda waves and kappa) for the high-frequency range estimated for the same seismological stations. Also, these values will be used in Chapter 5 to define propagation path effects in terms of $Q_C(f)$ for definition of the input $FAS(M_0, R, f)$ for the purpose of stochastic simulations using Random Vibration Theory-based site response analysis.
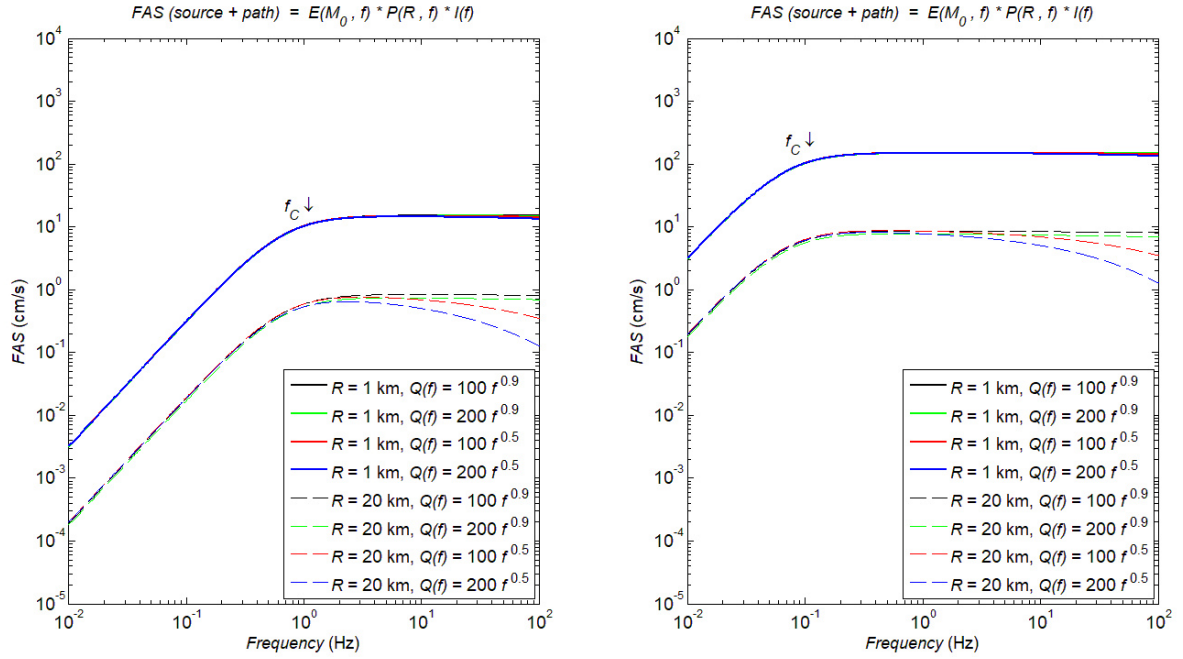
Figure 2.4. Comparison of acceleration $FAS(M_0, R, f)$ accounted for source and propagation path effects: $FAS(M_0, R, f) = E(M_0, f) \cdot P(R, f) \cdot I(f)$ for $R = 1 \text{ km}$ and $R = 20 \text{ km}$. Frequency dependent parameters $Q(f) = 100f^{0.5}, Q(f) = 200f^{0.5}, Q(f) = 100f^{0.9}, Q(f) = 200f^{0.9}$ are used for $M_W = 5$ (left), $M_W = 7$ (right) and constant value of $\Delta\sigma = 100$ bar.

2.3. Site effects

The crustal path attenuation effects shown in Figure 2.4 describe the change in $FAS(M_0, R, f)$ of ground acceleration from the source to the near-surface bedrock below the site (called engineering bedrock). As was mentioned at the beginning of this chapter, local site conditions (i.e., site effects) modify the spectral characteristics (amplitude, frequency, duration) of the incoming seismic waves when they pass through the uppermost soft soil layers (e.g., Reiter 1990; Kramer 1996). A simplified function given by frequency-dependent modification of spectrum $S(f)$ (e.g., Silva et al. 1997; Boore 2003) describes the site effects in terms of the amplification function $Amp(f)$ and the diminution parameter $D(f)$ (also called near-site attenuation parameter) as:

$$S(f) = Amp(f) \cdot D(f) \tag{2.16}$$

Boore and Joyner (1997) defined $Amp(f)$ as the FAS of the surface ground motion for un-attenuated incident plane waves divided by the FAS recorded at the surface of uniform half-space by the same incident plane (on the outcrop). $Amp(f)$ is given by Eq. (2.17) as the square-root of the ratio between seismic impedance at the earthquake source (product of density ρ_0

18

and shear wave velocity β_0 near the source) and average seismic impedance of materials near the surface (product of average density and shear wave velocity as a function of frequency f and depth z) up to a depth that corresponds to one quarter of the wavelength of interest:

$$Amp(f) = \sqrt{\frac{\rho_0 \beta_0}{\rho[z(f)]\beta[z(f)]}} = \sqrt{\frac{\rho_0 \beta_0}{\bar{\rho}(f)\bar{\beta}(f)}} \tag{2.17}$$

Quarter-wavelength approximation (introduced by Joyner et al. 1981 and later updated by Boore 2003) assumes that at any given frequency f, vertically heterogeneous soil profile can be characterized by average velocity down to a depth $z(f) = \bar{\beta}/4f = \lambda/4$ equivalent to a quarter-wavelength of interest as (Boore 2003):

$$f(z) = \frac{1}{4 \int_0^{z(f)} \frac{1}{\beta(z)} dz} \tag{2.18}$$

Near-surface seismic impedance varies with frequency f and depth $z(f)$ and represents the average velocity $\bar{\beta}(f)$ and density $\bar{\rho}(f)$ (Boore 2003):

$$\bar{\beta}(f) = \beta[z(f)] = z(f) \int_0^{z(f)} \frac{1}{\beta(z)} dz \tag{2.19a}$$

$$\bar{\rho}(f) = \rho[z(f)] = \frac{1}{z(f)} \int_0^{z(f)} \rho(z) dz \tag{2.19b}$$

Physically, using quarter-wavelength approximation in the simplified 1-D soil layer over a homogeneous half-space yields to observed maximum in SH-wave amplification at a defined frequency, the fundamental resonance frequency.

Boore and Joyner (1997) compiled the shear-wave velocity profiles for generic rock sites from borehole data and studies of crustal velocity to compute the frequency-dependent site amplification $Amp(f)$ model for zero attenuation as given in Table 2.1. Generic rock sites are defined as those whose velocity at shallow depths equals the average of those from rock sites sampled by the borehole data. $Amp(f)$ values are incorporated in the stochastic simulations when the FAS needs to be accounted for particular unattenuated generic sites (e.g., Boore and Joyner 1997; Boore 2003).

Table 2.1. Values of $Amp(f)$ for generic rock sites with average shear-wave velocity in top 30 m (V_{S30}): $V_{S30} = 620$ m/s (soft rock site), $V_{S30} = 760$ m/s (engineering bedrock), and $V_{S30} = 2900$ m/s (very hard rock site) (adapted from Boore and Joyner 1997).

Frequency (Hz)	$Amp(f)$ $V_{S30} = 2900$ m/s	$Amp(f)$ $V_{S30} = 760$ m/s	$Amp(f)$ $V_{S30} = 620$ m/s
0.01	1.00	1.00	1.00
0.09	1.02	1.09	1.10
0.16	1.03	1.18	1.18
0.51	1.05	1.32	1.42
0.84	1.07	1.51	1.58
1.25	1.09	1.64	1.74
2.26	1.11	1.99	2.06
3.17	1.12	2.18	2.25
6.05	1.13	2.38	2.58
16.60	1.14	2.95	3.13
61.20	1.15	3.68	4.00
100.00	1.15	3.96	4.40

The diminution function $D(f)$ given in Eq. (2.16) is used to model the path-independent loss of energy to account for the attenuation in the upper soil layers. In the 1980's, it was observed that empirical FAS of ground acceleration of shear waves decay rapidly after some site-specific cut-off frequency (f_{max}) (e.g., Hanks 1982). Rapid spectrum decay at the high frequencies has been attributed to the near-site attenuation effects (very shallow crust directly below the site) (e.g., Hanks 1982; Anderson and Hough 1984). The spectral decay parameter kappa (κ) was introduced by Anderson and Hough (1984) to describe the difference in the high frequencies between the observed acceleration FAS of the shear-waves from seismograms and the theoretical Brune (1970) ω^2 source model. The total path attenuation of shear-waves within the crust (e.g., Cormier 1982; Edwards et al. 2011) is separated into two attenuation parameters: frequency-dependent quality factor $Q(f)$ and the near site attenuation parameter kappa (zero distance parameter which describes near-surface site-specific attenuation called site kappa, κ_0). Details about the origin, physical interpretation, and field applications of κ and local-site specific component κ_0 will be provided in Chapter 4.

Diminution function $D(f)$ can be described using two alternatives (e.g., Silva et al. 1997; Boore 2003): i) the high-frequency cut-off filter represented by f_{max} (Eq. 2.20a) and ii) the simple exponential representation based on near-site attenuation κ_0 (Eq. 2.20b):

$$D(f) = \left[1 + \left(\frac{f}{f_{max}} \right)^8 \right]^{-\frac{1}{2}} \qquad (2.20a)$$

$$D(f) = exp(-\pi \kappa_0 f) \qquad (2.20b)$$

The combined site effects (Eqs. 2.16) in the Fourier Amplitude Spectrum expressed by amplification function $Amp(f)$ (Table 2.1) and near-site attenuation κ_0 (Eq. 2.20b) for a generic rock site with $V_{S30} = 760$ m/s is shown in Figure 2.5. Within reasonable values of κ_0 (higher than 0.01 s to 0.04 s for most rock sites), the large amplifications of FAS at high frequencies are greatly damped by the near-site attenuation κ_0 (Boore and Joyner 1997). In a similar manner, for a single value of κ_0 and for various V_{S30} site conditions, the site effect amplification exceeds factor 2 over different range of frequencies. The high-frequency site effects, particularly κ_0 value is important to be accounted in Fourier Amplitude Spectrum for the stochastic ground motion simulations for which the input motion is defined within reference generic bedrock.
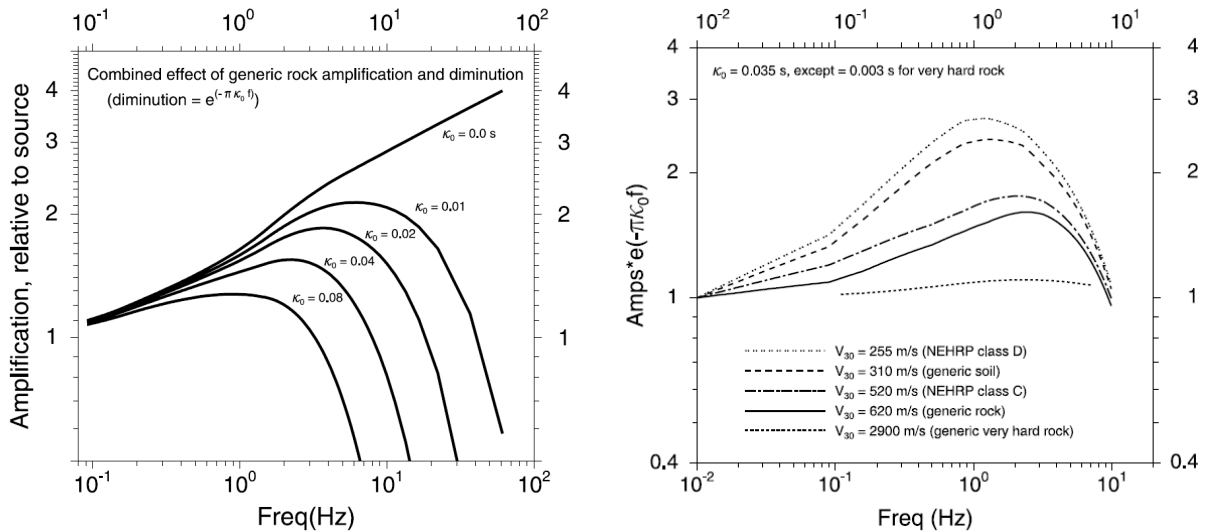
Figure 2.5. Combined site effects of the Fourier Amplitude Spectrum expressed by amplification function $Amp(f)$ and near-site attenuation κ_0. Left: Example for different values of κ_0 for single generic rock site with $V_{S30} = 760$ m/s. Right: Example for various V_{S30} site conditions for single value of κ_0 Taken from Boore (2003).

If the source, propagation path, and site effects are combined into theoretical FAS of ground acceleration of radiated shear-waves (Eqs. 2.15, 2.20b with the appropriate values of $Amp(f)$ for generic rock sites according to V_{S30} from Table 2.1), the final form of acceleration Fourier

Amplitude Spectrum of ground motion $FAS(M_0, R, f) = E(M_0, f) \cdot P(R, f) \cdot S(f) \cdot I(f)$ is given by Eq. (2.21):

$$FAS(M_0, R, f) = E(M_0, f) \cdot P(R, f) \cdot S(f) \cdot I(f)$$

$$= \left(0.78 \frac{\pi}{\rho_0 \beta_0^3} M_0 \frac{f^2}{1 + \left(\frac{f}{f_c}\right)^2} \right) \left[\frac{1}{R} exp\left(-\frac{\pi R f}{Q(f)\beta_0} \right) \right] [Amp(f) exp(-\pi \kappa_0 f)] \qquad (2.21)$$

The FAS for different seismological parameters based on Eq. (2.21) is provided in Figure 2.6, showing that the near-site attenuation parameter κ_0 changes the shape of FAS at higher frequencies more than quality factor $Q(f)$ (red vs. blue and green dash lines). If the value of near-site attenuation κ_0 is higher (e.g., green line), the decay of the high-frequency content of FAS is more rapid. When frequency-dependent site amplification effects in terms of $Amp(f)$ are taken into account, the amplitudes of FAS are amplified at higher frequencies for softer generic rock sites (Figure 2.6, left), whereas for for very hard rock sites (Figure 2.6, right) this effect is neglected.
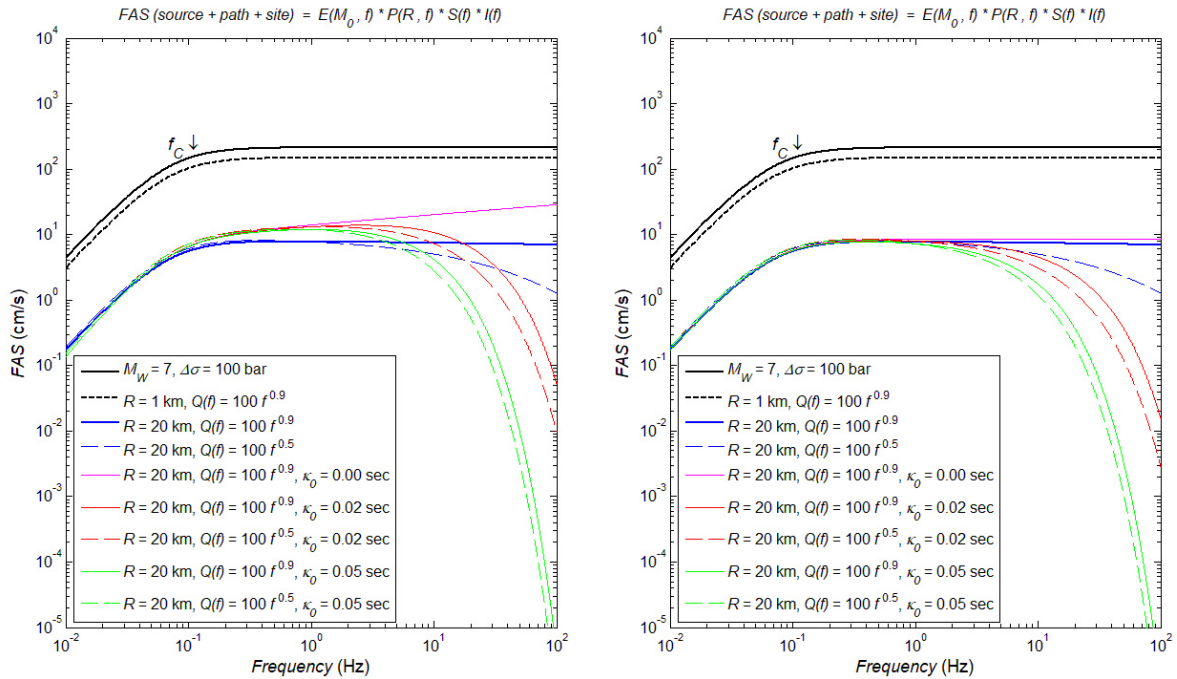
Figure 2.6. Comparison of acceleration shear-wave $FAS(M_0, R, f)$ accounted for source, propagation path effect and site effects: $FAS(M_0, R, f) = E(M_0, f) \cdot P(R, f) \cdot S(f) \cdot I(f)$ for $R = 1$ km and $R = 20$ km. Frequency dependent quality factors $Q(f) = 100 f^{0.5}, Q(f) = 100 f^{0.9}$, near-site attenuation values $\kappa_0 = 0.00$ s, 0.02 s, 0.05 s are used for constant values of moment magnitude $M_W = 7$ and $\Delta\sigma = 100$ bar. Left: $Amp(f)$ for generic rock site ($V_{S30} = 620$ m/s). Right: $Amp(f)$ for very hard generic rock site ($V_{S30} = 2900$ m/s).

Ground motion at the site (e.g., seismic station, city, etc.) is influenced by the complex system of parameters summarized in this chapter. A small change in one of these elements may have little impact on the FAS, but if combined with other elements, it can have disastrous effect on the damage (Reiter 1990; Kramer 1996). These parameters and the theoretical FAS described here are used in stochastic simulations (Boore 1983, 2003) to support the empirical strong motion datasets or used in site response analysis when combined by the Random Vibration Theory (Chapter 3). For all engineering applications, seismological parameters play an important role, particularly, the parameters which describe high-frequency part of FAS (frequency-dependent quality factor $Q(f)$ and site-specific attenuation parameter κ_0). Single corner frequency models have been proven to produce accurate results for specifying the spectra of far-field shear waves, which dominates the characteristics of high-frequency shaking (e.g., McGuire 1980; Hanks and McGuire 1981; Silva et al. 1997; Rathje and Ozbey 2006).

3. Methods to evaluate the local site effects on the site amplification factor of seismic ground motions

Estimating the effects of local site conditions upon the seismic ground motions is one of the most significant and controversial issues in the field of earthquake engineering. First evidence about local soil amplification effects and observed variations in building damage during shaking related to local geology was reported by Stur (1871) for the Klana earthquake of 1870. Stur (1871) observed that houses in Klana and Studena built on limestones sustained less damage than those situated in the alluvial parts. Herak et al. (2018) provided HVSR results that confirm these effects. Also, these effects were observed through years during the past earthquakes, for which the ground motions recorded on soft soils sites (e.g., alluvial basins, soft sediments) are found to be significantly larger than those recorded on nearby rock outcrops (e.g., Idriss and Seed 1968; Schnabel et al. 1972; Reiter 1990; Kramer 1996). One of the most important and most encountered problems in earthquake engineering practice is the evaluation of the ground response to predict the site amplification in surface ground motions for the future earthquakes, for the purpose of earthquake resistant design of structures under different ground shaking levels to ensure the health, safety, and security of building occupants and assets.

3.1. Equivalent–linear (EQL) site response analysis

Equivalent–linear (EQL) site response analysis method is a numerical technique that computes the surface ground motions from the input motion at the bedrock using the site-specific dynamic soil properties to predict the influence of local soil conditions on the amplification of seismic ground motion. 1-D EQL site response analysis was first introduced by Idriss and Seed (1968) and implemented by Schnabel et al. (1972) in SHAKE software, by Idriss and Sun (1992) in SHAKE91 and recently by Hashash et al. (2012) in DEEPSOIL. Later on, stochastic ground

motion simulation procedures (Hanks and McGuire 1981; Boore 1983, 2003; Rathje and Ozbey 2006; Kottke and Rathje 2013) have been introduced into the earthquake engineering community to predict site amplification factors based on the input earthquake scenario in terms of FAS to overcome the need for the use of the strong motion time series records. Silva and Lee (1987) introduced the RASCAL code for synthesizing the ground motions based on RVT procedure and Silva et al. (1997) provided a comprehensive validation of the RVT-based site response analysis procedure. Recently, Kottke and Rathje (2009) developed a new and publicly free available software (STRATA) that performs the RVT-based 1-D EQL site response analysis.

The 1-D EQL site response analysis approach proposed by Schnabel at al. (1972) is based on the assumption that superficial soil layers extend horizontally and vertically-propagating/horizontally-polarised waves (SH waves) dominate the earthquake ground motion wavefield. Shear wave velocities of the shallower soil layers are generally lower than those beneath them; therefore, inclined seismic rays on the horizontal layer boundaries are multi-reflected to a nearly-vertical direction (Figure 3.1). Representative soil profiles utilized in 1-D EQL analysis are described by horizontal multi-layered damped soil layers on the elastic rock that extends to the infinite depth (z) (N horizontal layers where N-th layer represents bedrock). Strain-compatible dynamic soil properties: the shear modulus (G) and damping ratio (ξ) as a function of strain (γ) are attributed to each soil layer in addition to layer thickness (h) and density (ρ) (Figure 3.2).

The EQL site response analysis procedure consists of four steps: 1) definition of the geometry of the soil layers and implementing the shear wave velocity profile, 2) selection of appropriate dynamic soil properties: the shear modulus reduction G/G_{max} and damping ξ curves (e.g., Seed et al. 1984; Vučetić and Dobry 1991), 3) specification of the input rock motions, and 4) propagation of the input rock motion through the soil profile to estimate the ground motions and maximum strains in each soil layer. The equivalent–linear soil model that will be defined in the next section is composed at the first two steps of the procedure. For the third step, two different ways of defining input bedrock motions will be introduced in Sections 3.2 and 3.3.
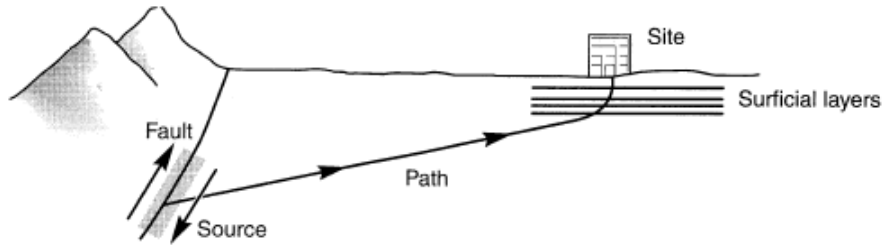
Figure 3.1. Ground motion propagation from source to the site. Nearly vertical wave propagation in the surficial soil layers is used in the 1-D equivalent–linear site response analysis (Kramer 1996).
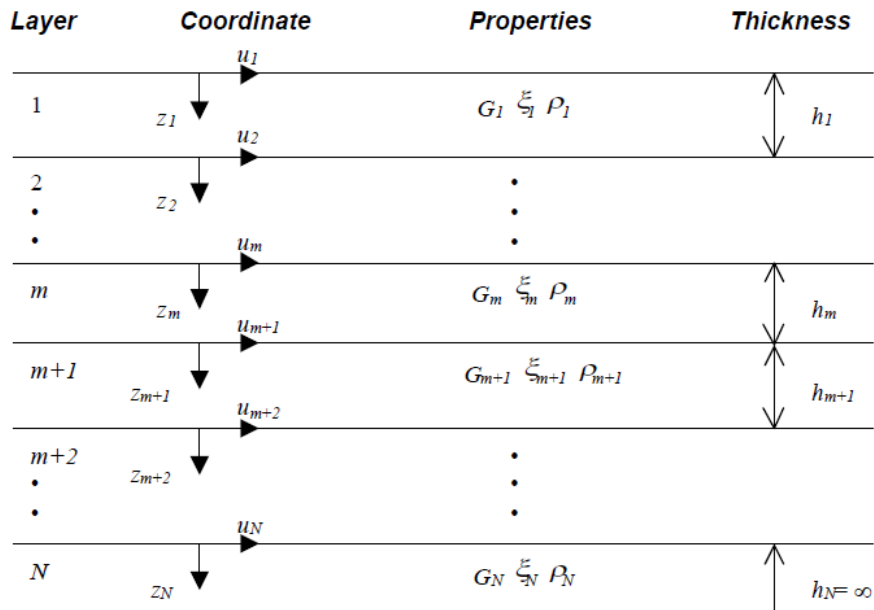
Figure 3.2. Multi-layered damped soil model on the elastic rock (Schnabel et al. 1972; Kramer 1996; Bardet et al. 2000). Soil layer properties are: shear modulus (G) and damping ratio (ξ) as a function of strain (γ) of each soil layer (1-surface to N-rock) of thickness (h) and density (ρ).

3.1.1. Equivalent–linear soil model

Soil undergoes inelastic deformations after a certain level of ground shaking; therefore, the non-linear behaviour of soil should be taken into account in ground response analysis. The equivalent–linear soil model utilizes the linear visco-elastic Kelvin-Voight model (Figure 3.3) as an approximation to the non-linear behaviour of soil under cycling loading (Schnabel et al. 1972; Seed et al. 1984). The shear stress τ is equal to shear stresses acting on both elements (elastic spring and viscous dashpot) and their changes with respect to time depends on the shear strain $\gamma(t)$ and its rate $\partial\gamma/\partial t$ as:

$$\tau(t) = G\,\gamma(t) + \eta\frac{\partial\gamma(t)}{\partial t} \tag{3.1}$$

where G is shear modulus of elastic spring and η is the viscosity of the damping material. If shear stress τ is applied continuously, the material deforms at a decreasing rate, asymptotically approaching to the steady-state. When τ is released, the material gradually relaxes back to its undeformed state. For a harmonic shear strain in the form of Eq. (3.2), τ is given by Eq. (3.3).

$$\gamma = \gamma_0 sin(\omega t) \tag{3.2}$$

$$\tau = G\gamma_0 sin(\omega t) + \omega\eta cos(\omega t) \tag{3.3}$$
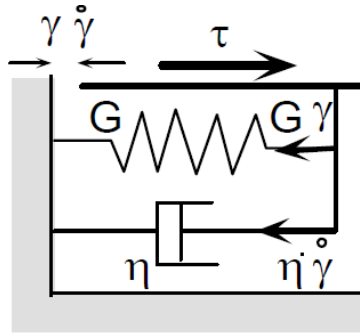
Figure 3.3. Schematic representation of shear stress (τ)-strain (γ) Kelvin-Voight model used in EQL analysis (Kramer 1996).

Eqs. (3.2) and (3.3) form the elliptic stress-strain loop of Kelvin-Voight model. Real soils dissipate elastic energy by a hysteresis stress-strain loop (Figure 3.4a) due to the slippage of the soil particles with respect to each other (Kramer 1996). The energy dissipated (Eq. 3.4) in one loading cycle (W_D) is equal to the area under the hysteresis stress-strain loop (i.e. energy demand of an earthquake). The maximum strain energy stored in the system (W_S) is given in Eq. (3.5). The equivalent–linear damping ratio ξ is the damping ratio in a particular loading cycle as shown in Eq. (3.6).

$$W_D = \oint_{\tau_c} \tau d\tau = \pi\omega\eta\gamma_c^2 \tag{3.4}$$

$$W_S = \frac{1}{2}\tau_c\gamma_c^2 = \frac{1}{2}G\gamma_c^2 \tag{3.5}$$

$$\xi = \frac{W_D}{4\pi W_S} = \frac{\eta\omega}{2G} \qquad (3.6)$$

The equivalent linear shear modulus is represented by the secant shear modulus G_{sec} which is equal to the ratio of shear stress τ_c and strain γ_c ($G_{sec} = \tau_c/\gamma_c$) at the tips of the strain-controlled loading cycles (Figure 3.4b, c). Generally, soils (particularly soft soils with small V_{S30} values; e.g., Seed et al. 1984; Vučetić and Dobry 1991) degrade under large deformations (strains); therefore, G decreases and ξ increases with increasing strains, explained as the *non-linearity* of soil response. The equivalent damping can be determined by the strain-controlled laboratory tests (e.g., Seed et al. 1984; Vučetić and Dobry 1991). Shear wave velocity (V_S) of each soil layer is a valuable indicator of the dynamic properties of soil and rock because of its relationship with the maximum value of equivalent linear shear modulus G defined as: $G_{max} = \rho V_S^2$, where V_S is measured from geophysical survey methods (small strains in the order to 10^{-4} or less). Values of G and ξ at large strains (of the order to 10^{-3} to 1 %) are usually determined from geotechnical in-situ testing methods (e.g. Standard Penetration Test–SPT, Cone Penetration Test–CPT). Provided that G_{max} is known, shear response at various levels of strain can be estimated using soil modulus reduction curves (G/G_{max}) that have been published before (e.g., Schnabel et al. 1972; Seed et al. 1984; Vučetić and Dobry 1991).
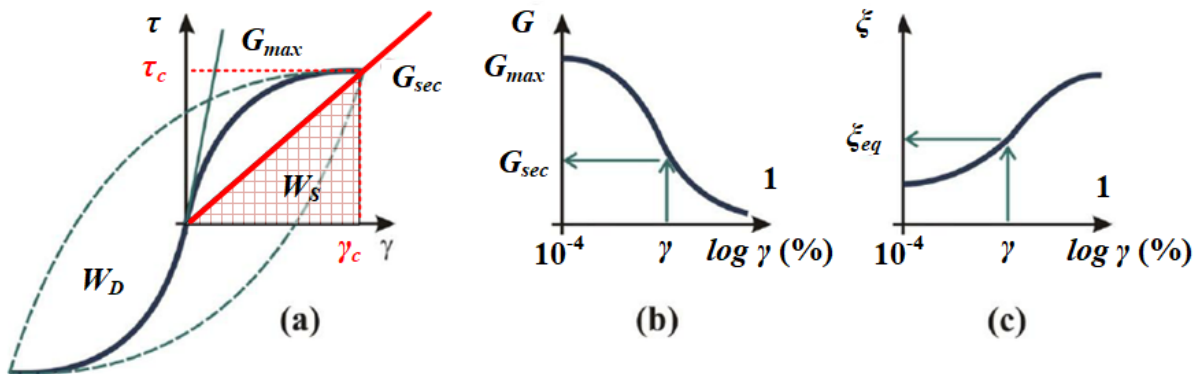
Figure 3.4. a) Hysteresis stress-strain loop representing equivalent–linear model. Variation of the: b) shear modulus G, and c) damping ratio ξ with shear strain γ (Kramer 1996; Bardet et al. 2000).

In the EQL site response analysis, the equivalent–linear approximation of the non-linear soil behaviour is represented by an iterative procedure: G and ξ are varied with the induced strain in each layer. This iterative procedure is illustrated in Figure 3.5. Initial values of $G_0(G_{max})$ and ξ_0 are defined at small strain values. Based on the initial values of G_0 and ξ_0 for each layer,

effective shear strain γ^1_{eff} is predicted in the EQL analysis. Usually, time history of shear strain of earthquake motions is irregular with peak amplitudes. Therefore, the effective shear strain is taken as 65 % of the maximum peak strain (e.g., Idriss and Sun 1992, Kramer 1996). The effective shear strain in each layer is determined based on the induced maximum shear strain as: $\gamma^i_{eff} = R_\gamma \cdot \gamma^i_{max} = 0.65 \cdot \gamma^i_{max}$. The new values G_{i+1} and ξ_{i+1} corresponding to the induced γ^i_{eff} in each layer are calculated for the next iteration. The non-linear site response is calculated using new soil properties and effective shear strains and γ^i_{eff} is re-determined. The procedure is repeated until the difference in strain-compatible values of G_i and ξ_i in two successive iterations is less than 5–10 % and predicted effective strains are consistent with assumed effective strains (Schnabel et al. 1972). The EQL approach is a first-order approximation to the effects of non-linear and inelastic soil behaviour under cycling conditions (e.g., earthquake) in which stiffness G decreases and damping ξ increases as induced shear strains increases.
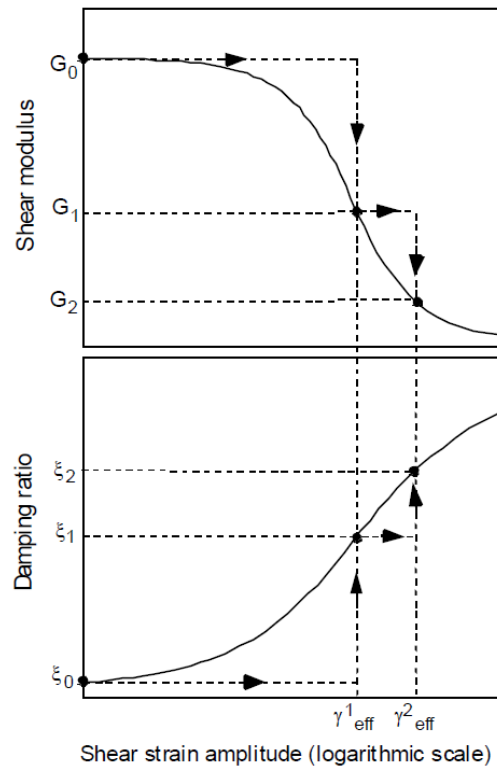
Figure 3.5. Iterative procedure of equivalent–linear approximation for soil with properties G and ξ to be consistent with the induced shear strain γ^i_{eff} in each layer (Bardet et al. 2000).

3.1.2. Site-specific response analysis based on the one-dimensional wave propagation theory

The EQL site-specific response analysis for the soil model shown in Figure 3.2 is based on the solution of 1-D wave equation for vertically propagating SH-waves of incident seismic ground motion propagating from the bedrock to the ground surface. In the 1-D wave equation, τ from Eq. (3.1) is substituted into Eq. (3.7a) to represent the response of Kelvin-Voight soil model to form Eq. (3.7b) (after Kramer 1996):

$$\rho \frac{\partial^2 u}{\partial t^2} = \frac{\partial \tau}{\partial z} \tag{3.7a}$$

$$\rho \frac{\partial^2 u}{\partial t^2} = G \frac{\partial^2 u}{\partial z^2} + \eta \frac{\partial^3 u}{\partial z^2 \partial t} \tag{3.7b}$$

Displacement $u(z,t)$ for harmonic waves can be written as:

$$u(z,t) = U(z) \exp(i\omega t) \tag{3.8}$$

Substituting Eq. (3.8) into Eq. (3.7b) yields to:

$$(G + i\omega\eta) \frac{d^2 U}{dt^2} = \rho \omega^2 U \tag{3.9a}$$

$$G^* \frac{d^2 U}{dt^2} = \rho \omega^2 U \tag{3.9b}$$

The complex shear modulus $G^* = G + i\omega\eta$ represents the complex stiffness matrix of real soils. Frequency dependence can be eliminated by substituting Eq. (3.6), so that complex shear modulus can be expressed as frequency independent $G^* = G(1 + 2i\xi)$. G^* is related to the shear wave velocity as $V_S^* = \sqrt{G^*/\rho} = V_S(1 + i\xi)$ and to the complex wave number as $k^* = \omega\sqrt{\rho/G^*}$.

General solution to the 1-D wave equation given in Eq. (3.9b) is:

$$u(z,t) = Ae^{i(\omega t - k^* z)} + Be^{i(\omega t + k^* z)} \tag{3.10}$$

where A and B represent amplitudes of upward (-z) and downward (+z) directions.

Corresponding shear stress τ using general solution from Eq. (3.10) is given by:

$$\tau(z,t) = G^*\gamma(z,t) = G^*\frac{\partial u}{\partial z} = ik^*G^*\left(Ae^{ik^*z} - Be^{-ik^*z}\right) \tag{3.11}$$

Boundary conditions for displacement at the top and bottom of layer m are:

$$u_m(z_m = 0, t) = (A_m + B_m)e^{i\omega t} \tag{3.12a}$$

$$u_m(z_m = h_m, t) = \left(A_m e^{ik_m^* h_m} + B_m e^{-ik_m^* h_m}\right)e^{i\omega t} \tag{3.12b}$$

Equality of displacements at the interface between layer m and $m+1$ implies that:

$$u_m(z_m = h_m, t) = u_{m+1}(z_{m+1} = 0, t) \tag{3.13a}$$

$$A_{m+1} + B_{m+1} = A_m e^{ik_m^* h_m} + B_m e^{-ik_m^* h_m} \tag{3.13b}$$

Boundary conditions for shear stresses at the top and bottom of layer m are:

$$\tau_m(z_m = 0, t) = ik_m^* G_m^* (A_m - B_m)e^{i\omega t} \tag{3.14a}$$

$$\tau_m(z_m = h_m, t) = ik_m^* G_m^* \left(A_m e^{ik_m^* h_m} - B_m e^{-ik_m^* h_m}\right)e^{i\omega t} \tag{3.14b}$$

Continuity of shear stresses at the interface between layer m and $m+1$ implies that:

$$\tau_m(z_m = h_m, t) = \tau_{m+1}(z_{m+1} = 0, t) \tag{3.15a}$$

$$A_{m+1} - B_{m+1} = \frac{k_m^* G_m^*}{k_{m+1}^* G_{m+1}^*}\left(A_m e^{ik_m^* h_m} - B_m e^{-ik_m^* h_m}\right) \tag{3.15b}$$

After adding Eq. (3.13b) to Eq. (3.15b) and subtracting Eq. (3.15b) from Eq. (3.13b), recursion formulas relates the amplitudes between layers m and $m+1$ as:

$$A_{m+1} = \frac{1}{2}A_m(1 + \alpha_m^*)e^{ik_m^* h_m} + \frac{1}{2}B_m(1 - \alpha_m^*)e^{-ik_m^* h_m} \tag{3.16a}$$

$$B_{m+1} = \frac{1}{2}A_m(1 - \alpha_m^*)e^{ik_m^* h_m} + \frac{1}{2}B_m(1 + \alpha_m^*)e^{-ik_m^* h_m} \tag{3.16b}$$

Complex impedance ratio α_m^* represents resistance to particle (soil or rock) motion and is inversely proportional to the shear wave velocity, i.e., as seismic wave travels through the region of increased impedance, resistance to motion increases and amplitude of seismic wave decreases due to energy preservation.

At the boundary of layers m and $m+1$ the complex impedance ratio α_m^* is given as:

$$\alpha_m^* = \frac{k_m^* G_m^*}{k_{m+1}^* G_{m+1}^*} = \frac{\rho_m (V_S^*)_m}{\rho_{m+1} (V_S^*)_{m+1}} \tag{3.17}$$

If the recursive algorithm starts from the top of the free surface and uses the boundary conditions at the free surface (shear stress is equal to zero), amplitudes at the free surface become equal to:

$$\tau_1(0,t) = i k_1^* G_1^* (A_1 - B_1) e^{i\omega t} = 0 \rightarrow A_1 = B_1 \tag{3.18}$$

When recursive algorithm is repeatedly applied from layers 2 to m, relationships between the amplitudes in layer m and those in surface layer are:

$$A_m = a_m(\omega) A_1 \tag{3.19a}$$

$$B_m = b_m(\omega) B_1 \tag{3.19b}$$

Transfer function $TF_{m,n}(\omega)$ relates the displacement amplitudes (a_n, b_n) in layer n to the amplitudes (a_m, b_m) in layer m:

$$TF_{m,n}(\omega) = \frac{u_m}{u_n} = \frac{\dot{u}_m}{\dot{u}_n} = \frac{\ddot{u}_m}{\ddot{u}_n} = \frac{a_m(\omega) + b_m(\omega)}{a_n(\omega) + b_n(\omega)} \tag{3.20}$$

Eq. (3.20) describes the amplification of displacements, velocities and accelerations from layer n to the layer m. Motion in any layer can be determined from the known motion at any point in the soil profile using the recursive relationships (Eq. 3.16). For $(m,n) = (1,N)$ transfer function $TF_{1,N}(\omega)$ relates the ground surface motion to the input bedrock motion (Kramer 1996).

3.1.3. Definition of the input motions used in site response analysis

The input motion in the EQL site response analysis is propagated from the elastic bedrock (bedrock motion) through the soil layers up to the soil surface (free surface motion). The rock outcropping motion is defined as a motion on the exposed bedrock at the location (Figure 3.6a). Outcrop motion does not involve the soil-rock interaction and its amplitude is twice the amplitude of the incoming motion due to the free surface effect $(2A_N)$. If elastic bedrock is defined in EQL site response analysis, the bedrock motion includes the soil-rock interaction (reflection at the interface of soil-rock layer) and the amplitude of bedrock motion $(A_N + B_N)$ is not equal to that of the outcrop motion $(2A_N)$. If the bedrock is rigid, there is no interaction between soil and rock, and the input motion is identical to the outcrop motion $(A_N = B_N = 2A_N)$. The amplitude of the incoming motion (A_N) in the halfspace is independent of the media properties above, since the reflected motion (B_N) is absorbed in the halfspace (e.g., Kramer 1996; Bardet et al. 2000; Ordonez 2011).

The amplification relating the bedrock motion to the outcrop motion and the surface motion (for the illustrated cases in the Figure 3.6b) is defined using transfer function $TF_{m,n}(\omega)$ (Eq. 3.20) (Bardet et al. 2000; Ordonez 2011):

- Soil surface-bedrock:

$$T_{1,b} = \frac{u_1}{u_b} = \frac{2A_1}{A_N + B_N} = \{A_1 = 1\} = \frac{2}{A_N + B_N} \tag{3.21a}$$

- Soil surface-outcrop:

$$T_{1,o} = \frac{u_1}{u_o} = \frac{2A_1}{2A_N} = \{A_1 = 1\} = \frac{1}{A_N} \tag{3.21b}$$

- Bedrock-outcrop:

$$T_{b,o} = \frac{u_b}{u_o} = \frac{A_N + B_N}{2A_N} \tag{3.21c}$$

Difference between transfer functions, surface to bedrock $(T_{1,b})$ and surface to outcrop $(T_{1,o})$, changes depending on the definition of the bedrock: as rigid base or an elastic base. The use of input bedrock motion on the elastic bedrock, or the input outcrop motion on the rigid bedrock is not recommended due to the over-amplification $(T_{1,b})$ (Eq. 3.21a) at the peak frequency (Schanbel et al. 1972; Hashash et al. 2012). Typically, in the EQL site response analysis, previously recorded or simulated rock motions on the outcrop are used to define input rock

motions: outcrop motion on the elastic bedrock is approx. equal to bedrock motion on the rigid bedrock with minimum values $(T_{b,o} < 1)$ at resonance peak frequency of the soil model. This is reflected in the transfer function peak (Eq. 3.21b) between surface and outcrop/bedrock amplitudes: $(T_{1,o})$ is approx. 65 % of the $(T_{1,b})$ (Kramer 1996; Bardet et al. 2000; Hashash et al. 2012).
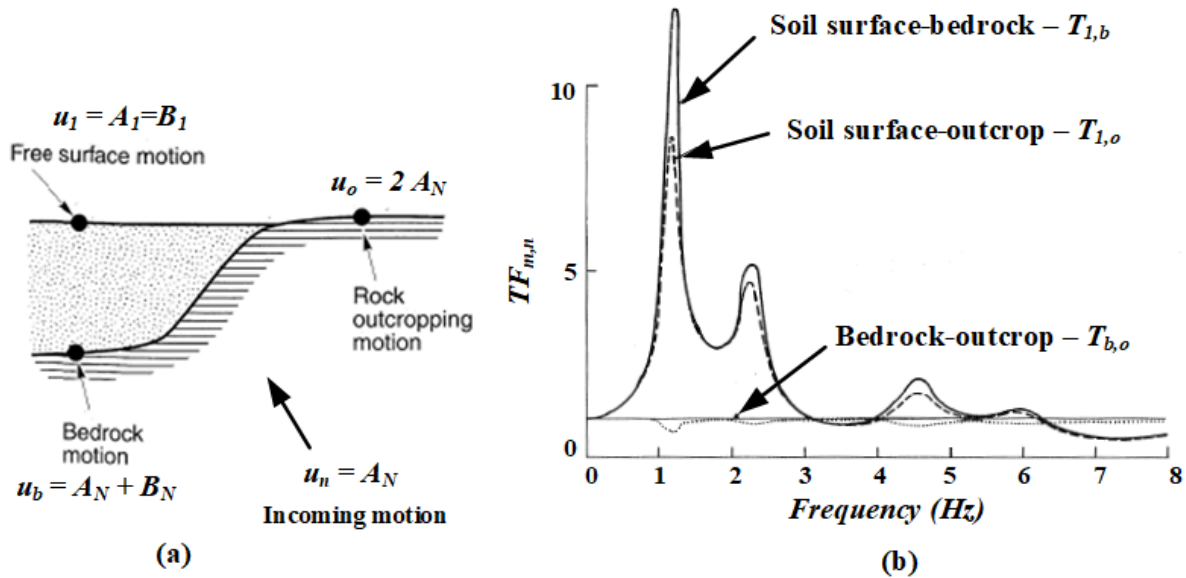
Figure 3.6. a) Definition of the input motions used in site response analysis. b) Transfer function (Eq. 3.20) $TF_{m,n}(\omega)$ that defines the amplification of the input motion at the bedrock to the outcrop and surface motion (after Kramer 1996 and Bardet et al. 2000). The largest amplification (transfer function) in this case occurs at the lowest natural frequency (or largest period) with higher peak characteristic frequencies.

3.2. EQL site response analysis using Time Series (TS) approach

The input rock motions in the EQL site response analysis can be defined using previously recorded, or simulated rock acceleration motions in time series approach (TS-approach). The TS-approach is widely used in the site-specific EQL site response analysis for decades (e.g., Idriss and Seed 1968; Schnabel et al. 1972; Idriss and Sun 1992; Hashash et al. 2012). To use the real recordings of acceleration time histories as an input motion in the 1-D EQL site response analysis, Fourier transformation is used to represent transient motions. Real or simulated seismogram with n equidistant acceleration values $\ddot{u}_j(\Delta t), j = 0, \dots, n - 1$ can be approximated by a finite sum of harmonic motions (Ordonez 2011):

$$\ddot{u}(t) = \sum_{s=0}^{n/2} [e_s exp(i\omega_s t) + f_s exp(-i\omega_s t)] \tag{3.22}$$

where $\omega_s, s = 0, \dots, n/2$ are the equidistant frequencies: $\omega_s = \frac{2\pi}{n\Delta t}s$, and e_s and f_s are complex Fourier coefficients:

$$e_s = \frac{1}{n}\sum_{s=0}^{n/2} \ddot{u}(t)exp(-i\omega_s t) \qquad f_s = \frac{1}{n}\sum_{s=0}^{n/2} \ddot{u}(t)exp(i\omega_s t) \tag{3.23}$$

If a discrete acceleration time series (Eq. 3.22) represents the motion in layer m, using the transfer function $TF_{m,n}(\omega)$ (Eq. 3.20), a new acceleration time series representing the motion in any other layer n can be calculated as:

$$\ddot{u}(t) = \sum_{s=0}^{n/2} TF_{m,n}(\omega_s)[e_{m,s}exp(i\omega_s t) + f_{m,s}exp(-i\omega_s t)] \tag{3.24}$$

The computational steps in TS-approach are presented in Figure 3.7 and briefly include the following stages:

a) The acceleration time series is applied to the bedrock or to the outcrop as the input;

b) Fourier Amplitude Spectrum (FAS) of the input motion is computed using Fast Fourier Transform in order to obtain the discrete Fourier transformations;

c) Transfer function $TF_{m,n}(\omega)$ (Eq. 3.20) is computed using the strain-compatible soil properties of each soil layer; the shear modulus (G), and damping ratio (ξ) as a function of strain (γ);

d) Surface FAS is computed as a product of transfer function (c) and the input FAS (b) (Eq. 3.24);

e) The time history of ground surface acceleration is produced using inverse FFT of (d).

The effect of the selected time series on the analysis results is significant (Boore 2004; Rathje et al. 2010; Dhakal et al. 2013; Kottke and Rathje 2013); therefore, the uncertainty brought in by the record selection procedure is quite large. This uncertainty can be modelled by using a large number of ground motion recordings, which increases the computational time and requires a well-defined ground motion selection and scaling scheme that lacks in standard engineering applications. Usually, a stable median of the target input motion levels is obtained with implementing five to ten different input rock time series that fit the chosen target acceleration

response spectrum such as those provided in Eurocode 8 or NEHRP (National Earthquake Hazard Reduction Program, BSSC 2009). However, the motion-to-motion variability for the same earthquake may not be captured due to different characteristics in terms of amplitude, ground motion duration and frequency content (e.g., Rathje et al. 2010). This is the main disadvantage of the TS-approach, particularly in the low seismicity areas where the database of strong motion records is sparse. In the last few years, previously recorded ground motions at rock stations (e.g. from $V_{S30} > 800$ m/s sites) are collected in the growing database of Pacific Earthquake Engineering Research Center (PEER) in the context of Next Generation Attenuation (NGA) project for active tectonic regions such as California. The NGA-W2 database (http://ngawest2.berkeley.edu/) includes a large set of ground motions recorded in worldwide shallow crustal earthquakes in active tectonic regimes.
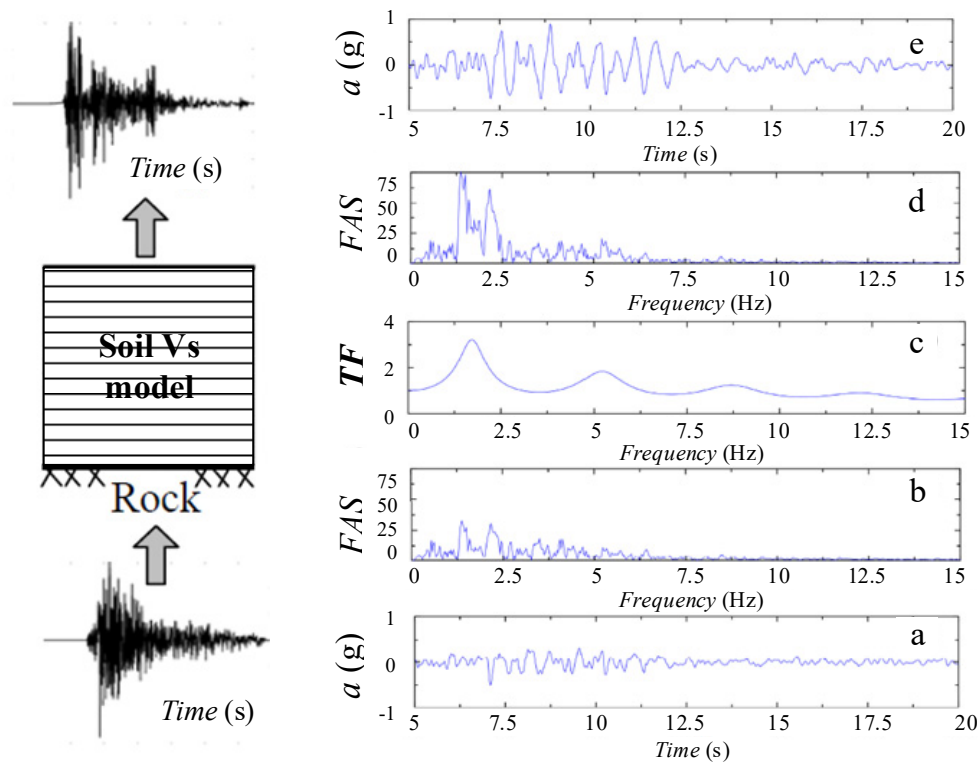
Figure 3.7. 1-D EQL-TS approach. a) Input rock acceleration time series (outcrop motion), b) Fourier Amplitude Spectrum *FAS* of input motion, c) transfer function $TF_{m,n}(\omega)$ from input to surface, d) surface *FAS*, e) surface acceleration time series (after Kramer 1996 and Kottke and Rathje 2009).

To present an example for the above-mentioned effects in motion-to-motion differences and effect on the site response analysis results, a suite of previously recorded rock motions ($V_{S30} > 800$ m/s) were selected from the NGA-W2 database (available at https://ngawest2.berkeley.edu/). 82 individual records were downloaded from the database and

scaled to target input motion represented by peak ground acceleration $PGA_{ROCK} = 0.05$ g (Figure 3.8). Note that each record has different record characteristics such as duration and number of cycles as shown in Figure 3.8a (only few examples are shown). After these records are employed in the EQL site response analysis based on the TS-approach, the rock response spectrum (Sa_{ROCK}) and surface response spectrum (Sa_{SURF}) from each individual analysis are presented by the black lines in Figure 3.8b. The site effects can be represented in terms of the site amplification factor $AF(T)$, calculated as the ratio of the surface and rock (bedrock) response spectra as a function of the spectral period. In Figure 3.8, right panel, the $AF(T = 0.0\ s)$ ($@PGA$) is presented with the horizontal red line, while at the predominant spectral period $T_{pp}(s)$ (soil natural period or frequency), peak of the $AF(T_{pp})$ is shown with the crossings of blue lines. Note that response spectra are usually presented with spectral period (inversely proportional to frequency) on the x-axis.

Figure 3.8 shows that the record selection has a significant effect on the calculated AFs for all period ranges; the standard deviations of the medians ($\pm 1\ \sigma$ in log units) shown with red dashed lines are quite large. For seismically active shallow crustal regions (e.g., California or Turkey), this uncertainty can be modelled using a large database of previously recorded rock motions, favoring the use of straightforward EQL site response analysis based on TS-approach. On the other hand, the ground motion datasets for moderate seismicity areas (e.g., Croatia) is relatively sparse and performing a well-designed ground motion selecting procedure is hard to achieve. Data from global strong motion datasets (e.g., PEER Ground Motion Database – NGA-W2 database available at https://ngawest2.berkeley.edu/), European strong-motion records – ESD available at http://www.isesd.hi.is/ESD_Local/frameset.htm, Engineering Strong-Motion database – ESM developed in the framework of the Network of European Research Infrastructures for Earthquake Risk Assessment and Mitigation – NERA available at http://esm.mi.ingv.it/, Observatories and Research Facilities for European Seismology – ORFEUS avaialble at http:/www.orfeus-eu.org/data/eida) can be used to fill this gap if same/similar tectonic settings can be assumed with similar source and propagation path effects. Alternatively, the Random Vibration Theory based EQL site response analysis can be preferred for these regions.
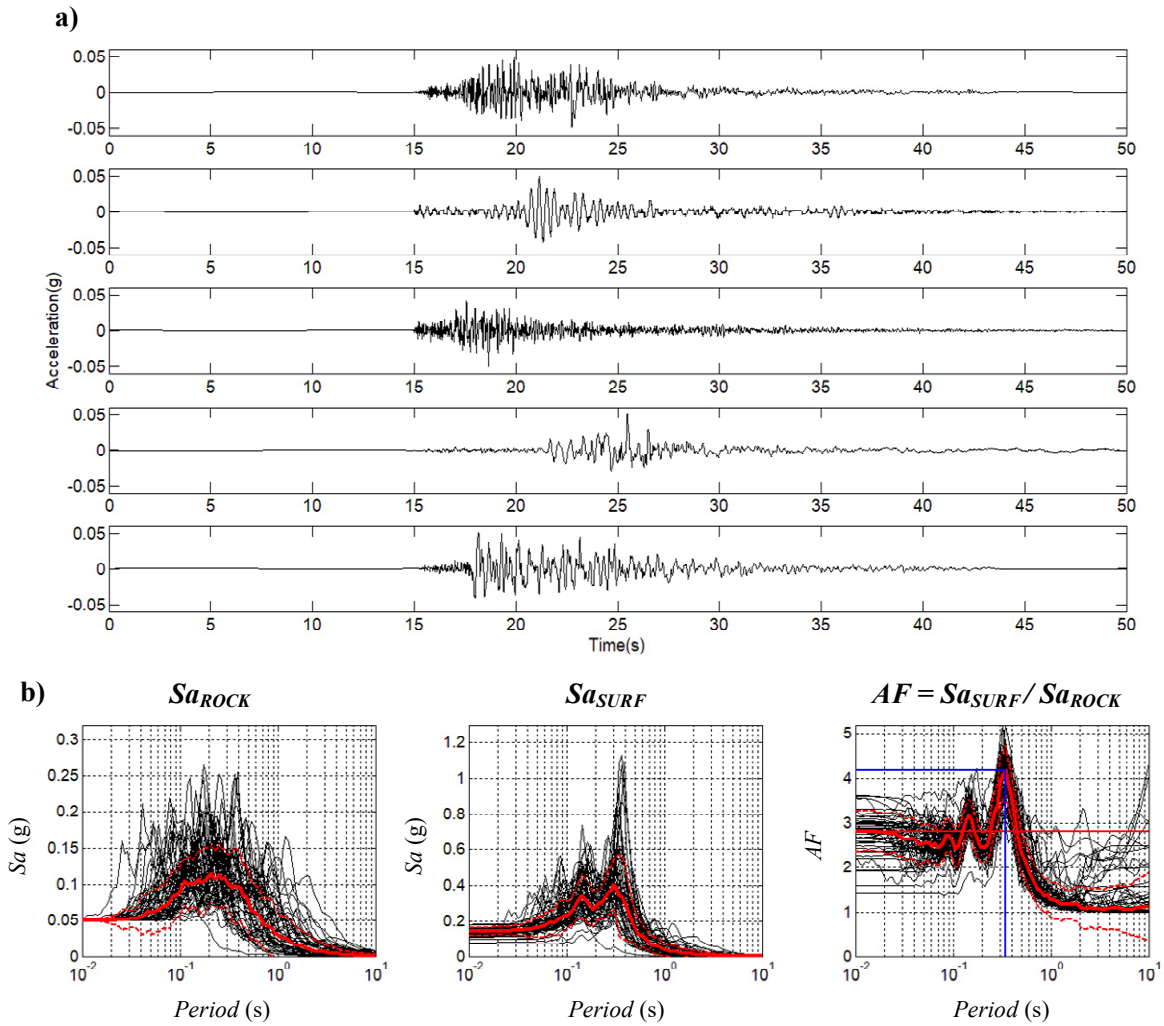
Figure 3.8. a) Example of few recorded rock $(V_{S30} > 800 \text{ m/s})$ acceleration time series from NGA-W2 database (http://ngawest2.berkeley.edu/) scaled to target rock peak ground acceleration $PGA_{ROCK} = 0.05$ g. b) Bedrock (left) and surface (middle) response spectrum for each individual recording marked with black lines. Amplification factor $AF(T)$ is calculated as the ratio of the surface response spectrum to the rock (bedrock) response spectrum (at 5% of critical damping): $AF(T) = Sa_{SURF}/Sa_{ROCK}$. Solid red lines represent the median Sa_{ROCK}, median Sa_{SURF}, and median $AF(T)$. Dashed red lines represent standard deviations of the medians ($\pm$ 1 σ in log units) in each panel. Horizontal red lines mark the $AF(@PGA)$ at the top of the soil model (surface) and crossings of blue lines indicate $AF(T_{pp})$ at the predominant spectral period (predominant peak).

3.3. Random Vibration Theory (RVT) based EQL site response analysis

3.3.1. Theoretical background of RVT methodology

The pioneering work of Hanks and McGuire (1981) represents the first use of the Random Vibration Theory (RVT) in engineering seismology to predict PGA as a function of FAS of ground motion. Please note that the FAS is defined using the seismological parameters described in Chapter 2 based on Brune (1970) single-corner frequency ω^2 source spectrum. Basic assumption of Hanks and McGuire (1981) is that the high-frequency strong ground motion can be approximated with a finite duration within the S-wave arrival window $\left(0 \leq t - R/\beta_0 \leq T_{gm}\right)$ stationary band-limited $(f_C \leq f \leq f_{max})$ white Gaussian noise over duration interval (Vanmarcke 1975; Vanmarcke and Lai 1980). Here, R is the hypocentral distance, β_0 is shear wave velocity in the crust, T_{gm} represents the duration of high-frequency strong ground motion, and source and path effects on the FAS are defined with corner frequency f_C and high-frequency cut-off frequency f_{max} that represents property of local site conditions (Hanks 1982). Hanks and McGuire (1981) developed a simple theoretical model of ground motion to estimate peak acceleration (a_{max}) from root-mean-square acceleration (a_{rms}) for earthquakes with local magnitude $4.0 \leq M_L \leq 6.5$ with constant value of stress drop $\Delta\sigma = 100$ bar:

$$a_{max} = \left[0.85 \frac{(2\pi)^2}{106} \frac{\Delta\sigma}{\rho R^{3/2}} \sqrt{\frac{Q\beta_0}{\pi f_C}}\right] \sqrt{2ln\left(\frac{2Q\beta_0}{\pi f_C R}\right)} = a_{rms} \sqrt{2ln\left(\frac{2f_{max}}{f_C}\right)} \qquad (3.25a)$$

$$\frac{a_{max}}{a_{rms}} = \sqrt{2ln\left(\frac{2f_{max}}{f_C}\right)} \qquad (3.25b)$$

Boore (1983, 2003) extended the work of Hanks and McGuire (1981) to stochastic simulation method to simulate site-specific and earthquake-specific ground motions. The key feature of the RVT analysis is the prediction of peak value of the ground motion from the FAS and its duration through Parseval's theorem and extreme value statistics (EVS) (e.g., Vanmarcke and Lai 1980; Hanks and McGuire 1981; Boore 1983, 2003). Parseval's theorem states that energy

is conserved both in time and frequency, and any time-varying signal, i.e., acceleration time series $a(t)$ can be related with its FAS as (e.g., Silva and Lee 1987; Rathje and Ozbey 2006):

$$a_{rms} = \sqrt{\frac{1}{T_{rms}} \int_0^{T_{rms}} |a(t)|^2 dt} = \sqrt{\frac{2}{T_{rms}} \int_0^\infty |FAS|^2 df} = \sqrt{\frac{m_0}{T_{gm}}} \qquad (3.26)$$

Power spectral density function or spectral moments of the motion (m_k) indicates how the ground motion "power" (energy per time) is distributed with frequency (e.g., Vanmarcke and Lai 1980; Boore 1983, 2003; Rathje and Ozbey 2006). In Eq. (3.26), m_0 represents zero-moment of the power spectral density of the FAS defined for *k-th* moment ($k = 0, 2, 4$):

$$m_k = 2 \int_0^\infty (2\pi f)^k |FAS|^2 df \qquad (3.27)$$

For peak accelerations, T_{rms} in Eq. (3.26) is set to be equal to the ground motion duration T_{gm} as the sum of source duration (inverse of corner frequency) which depends on the fault dimensions and magnitude, and path dependent duration (Atkinson and Boore 1995; Boore 1983, 2003):

$$T_{gm} = \frac{1}{f_c} + 0.05R \qquad (3.28)$$

where, the coefficient 0.05 is taken from empirical distance-dependent model (Atkinson and Boore 1995).

a_{max} is related to a_{rms} through a certain factor defined using extreme values statistics. Cartwright and Longuet-Higgins (1956) developed the expression for the most probable value of peak factor (PF) by studying the statistics of ocean wave amplitudes and considered the probability distribution of the signal maximum in terms of number of extrema (N_e) and the bandwidth (B_w) of time series (Boore 2003):

$$PF = \frac{a_{max}}{a_{rms}} = \sqrt{2} \int_0^\infty \{1 - [1 - B_w exp(-Z^2)]^{N_e} dZ\} \qquad (3.29)$$

Bandwidth (B_w) of motion time series is expressed as the ratio of number of zero crossings (N_z) and number of extrema (N_e) and can be expressed in terms of spectral moments (m_0, m_2, m_4) of the motion:

$$B_w = \frac{N_z}{N_e} = \sqrt{\frac{m_2^2}{m_0 m_4}} \qquad (3.30)$$

For narrowband signals, N_z is equal to N_e and B_w is equal to 1.0. Earthquake motions represent signals which are spread over a range of frequencies, N_z is smaller than N_e and B_w is smaller than 1.0 (broadband signal). The number of zero crossings N_z and extrema N_e are related to the frequencies of zero crossings (f_z) and extrema (f_e) and to ground motion duration (T_{gm}) in the form:

$$N_z = 2f_z T_{gm} \Rightarrow f_z = \frac{1}{2\pi}\left(\frac{m_2}{m_0}\right)^{1/2} \qquad (3.31a)$$

$$N_e = 2f_e T_{gm} \Rightarrow f_e = \frac{1}{2\pi}\left(\frac{m_4}{m_2}\right)^{1/2} \qquad (3.31b)$$

For a large number of N_e, Boore (1983, 2003) simplified Cartwright and Longuet-Higgins (1956) peak factor PF expression to its asymptotic form:

$$PF = \frac{a_{max}}{a_{rms}} = [2ln(B_w N_e)]^{1/2} + \frac{0.5772}{[2ln(B_w N_e)]^{1/2}} \qquad (3.32)$$

The expression of PF in Eq. (3.32) is different than the original formulation of Hanks and McGuire (1981), (Eq. 3.25b, proposed by Vanmarcke and Lai 1980) for the first term of the equation. Difference between these two expressions lies in the definition of root-mean-square duration T_{rms}; Hanks and McGuire (1981) expressed T_{rms} as the ground motion duration as a function of the source $T_{rms} \sim 1/f_C$, while Boore (1983, 2003) expressed T_{rms} as the ground motion duration by including source and path duration (Eq. 3.28). As it is stated in Boore (1983), difference is about 10 % between these two PF expressions (Eq. 3.25b and Eq. 3.32) which affects predicted ground motion peak values.

In order to employ the RVT approach to estimate the response spectrum, the response of a linear single-degree-of-freedom (SDOF) oscillator is included before the RMS acceleration a_{rms} (Eq. 3.26) is calculated (e.g., Silva and Lee 1987). The spectrum $|FAS|^2$ in Eq. (3.26) is multiplied

by the square of the transfer function $\left|H_{f_n}(f)\right|^2$ (given in Eq. 3.34) for a SDOF oscillator with different natural frequencies f_n for a given damping. The resulting spectrum is used to calculate spectral acceleration Sa_{rms} and peak factor PF in Eqs. (3.26), (3.29) and (3.32) that yields to:

$$(Sa_{rms})^2 = \frac{2}{T_{rms}} \int_0^\infty |FAS|^2 \cdot \left|H_{f_n}(f)\right|^2 df \qquad (3.33)$$

Transfer function $\left|H_{f_n}(f)\right|$ of a SDOF oscillator with natural frequency f_n and damping ξ_{osc} is defined as:

$$\left|H_{f_n}(f)\right| = \frac{f_n^2}{\sqrt{(f_n^2 - f^2)^2 + (2\xi_{osc}ff_n)^2}} \qquad (3.34)$$

The peak acceleration value a_{max} from Eqs. (3.29) and (3.32) is then the response spectral ordinate; i.e., spectral acceleration Sa for a particular oscillator damping ξ_{osc} (usually 5 % of the critical damping) and resonant frequency f_n:

$$(Sa)^2 = PF^2 \cdot (Sa_{rms})^2 \qquad (3.35)$$

In order to employ RVT-based approach into EQL site response analysis to estimate the response of the soil upon the input FAS of the ground motion, the response of the characteristics of the SDOF oscillator transfer functions must be included as a correction of duration models T_{rms} for the root-mean-square acceleration (a_{rms}) or calculation (Eqs. 3.26 and 3.33) (Boore 2003; Rathje and Ozbey 2006; Kottke and Rathje 2013). Small earthquakes have short ground motion durations, and the approximation $T_{rms} = T_{gm}$ as a function of source and path (Eq. 3.28) covers the response of the resonant soil system. Root-mean-square duration T_{rms} must be increased for larger earthquakes to capture the response of oscillator. Boore and Joyner (1984) proposed a modification on T_{rms} to cover the peak response of small and large earthquakes:

$$T_{rms} = T_{gm} + T_n \frac{\eta^c}{\eta^c + \alpha} \qquad (3.36)$$

where $T_n = 1/f_n$ is the SDOF oscillator natural period, $\eta = T_{gm}/T_n$ and parameters $c = 3$ and $\alpha = 1/3$ are adjustable determined from comparison between RVT and time simulations (e.g., Boore and Joyner 1984; Liu and Pezeshk 1999). The T_{rms} correction approaches to T_{gm} for shorter durations and to $T_{gm} + T_n$ for longer durations of ground motion.

Recently, Wang and Rathje (2016) and Chi-Miranda and Montejo (2017) proposed that the difference between TS and RVT-based approaches is related to the peak factor *PF* used in RVT-based method based on the analysis of a limited number of soil profiles. An adjustment for the duration is suggested by Wang and Rathje (2016) to minimize the difference. Available T_{rms} models have been developed empirically (e.g., Boore and Thompson 2012, 2015) using Cartwright and Longuet-Higgins (1956) and Vanmarcke (1975) peak factor expressions (Eqs. 3.29 and 3.32). These corrections are employed into the available software that performs RVT-based EQL site response analysis (e.g., RASCAL, STRATA).

3.3.2. RVT-based EQL site response analysis approach

The first software, "RASCAL", for synthesizing the ground motions based on the RVT method described above was introduced by Silva and Lee (1987). Kottke and Rathje (2009) incorporated the RVT-based EQL site response analysis approach into the new and publicly available software, STRATA. The EQL RVT-based approach does not require strong motion records for input as in the classical TS-approach. In the RVT-based method, the only required input is the *FAS* that represents the input bedrock motion based on certain earthquake scenario scaled to match chosen target response spectrum (e.g., EC8 or NEHRP) (Rathje and Ozbey 2006). Figure 3.9 shows schematic difference between TS and RVT-based site response analysis.
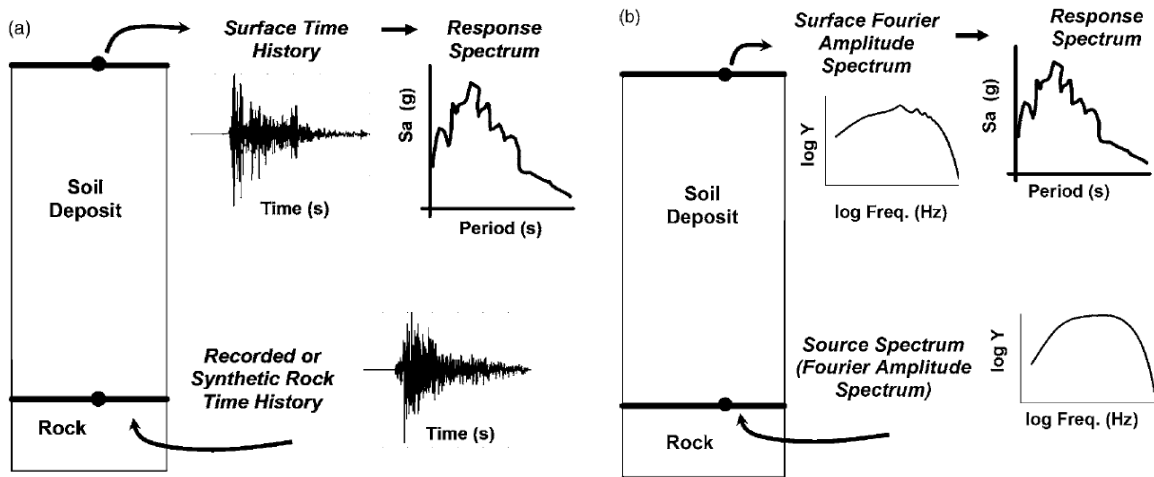
Figure 3.9. Schematic difference between a) TS-approach and b) RVT-based site response analysis. From Rathje and Ozbey (2006).

The computational steps in RVT-based EQL analysis are presented in Figure 3.10 and briefly include the following stages:

a) FAS at the base rock is utilized as the input at the bedrock level;

b) The transfer function $TF_{m,n}(\omega)$ given in Eq. (3.20) is computed using the strain-compatible soil properties of each soil layer; shear modulus (G), and damping ratio (ξ) as a function of strain (γ);

c) The FAS at the surface is computed as a product of the transfer function $TF_{m,n}(\omega)$ and input FAS.
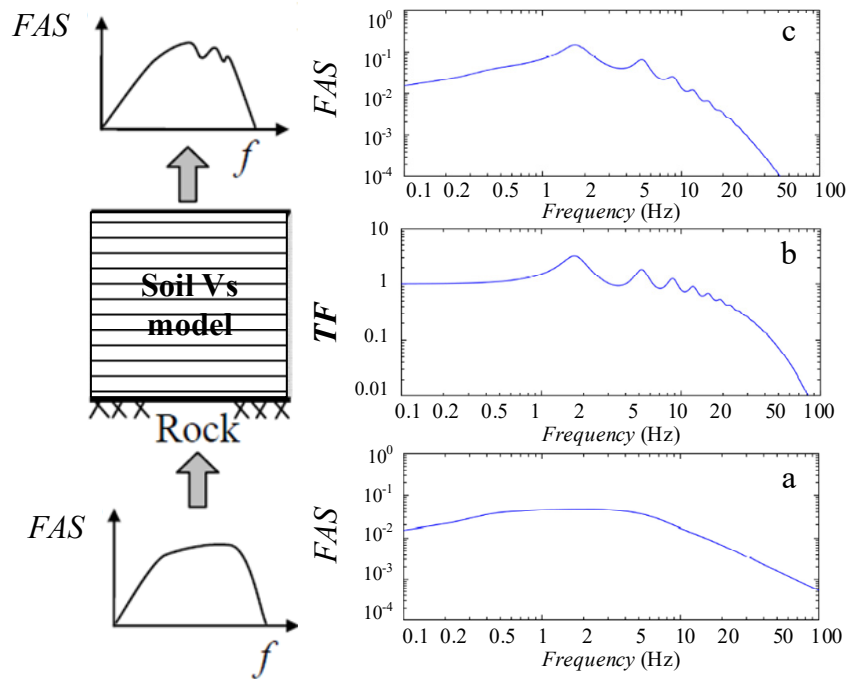
Figure 3.10. RVT-based EQL approach. a) Input FAS defined by seismological parameters (outcrop motion), b) transfer function $TF_{m,n}(\omega)$ from input to surface, c) surface FAS (after Kottke and Rathje 2009).

The essence of the RVT-based method is the use of extreme values statistics to generate filtered, stochastic, finite duration, stationary random time series where the amplitude spectrum equals the average theoretical acceleration spectrum of the certain earthquake scenario (Boore 1983). Earthquake ground motions violate assumptions on stationarity, Gaussian nature and random phase. Therefore, major difference between the input motions in the TS-approach and the RVT-based method is the phase information. In the TS-approach, phase information is known (as the empirical earthquake recordings are utilized) and the transfer function $TF_{m,n}(\omega)$ propagates both the amplitude and the phase information to the surface. In the RVT-based EQL approach, only the amplitude of the ground motion is known because $|FAS|^2$ is used as the input motion

(Eqs. 3.26 and 3.33) and the transfer function $TF_{m,n}(\omega)$ propagates only the amplitude to the surface.

Recently developed software STRATA (Figure 3.11a) can predict a statistically stable estimate of the surface response spectrum (in terms of spectral acceleration) based on the earthquake scenario defined by the FAS at the bedrock using RVT-approach. Input response spectrum (Sa_{ROCK}) is generated from the input spectrum $|FAS|^2$, by multiplication with the square of the transfer function $\left|H_{f_n}(f)\right|^2$ of a SDOF oscillator with natural frequency f_n and for a given damping following the RVT procedure (Eqs. 3.26–3.35). Following the same procedure, surface response spectrum (Sa_{SURF}) is generated from the surface spectrum FAS. The AFs that are calculated by a single RVT-based analysis found to be similar to the median AFs estimated by using a large suite of input rock motions in the TS-approach (Rathje and Ozbey 2006; Kottke and Rathje 2009, 2013; Kottke 2010; Rathje et al. 2010). Generally, differences between the estimated AFs of two approaches are lower than 10 % over the whole range of spectral periods. Difference is most prominent at the predominant period of the soil: the AF calculated by the RVT-based method is approx. 5–25 % higher than the AF calculated by TS-approach (Kottke and Rathje 2013). The same soil profile and input ground motion levels used for the analysis given in Figure 3.8b are employed as the example case for the AF estimated using the RVT-based EQL analysis. Results of the TS-approach and the RVT-based method are compared in Figure 3.11b. Figure 3.11b shows that the AFs calculated using the RVT-based method lie within $\pm 1\,\sigma$ range of the AFs from the TS-approach.

One of the main concerns for the use of RVT-based method is that the point source approximation is not valid for large earthquakes where the assumed single corner frequency scaling is not appropriate to describe the FAS (Boore 1983). An extensive literature that compares the RVT predictions with recorded ground motion time series is available (e.g., Boore 1983, 2003; McGuire et al. 1984; Silva and Lee 1987; Silva et al. 1997; Rathje and Ozbey 2006; Kottke and Rathe 2013). For the magnitude range of $M_W = 5.0-7.7$, convincing evidence is provided that the RVT method can provide reasonable and similar response to those of earthquake ground motion time series. An equivalent point-source model based on the effective distance concept is incorporated into RVT through hypocentral distance $R = \sqrt{(R_e^2 + h^2)}$ in the geometrical attenuation spreading function $Z(R)$ to predict the average ground motions from M_W 6+ earthquakes over wide distance range (Yenier and Atkinson 2014).
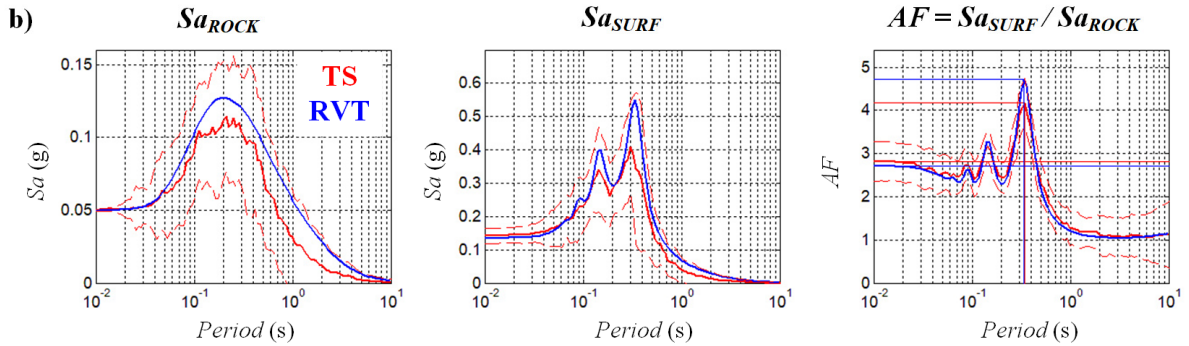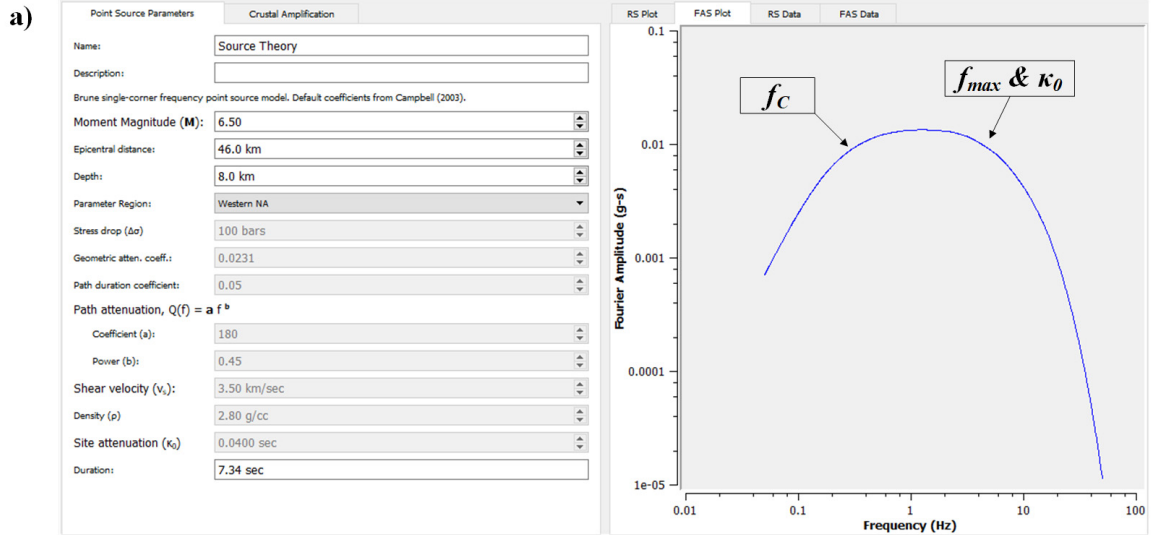
Figure 3.11. a) Example of the earthquake scenario used to define the input FAS in STRATA. Seismological parameters defined for Western North America (WNA). On the FAS marked corner frequency (f_C) and cut-off frequency (f_{max}) are related to the near-site attenuation parameter κ_0. b) Example of the RVT-based EQL site response analysis approach compared to TS-approach for the input rock peak ground acceleration $PGA_{ROCK} = 0.05$ g. Bedrock (left) and surface (middle) response spectrum marked with thick black lines. Amplification $AF(T)$ is calculated as the ratio of the surface response spectrum to the rock (bedrock) response spectrum (at 5% of critical damping): $AF(T) = Sa_{SURF}/Sa_{ROCK}$. Solid red lines represent the median TS-approach and blue lines single RVT-based EQL approach: Sa_{ROCK}, median Sa_{SURF}, and median $AF(T)$. Dashed red lines represent standard deviations of the medians (± 1 σ in log units) in each panel. Horizontal lines mark the $AF(@PGA)$ at the top of the soil model (surface) and crossings of lines indicate $AF(T_{pp})$ at the predominant spectral period T_{pp}.

A critical issue in the RVT-based EQL site response analysis is the definition of the input FAS using proper seismological parameters as described in Chapter 2. The choice of the seismological parameters, particularly the parameters which describe high-frequency part of the FAS ($Q(f)$ and κ_0), plays an important role in the calculated surface spectrum (Rathje and Ozbey 2006). Using the regional seismological source and high frequency parameters over the best fit source parameters for Western North America (WNA) in RVT-based site response

analysis approach, Rathje and Ozbey (2006) found that the estimated surface response spectra are generally smaller for the case of regional parameters (within ± 15 % compared to the response using best fit source parameters for WNA). If the regional seismological parameters can be used to define the regional *FAS*, the computed soil response parameters are comparable with the TS-approach (e.g., Rathje and Ozbey 2006; Kottke and Rathje 2013). Therefore, the TS-approach which introduces the uncertainty from time series selection can be replaced with powerful and computationally effective RVT-based method for the evaluation of the site amplification factors using EQL site response analysis (Rathje and Ozbey 2006; Kottke and Rathje 2009, 2013; Kottke 2010; Rathje et al. 2010).

3.4. Nonlinear site amplification models utilized in the Ground Motion Prediction Equations (GMPEs)

Pre-defined site amplification models have been utilized in the recently proposed ground motion models (GMPEs) for shallow crustal and active tectonic regions (e.g. global NGA-West 1 and West 2 GMPEs, RESORCE models). These pre-defined site factors include both linear and non-linear site amplification components. Typically, the non-linear site response effects are directly adopted from the 1-D EQL site response analysis of soil profiles representing the target region (e.g., Walling et al. 2008; Kamai et al. 2014 for California) or developed based on empirical ground motion datasets (e.g., Choi and Stewart 2005; Sandikkaya et al. 2013), whereas linear site amplification parameter is estimated with the other parameters of the GMPE.

3.4.1. Short overview of GMPEs in regional, European, and global context

Attenuation relations or ground motion prediction equations (GMPEs), provide statistical predictions of the level of ground shaking and its associated uncertainty at any given site or location, based on earthquake magnitude, source-to-site distance, local soil conditions, fault mechanism, etc., (e.g., Atkinson and Boore 2006; Akkar and Bommer 2010; Bommer and Akkar 2012; Akkar et al. 2014). GMPEs are an important input for: a) site-specific seismic analysis and design of structures and facilities; b) development of regional seismic hazard maps for use in building codes, financial estimation, and, c) social and financial loss estimation

(http://peer.berkeley.edu/globalgmpe/). A large number of global and regional GMPEs were developed in the last 20 years that are applicable to shallow crustal and active tectonic regions. Constructing the GMPE logic tree for seismic hazard assessment is a controversial issue since: (i) locally used GMPEs are developed from the regional datasets so they are expected to reflect the regional tectonic characteristics better than the others, (ii) the uncertainties introduced by local GMPEs are higher than those of the global GMPEs because they are based on statistically less stable and limited datasets (Gülerce et al. 2016). Douglas (2017) summarized worldwide empirical GMPEs to estimate earthquake peak ground acceleration and elastic response spectral ordinates published between 1964–2017 (http://www.gmpe.org.uk./), showing that the GMPE modelling in Europe has been behind the western United States (US) for many years. In Europe, first GMPEs were derived about 20 years after the first predictive models were derived in US (Akkar et al. 2014).

First set of ground motion models (attenuation relations) in terms of peak horizontal and vertical acceleration relations for Croatia (Dinarides area) were published by Herak et al. (2001) using the functional form (Eq. 3.37) proposed by Ambraseys et al. (1995):

$$log\ a_{max} = c_1 + c_2 M_L + c_3 log \sqrt{c_4^2 + R_e^2} \qquad (3.37)$$

The peak horizontal and vertical acceleration attenuation relations for Croatia published by Herak et al. (2001) are:

$$log\ a_{max}^{hor} = -1.300 + 0.331 M_L - 1.152 log \sqrt{11.8^2 + R_e^2} + 0.311P \qquad (3.38a)$$

$$log\ a_{max}^{ver} = -1.518 + 0.302 M_L - 1.061 log \sqrt{11.0^2 + R_e^2} + 0.313P \qquad (3.38b)$$

In Eqs. (3.37 and 3.38), $a_{max}^{hor,\ ver}$ is the larger horizontal or vertical PGA_{ROCK} (for rock or stiff soil) in g, M_L is local magnitude and R_e is epicentral distance in km. Standard errors of the coefficients are: a) a_{max}^{hor}: $c_1 = -1.300 \pm 0.192$, $c_2 = 0.331 \pm 0.040$, $c_3 = -1.152 \pm 0.099$, $c_4 = 11.8 \pm 4.8$ km; b) a_{max}^{ver}: $c_1 = -1.518 \pm 0.293$, $c_2 = 0.302 \pm 0.035$, $c_3 = -1.061 \pm 0.096$, $c_4 = 11.0 \pm 5.5$ km and standard error of the fit are $0.311P$ and $0.313P$ for horizontal and vertical components where P is equal to zero for mean values, and one for 84-percentile of $log\ a_{max}$.

Markušić et al. (2002) updated the horizontal acceleration attenuation relation coefficients proposed by Herak et al. (2001) by including "standard" independent site condition terms based on peak horizontal/vertical acceleration ratio. The same form of horizontal acceleration attenuation relation (Eqs. 3.37, 3.38a) was used and the updated coefficients were:

$$log\ a_{max}^{hor} = -1.461 + 0.326M_L - 1.086 log\sqrt{10.2^2 + R_e^2} + 0.308P \qquad (3.39)$$

Standard errors of the coefficients are: a) a_{max}^{hor}: $c_1 = -1.461 \pm 0.188$, $c_2 = 0.326 \pm 0.035$, $c_3 = -1.086 \pm 0.092$, $c_4 = 10.2 \pm 4.5$ km standard error of the fit are $0.308P$ for horizontal component where P is equal to zero for mean values, and one for 84-percentile of $log\ a_{max}$.

Most recent empirical GMPEs models for point source and extended source crustal earthquake scenarios in Europe (mostly based on the data from Italy, Greece and Turkey) were developed by Akkar et al. (2014) which included the nonlinear site amplification model developed by Sandikkaya et al. (2013). Functional form of Akkar et al. (2014) ground motion predictive model is given as:

$$\ln(Y) = ln[Y_{REF}(M_W, R, SoF)] + ln[AF(V_{S30}, PGA_{REF})] + \varepsilon \qquad (3.40)$$

The first term in Eq. (3.40) describes the reference ground motion model in terms of magnitude, distance, and style-of-faulting scaling (see Eq. 3.41 below); whereas the second term represent the nonlinear site amplification model that includes the linear and nonlinear soil response expressed by V_{S30} and PGA_{REF} (or PGA_{ROCK}). The functional form of the reference ground motion model $Y_{REF}(M_W, R, SoF)$ in Eq. 3.41 proposed by Akkar et al. (2014) is similar to the attenuation relations for Dinarides (3.38 and 3.39) by Herak et al (2001) and Markušić et al. (2002), however it includes additional terms such as the quadratic magnitude term, the distance dependent magnitude scaling term, and style-of-faulting terms. Additionally, moment magnitude M_W is employed instead of local magnitude M_L and the adopted source-to-site distance measures are different.

$$\ln(Y_{REF}) = a_1 + a_2(M_W - 6.75) + a_3(8.5 - M_W)^2 + [a_4 + a_5(M_W - 6.75)]ln\sqrt{R^2 + a_6^2} +$$
$$+ a_8F_N + a_9F_R; M_W \leq 6.75 \qquad (3.41a)$$
$$\ln(Y_{REF}) = a_1 + a_7(M_W - 6.75) + a_3(8.5 - M_W)^2 + [a_4 + a_5(M_W - 6.75)]ln\sqrt{R^2 + a_6^2} +$$
$$+a_8F_N + a_9F_R; M_W \geq 6.75 \qquad (3.41b)$$

In Eq. (3.41), R is source-to-site distance which can be the R_{JB} representing the Joyner-Boore distance, R_e (epicentral distance) and R_h (hypocentral distance). The style-of-faulting SoF variables F_N and F_R are unity for normal and reverse faults, and zero otherwise (strike-slips). Period independent coefficient for all distance metrics are: $a_2 = 0.0029, a_5 = 0.2529, a_6 = 7.5, a_7 = -0.5096$. Coefficients a_1, a_3, a_4, a_8, a_9 are period dependent coefficients which depends on the style-of-faulting, and at PGA (at 0.0 s) are: a) R_{JB}: $a_1 = 1.85329, a_3 = -0.02807, a_4 = -1.23452, a_8 = -1.1091, a_9 = 0.0937$; b) R_h: $a_1 = 2.52977, a_3 = -0.05496, a_4 = -1.31001, a_8 = -1.1091, a_9 = 0.0937$; c) R_e: $a_1 = 3.26685, a_3 = -0.04846, a_4 = -1.47905, a_8 = -1.1091, a_9 = 0.0937$. Full list of period dependent coefficients a_1, a_3, a_4, a_8, a_9 is provided in Akkar et al. (2014).

The Next Generation Attenuation (NGA) West1 and West2 projects (Power et al. 2008, Bozorgnia at al. 2014) developed GMPEs for shallow crustal earthquakes in active tectonic regions. Even though the target area was Western US (WUS), the GMPEs were intended to be applicable in other shallow crustal and active tectonic regions around the world. Slowly, NGA GMPEs have been used in probabilistic seismic hazard assessment (PSHA) studies in various regions, raising the issue of their applicability outside WUS. During the recent Harmonization of Seismic Hazard Maps in the Western Balkan Countries Project (BSHAP), a comprehensive methodology for choosing and testing the applicability of recently published global GMPEs for the PSHA studies in the Western Balkan area was proposed (Šalić et al. 2016). Using the residual analysis methods, evaluation of the trellis plots showing the scaling and functional form of candidate GMPEs, and recently published quantitative model-data comparison methods, four GMPEs (2 global NGA-West 2 models and 2 recently published European models) were selected based on the behavioural analysis of the BSHAP strong motion dataset. The GMPEs proposed by Akkar et al. (2014), Boore et al. (2014), Bindi et al. (2014), and Chiou and Youngs (2014) were found to be suitable for the Western Balkan Region with different weights assigned in the logic tree.

3.4.2. Development of the recent nonlinear site amplification models

The nonlinear site amplification model (second term in Eq. 3.40) developed by Sandikkaya et al. (2013) is the first site amplification model based on the regression analysis of the empirical datasets using a reference rock model explicitly for Pan-European ground motion database. The AF model has the following functional form:

$$\ln(AF) = a(T)ln\left(\frac{V_{S30}}{V_{REF}}\right) + b(T)ln\left[\frac{PGA_{REF} + c\left(\frac{V_{S30}}{V_{REF}}\right)^n}{(PGA_{REF} + c)\left(\frac{V_{S30}}{V_{REF}}\right)^n}\right] \; ; \; V_{S30} < V_{REF} \tag{3.42a}$$

$$\ln(AF) = a(T)ln\left(\frac{\min(V_{S30}, V_{CON})}{V_{REF}}\right) \; ; \; V_{S30} \geq V_{REF} \tag{3.42b}$$

In Eq. (3.42), PGA_{REF} is reference rock peak ground acceleration from Eq. (3.41), V_{S30} is the average shear-wave velocity in top 30 m, a general parameter representing the local site conditions, V_{REF} is reference shear wave velocity of the bedrock (750 or 1100 m/s, depending on the definition), $V_{CON} = 1100$ m/s that stands for the limiting V_{S30} after which the site amplification is constant, and coefficients $c = 2.5$ and $n = 3.2$ are period independent. The coefficient c relates the transition between higher and lower ground motion amplitudes and coefficient n captures the soil non-linearity at lower V_{S30} values. Period dependent coefficients $a(T)$ and $b(T)$ at PGA are $a = -0.41997$ and $b = -0.28846$. The coefficient $a(T)$ represents the linear change of AF with V_{S30} up to V_{REF}, and $b(T)$ controls the non-linear soil behaviour with increasing PGA_{REF}. Full list of period dependent coefficients $a(T)$ and $b(T)$ is provided in Akkar et al. (2014).

Integration of the site effects into GMPEs in terms of pre-defined AF models as given by Sandikkaya et al. (2013) (Eqs. 3.40–3.42) was evolved progressively in the western US over the years. One of the first uses of V_{S30} in the site amplification model was presented by Boore et al. (1997) in the linear form:

$$\ln(AF) = a(T)ln\left(\frac{V_{S30}}{V_{REF}}\right) \tag{3.43}$$

Boore et al. (1997) model (Eq. 3.43) did not include the non-linearity of the soil response controlled by the level of input rock motion (PGA_{ROCK}). Later on, Abrahamson and Silva

(1997) included the nonlinear effects into period dependent site amplification model as function of the input rock motion level (PGA_{ROCK}):

$$\ln(AF) = a(T) + b(T)ln(PGA_{ROCK} + c) \tag{3.44}$$

Because this model classified sites as generic soil and rock with dummy variables, the AF model did not include the local site parameter V_{S30}. A couple years later, Choi and Stewart (2005) combined models given by Eq. (3.43) and Eq. (3.44) to obtain site amplification model that considers both linear and nonlinear site effects as shown below:

$$\ln(AF) = a(T)ln\left(\frac{V_{S30}}{V_{REF}}\right) + b(T, V_{S30})ln\left(\frac{PGA_{ROCK}}{0.1}\right) \tag{3.45}$$

In the site amplification models given in Eqs. (3.42–3.44), coefficients $a(T)$ and $b(T)$ are period dependent and determined by the regression analysis. Coefficient $b(T, V_{S30})$ in Choi and Stewart (2005) model (Eq. 3.45) is a function of period and V_{S30} but varies for each soil category (e.g., NEHRP, EC8), and quantifies the evidence of non-linearity in soft sediments by the reduction of amplification factors with increasing reference rock motion PGA_{ROCK} (Figure 3.12). V_{REF} is the reference shear wave velocity of the rock, taken as 760 m/s. Two of the NGA-West 1 GMPEs, GMPEs proposed by Boore and Atkinson (2008) and Chiou and Youngs (2008), integrated the modified form of Choi and Stewart (2005) AF model. The AF model was not directly implemented in these GMPEs because: i) the linear term represented by $a(T)$ of Choi and Stewart (2005) model was re-estimated by the empirical ground motion dataset and ii) V_{REF} was set to 1130 m/s. Differences in the modified forms are presented in Figure 3.12.
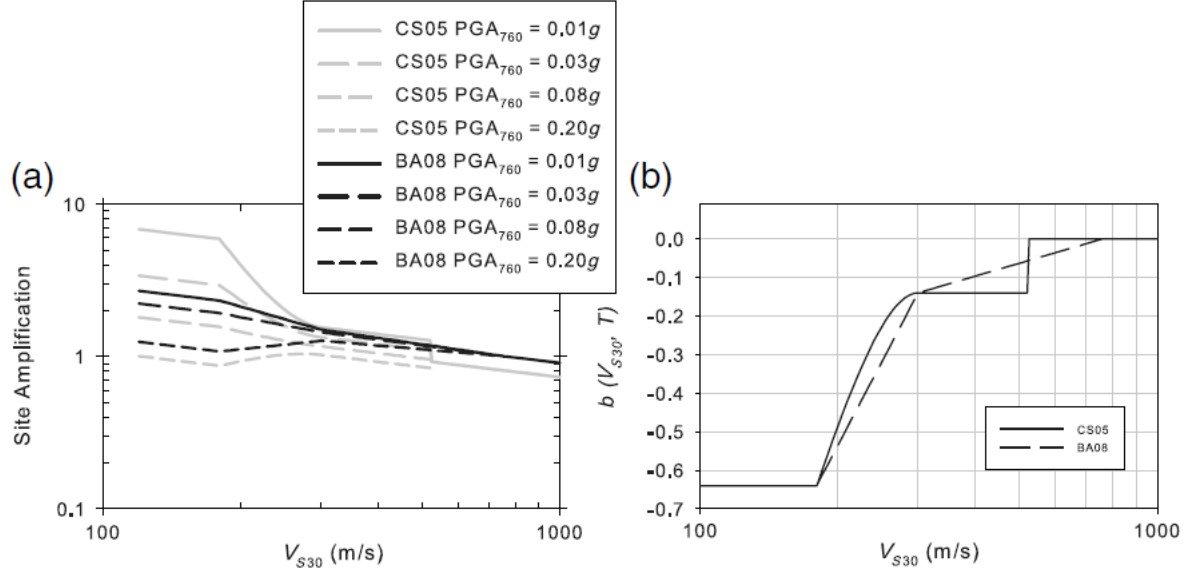
Figure 3.12. a) Comparison of site AF from Choi and Stewart (2005) and Boore and Atkinson (2008) for the reference rock $V_{REF} = 760$ m/s and different input PGA_{ROCK}. b) Variation of coefficient $b(T)$ with V_{S30} from Choi and Stewart (2005) model (Eq.3.42). Both figures represent AF at PGA (at 0.0 s). (taken from Sandikkaya et al. 2013).

A more complex site response model was proposed by Walling et al. (2008) using stochastic simulations and RVT-based EQL site-response analysis approach for randomized soil profiles and given by the following functional form:

$$\ln(AF) = a(T)ln\left(\frac{V_{S30}}{V_{LIN}(T)}\right) - b(T)ln(PGA_{ROCK} + c)$$

$$+ b(T)ln\left[PGA_{ROCK} + c\left(\frac{V_{S30}}{V_{LIN}(T)}\right)^n\right]; \quad V_{S30} < V_{LIN}(T) \tag{3.46a}$$

$$\ln(AF) = [a(T) + b(T)]ln\left(\frac{V_{S30}}{V_{LIN}(T)}\right) + d; \quad V_{S30} \geq V_{LIN}(T) \tag{3.46b}$$

where $V_{LIN}(T)$ represents the cut-off V_{S30} value for the end of non-linear site amplification zone at each period, parameter d implicitly relates the linear transition between $V_{LIN}(T)$ and the reference-rock shear wave velocity $V_{REF} = 1100$ m/s and coefficients n and c are period independent. Main differences between the Choi and Stewart (2005) and Walling et al. (2008) models are the treatment of coefficients $b(T)$ to be independent of V_{S30} and change in the functional form of the PGA_{ROCK} term. Two of the NGA-West 1 GMPEs, GMPEs proposed by Abrahamson and Silva (2008) and Campbell and Bozorgnia (2008), integrated the modified

53

form of Walling et al. (2008) model (Figure 3.12). Again, the linear site amplification terms were re-estimated using the empirical ground motion dataset by the GMPE developers.

All AF models (Eqs. 3.42–3.46) aim to mimic the non-linear soil behaviour by a simple site parameter, V_{S30}, and a parameter that represents the level of ground shaking at the bedrock, PGA_{ROCK}. Choi and Stewart (2005) and Boore and Atkinson (2008) showed that the coefficient $b(T)$ is negative and generally increase towards zero as soil gets stiffer (higher V_{S30}) since the non-linearity becomes less significant (Figure 3.12). Also, AF decreases significantly (de-amplification) with increasing intensity of input PGA_{ROCK} for softer sites (smaller V_{S30}) and non-linearity becomes significant, particularly for the large PGA_{ROCK} (Figures 3.13 and 3.14) (e.g., Walling et al. 2008; Abrahamson and Silva 2008; Campbell and Bozorgnia 2008; Sandikkaya et al. 2013). Nonlinear soil effects are more prominent for softer sites at lower spectral periods (at 0.0–0.2 s) than at longer periods (at 1.0 s) as shown in Figure 3.14. Findings of Sandikkaya et al. (2013) study compared to Abrahamson and Silva (2008) and Boore and Atkinson (2008) studies, emphasize the importance of period dependency in site amplification factors for different PGA_{ROCK} levels; however, these effects are poorly constrained with period-dependent site amplification factors given in Eurocode 8 (EC8) for Type 1 ($M_S > 5.5$) and Type 2 ($M_S \leq 5.5$) earthquake scenarios (Figure 3.15). Here it needs to be mentioned that the site amplification curves for soil categories B, C and D from Eurocode 8 are actually not period-independent as suggested in Figure 3.15 and in Sandikkaya et al. (2013). This issue was corrected in the recent work by Sandikkaya et al. (2018), properly presenting period-dependent site amplification factors and this will be shown in Chapter 6. Site amplification factors tends to normalize to a constant value for stiffer sites ($V_{S30} > 300$ m/s) since the soil behaviour is presumably linear and all models (Eqs. 3.42–3.46) yield to similar amplification factors.
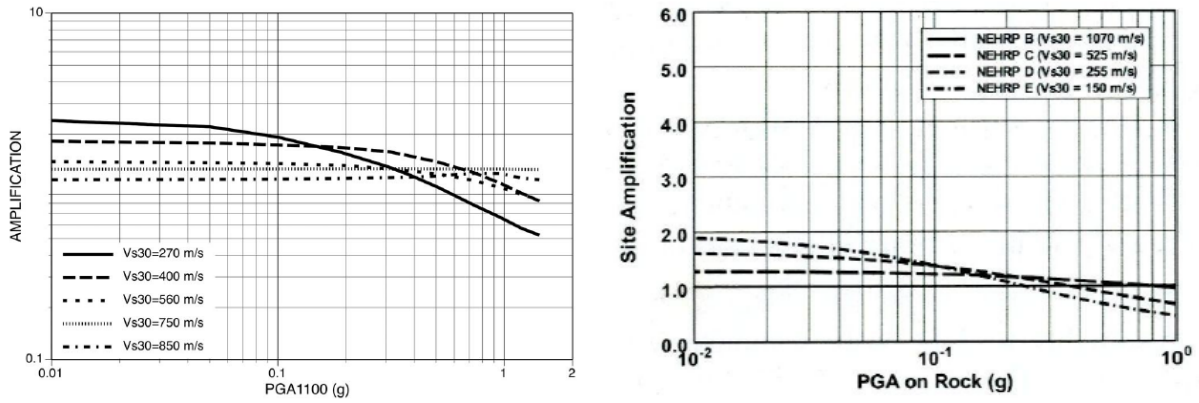
Figure 3.13. Example of the site AF for different site V_{S30} and different input PGA_{ROCK} for spectral period $T = 0.0\ s$. Left: Walling et al. (2008). Right: Campbell and Bozorgnia (2008).
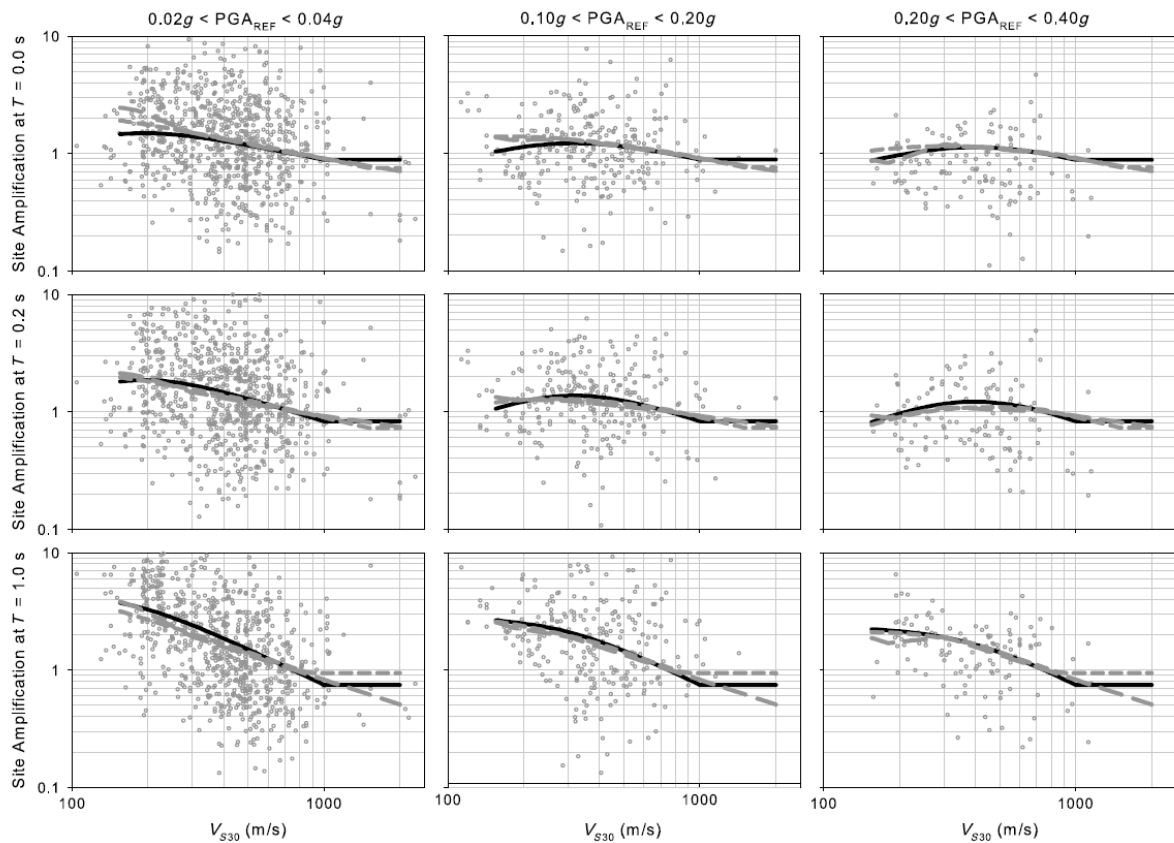
Figure 3.14. Comparison of proposed models from well-constrained empirical dataset by Sandikkaya et al. (2013) (black solid line) with Abrahamson and Silva (2008) (dashed grey line) and Boore and Atkinson (2008) (long dashed grey line) for $T = 0.0\ s, 0.2\ s$ and $1.0\ s$ at different levels of input rock PGA_{ROCK}. From Sandikkaya et al. (2013).
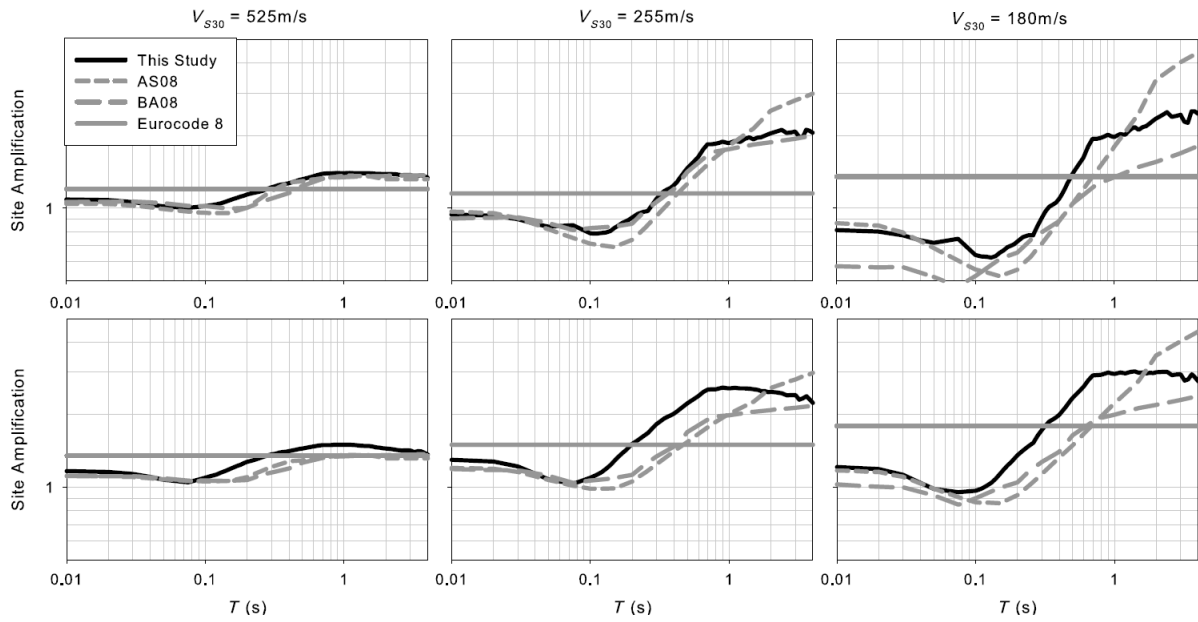
Figure 3.15. Period dependent variation of site amplification factor from proposed model of Sandikkaya et al. (2013) (black solid line) with Abrahamson and Silva (2008) and Boore and Atkinson (2008) compared to Eurocode 8 site classes (B: $360 \leq V_{S30} < 800$ m/s, C: $180 \leq V_{S30} < 360$ m/s and D: $V_{S30} < 180$ m/s). Top row: Type 1 $(M_S > 5.5)$, Bottom row: Type 2 $(M_S \leq 5.5)$.

4. Estimation of the high-frequency attenuation parameter kappa (κ) in Croatia

The Fourier Amplitude Spectrum (FAS) of ground motions is influenced by the effects of the source, propagation path, and local site conditions as modelled by the theoretical ω-square source model as presented in Chapter 2. The importance of high-frequency attenuation parameter κ on the shape of FAS was demonstrated in Figure 2.6 (Chapter 2.3) as a phenomenon attributed to the local site effects.

The main objective of this study is to perform a systematic evaluation of the local site effects influence on the amplification factor (AF) in Croatia, calculated in the RVT-based 1-D EQL site response analysis approach that uses only single FAS to represent the input ground motion instead of traditional and time-consuming TS-approach. Critical issue in the RVT-based EQL site response analysis approach is the definition of the input FAS (e.g., as presented in Chapter 3.3). The choice of the seismological parameters play an important role (e.g., Rathje and Ozbey 2006), particularly parameters describing the high-frequency part of FAS (frequency dependent quality factor $Q(f)$ and near-surface site-specific attenuation κ_0 which will be described in more detail in Chapters 4.1 and 4.3).

In this chapter estimation of the high-frequency attenuation parameter kappa (κ) in Croatia using classical "AH84" approach Anderson and Hough (1984) will be presented. This research presents "for the first time" calculation of the spectral parameter κ and its local site-specific component κ_0 (also called near-site or near-surface attenuation) in Croatia using seismograms from ten seismological stations of the Croatian network. Estimated regional and local variations of spectral parameter κ are compared with seismotectonic and geological characteristics of the study area, findings of the geophysical fieldwork, properties of the compiled dataset, as well as regional and global values from previous κ studies and from recent attenuation studies of coda waves in the region.

Over the last three decades, near-site attenuation parameter κ_0 (described later in Chapter 4.1 and 4.3) has been used in a variety of applications, particularly in the creation and calibration of ground-motion prediction equations (GMPEs) based on stochastic simulations (e.g., Hanks and McGuire 1981; Boore 1983; 2003; Ktenidou et al. 2014), host-to-target adjustments of GMPEs (e.g., Campbell 2003; Biro and Renault 2012; Delavaud et al. 2012) and site-specific ground response analysis for critical facilities.

4.1. Background on the κ estimation method

The spectral decay parameter kappa (κ) was introduced in the 1980's to describe the high-frequency attenuation of shear waves (S-waves) from the seismograms since existing attenuation models were not adequate to explain the deviation of the high-frequency spectrum of S-waves from the ω-square model of Brune (1970). Several attenuation studies attributed decay of coda waves from the tail of seismograms to backscattering on the randomly distributed heterogeneities of the Earth medium and show that quality factor $Q_C(f)$ of coda waves is strongly frequency dependent at greater depths within the earth (e.g., Aki and Chouet 1975). Effective frequency dependent quality factor $Q(f)$ of shear waves within the crust for whole-path attenuation is modelled in the exponential formulation (e.g., Futterman 1962):

$$A(R,f) = A_0 exp\left(-\frac{\pi R f}{Q(f)\beta_0}\right) \qquad (4.1)$$

where A_0 represent acceleration spectrum that contains the effects of source, distance and perhaps other factors, f is the frequency, R is distance, and β_0 is the shear wave velocity of the Earth medium, and the effective frequency dependent quality factor $Q(f)$ represents the inverse sum of intrinsic or anelastic attenuation and scattering attenuation (e.g., Giampiccolo et al. 2004).

One of the early attempts to explain the observed decay in the spectral amplitude at high frequencies of FAS from the theoretical Brune (1970) ω-square model was made by Hanks (1982) through the high-frequency band limitation parameter f_{max} which is predecessor to the κ. The study of Hanks (1982) was one of the first works that observed "crashing spectrum syndrome" from recordings (strong-motion accelerograms) at close distances in the form of

acceleration spectrum of S-waves. The high-frequency band limitation parameter f_{max} indicates cut-off frequency at which spectrum start to decay very rapidly and with observational definition varies from station-to-station. Hanks (1982) concludes that f_{max} observed in acceleration FAS is controlled by local site conditions, particularly by the geological structures below and near the site. Although primary effect of the high-frequency decay of FAS was attributed to the local site conditions, Hanks (1982) did not eliminate source-controlled effect as a mechanism for high-frequency band-limited radiated field of earthquakes. Boore (1983) included high-frequency parameter f_{max} as a low-pass filter in the simulation of synthetic accelerograms by extending stochastic ground motion simulation method of Hanks and McGuire (1981).

One of the first uses of the term "site attenuation parameter" to incorporate effects of attenuation to model high-frequency spectral attenuation was introduced by Cormier (1982) by t^* factor (attenuation time). Parameter t^* is predecessor of near-site attenuation parameter κ to describe the effects of regional and local geological conditions upon the acceleration FAS of S-waves. Empirical spectral decay parameter kappa (κ) was introduced by Anderson and Hough (1984) to present a model for the shape of the high-frequency FAS to describe the difference between the observed acceleration spectrum of shear waves (S-waves) from seismograms and simple Brune's (1970) ω-square source model. Anderson and Hough (1984) extended Eq. (4.1) and hypothesize that to the first order the shape of the acceleration FAS at high frequencies can be described as:

$$A(f, t) = A_0 \exp(-\pi f t^*) = A_0 \exp\left[-\pi f \left(\frac{R}{Q(f)\beta_0} + \kappa_0\right)\right] = A_0 \exp(-\pi \kappa f) \qquad (4.2)$$

If the effective quality factor $Q(f)$ in the near-surface rocks (up to a few hundred meters to few kilometres depth) is assumed to be frequency independent in the high-frequency range, particularly in the shallow upper layers of rock and soil as they significantly attenuate seismic energy more than the lithospheric crust (Anderson and Hough 1984; Edwards et al. 2011; Ktenidou et al. 2013), then the approximation in the Eq. (4.2) is valid for frequencies higher then corner frequency f_C. In this case t^* is also frequency independent and equal to κ for frequencies and distances at which the shallow attenuation dominates (Anderson and Hough 1984). The t^* parameter for seismic phases along the whole ray path is simplified by assuming a layer over the half-space (Cormier 1982; Edwards et al. 2011; Gentili and Franceschina 2011):

$$t^* = \int_{r=0}^{R} \frac{dr}{Q(r)\beta(r)} = \frac{r_{ij}}{Q\beta_0} + \kappa_0^j = \kappa(r) \qquad (4.3)$$

where Q and β_0 are the average reference crustal values of $Q(r)$ and $\beta(r)$, i and j refer to the *i-th* source and *j-th* site, and κ_0^j represents the attenuation of the uppermost crust layer of the recording site (Hanks 1982; Anderson and Hough 1984) . The total path attenuation of S-waves within the crust (t^* in Eqs. 4.2 and 4.3) is separated into two attenuation parameters: frequency-dependent quality factor (anelastic attenuation along the path, $Q(f)$) and the near-surface site-specific attenuation parameter kappa (also termed site diminution parameter κ_0) (Cormier 1982; Edwards et al. 2011). For the κ_0, term near-site attenuation is also used, since it "catches" the effects of attenuation below and near the site (few kilometres around the site).

Anderson and Hough (1984) (later in the text referred as AH84) classical method to estimate spectral parameter κ (Eq. 4.2) was developed by studying shear-wave spectra for horizontal components of strong ground acceleration for earthquakes with range of magnitudes $M_L = 3.5$−6.8 which also excludes possible source contribution to κ. The essence of κ estimation method lies first in Fourier transform of S-wave accelerograms where time window was chosen to include direct S-wave arrivals. In most cases coda was not included, except for cases where transition between S-wave direct arrival and coda was not clearly observed. Acceleration spectrum is flat above corner frequency f_C to the cut-off frequency f_{max} where spectrum start to decay rapidly (Figure 4.1, top figure). Anderson and Hough (1984) estimated κ directly from linear–logarithmic space on the high-frequency part (Δf) of *FAS* of S-waves, above a specific frequency (f_1) where spectrum starts to decay down to noise part of spectrum (f_2) (Figure 4.1, bottom figure). Spectral parameter κ for a given acceleration record at some distance from the source was related to the slope of the high-frequency part Δf of *FAS* as:

$$A(f) = A_0 \exp(-\pi\kappa f)$$
$$\Delta \ln(A) = -\pi\kappa\Delta f$$
$$(y = slope \cdot x)$$
$$slope = \frac{\Delta ln(A)}{\Delta f}$$
$$\kappa = -\frac{slope}{\pi} \qquad (4.4)$$
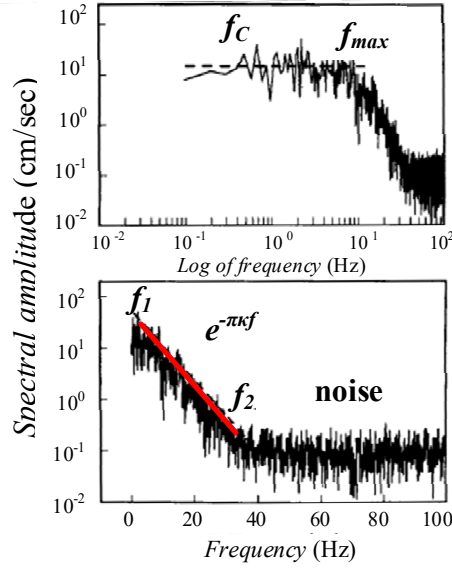
Figure 4.1. Anderson and Hough (1984) classical method to estimate high-frequency spectral parameter κ from the FAS of S-waves for individual acceleration record ($M_L = 6.2$, Mexicalli Valley earthquake of 9 June 1980). f_C marks corner frequency, f_{max} high-frequency cut-off frequency, f_1 the frequency above which spectrum decay starts and is usually lower (or nearly the same as will be shown later) as f_{max}, and f_2 is the start of noise-dominated part of the spectrum. For this example, $f_C \approx 0.2$ Hz, $f_1 \sim 2–5$ Hz, $f_{max} \sim 8–10$ Hz and $f_2 \approx 30$ Hz.

Anderson and Hough (1984) observed a linear dependence between the calculated κ of the ground motion and the epicentral distance (R_e) of the recording station and proposed a mathematical formula that treats κ as a function of R_e:

$$\kappa = \kappa_0 + \kappa_R \cdot R_e \qquad (4.5)$$

In the Eq. (4.5), the zero-distance intercept κ_0 represents the attenuation contribution to κ from geological structure beneath the site (called near-site attenuation or site-kappa), and the distance dependent part in term of the slope (κ_R) is related to the regional attenution due to the horizontal propagation of S-waves through the crust below and near the site within few kilometers (e.g., Anderson and Hough 1984; Edwards et al. 2011; Ktenidou et al. 2013). The example of linear function $\kappa–R_e$ from Anderson and Hough (1984) study is shown in Figure 4.2; κ gradually increases with distance, and degree of the slope κ_R depends on the local and regional geology. Since its introduction, general observation of Anderson and Hough (1984) study that κ is a linear function of R_e has proven to be good approximation as shown in the recent studies that estimated κ (e.g., Douglas et al. 2010; Drouet et al. 2010; Edwards et al. 2011; Gentili and Franceschina 2011; Van Houtte et al. 2011, 2014; Ktenidou et al. 2013, 2014, 2015; Perron et al. 2017).
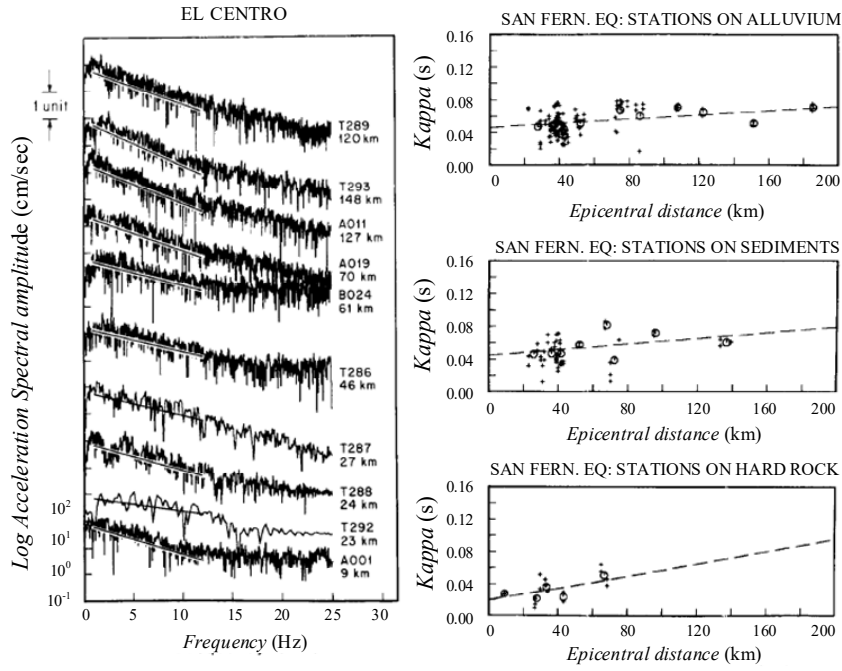
Figure 4.2. Left: Example of estimation of κ from high-frequency part of *FAS* for El Centro station (California) for the same or different earthquakes corresponding to different epicentres. Years and magnitudes are: T289 (1954, 6.3), T293 (1966, 6.3), A011 (1956, 6.8), A019 (1968, 6.4), B024 (1934, 6.5), T286 (1942, 6.5), T287 (1951, 5.6), T288 (1953, 5.5), T292 (1955, 5.4), A001 (1940, 6.7). Linear least-square fit is shown by black curve over frequency band 2–12 Hz. Right: The example of linear function $\kappa - R_e$ for the San Fernando earthquake 9 February 1971 recorded on stations on different soil types. Taken from Anderson and Hough (1984).

In the last decade relationship between estimated κ_0 and measured V_{S30} values are proposed and existing $\kappa_0 - V_{S30}$ correlations are shown in Figure 4.3; κ_0 has lower values for sites on harder rocks (higher V_{S30} values) and higher κ_0 values on softer rocks (sedimentary soils with lower V_{S30} values) (e.g., Anderson and Hough 1984; Ktenidou et al. 2014). The major contribution to the seismic energy dissipation at sites and contribution to the high-frequency part of *FAS* of S-waves (for which near-site attenuation parameter κ_0 describes rapid decay) occurs in a top surface layers up to depths of 1–2 km of the crust (sedimentary soils and rocks) at close rupture distances (less than about 50 km) (e.g., Anderson and Hough 1984; Edwards et al. 2011; Gentili and Franceschina 2011; Ktenidou et al. 2015). Although dominant contribution to the κ has been attributed to the attenuation below and near the site, it may also have potential source contributions. Potential source dependence in Eq. (4.5) can be considered if the information of the focal mechanism (type of faults) or fault-plane solution are available for each earthquake record (e.g., Purvance and Anderson 2003; Ktenidou et al. 2013). Kilb et al. (2012) observe the large scatter of κ with M_L and showed that κ from small

earthquakes ($M_L < 1$) predicts the relative values of κ for larger earthquakes ($M_L > 3.5$) with possible overestimation indicating that the influence of source effects is negligible for larger magnitudes. Perron et al. (2017) evaluated source dependence of κ and M_L for earthquakes approximately in the same epicentral distance and azimuthal direction with observed scatter, but did not ruled out source influence on κ.
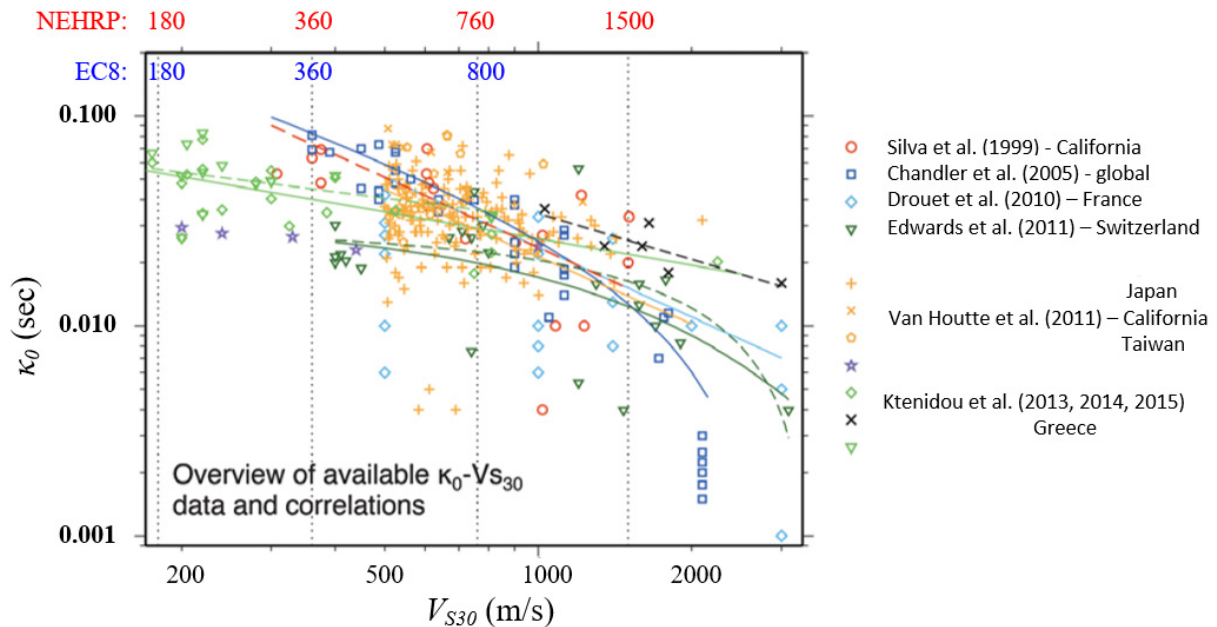
Figure 4.3. Existing $\kappa_0 - V_{S30}$ correlations in the literature (coloured markers and their fit lines for particular regions are shown in legend). Adapted from Ktenidou et al. (2014). Site V_{S30} classes from NEHRP (see BSSC 2009) (red numbers, dashed lines) and Eurocode 8 (blue numbers) are shown above the plot. For full description of Eurocode 8 soil V_{S30} classes see Table 5.2. Note that NEHRP and Eurocode 8 has different site classifications.

4.2. Study area and ground motion database

Even though the spectral parameter κ had been calculated and applied extensively in Western United States (a full collection of previous works is given in Campbell et al. 2014) and Europe (e.g., Castro et al. (2000) for Italy; Drouet et al. (2010) and Douglas et al. (2010) for France; Edwards et al. (2011) for Switzerland; Gentili and Franceschina (2011) in southeastern Alps and northern Dinarides; Ktenidou et al. (2013, 2015) for Greece), no previous attempts to estimate spectral parameter κ in Croatia were made.

4.2.1. Seismotectonic characteristics of the study area

The study area shown in Figure 4.4 covers the central part of convergent boundary zone between the African and Eurasian plates; the Dinarides extending from NW to SE of Croatia between the unaccreted part of the Adriatic microplate (as a part of the African plate) and Pannonian segment (Euroasian plate), and the southwestern corner of the Pannonian Basin in the NW Croatia (e.g., Tomljenović et al. 2008; Schmid et al. 2008; Ustazewski et al. 2008; Handy et al. 2015). The collision between Adria and Eurasia is complex and many different explanation mechanisms have been proposed. The most recent geodynamic schemes suggest that Eurasia subducts under the Adria in the whole Alpine region, together with a less pronounced under-thrusting of the Adria beneath the Eurasia at the northeastern collisional boundary (e.g., Ustazewski et al. 2008; Handy et al. 2015). Along the northeastern coast of the Adriatic Sea this process resulted in the formation of the Dinarides and thickening of the crust. The Dinarides represent active fold-and-thrust belt zone of elevated and deformed deposits striking NW–SE from the Southern Alps in the NW to the Albanides and the Helenides in the SE. Reverse faulting is prevalent for the Dinaridic region. The fold-thrust belt of the Dinarides in its northwestern and central parts is subdivided into two tectonic units; External and Internal Dinarides bounded by the southeastern Alps and Tisia to the north and northeast (e.g., Schmid 2008). The External Dinarides encompass the NW–SE striking faults and southwest-verging thrust belt formed along the eastern part of the Adriatic coast largely composed of Mesozoic to Tertiary shallow-marine carbonate platform deposits (Vlahović et al. 2005; Tomljenović et al. 2008). The Internal Dinarides encompass central and northern part of Bosnia and Herzegovina (narrow belt in the inland) extending toward the Pannonian Basin comprised of the Bosnian flysch zone of Upper Jurassic to Cretaceous mixed carbonate and siliciclastic sedimentary units, and the Central Dinaridic ophiolite zone and the Sava–Vardar suture zone (e.g., Tomljenović et al. 2008; Handy et al. 2015). To the northeast, Dinarides are bounded by the Pannonian basin with a wide transition zone in-between. The formation of the Pannonian basin is most frequently considered to be a 'backarc' basin behind the Carpathian arc bordered by the Southern Alps in the west and the Dinarides in the south (e.g., Šumanovac et al. 2009). The largest depressions in this part of the Pannonian basin are the Sava and Drava river basins. The faulting system is complex, and mostly follows the trend of the rivers Sava and Drava, and mountains chains (Medvednica Mt., Žumberak Mt., Ivanščica Mt. and Kalnik Mt.).
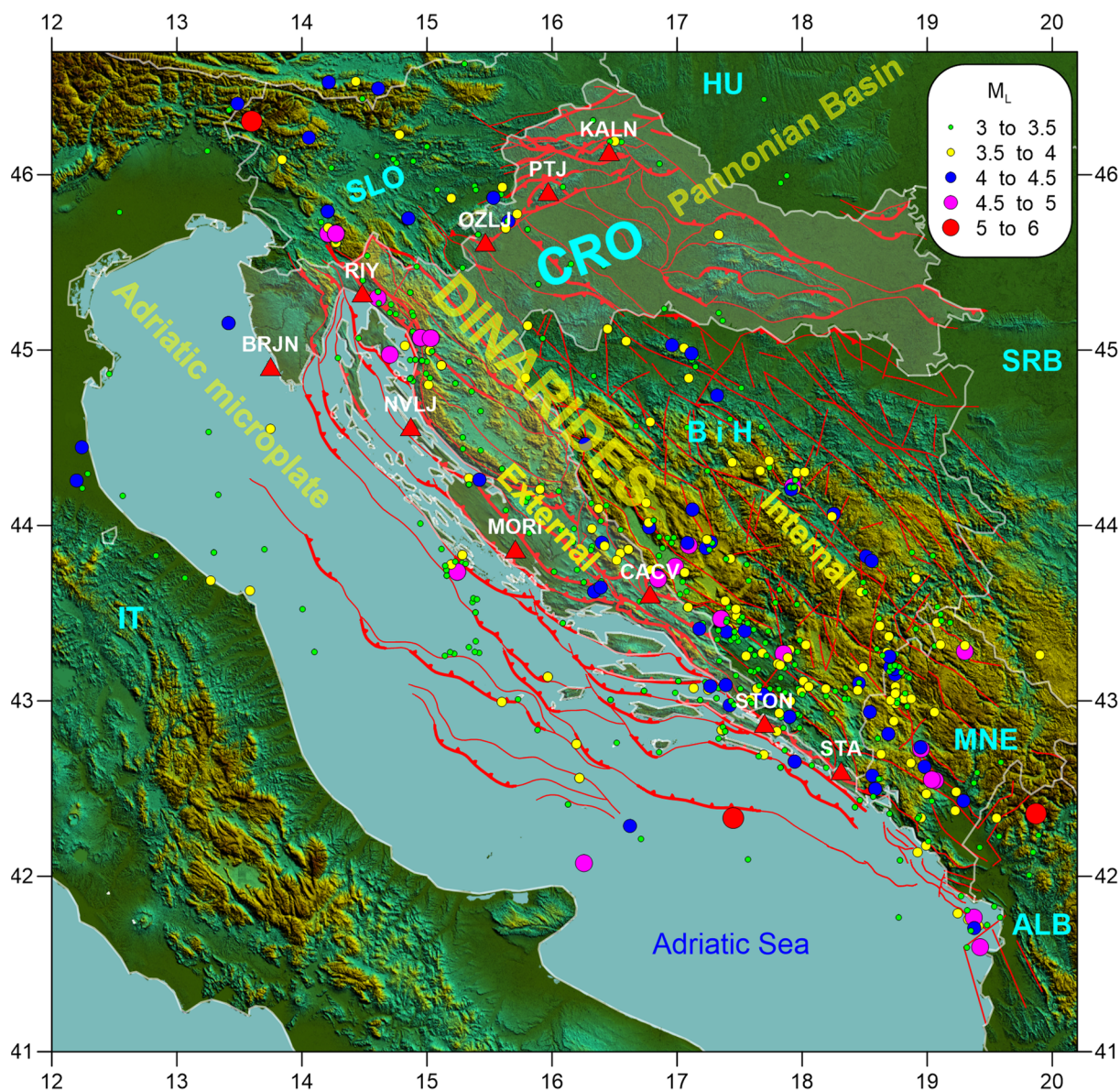
Figure 4.4. Topographic and tectonic map of the study area with earthquake epicentres (2002–2016). Locations of considered seismic stations are marked with red triangles. Thin red lines represent known surface faults and thick red lines active faults in Croatia and Bosnia and Hercegovina (Ivančić et al. 2006).

Highest seismicity in the study area is occurring in the coastal part of Croatia: intense seismicity around Ston and Dubrovnik in the south-east and moderate seismicity around Ilirska Bistrica–Rijeka–Vinodol–Senj fault zone (e.g., Ivančić et al. 2006). In addition to the instrumental era events, the historical earthquake catalogue shows that Dubrovnik area was repeatedly hit by strong earthquakes (Markušić et al. 2017). Continental part of Croatia experienced moderate seismicity – around Zagreb and in north-western part spreading from Žumberak Mt., Medvednica Mt., Ivanščica Mt., through Kalnik Mt. towards Koprivnica (e.g., Ivančić et al. 2006; Herak et al. 2009). Moreover, historical seismicity in this area is apparent

by strong earthquakes in the past: e.g., great Zagreb earthquake in 1880 or strong earthquakes near Varaždin in 1459 and 1738 (Herak et al. 2009), etc.

The Croatian seismological stations included in this study listed from northwest to southeast are: Kalnik (KALN), Puntijarka (PTJ), Ozalj (OZLJ), Rijeka (RIY), Brijuni (BRJN), Novalja (NVLJ), Morići (MORI), Čačvina (CACV), Ston (STON) and Stravča (STA) and are represented by red triangles in Figure 4.4. Seismograms used were recorded at each station between 2002 and 2016 for the earthquakes with $3.0 \leq M_L \leq 5.7$, $R_e \leq 150$ km and focal depths of $h < 30$ km (see Figure 4.4). Record selection in terms of the local magnitude and epicentral distance plays a major role in the calculation of κ (Anderson and Hough 1984; Drouet et al. 2010; Ktenidou et al. 2013). Magnitude limit was applied to the selected recordings ($M_L \geq 3.0$) to exclude possible source contribution to κ.

Figure 4.5 evaluates the compiled dataset in terms of the azimuthal rose diagrams and R_e-M_L distribution of the recordings for each station. The azimuthal distribution of epicentres of the recordings from southeastern stations (MORI, CACV, STON and STA) are densely distributed along the vicinity of faults stretching from northwestern part of Bosnia and Hercegovina to the east and southeastern region around Ston, Dubrovnik, Montenegro, and Albania. Only a minor portion of epicentres are distributed from the Adriatic Sea and recorded at stations MORI and NVLJ. Epicentre distribution of the recordings at stations RIY and NVLJ are from northwestern parts of Slovenia to the southeast of wider Rijeka area along the Velebit Mt. At station BRJN most of earthquakes are recorded from Italy in the southwest and around Rijeka in the northeast. For the northern stations, OZLJ, PTJ and KALN, recordings are distributed from northwestern and southwestern parts of Slovenia and Croatia around mountains in this area and only small portion of KALN recordings are from Hungary.

Most of recordings are from $3.0 \leq M_L \leq 4.0$ earthquakes (max. $M_L = 5.7$) distributed within $30 \leq R_e \leq 150$ km for southeastern stations (STA, STON and CACV), while other stations show limited lower epicentral distances (around 40–60 km) (Figure 4.5). Chosen data limits ($3.0 \leq M_L \leq 5.7$, $R_e \leq 150$ km) play a major role in kappa calculation analysis in terms of number of recorded earthquakes by each station. Number of recordings on each station depends on the seismicity (shown by peak ground accelerations corresponding to return periods of 95, 200 and 475 years, in Table 4.1) and by operative period from the year when stations started to be active until the end of 2016. Stations STA, STON, CACV and NVLJ recorded more than one hundred earthquakes in the seismically most active part of Croatia

(except stations MORI which operates since 2011), RIY and PTJ recorded between 50–70 earthquakes in moderate seismic areas while BRJN (data only from 2009 to the end of 2013), OZLJ (operates since 2010) and KALN (operates since 2011) recorded only around 20–35 earthquakes (Table 4.1).

Table 4.1. A number of analysed earthquakes, peak ground accelerations (PGA) corresponding to return periods of 95, 200, 475 years and V_{S30} and HVSR values for each station (later shown in Figures 4.7 and 4.8, Chapter 4.2.3). *Approximated as a soil category A from the EC8 based on HVSR measured curves (Figure 4.8) and local geological maps (Figure 4.6).

Station	Period	Nr. EQs	PGA 95-years	PGA 200-years	PGA 475-years	V_{S30} (m/s)	HVSR
KALN	2010–2016	24	0.087	0.128	0.191	≈ 760	HV ≈ 3 @ 4 Hz
PTJ	2005–2016	70	0.137	0.202	0.302	*EC8–A	HV ≈ 2 @ 5 and 10 Hz
OZLJ	2011–2016	35	0.103	0.146	0.208	≈ 850	HV ≈ 2 @ 5 and 10 Hz
RIY	2006–2016	60	0.093	0.130	0.184	≈ 1190	No expressed clear HV peaks.
BRJN	2009–2013	33	0.036	0.047	0.064	*EC8–A	
NVLJ	2002–2016	107	0.078	0.105	0.146	≈ 1270	
MORI	2011–2016	51	0.095	0.135	0.198	≈ 1290	
CACV	2007–2016	132	0.161	0.230	0.338	≈ 1050	
STON	2003–2016	222	0.180	0.254	0.367	≈ 1390	
STA	2005–2016	157	0.137	0.199	0.295	≈1280	

Peak ground accelerations (PGA) corresponding to return periods of 95, 200, 475 years in Table 4.1 were estimated (Snježana Markušić, personal communication) by the same procedure which was used for compilation of the seismic hazard map of Republic of Croatia (Herak et al. 2011b; http://seizkarta.gfz.hr), but with updated and expanded earthquake catalogue and thus new seismicity models. This is an algorithm by which seismic hazard is expressed as PGA estimated by stochastic (Monte-Carlo) procedure using the smoothed seismicity approach. In the procedure the probability of the exceedance of particular acceleration is determined by statistical analysis of synthetic earthquake catalogue generated for a very long time period (three million years here) for earthquake magnitudes greater than M_0 ($M_0 = 4.0$ in this study). Maximum theoretical horizontal acceleration is calculated for every generated earthquake in every node of the computation grid with the assumption that the location is situated on bedrock, and using several empirical attenuation relations (AR). Uncertainties related to modelling the dependence of PGA on source distance, earthquake

magnitude, faulting style and other commonly considered parameters are considered by applying five rather recent and for this area relevant ground motion prediction models. In this way epistemic uncertainties are taken into account using a simple logic tree with 10 branches (two seismicity models with different seismicity discretization and smoothing parameters, and five attenuation relations). Following five attenuation relations were used: a) AR1: Akkar et al. (2014) [w = 0.25], b) AR2: Bindi et al. (2014) [w = 0.25], c) AR3: Chiou and Youngs (2008) [w = 0.15], d) AR4: Zhao et al. (2006) [w = 0.15], e) AR5: Herak et al. (2001). These ground motion prediction models were chosen among dozens of available attenuation relations, because each of them is in a way representative for the studied area – either by geographical criteria or by tectonic regime of the earthquakes used in their derivation. AR1 is a new relation developed for the area of Near East and Europe. AR2 uses RESORCE database which is a subset of European data in SHARE database. AR3 is one of the NGA relations based on PEER-NGA dataset of empirical data. AR4 is based mainly on the dataset from Japan. AR5 relation is the only one developed for the greater area of the Dinarides and was therefore used for *PGA* estimate (but not for the estimate of the uniform hazard spectra shape, UHS, because it relates only to *PGA*). *PGA* estimates calculated from AR5 were multiplied by an empirical corrective coefficient F = 0.85 in order to reduce the value to bedrock. Square brackets denote weights in the logic tree for every AR, with a sum of coefficients that equals 1.0. Once the synthetic seismic history of the *PGA* during three million years in every node had been generated as previously described, it was possible to statistically assess accelerations that are exceeded in any node on average once in 95, 200 and 475 years.
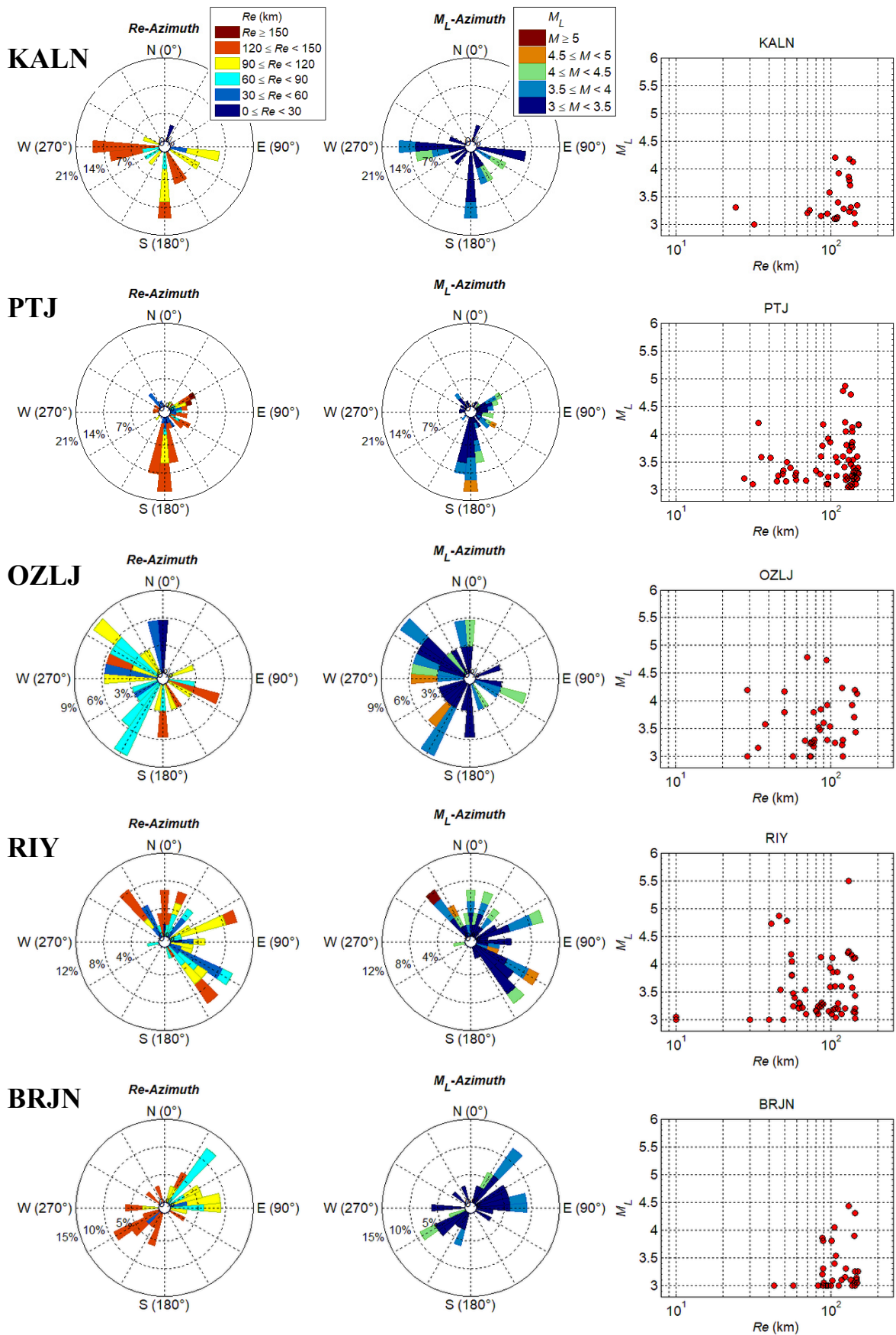
Figure 4.5. Statistics of the compiled ground motion datasets. Left: Azimuthal distribution of R_e. Middle: Azimuthal distribution of M_L. Right: R_e–M_L distribution of recordings for each station.
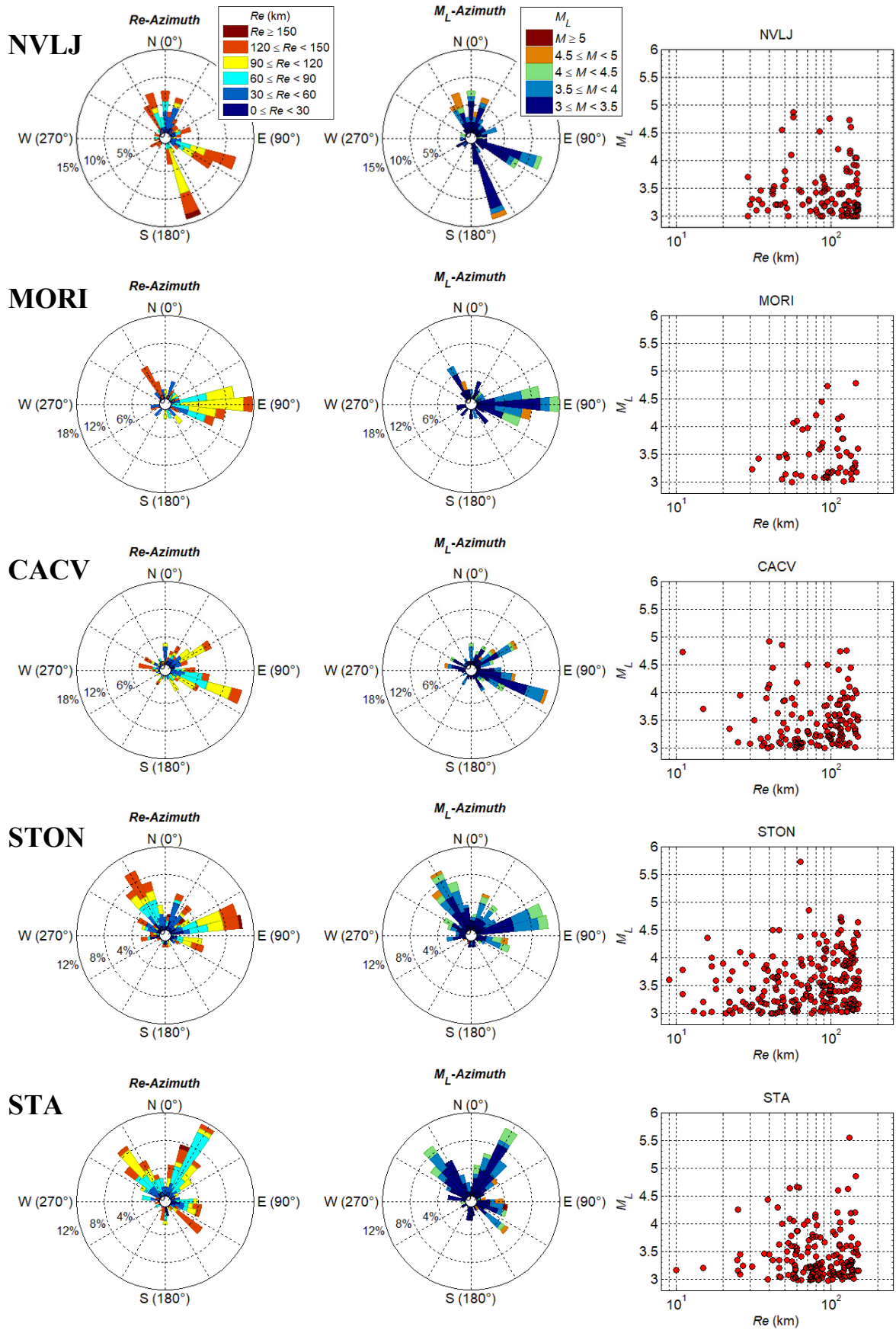
Figure 4.5. ▶continued

4.2.2. Local geological characteristics of seismological stations

Local geological maps of the area in the close vicinity (approx. 30 km) of seismological stations are shown in Figure 4.6 with short geological description in the text below based on the Geological Map of Republic of Croatia at the 1:300.000 scale and accompanying Explanatory notes (HGI-CGS 2009 a, b).

1) Wider area of the seismological station Kalnik (KALN) represents part of the Kalnik Mt. horst, highland region that was formed during tectonic movements during the Middle Miocene. Due to the N–S oriented tectonic stress, Jurassic magmatic rocks (31b) and Palaeogene deposits are thrusted over folded Oligocene and Lower Miocene clastic deposits and volcanic rocks (43). Miocene transgression completely covered whole area and marine deposition continued until Middle Pliocene. Kalnik Mt. presents main core during folding process. Vertical movements during Late Pliocene and Quaternary tectonic activity had significant role in the formation of Kalnik Mt. causing elevations up to several hundreds of meters. In a local geological sense, seismological station KALN is situated near the highest point of the Kalnik Mt. (altitude 642 m) in a hilly area oriented W–E. Main elevation of the Kalnik Mt. and relative descend of the Kalnik slopes was formed during Late Pliocene and Pleistocene period as indicated by thick Pliocene–Quaternary gravel, sand and clay deposits (49) that can be found at the lowest southern parts of the Kalnik. Also, terraces of Pleistocene loess from small streams (54a) near the town of Križevci to the south, and Holocene proluvial–limnic deposits (58b) near Varaždinske Toplice to the northwest alongside rijeka Bednja, can be found.

2) Wider area of the seismological station Puntijarka (PTJ) can be morphologically subdivided into three parts: Medvednica Mt. area, slope area and lowland Zagreb area. Slope area is mostly built-up of Tertiary deposits (47, 48). Lowland area is mainly composed of Holocene alluvial terraces (58b) of the rivers Sava to the south and Krapina to the west from Medvednica Mt. as well as Pleistocene (54a, 54b) and Plio-Quaternary deposits (52) towards Medvednica Mt. slope. Seismological station PTJ (altitude 957 m) is situated in the Medvednica Mt. area close to the highest peak, Sljeme (1035 m). This area is mostly built-up of Palaeozoic–Triassic ortometamorphites (5) and parametamorphites (6). During the Palaeogene, some of the older faults oriented NE–SW became reactived. At the end of the

Pleistocene, tectonic reactivation of Dinaric strike faults (NW–SE) formed Sava depression with thick fluvial sedimentary deposits (gravels and sands).

3) Wider area of the seismological station Ozalj (OZLJ) represents part of the Adriatic Carbonate Platform representing overthrust with SW vergence. It is composed of Upper Jurassic carbonate deposits (25), Lower Cretaceous limestones (32) and transgressive clastic sequence that culminated during Senonian (36). Thrusted complex is intensively folded and faulted. In the eastern part of the area Miocene clastic deposits (47, 48) and Holocene alluvial deposits (58b) of the Kupa river can be found. Seismological station OZLJ (altitude 186 m) is situated on the cliff above the Kupa river terrace composed of Senonian flysch deposits (36) which transgressively cover Upper Jurassic peri-reefal dolomites (25).

4) Wider area of the seismological station Rijeka (RIY) is mainly composed of Lower and Upper Cretaceous deposits (32, 33, 34) with subordinated Eocene foraminiferal limestones (39) and flysch (40). Lower Cretaceous (32) limestones and dolomites represent continuous sedimentation in the shallow-marine platform environments, while transition into Upper Cretaceous sedimentary rocks (33) in this part of the Dinarides is characterized by late-diagenetic dolomites and limestone–dolomite breccias. Seismological station RIY (altitude 70 m) is situated in the city of Rijeka on the Lower Cretaceous limestones and dolomites (32), SW of zone characterized by numerous reverse faults oriented NNW–SSE.

5) Wider area of the seismological station Brijuni (BRJN) situated on western coast of the Istrian Peninsula is represented by Lower Cretaceous deposits (32). Seismological station BRJN (altitude 22 m) is situated on the island of Veliki Brijuni, in the Brijuni National park. Tectonic structure of the area is very simple, since deposits represent SW limb of relatively undisturbed wide Western Istrian anticline with maximum dip angle of 10°.

6) Wider area of the seismological station Novalja (NVLJ) situated on the island of Pag is composed of Upper Cretaceous deposits (34), transgressive Palaeocene–Eocene foraminiferal limestones (39) and Palaeogene–Neogene limestone breccias (42). Seismological station NVLJ (altitude 10 m) is situated in Novalja at the contact of Palaeogene–Neogene limestone breccias (42) and rudist limestones (34). Large amounts of similar limestone breccias (42) composed of different, mostly angular to sub-angular, poorly sorted fragments are covering SW Velebit slopes.

7) Wider area of the seismological station Morići (MORI) situated in the Central Dalmatia represents intensely folded area with numerous NW–SE striking reverse faults. Central and SW part belongs to the Cretaceous–Palaeogene folded and faulted complex. Northeastern part of the area belongs to the Palaeogene synclinorium composed of Eocene–Oligocene Promina deposits (41). Seismological station MORI (altitude 136 m) is situated within the Cretaceous–Palaeogene folded complex in-between Vransko and Prokljansko lakes close to the transgressive contact between Upper Cretaceous rudist limestones (34) and Palaeocene–Eocene foraminiferal limestones (39). Holocene diluvial–proluvial deposits (58a) and Holocene Mediterranean red soil (55) are covering relatively large areas.

8) Wider area of the seismological station Čačvina (CACV) situated in the Central Dalmatia represents complex geological structure composed of Jurassic (21, 22, 23) and Lower Cretaceous (32) carbonate deposits, Upper Cretaceous rudist limestones (34), Palaeocene–Eocene foraminiferal limestones (39) and Miocene deposits (51). Seismological station CACV (altitude 525 m) is situated SE of Sinj in the hilly area. The area is composed of Jurassic deposits (21, 22, 23) thrusted over the Upper Cretaceous deposits (station is located at the boundary between Lower and Middle Jurassic rocks).

9) Wider area of the seismological station Ston (STON) is characterized by contact of Cretaceous and Palaeogene rocks of the Adriatic Zone to the SW and High Karst Nappe striking NW–SE to the NE. High Karst Nappe is composed of Triassic dolomites (20) and Jurassic deposits (21, 22, 23) and is thrusted over Upper Cretaceous rudist limestones (34), Eocene foraminiferal limestones (39) or Eocene clastic rocks (40). Seismological station STON (altitude 3 m) is situated in the Bistrina bay in the Mali Ston channel within zone of the Cenomanian rudist limestones (34).

10) Wider area of the seismological station Stravča (STA) is located in the region of Konavle within the High Karst Nappe thrusted over Eocene flysch deposits of the Adriatic Zone. SW part of the area represents succession of Upper Cretaceous limestones (34), transgressive Eocene foraminiferal limestones (39) and Eocene flysch deposits (40). High Karst Nappe to the NE is composed of Upper Triassic dolomites (20), Lower, Middle and Upper Jurassic deposits (21, 22 and 23) and Lower to Middle Cretaceous deposits (32 and 33). Seismological station STA (altitude 478 m) is situated on the NE slopes of the Sniježnica Mt., on the contact between Upper Jurassic (23) and Lower Cretaceous (32) carbonates (limestones and dolomites) as a part of the High Karst Nappe.
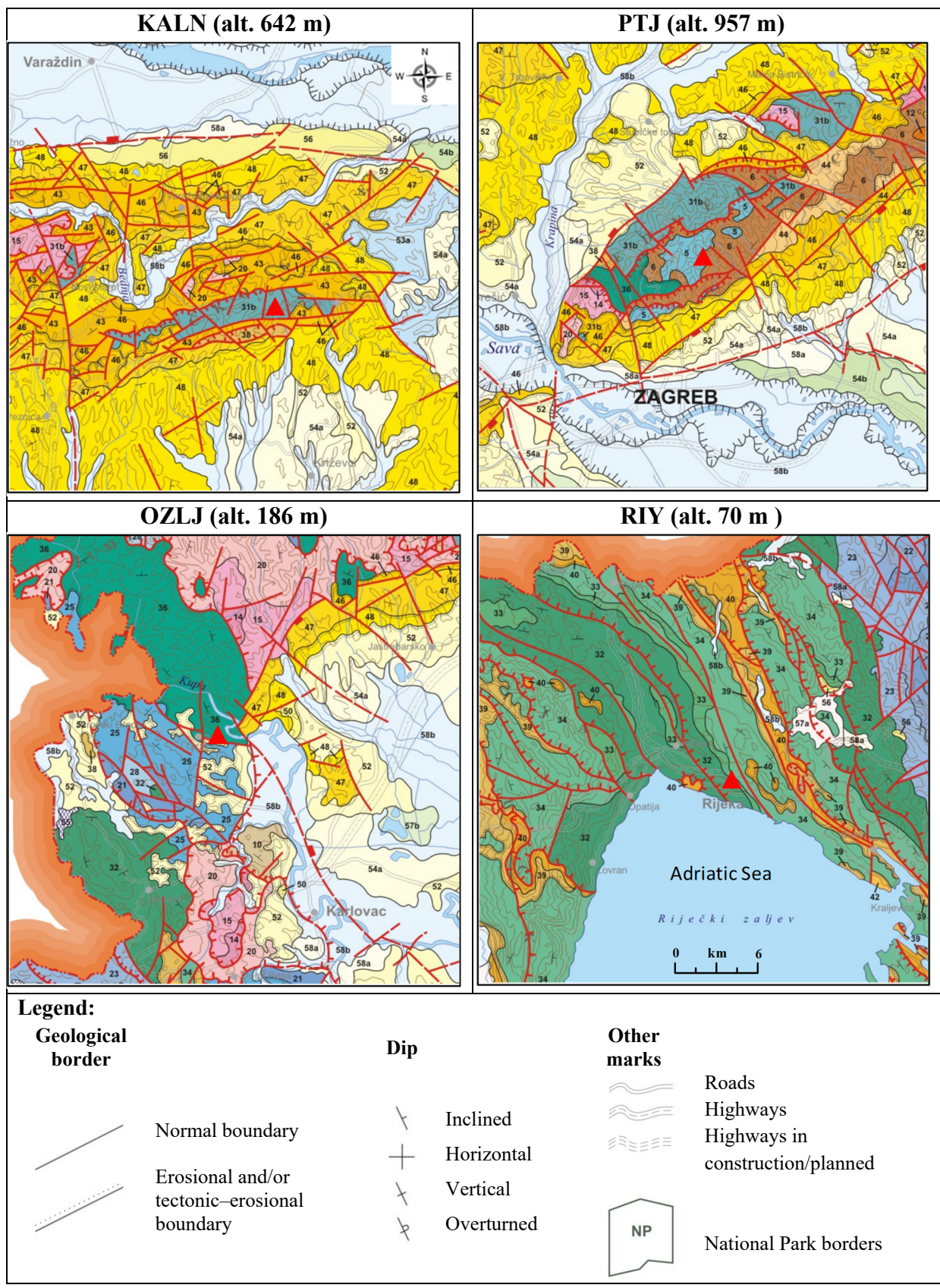
Figure 4.6. Segments of geological maps around seismological stations; locations of stations are marked with red triangles. Modified after Geological Map of the Republic of Croatia in 1:300,000 Scale (HGI-CGS 2009a). Stratigraphic units mentioned in the text are described in Explanatory notes of the Geological Map of the Republic of Croatia (HGI-CGS 2009b).

74

BRJN (alt. 22 m)

NVLJ (alt. 10 m)

MORI (alt. 136 m)

CACV (alt. 525 m)

Legend:

Structural marks

Foliation

Cleavage plane

Fault without sense of movement
a)
b)

Relatively downthrown block
a)
b)

a) defined
b) covered

Reverse fault
a)
b)

Thrust contact
a)
b)

Thrust contact relatively downthrown by normal fault
a)
b)

a) defined
b) covered

Tectonic window

Klippen

Tectonic intrusion–diapiric contact

Slope of river terrace

Figure 4.6. ►continued

75

Figure 4.6.► continued

4.2.3. Geophysical measurements at seismological stations

Local geology is important factor as a dominant contribution to the κ below and close to the site. The average seismic shear-wave velocity from the surface to a depth of 30 m (V_{S30}) and dominant/natural soil frequency (f_{res}) (also called resonant soil frequency) are strongly correlated with the local geology (various thicknesses of sedimentary surface layers above bedrock) (e.g., Seht and Wohlenberg 1999; Leyton et al. 2013; Paolucci et al. 2015).

In the study of Herak et al. (2001) an educated assumption about local soil properties at the locations of accelerometric stations was made based on regional geological settings (e.g., Figure 4.6) that the most of station sites may be classified as "rock" or "stiff soil". To the authors' knowledge, no reliable information regarding measured shear wave velocity V_S profiles and site parameter V_{S30} at seismological (and accelerometric) stations had been documented so far. For this study, site parameter V_{S30} is important for three reasons: a) to correlate with local site-specific attenuation parameter κ_0 of seismological station (in Chapter 4.3), b) to be used in RVT-based site response analysis (in Chapter 5), and c) to be implemented into nonlinear-site amplification models developed for Croatia (in Chapter 6).

Shear wave velocity can be measured in the field using geophysical methods (e.g., Spectral Analysis of Surface Waves—SASW, Multichannel Analysis of Surface Waves—MASW,

Seismic Refraction—RF, Refraction Microtremor—ReMI, Down-hole and Cross-Hole) (e.g., Šumanovac 2012). In this study variation of the seismic refraction method, S-wave Seismic Refraction is used during fieldwork to determine shallow shear-wave velocity (V_S) structures by generating seismic SH waves (particle motion parallel to the surface) to define V_{S30}:

$$V_{S30} = \frac{30}{\sum_{i=1}^{N} \frac{h_i}{V_i}}$$
(4.6)

where h_i and V_i represent the thickness and shear wave velocity of *i-th* formation or layer in total of *N*-layers existing in the top 30 m. Soil is classified by V_{S30} categories according to the Eurocode 8 (EC8) standard (e.g., soil category A represents rock or other rock-like geological formations with $V_{S30} > 800$ m/s).

Results of geophysical measurements at locations of seismological stations are shown in Figure 4.7 with 1-D V_S profile by depth with estimated value of site parameter V_{S30}. Due to terrain features, forestry environment and inability to conduct geophysical measurements at the top of Medvednica Mt. (PTJ station) and problems with permits for geophysical survey at the National Park Brijuni (BRJN station), site parameter V_{S30} at those sites was approximated according to the local geological map (Figure 4.6) as a soil category A according to EC8 with $V_{S30} > 800$ m/s. Generally, all stations can be categorized with $V_{S30} > 800$ m/s (category A by EC8) as rock or rock-like geological formations with less than 5 m of weaker material at the surface $V_S < 400$ m/s. Only station KALN shows $V_{S30} = 760$ m/s (category B by EC8), for which generally rock classified formations with $V_S > 800$ m/s occur at depth of 20 m, while at other stations these formations are at depths of 10 m or closer to the surface. Stations with $V_{S30} \geq 1100$ m/s show hard rock formations usually with $V_S > 1500$ m/s or higher at depths of 20–30 m. **For this study $V_{S30REF} = 1100$ m/s is taken as a reference rock shear wave velocity in the upper 30 m.**
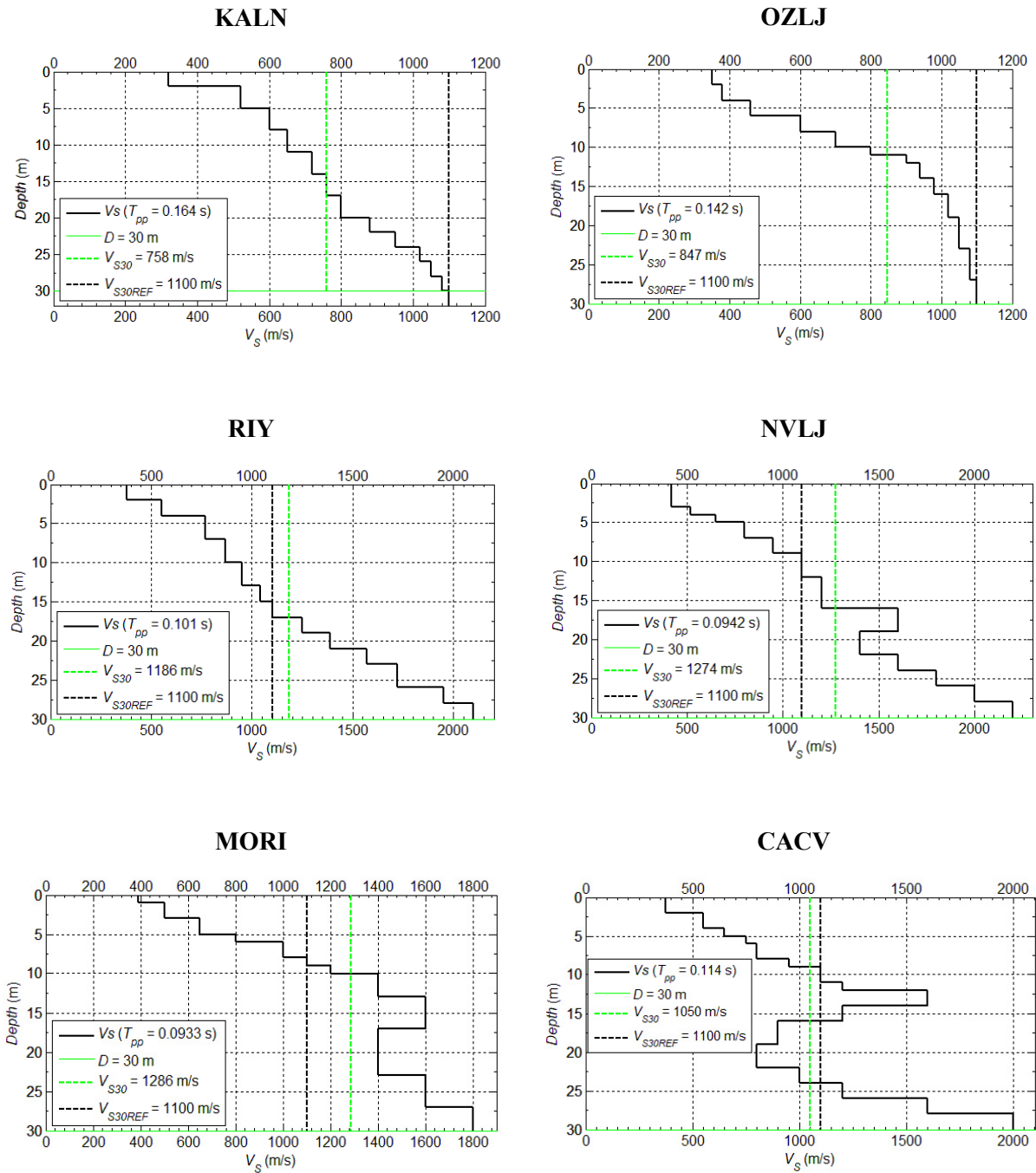
Figure 4.7. 1-D shear wave velocity V_S profiles from S-wave Refraction at seismological stations. On each V_S profile for depths up to 30 m, site V_{S30} value, site predominant period T_{pp} and reference rock $V_{S30REF} = 1100$ m/s are marked. Stations PTJ and BRJN are approximated as a soil category A from the EC8 due to terrain features and inability to conduct geophysical measurements (PTJ) and problems with research permits for geophysical survey at the National Park Brijuni (BRJN).

STON

STA
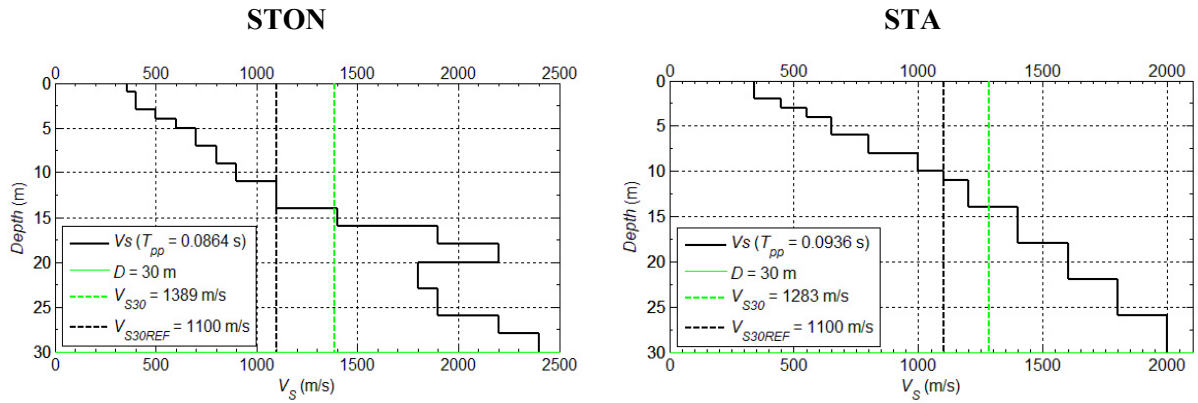
Figure 4.7. ► continued

Measured soil profiles and V_{S30} values are in good agreement with local geological characteristics of each seismological station site, mostly composed of rock formations. To exclude or detect potential site amplification at the locations of seismological stations due to presence of surficial weaker material with low V_S values as observed in Figure 4.7 for some sites, set of ambient noise measurements were performed. In the last two to three decades the microtremor Horizontal-to-Vertical Spectral Ratio (HVSR) methodology proposed by Nakamura (1989) was used in many studies for estimation of local seismic ground response expressed by natural/fundamental soil frequency (f_{res}) and HVSR spectral peak amplification, particularly in the regional area (e.g., Gosar 2007; Gosar and Martinec 2009; Gosar et al. 2010 in Slovenia; Mucciarelli and Gallipoli 2001; Di Giacomo et al. 2005; Del Monaco et al. 2013; Panzera et al. 2013 and others in Italy; Herak et al. 2010; Herak 2011a; Stanko et al. 2016, 2017 in Croatia).

In the extensive HVSR literature, it is widely accepted that higher HVSR spectral peak frequencies correspond to shallower sedimentary structures above the bedrock, and vice versa, that lower HVSR frequencies indicate deeper soft sediments above the bedrock. The basis of this assumption is simple representation of soil with two layers: sedimentary cover and bedrock for which formula $f_{res} = \overline{V}_S/4h$ describes the relation between resonant HVSR soil frequency, average shear wave velocity $\overline{V}_S$ of sedimentary cover and depth h to the bedrock. In case of several HVSR peaks, the peak with the lowest frequency represents the fundamental frequency (sedimentary cover-bedrock limit), while other peaks are influenced by shallower soil layers (e.g., SESAME 2004).

HVSR spectral peak is generally higher than 2 for softer sites with lower values of V_S which indicates site amplification (high impedance contrast between surface deposits and the underlying bedrock). It is accepted that flat HVSR spectral curve with HVSR amplitudes generally less than 2 or closer to unity are an indicator of rock reference site with higher V_S (represented as soil category A in EC8) which does not show site amplification (SESAME 2004). For a better interpretation of measured HVSR spectral curves it is best to combine geophysical measurements and local geology maps to exclude or detect potential site amplification due to the presence of weaker material at the surface.

The Horizontal-to-Vertical Spectral Ratio (HVSR) vs. frequency curves from microtremor measurements (red lines) and their standard deviation (dashed black lines) are given in Figure 4.8. Observed HVSR curves are strongly related to the soil structure of the study area. The average amplitudes of HVSR curves gathered from microtremor measurements do not show expressed clear peaks and are generally below reference amplitude (HVSR < 2) for most of stations. Therefore, these sites can be considered as a good reference rock sites since they do not indicate strong HVSR site amplifications and are in good agreement with geophysical measurements ($V_{S30REF} = 1100$ m/s) and local geology maps.

At stations PTJ (situated on the top of Medvednica Mt.) and OZLJ (situated on the cliff hillside of Kupa river terrace) two peaks with HVSR amplitude slightly higher than 2 are observed: one at approx. 5 Hz which could be due to the topographic effects of the hill geometry from the HVSR polarization effects or the presence of the forestry environment (SESAME 2004) and the second one at approx. 10–12 Hz which represents the presence of few meters surficial marly-clay soil layers overlying bedrock (geophysical profile for OZLJ in Figure 4.6). Similar observation about HVSR topographic effects on a rocky hilltop was observed in the study of seismic response on the site of Trakošćan Castle (Stanko et al. 2016). Presence of softer surficial material up to 10–20 m depth overlying bedrock at station KALN (geophysical profile for KALN in Figure 4.6) can explain slightly higher HVSR amplitude of approx. 3 at 4 Hz, but since station is situated on the tophill of Kalnik Mt., presence of the topographic effects on the HVSR cannot be ruled out.

The use of certain geophysical survey methods which require a long distance profile (at least 70 m) is a challenge for terrains like steep hills, mountains, ridges, slopes, cliffs, etc., due to lack of space, which makes geophysical surveys practically impossible. The application of a quick and non-invasive microtremor HVSR methodology can overcome this limitation with

no environmental impacts. Following the above-mentioned conclusions and good agreement of HVSR curves, geophysical profiles and local geology maps, approximation for the PTJ as a soil category A–EC8 is justified. The same approximation as a soil category A–EC8 for the station BRJN is used based on almost flat HVSR curve without expressed clear peaks that do not present HVSR site amplification (< 2). Note that microtremor HVSR measurement was performed at the National Park Brijuni since this method has no environmental impact and does not require distance profiling as in geophysical methods.
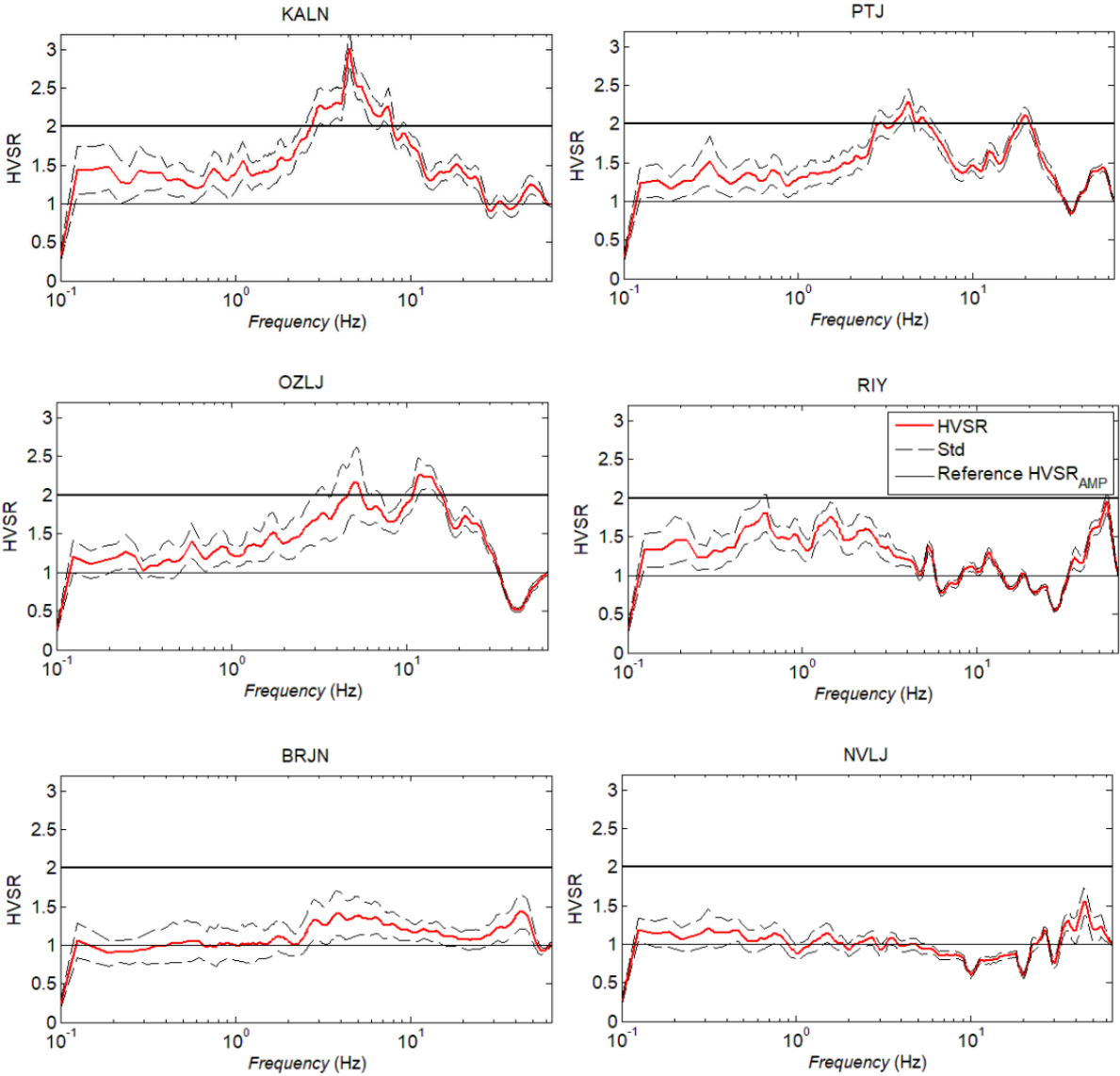
Figure 4.8. Average HVSR frequency curves from microtremor measurements (red lines) and standard deviation (dashed black lines) for each seismological station. Rock reference "no-amplification" HVSR$_{AMP}$ range is marked with black lines according to SESAME (2004) guidelines.
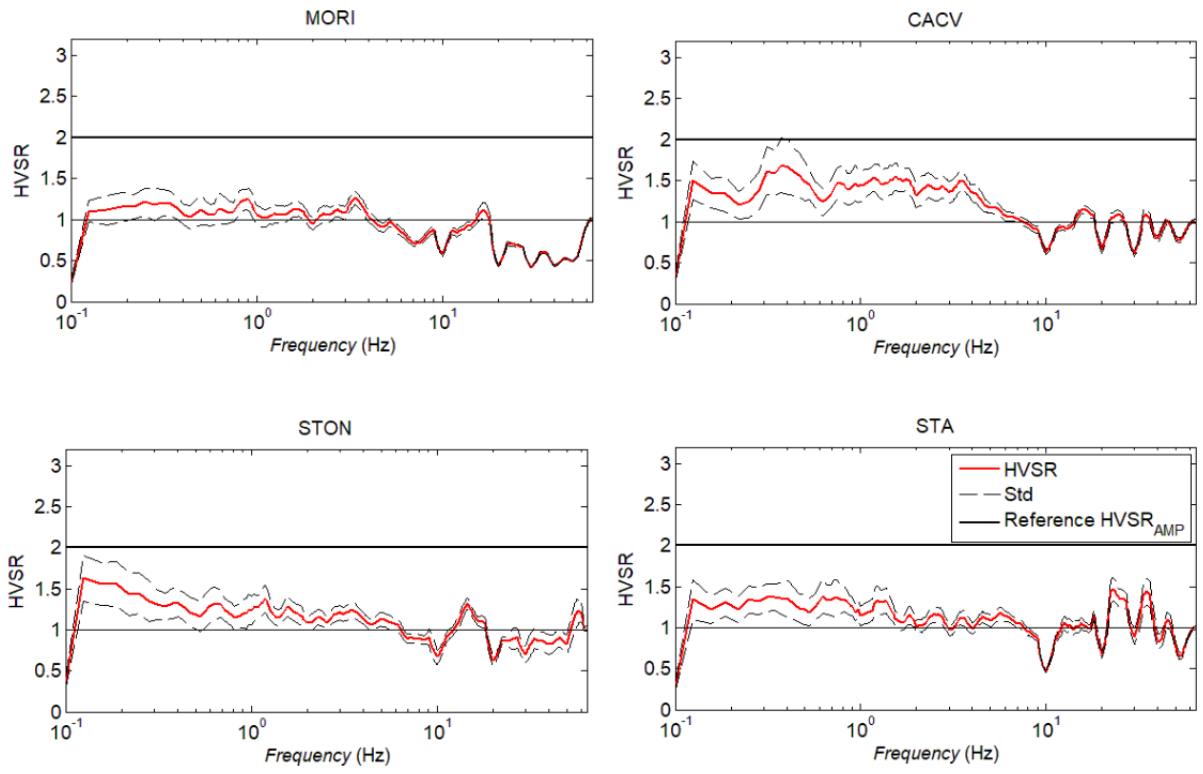
Figure 4.8. ► continued

4.3. Results of the κ calculation in Croatia

The original AH84 approach (Anderson and Hough 1984) utilized in this study was also preferred in the recent studies for κ calculation (e.g., Douglas et al. 2010; Edwards et al. 2011; Gentili and Franceschina 2011; Van Houtte et al. 2011; Ktenidou et al. 2013, 2015; Perron et al. 2017).

4.3.1. κ calculation procedure

The calculation process of the high-frequency decay parameter κ in Croatia using AH84 method (Anderson and Hough 1984) follows Eqs. (4.2–4.4). Three-component (north-south—NS, east-west—EW and vertical—Z) weak motion seismograms (only those of good quality are used) recorded on each station with the frequency sampling rate of 50 Hz were used (Nyquist frequency of 25 Hz). The examples of calculation of the high-frequency decay parameter κ and spectrum processing from earthquake acceleration (derived velocity-seismograms) recordings in Croatia using AH84 classical approach are shown in Figures 4.9 and 4.10 for two earthquakes of magnitudes $M_L = 3.60$ and $M_L = 3.04$, and epicentral distances $R_e = 149$ km and $R_e = 59$ km, recorded at stations MORI and STA.

Recordings are filtered using the band-pass filter between 0.5–25 Hz to exclude the low frequency noise. Dropout of FAS at frequencies > 24 Hz is due to the anti-alias filter and does not affect the κ estimation from the slope of the high-frequency part of FAS. The adequate acceleration S-wave window (in some cases with part of coda which cannot be avoided) was chosen for each record with a minimum duration of 3 s (Figures 4.9 and 4.10, upper row). Selected S-wave windows were processed using the Fast Fourier Transform to obtain FAS of the S-waves (Figures 4.9 and 4.10, middle row). Each FAS is checked to have the Signal-to-Noise-Ratio above 3 ($SNR > 3$). Recordings with deviating FAS from the exponential decay trend at high frequencies (e.g., flat spectrum), with presence of strong site resonance peaks, and other noise effects were not used in κ calculations (e.g., Anderson and Hough 1984; Ktenidou et al. 2013). HVSR curves (Figure 4.8) at the seismological station sites were used as an indicator of possible strong local site resonance peaks which can have impact on the κ estimation from the FAS.

Initially, corner frequency f_C is handpicked approximately as the frequency at which the increase of FAS with the square of frequency stops, or where the FAS becomes theoretically flat following the Brune (1970) omega-square model (Figures 4.9 and 4.10, middle row). Note that f_C is a characteristic of the source and is directly related to magnitude and stress drop. The high-frequency range from which the κ is calculated (Δf, defined as the high-frequency window between f_1 and f_2), is selected manually and is different for each record. f_{max} is determined as the cut-off frequency at which FAS starts to decay rapidly (Figures 4.9 and 4.10, middle row). In most cases, f_1 is picked as the lower bound of the high-frequency slope before the FAS starts to decrease rapidly (f_1 is slightly lower than f_{max}), whereas f_2 is the frequency at which the noise is significantly present in the FAS (except in cases where high resonance peaks are present).

High-frequency decay parameter κ is calculated from the slope of FAS (Eq. 4.4) in the linear–logarithmic space for the high-frequency range $\Delta f = f_1 - f_2$ as shown in Figures 4.9 and 4.10, bottom row. The original AH84 definition was followed to visually choose high-frequency range Δf where the spectrum decay is mostly linear. Although automatic procedure can speed up the whole κ calculation as used by some researchers (e.g., Edwards et al. 2011; Kilb et al. 2012), manual procedure is applied to record by record analysis for each station, to visually inspect previously noted exclusions which can strongly affect calculated κ values (Anderson and Hough 1984; Ktenidou et al. 2013, 2014, 2015).
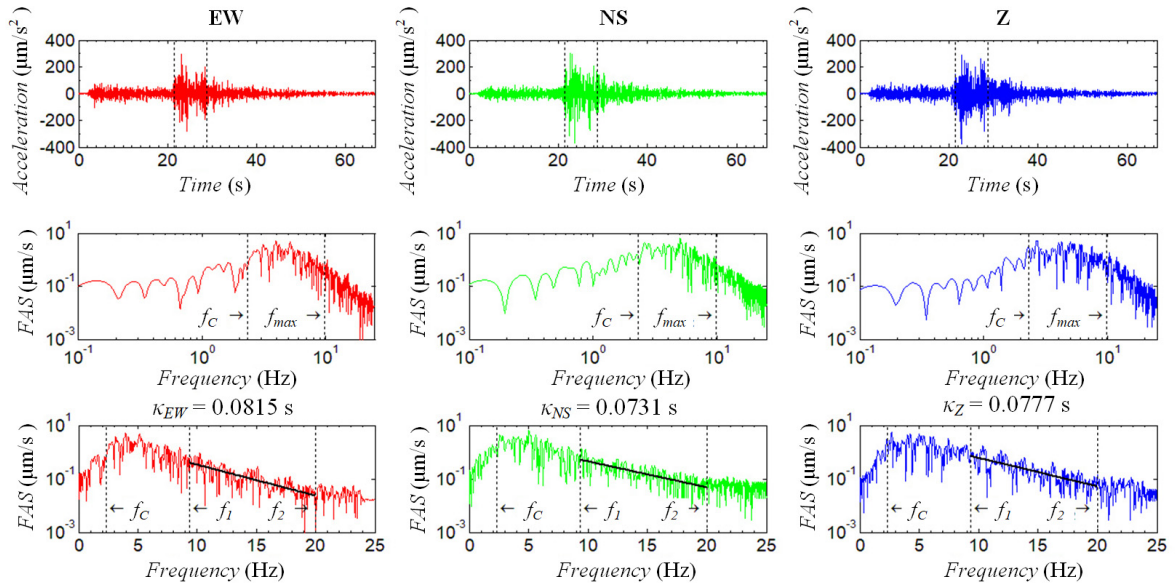
Figure 4.9. Example of κ calculation using AH84 method for three component (EW, NS and Z) seismogram (station: MORI, date: 05/07/2014, time: 03:50, $M_L = 3.60, R_e = 149$ km). Top row: acceleration time history with selected S-wave window (dashed lines). Middle row: log–log plot of FAS. Bottom row: linear–logarithmic plot of FAS. Corner frequency f_C, high frequency range $\Delta f = f_1 - f_2$ where κ is calculated from the slope of FAS and f_{max} at which FAS start to decay rapidly are marked with dashed vertical lines.
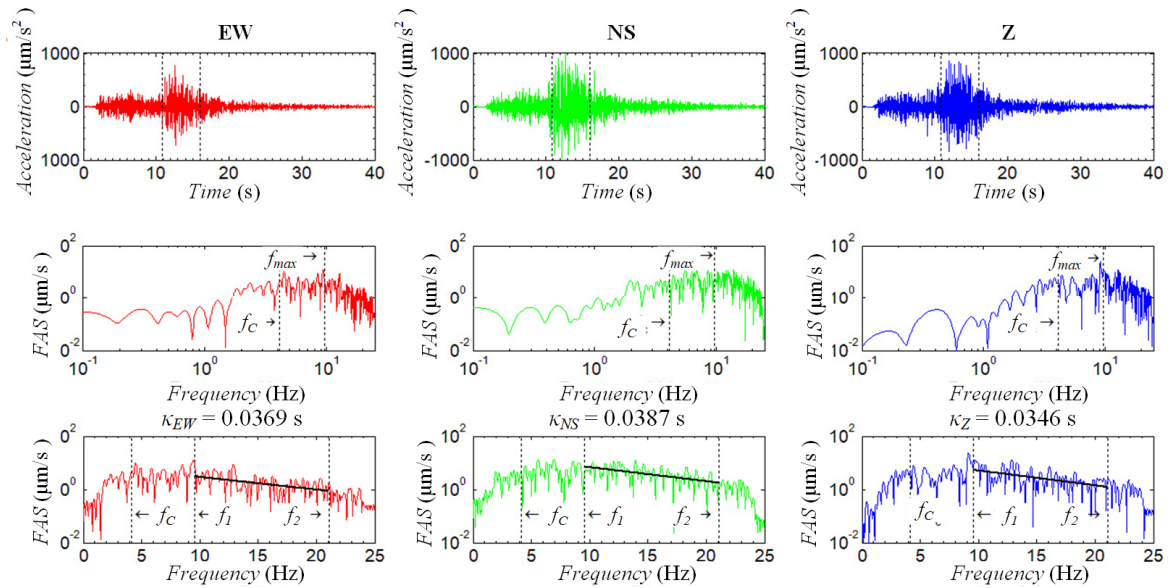
Figure 4.10. Example of κ calculation using AH84 method for three component (EW, NS, and Z) seismogram (station STA, 24/06/2014, time 01:23, $M_L = 3.04, R_e = 59$ km). Top row: acceleration time history with selected S-wave window (dashed lines). Middle row: log–log plot of FAS. Bottom row: linear–logarithmic plot of FAS. Corner frequency f_C, high frequency range $\Delta f = f_1 - f_2$ where κ is calculated from the slope of FAS and f_{max} at which FAS start to decay rapidly are marked with dashed vertical lines.

85

Manually selected frequencies f_C, f_2 and f_{max} (approximately equal to f_1) for all ground motions are plotted against magnitude and epicentral distance for each station to identify the possible source, path, and site contributions to κ regarding frequency selection (Figure 4.11). Distribution of f_{max} and f_2 with magnitude and epicentral distance is nearly-uniform and within the expected scatter. f_2 in most cases is the frequency where the spectrum hits the noise floor (approx. 20–22 Hz). On the other hand, local site conditions control f_{max} (Hanks 1982; Anderson and Hough 1984; Boore 2003) and the average values given in Figure 4.11 are comparable with the estimated site resonant frequencies/periods (approx. 8–12 Hz or 0.09–0.16 s) for the stations provided in Figure 4.7. Figure 4.11 shows that the f_C is correlated with the magnitude and epicentral distance: f_C decreases with increasing magnitude (especially when $M_L > 3.5$) and epicentral distance. Note that most of higher M_L values are at larger epicentral distances (Figure 4.5) which explains decrease of f_C with epicentral distance. Although the trend of f_C correlation with magnitude is well-known (e.g., Brune 1970; Boore 2003; Allmann and Shearer 2009), observed large scatter ($f_C \sim 2-6$ Hz) at the small magnitude range might be the indication of possible source contribution of small magnitude earthquakes at short-to-moderate epicentral distances ($R_e < 60$ km) to κ (probably due to near-source scattering as observed in Kilb et al. (2012).
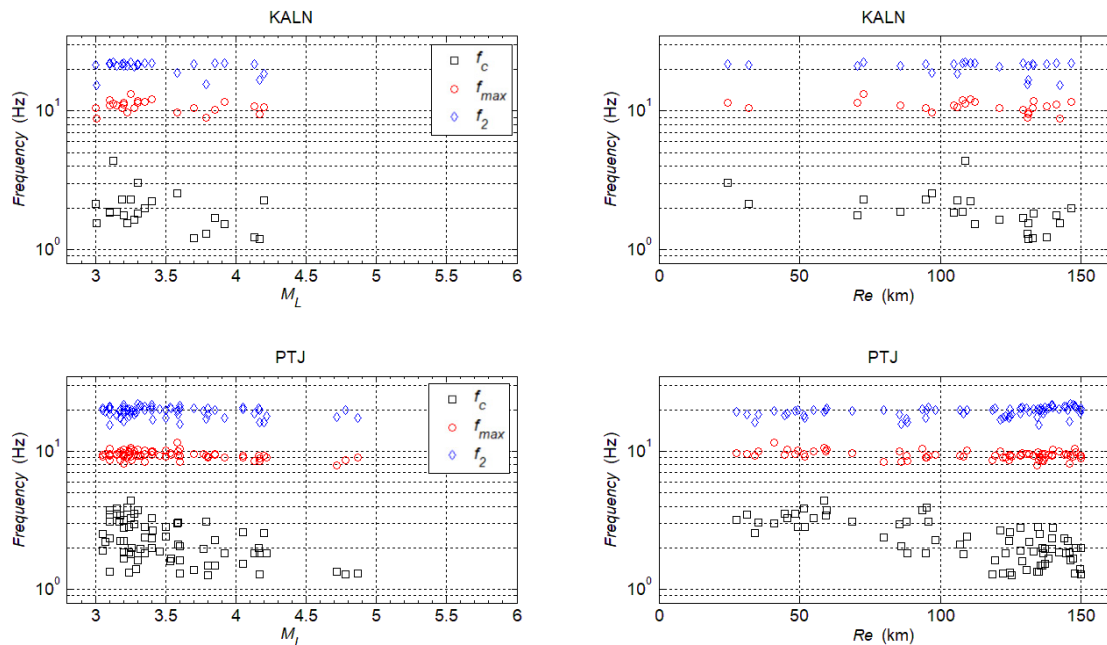
Figure 4.11. Selected frequencies: corner (f_C), cut-off (f_{max}) and noise (f_2) vs. magnitude (M_L) (left column figures) and epicentral distance (R_e) (right column figures) for each seismological station.
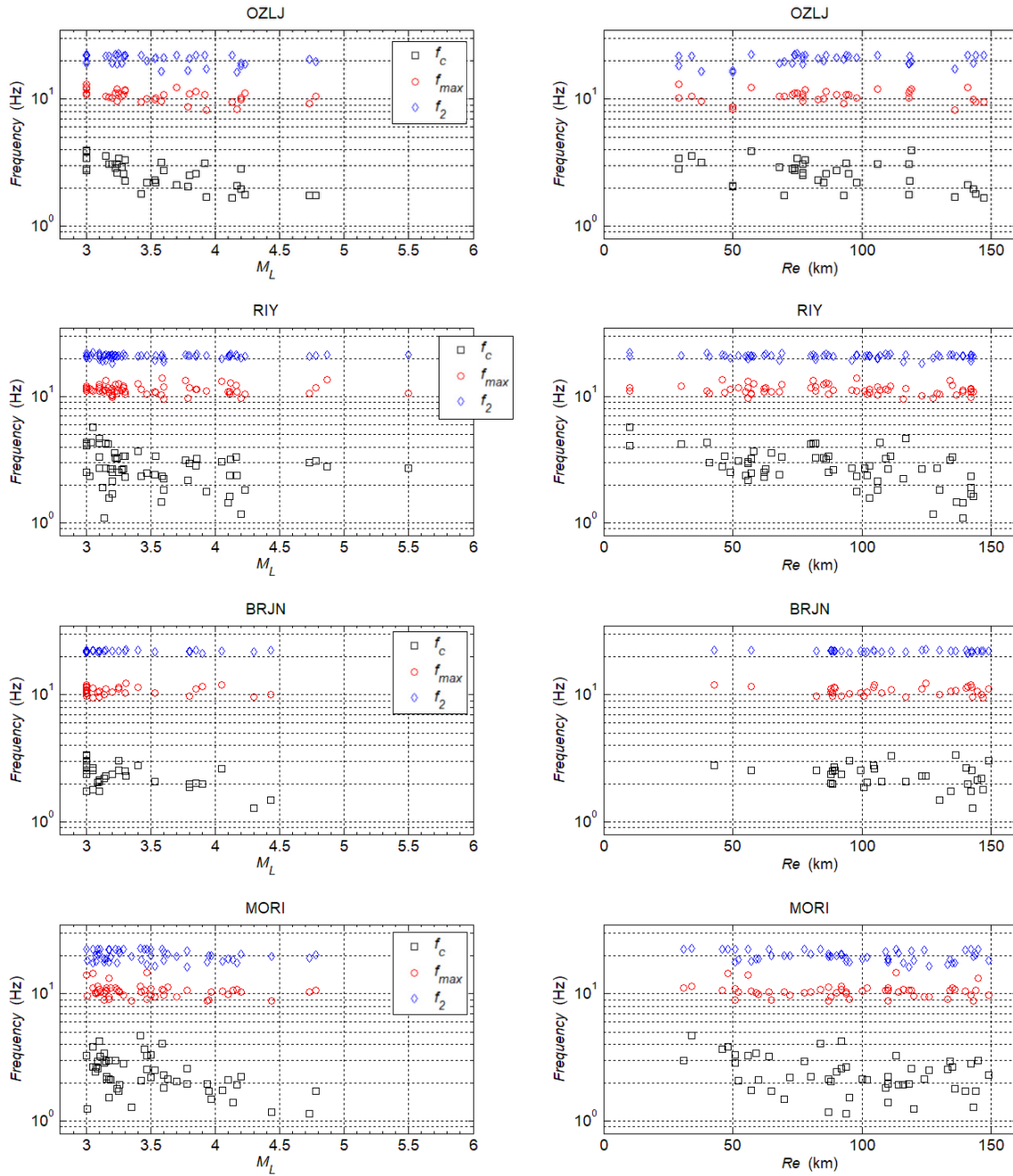
Figure 4.11. ►continued
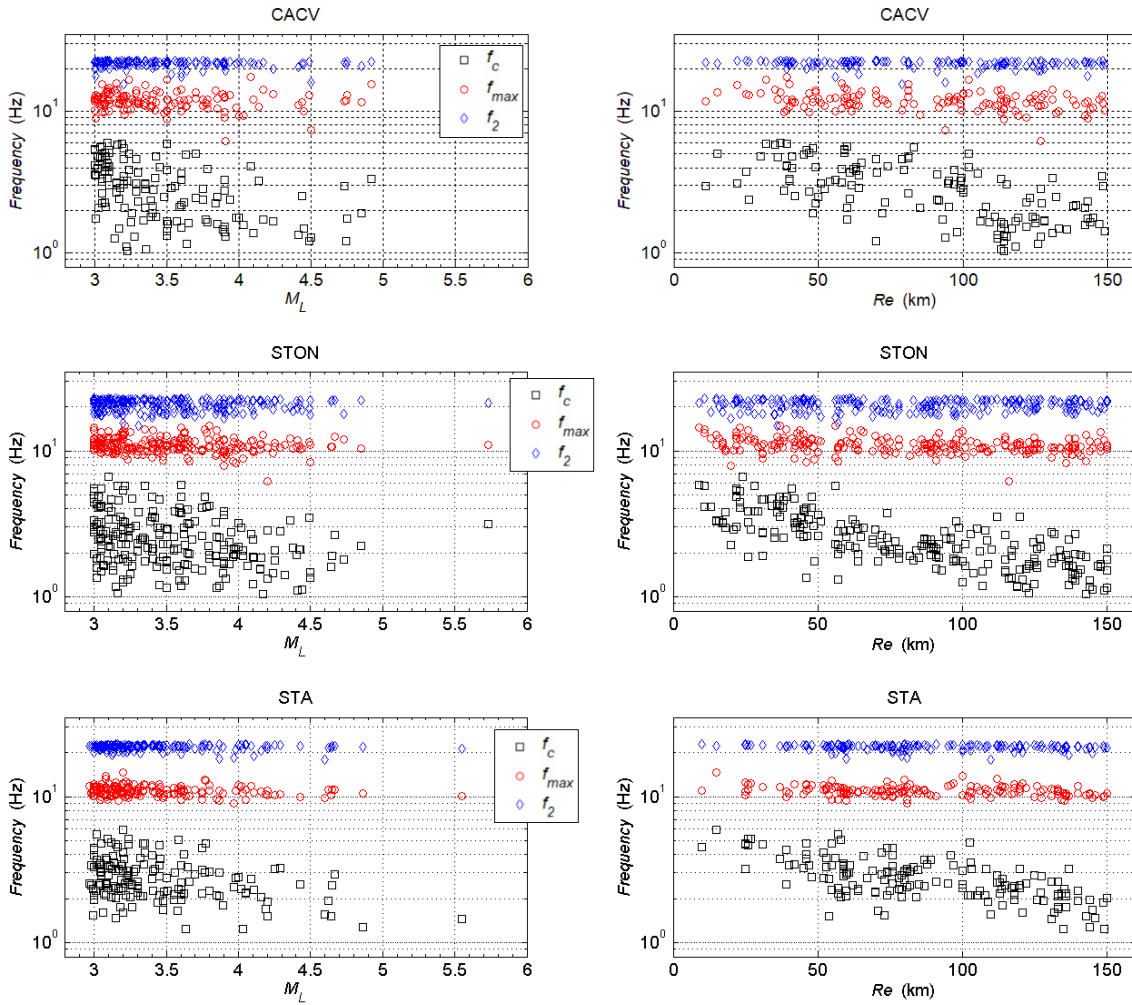
Figure 4.11. ►continued

In this study, κ was calculated for the three component seismograms for each station. Calculated κ values for NS and EW were averaged into one value $\kappa_{hor} = (\kappa_{NS} + \kappa_{EW})/2$ for both horizontal components. In the recent κ studies (e.g., Douglas et al. 2010; Van Houtte et al. 2011; Ktenidou et al. 2013, 2015; Perron et al. 2017) only horizontal components were used to estimate κ from the FAS of the ground motions to propose κ models as a function of distance (Eq. 4.5). Douglas et al. (2010) and Ktenidou et al. (2013) estimated κ from the vertical component of ground motion and observed that the κ_{ver} values for the vertical component are slightly lower than the average κ_{hor} for the horizontal components of the record. Generally, the vertical component of the ground motion is mainly controlled by the source effect and exhibits relatively less sediment-induced amplification than horizontal components (e.g., Reiter 1990; Castro et al. 1996; Elgamal and He 2004). Significant problem of site amplification for the vertical component represents the presence of weaker soil material within deformation zone

overlying more compact rocks with the presence of groundwater (i.e., ridge-and-valley topography slopes; Meunier et al. 2008).

Figure 4.12 compares the ratio of κ_{ver} versus κ_{EW} and κ_{NS} values and averaged horizontal values $\kappa_{hor} = (\kappa_{NS} + \kappa_{EW})/2$ with the $\kappa_{ver}/\kappa_{EW,NS,hor} = 1:1$ (black line) as a function of epicentral distance R_e for each seismic station. Mean ratio between κ components (vertical vs. horizontal) is used since on the plots no clear trends are observed with epicentral distance R_e. Also, the scatter of individual ratios $\kappa_{ver}/\kappa_{EW,NS,hor}$ is almost equally distributed with R_e. where the mean ratio line shows how individual κ_{ver} values are comparable with $\kappa_{EW,NS,hor}$ values as a function of R_e for each seismic station. Differences between mean ratios κ_{ver}/κ_{EW} , κ_{ver}/κ_{NS} and $\kappa_{ver}/\kappa_{hor}$, show that variation of κ_{EW} and κ_{NS} is comparable with $\kappa_{ver}/\kappa_{hor}$. This also justifes averaging both horizontal values κ_{EW} and κ_{NS} into a single value κ_{hor}.

Compared to previous studies (Douglas et al. 2010; Ktenidou et al. 2013), calculated κ_{ver} values are lower than the averaged κ_{hor} in terms of mean ratio line $\kappa_{ver}/\kappa_{hor} < 0.90$ only for stations MORI, CACV and STON. For stations KALN, OZLJ, RIY, NVLJ and STA displayed mean ratio line $\kappa_{ver}/\kappa_{hor} \approx 1.00$. Significant difference between κ_{ver} and κ_{hor} is observed for stations PTJ and BRJN for which the mean ratio line $\kappa_{ver}/\kappa_{hor} > 1.20$. This observation could be possibly attributed to mountainous area that could affect vertical component as disscussed previously with HVSR observations around PTJ station located on the top of Medvednica Mt. Also, BRJN station is located on the island and the station's location is on a small hill. The island location could have some effect on the vertical component due to polarization effects (geometry is similar to those of hilltops). However, the stations KALN, OZLJ, CACV and STA are also located in mountainous area (on hilltop, on ridge or on top of mountain) where these effects are not observed. Possible influence of site amplification due to the topographic effects or/and the presence of shallower soil layers above bedrock (Figure 4.7) could affect the vertical component of ground motion at some stations, e.g., PTJ, BRJN, and CACV, which could explain observed $\kappa_{ver}/\kappa_{hor}$ ratios. These effects and the relation of $\kappa_{ver}/\kappa_{hor}$ need to be studied in more detail in future, particularly when more data will be available, in order to arrive at more robust conclusions.
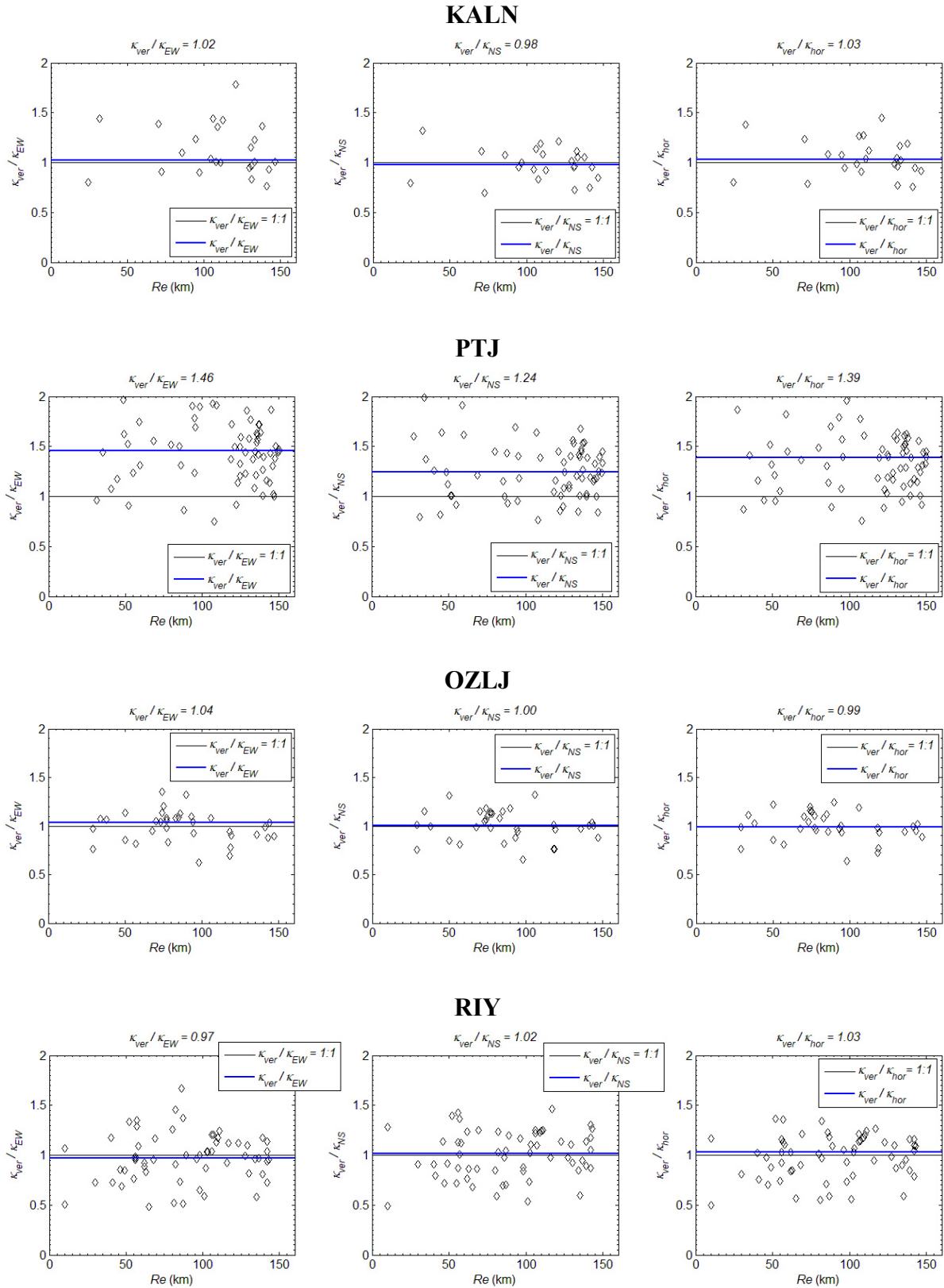
Figure 4.12. Comparison of ratio of κ_{ver} versus κ_{EW} and κ_{NS} values and averaged horizontal $\kappa_{hor} = (\kappa_{NS} + \kappa_{EW})/2$ values as a function of epicentral distance R_e for each seismic station. Black line indicate $\kappa_{ver}/\kappa_{EW,NS,hor} = 1:1$ ratio line, and thick blue line indicate Mean ratio line for κ_{ver}/κ_{EW}, κ_{ver}/κ_{NS} and $\kappa_{ver}/\kappa_{hor}$ and mean ratio values are shown above each figure.

Figure 4.12. ▶ continued

STON

STA
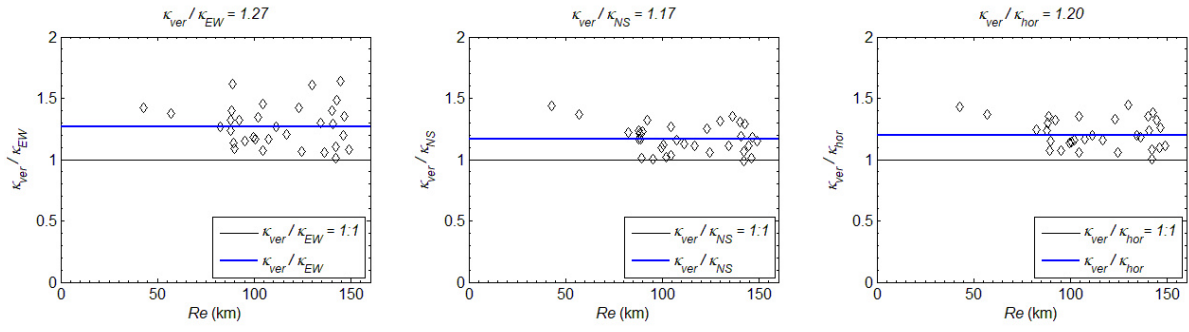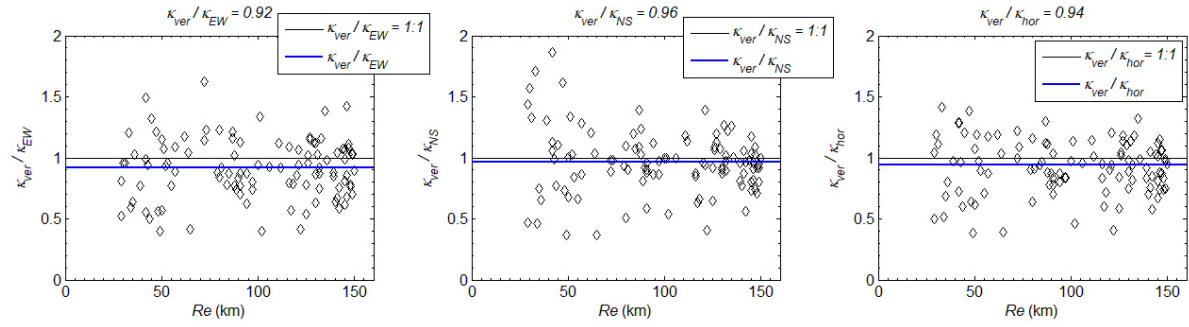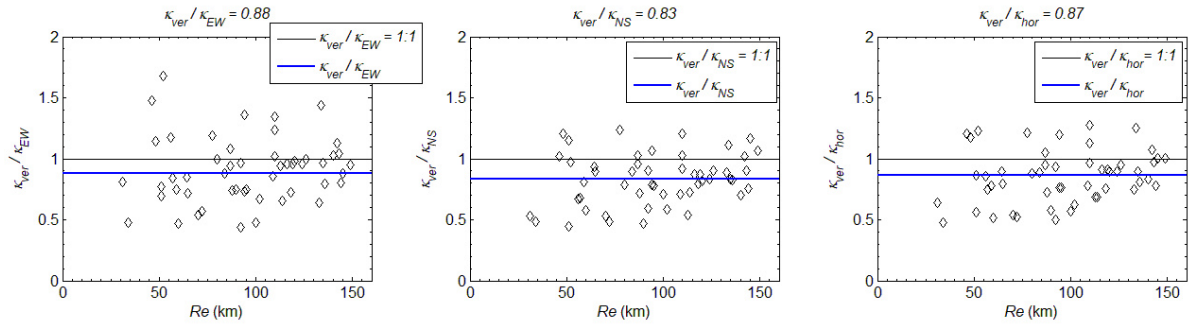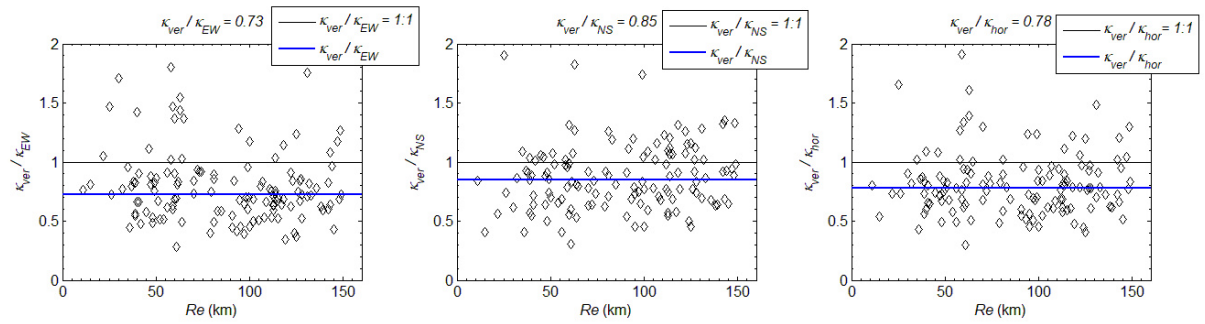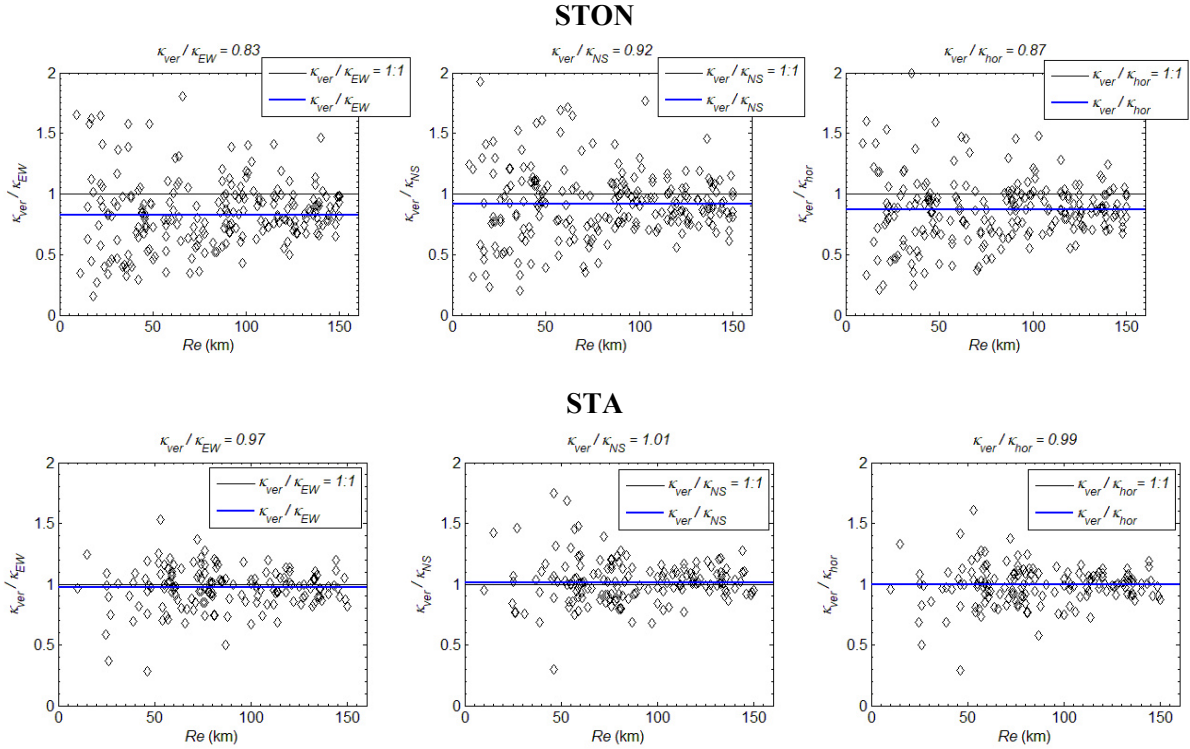
Figure 4.12. ► **continued**

4.3.2. Linear least-square regression (κ dependence on distance)

Linear $\kappa - R_e$ formulation (Anderson and Hough 1984; Eq. 4.5) pairs individual values of κ and epicentral distances R_e for all records at each station to propose κ models as a function of epicentral distance to estimate value of site-specific (near-site) attenuation parameter κ_0. Van Houtte et al. (2011), Kilb et al. (2012) and Ktenidou et al. (2013) reported that hypocentral distance may have a stronger correlation with the propagation path from source to the site than the epicentral distance, and is thus more appropriate to describe the regional effect on κ. Study of Ktenidou et al. (2013) found that choice of distance (epicentral vs. hypocentral) systematically affects κ_0 and the difference in κ_0 estimates with the use of hypocentral distance can be 20–40 % lower when compared to κ_0 estimates with the use of epicentral distance. The main goal of studying the κ dependence on distance is to extrapolate the $\kappa(R)$ function to $R = 0$ km to estimate κ at the site under study (κ_0), and it is more convenient to use epicentral distance, as the hypocentral distance cannot be zero unless the focal depth is zero. Epicentral distance was originally used by Anderson and Hough (1984) in analogy with the problem of inverting travel times for the velocity in a layered Earth using ray tracing and with the use of

hypocentral distance in regression, the analogy is lost. One should note that the use of epicentral distance in $\kappa-R_e$ regression could present a problem at shorter epicentral distances with deep foci (> 30 km) (e.g., Vrancea intermediate-depth earthquakes) and the use of hypocentral distance could then be a better choice. For the compiled dataset in this study, all earthquakes are shallow, therefore the suggestion from Ktenidou et al. (2013) to use epicentral distance for κ_0 extrapolation was followed, which also limits the adverse influence of uncertainty of focal depth estimations.

Calculated individual horizontal κ values for EW and NS components were combined into an average value of $\kappa_{hor} = (\kappa_{NS} + \kappa_{EW})/2$ for single earthquake, and in certain cases where they differ significantly from each other (difference > 25 %), the recording is excluded from the dataset (Gentili and Franceschina 2011; Van Houtte et al. 2011, 2014; Ktenidou et al. 2013, 2014). Although Douglas et al. (2010) and Ktenidou et al. (2013) estimated κ from the vertical component, they did not propose κ_{ver} models as a function of distance. In this study, both κ models κ_{hor} and κ_{ver} as a function of epicentral distance are proposed (Figures 4.13 and 4.14) to estimate site-specific parameters κ_0^{hor} and κ_0^{ver} (Eq. 4.5) and their comparison is discussed. Red lines in Figures 4.13 and 4.14 (left hand side) show the median values and 95 % confidence intervals from the regression analysis for averaged horizontal component κ_{hor} and vertical component κ_{ver}, respectively. Vertical error-bars show the uncertainty of κ_{hor} values and horizontal error-bars show uncertainty in epicentral distances with standard error set to $\pm$ 5 km. In these figures, right hand side plots represent the distribution of the residuals (actual kappa minus predicted kappa) with epicentral distance. Residual plots show no visible trends with epicentral distance and most of data are distributed equally from regression line and 95 % confidence interval.

Linear least-square regression is performed to estimate parameters of Eq. (4.5), site-specific attenuation parameter expressed as the intercept κ_0 extrapolated to zero distance R_e and the regression slope κ_R by rejecting the points outside the 95 % confidence intervals (full green circles in Figures 4.13 and 4.14) as suggested by Ktenidou et al. (2013). Outliers removal is important if data sets used for the regression $\kappa-R_e$ are not complete in terms of distance as was shown in Figure 4.5 (right column). Also, as Ktenidou et al. (2013) suggested, if there is only single analyst, the use of so-called robust linear least-square regression with outlier removal is recommended to minimize bias of the outliers on the overall records. Most of outliers are at

larger epicentral distances ($R_e > 100$ km) with few cases observed at shorter R_e probably due to the some local and regional effects.

Simple linear least-squares regression was used in this study with the assumption that R_e is independent variable with standard error in $R_e = \pm\ 0$ km. In fact, both variables, κ and R_e, are imperfectly known and errors in R_e could have impact on the final values of κ_0 and slope κ_R. For this reason, error-bars with standard error in $R_e = \pm\ 5$ km were plotted too.

To address the effect of the uncertainty in R_e on the κ, instead of using the traditional linear least-squares regression, the linear regression suitable for data with errors following the method in York et al. (2004) was tested to check how the existence and correlation for the observational errors in the two coordinates (R_e and κ) affect values of κ_0 and κ_R, and if there exists significant difference regarding the standard linear regression. To check this, 6 different variations in standard errors for the R_e and κ were used in testing linear regression using York et al. (2014) method. For the cases where standard errors for R_e and κ are set to: $R_e = \pm\ 2$–5 km and $\kappa \sim 1$–2 standard deviations (residuals from Figures 4.13 and 4.14, right plots), differences between two regression methods (standard vs. error-in-variables) are less than 5 %. If the standard error for $R_e = \pm\ 10$–15 km, differences between two regression methods (standard vs. error-in-variables) are higher than 10 % and can go up to 20 %, particularly for the stations with less data, large data scatter and lack of data at shorter epicentral distances. This needs to addressed in more detail in future, particularly for the stations with few data (e.g., KALN, BRJN).

Typically, the standard error for R_e amounts to $\pm\ 3$–5 km (Marijan Herak, personal communication) and for these particular cases, with error in κ set to 2 standard deviations (~ 0.01–0.02 s), differences between standard linear regression and error-in-variables linear regression are less than 5 %. Summarized results of a standard least-square regressions of κ–R_e dependence for horizontal and vertical κ models (κ_{hor} and κ_{ver}) using AH84 approach are given in Table 4.2 with estimated site-specific attenuation values of κ_0^{hor} and κ_0^{ver} and regression slopes κ_R^{hor} and κ_R^{ver} for each seismological station.
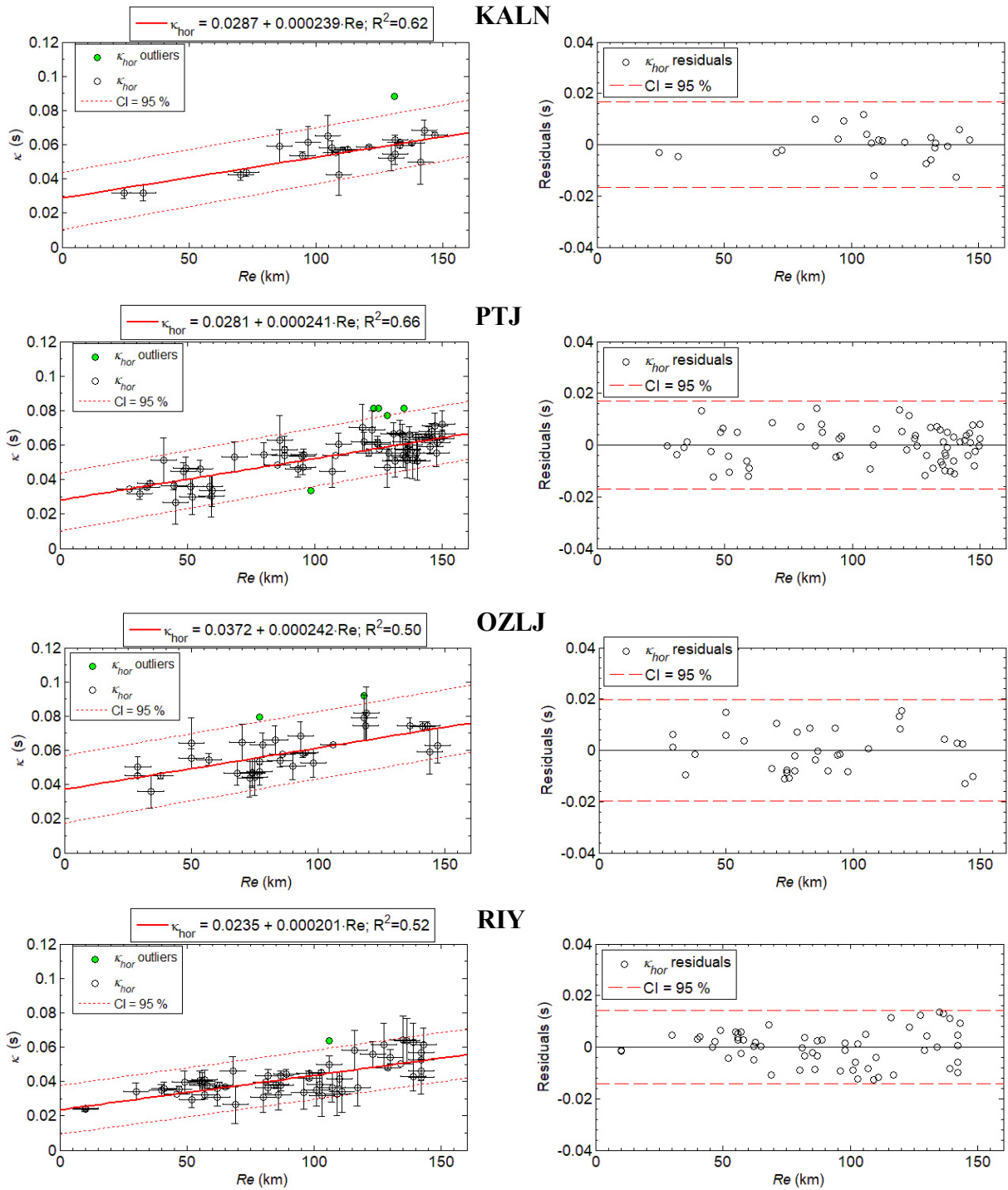
Figure 4.13. Horizontal $\kappa_{hor} - R_e$ models for each seismological station. Left: least-squares regression of $\kappa_{hor} - R_e$ dependence (Eq. 4.5) (fit regression line shown by red thick line) with the rejection of outlier points (green points) from 95 % confidence interval (dashed red lines). Site-specific attenuation values of κ_0^{hor} (intercept at zero distance R_e) and regression slopes κ_R^{hor} with R^2 are given above figure. Vertical error-bars show the uncertainty of κ_{hor} values and horizontal error-bars show uncertainty in epicentral distances with standard error set to $\pm$ 5 km. Right: Residuals from regression lines – only points inside 95 % confidence interval are plotted.
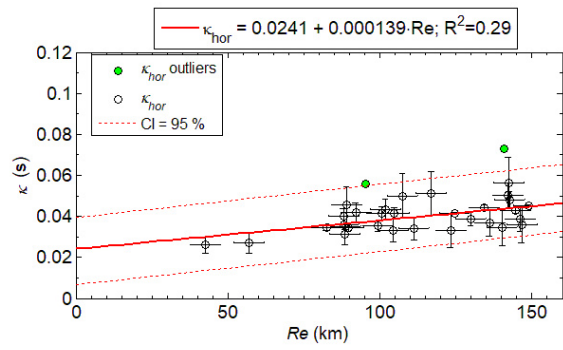
BRJN
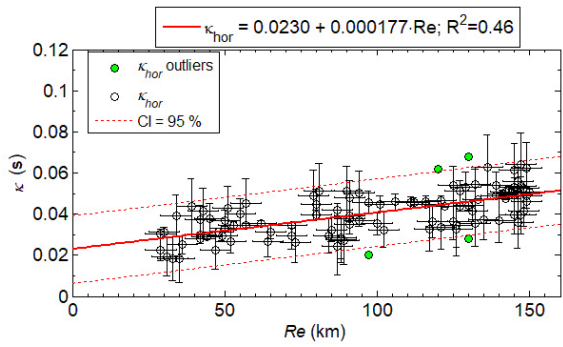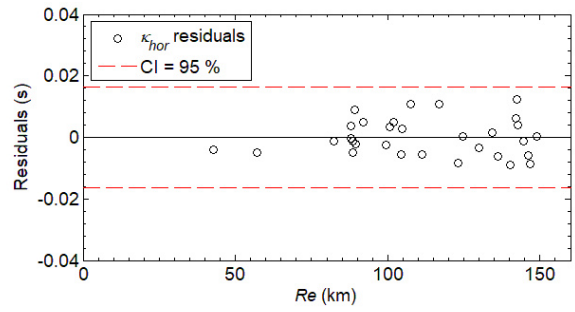
NVLJ
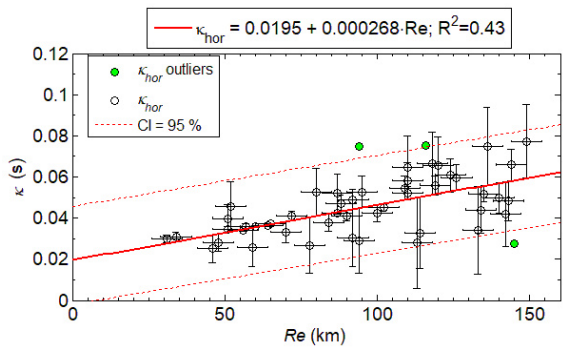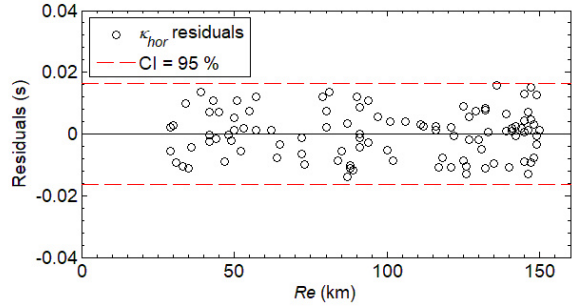
MORI
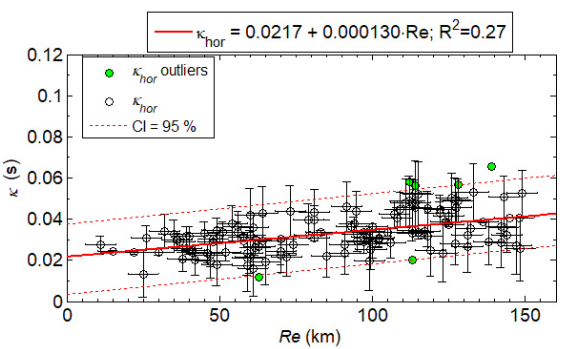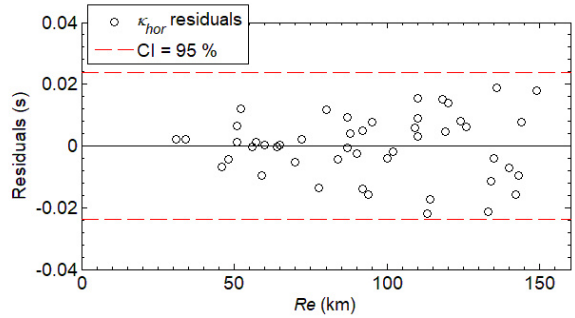
CACV
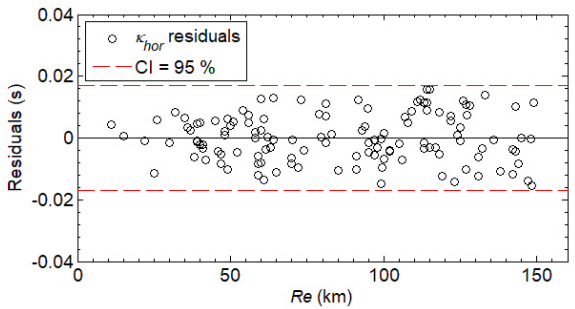
Figure 4.13. ► continued
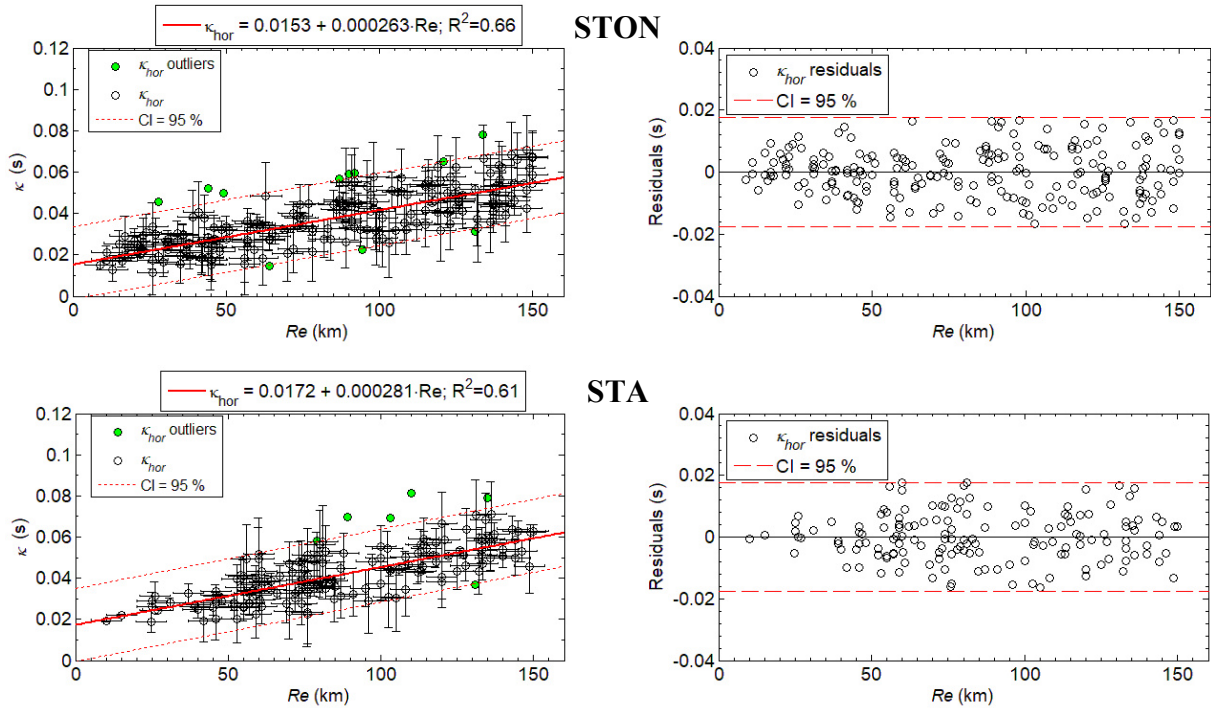
Figure 4.13. ► continued
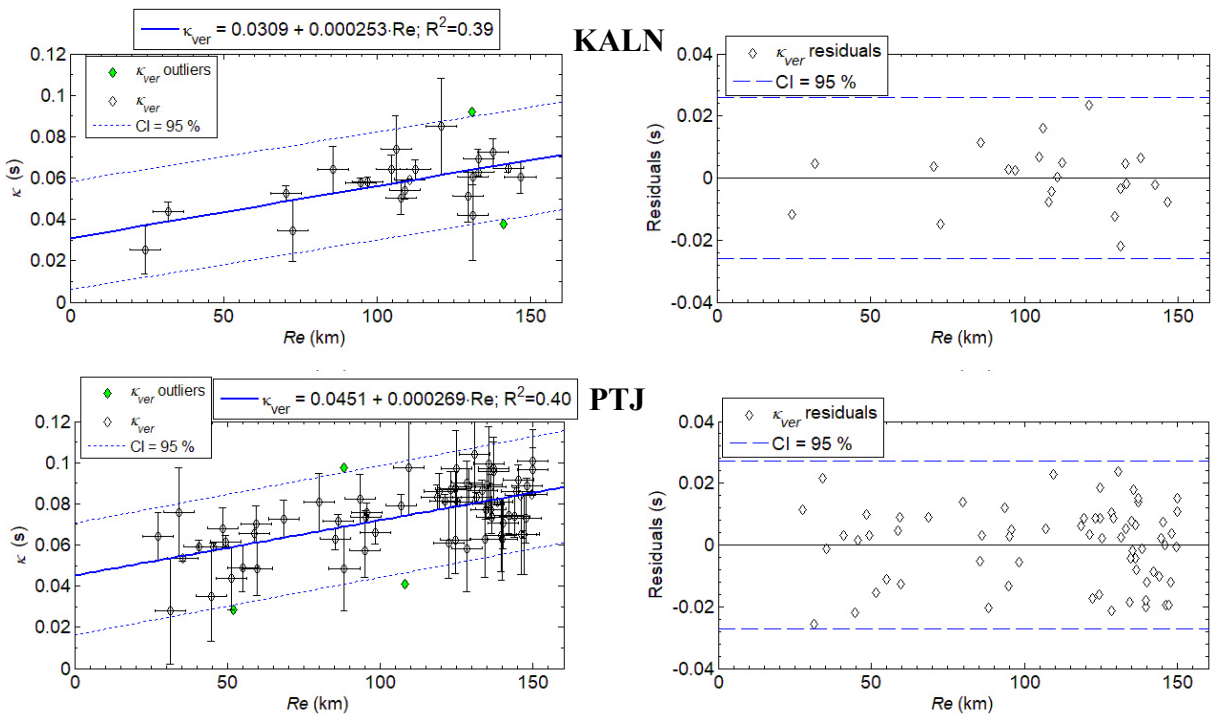
Figure 4.14. Vertical $\kappa_{ver}-R_e$ models for each seismological station. Left: least-squares regression of $\kappa_{ver}-R_e$ dependence (Eq. 4.5) (fit regression line shown by blue thick line) with the rejection of outlier points from 95 % confidence interval (dashed blue line). Site-specific attenuation values of κ_0^{ver} (intercept at zero distance R_e) and regression slopes κ_R^{ver} with R^2 are given above figure. Vertical error-bars show the uncertainty of κ_{ver} values and horizontal error-bars show uncertainty in epicentral distances with standard error set to $\pm$ 5 km. Right: Residuals from regressed lines – only points inside 95 % confidence interval are plotted.
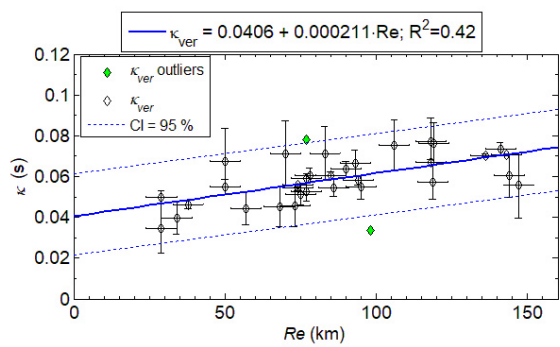
OZLJ
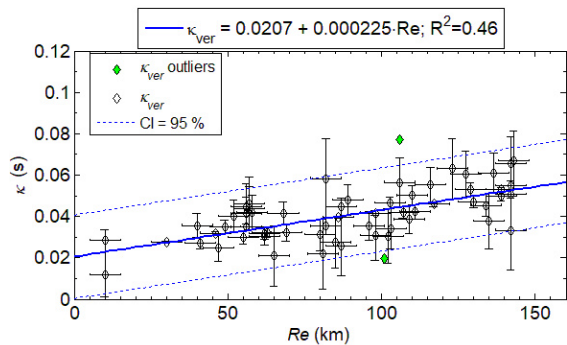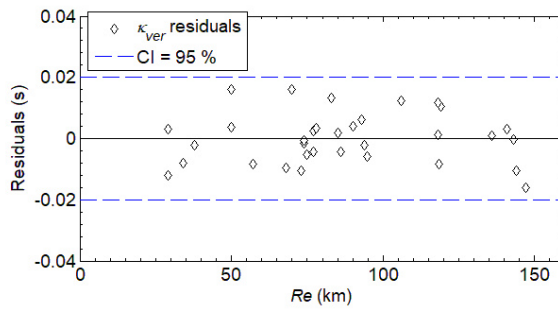
RIY
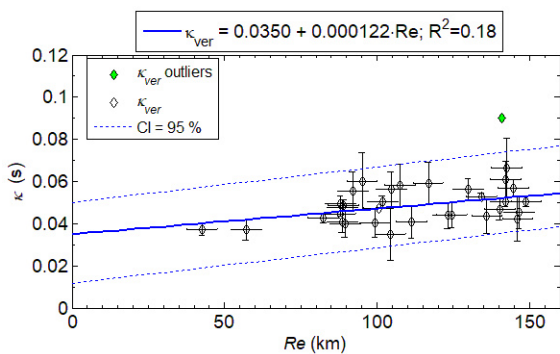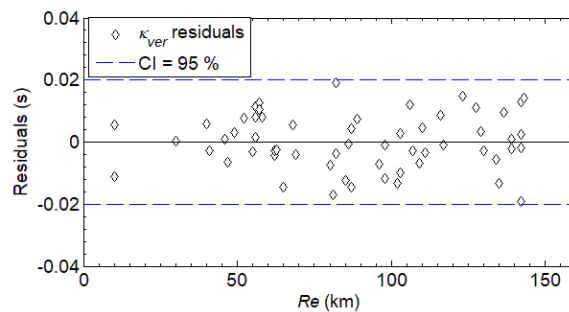
BRJN

NVLJ

Figure 4.14. ► continued

98

MORI

$\kappa_{ver} = 0.0101 + 0.000300 \cdot Re; R^2 = 0.37$

CACV

$\kappa_{ver} = 0.0160 + 0.000116 \cdot Re; R^2 = 0.21$

STON

$\kappa_{ver} = 0.0126 + 0.000238 \cdot Re; R^2 = 0.50$

STA

$\kappa_{ver} = 0.0159 + 0.000287 \cdot Re; R^2 = 0.60$
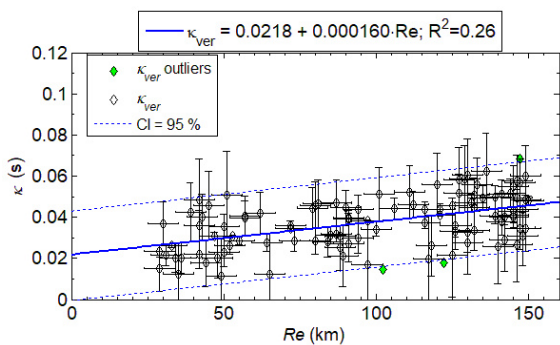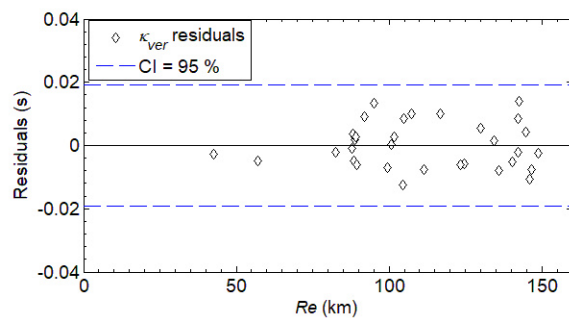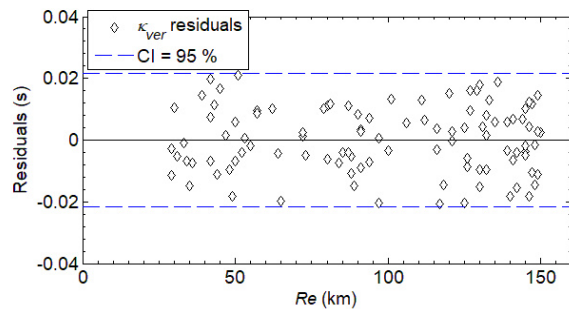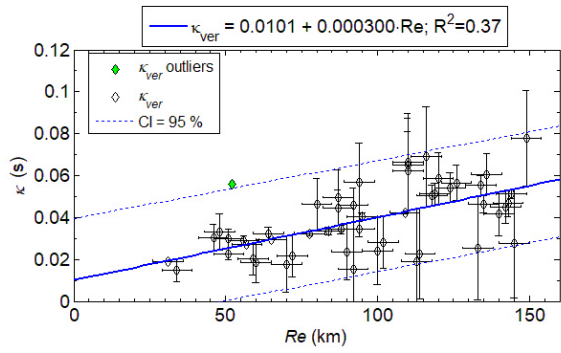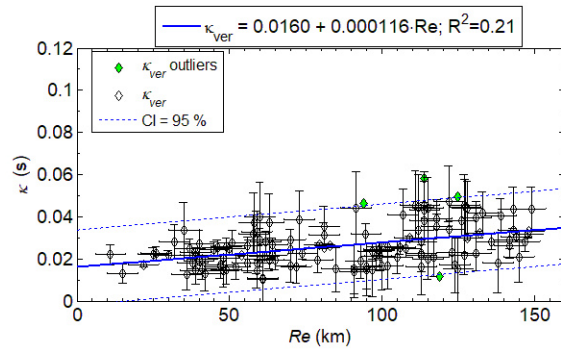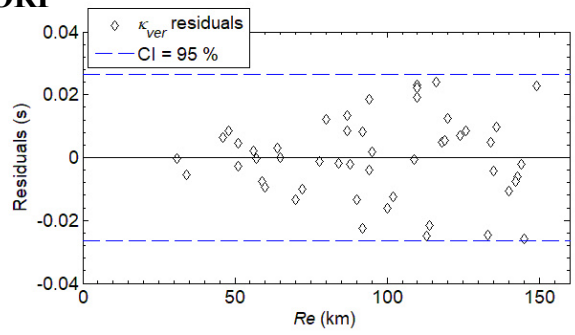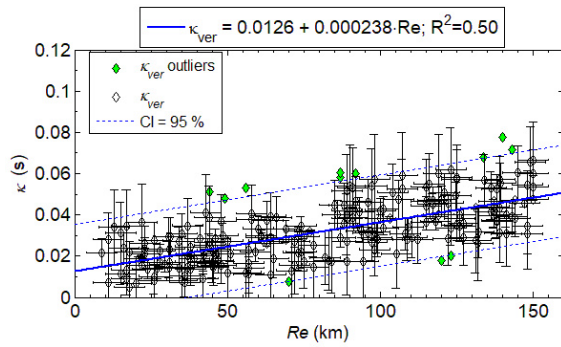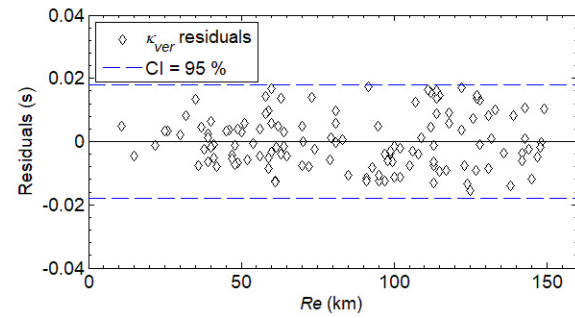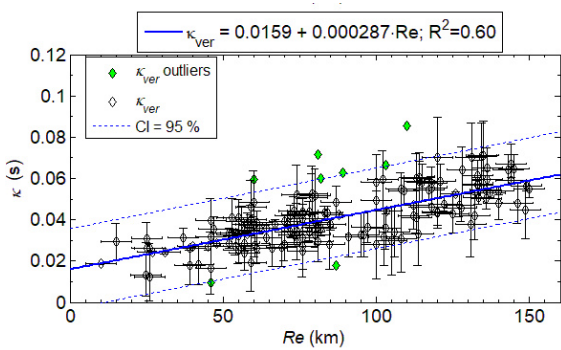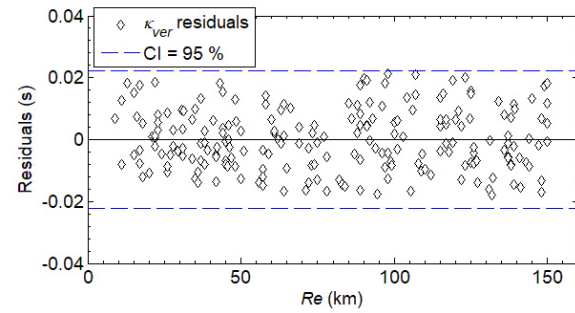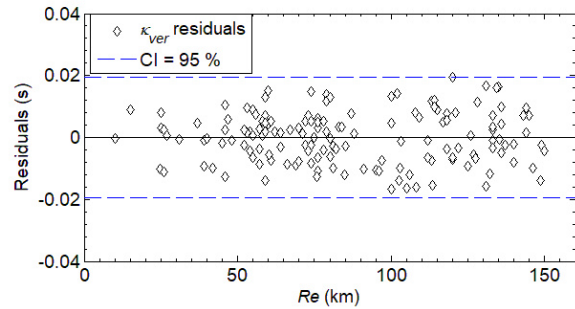
Figure 4.14. ► continued

Table 4.2: Summarized results of the least-squares regression of $\kappa - R_e$ dependence for horizontal and vertical component κ models (κ_{hor} and κ_{ver}) using AH84 model (Eq. 4.5). Site-specific (near-site) attenuation values κ_0^{hor} and κ_0^{ver} and slopes of regression in terms of κ_R^{hor} and κ_R^{ver} and their standard errors ($\pm$) with coefficient of determination $R_{hor,ver}^2$ are listed. Ratio of $\kappa_0^{ver}/\kappa_0^{hor}$ and $\kappa_R^{ver}/\kappa_R^{hor}$ is listed for each seismological station at the bottom of the table.

HORIZONTAL COMPONENT			
Station	κ_0^{hor} (s)	κ_R^{hor} (skm^{-1})	R_{hor}^2
KALN	0.0287 ± 0.0046	0.000239 ± 0.000041	0.62
PTJ	0.0281 ± 0.0025	0.000241 ± 0.000022	0.66
OZLJ	0.0372 ± 0.0041	0.000242 ± 0.000044	0.50
RIY	0.0235 ± 0.0024	0.000200 ± 0.000025	0.52
BRJN	0.0241 ± 0.0046	0.000139 ± 0.000040	0.29
NVLJ	0.0230 ± 0.0020	0.000177 ± 0.000019	0.46
MORI	0.0194 ± 0.0045	0.000270 ± 0.000045	0.43
CACV	0.0217 ± 0.0018	0.000130 ± 0.000019	0.27
STON	0.0153 ± 0.0012	0.000263 ± 0.000013	0.66
STA	0.0173 ± 0.0017	0.000280 ± 0.000019	0.60
VERTICAL COMPONENT			
Station	κ_0^{ver} (s)	κ_R^{ver} (skm^{-1})	R_{ver}^2
KALN	0.0309 ± 0.0078	0.000253 ± 0.000071	0.39
PTJ	0.0451 ± 0.0047	0.000269 ± 0.000041	0.40
OZLJ	0.0406 ± 0.0041	0.000211 ± 0.000044	0.42
RIY	0.0207 ± 0.0031	0.000225 ± 0.000033	0.46
BRJN	0.0350 ± 0.0055	0.000122 ± 0.000048	0.18
NVLJ	0.0218 ± 0.0028	0.000160 ± 0.000026	0.26
MORI	0.0102 ± 0.0058	0.000299 ± 0.000057	0.37
CACV	0.0160 ± 0.0019	0.000116 ± 0.000020	0.21
STON	0.0126 ± 0.0015	0.000238 ± 0.000017	0.50
STA	0.0161 ± 0.0018	0.000286 ± 0.000019	0.59

RATIO VERTICAL / HORIZONTAL										
Ratio	**KALN**	**PTJ**	**OZLJ**	**RIY**	**BRJN**	**NVLJ**	**MORI**	**CACV**	**STON**	**STA**
$\kappa_0^{ver}/\kappa_0^{hor}$	1.07	1.61	1.09	0.88	1.45	0.95	0.52	0.74	0.82	0.92
$\kappa_R^{ver}/\kappa_R^{hor}$	1.06	1.12	0.87	1.12	0.87	0.90	1.12	0.89	0.91	1.02

The regression slopes κ_R of linear function (Eq. 4.5) indicate gradual increase of κ with epicentral distance R_e for all stations, consistent with the findings of Anderson and Hough (1984), Ktenidou et al. (2013, 2015). Nearby recordings can constrain site-specific κ_0 and distant recordings can constrain propagation path effects through the slope of regression κ_R. Numerous kappa researchers reported in their studies that the gradual increase may begin after distances of 15–20 km implying the effect of regional attenuation in the crust, whereas at short distances mean κ values are approximately constant (and similar to the site-specific κ_0). This effect is hinted at in Figures 4.13 and 4.14, mainly due to limited data at shorter epicentral distances. Main attenuation contribution in κ_0 is due to the local site effects of the shallow crust near and below the site (up to depths of 1–2 km) as reported by Van Houtte et al. (2014) and Ktenidou et al. (2015). This is the reason why kappa-researchers use several terms (near-site attenuation, site-specific attenuation, or simply site attenuation) to describe parameter κ_0 at zero-distance or at short epicentral distances. This study lacks short epicentral distances at almost all stations (only STON have some data closer than 20 km), but the distance dependence is visible even at the shortest distances for the cases where they exist as observed in Figures 4.13 and 4.14. Large scatter in the data points is typical in κ studies as it was reported in the cited literature.

The important indicator of a good linear form of κ–R_e models (horizontal and vertical) is coefficient of determination R^2 (Table 4.2). For this kind of κ studies, values of $R^2 > 0.60$ represent strong correlation (Ktenidou et al. 2013, 2014), whereas $0.40 < R^2 < 0.60$ are acceptable as good correlations, but it depends on the number and scatter of data with R_e, and possible other factors that can affect the κ values (frequency windows for the κ calculation from the FAS, source effects, azimuthal and geographical distribution) (e.g., Perron et al. 2017). Low correlations $0.20 < R^2 < 0.40$ are questionable due to large scatter of data particularly for the vertical κ_{ver}–R_e models as observed in Figure 4.14. In general, if linear trend with epicentral distance is visible for large or limited number of data despite low value of R^2 (CACV and BRJN), estimated value of site-specific parameter κ_0 can be used as a good indicator of near-site attenuation of certain local site (or station) (Ktenidou et al. 2014).

As it was previously mentioned and discussed (Figure 4.12), individual values of κ_{ver} are lower than κ_{hor} only for few stations, whereas in some cases they differ under influence of typical local site effects (topography, shallow soft materials, velocity inversion). Generally, the observations from this study does not confirm observations from studies of Douglas et al.

(2010) and Ktenidou et al. (2013) that values of κ_{ver} are lower than the κ_{hor}. Major influence on the site-specific (near-site) parameter κ_0 have the local site effects below and near site and it is convenient to see if the individual differences between κ_{ver} and κ_{hor} have effect on the κ_0^{hor} and κ_0^{ver}. The ratio of site-specific values $\kappa_0^{ver}/\kappa_0^{hor}$ (Table 4.2) for stations varies between 0.53 and 1.61. Stations STA, STON, NVLJ, RIY, OZLJ and KALN show ratios $\kappa_0^{ver}/\kappa_0^{hor}$ near and around "1" (0.82–1.09) and are comparable with $\kappa_{ver}/\kappa_{hor}$ observations (Figure 4.12). Ktenidou et al. (2013) found the ratio of $\kappa_0^{ver}/\kappa_0^{hor} \approx 1$ for the stations at depth (in borehole), and $\kappa_0^{ver}/\kappa_0^{hor} \approx 0.71$ for the station at the surface. This is the only reported literature comparison between site-specific attenuation values $\kappa_0^{ver}/\kappa_0^{hor}$. One possible explanation of low value of the ratio $\kappa_0^{ver}/\kappa_0^{hor} < 0.74$ (CACV and MORI) could be geomorphological characteristics of the station area, presence of shear wave velocity inversion (weathered zone that affect the limestone within the first few meters beneath the surface) and local near-source scattering (Figures 4.6 and 4.7) (Kilb et al. 2012; Pischiutta et al. 2012; Perron et al. 2017). For the ratio of site-specific attenuation values $\kappa_0^{ver}/\kappa_0^{hor} \gg 1$ (PTJ and BRJN), it could be due to their geo-location effects, shallow soft-surface layers and topographic effects as disccused previously (Figure 4.12). Perron et al. (2017) stated that topography of the free surface near the site can modify spectral shape of ground motion and thus the evaluation of the individual values of κ, which then affects the estimation of site-specific parameter κ_0, especially for the rock sites situated in hilly areas.

More interestingly, the slopes κ_R^{hor} and κ_R^{ver} from the κ_{hor} and κ_{ver} distance models are similar, and the ratio of $\kappa_R^{ver}/\kappa_R^{hor}$ varies between 0.87–1.12 (Table 4.2). This could imply that the effect of regional attenuation in the upper crust is similar for κ_{hor} and κ_{ver} distance models, consistent with similar reported findings regarding horizontal and vertical kappa models (Douglas et al. 2010; Ktenidou et al. 2013, 2014, 2015). In addition to the similar values of the regression slopes κ_R^{hor} and κ_R^{ver}, large differences between site-specific attenuation values of κ_0^{hor} and κ_0^{ver} and low values of R^2_{ver} for some sites, point out that full κ models and site values of κ_0^{ver} should be used with "caution", as reported in Ktenidou et al. (2013). For the stations where ratios $\kappa_0^{ver}/\kappa_0^{hor}$ and $\kappa_R^{ver}/\kappa_R^{hor}$ are near and around 1 (KALN, OZLJ, RIY, NVLJ, STON, STA) both $\kappa_{hor,ver}$ models can be combined only if the R^2 is high enough (at least $R^2 > 0.50$). For the stations for which significant difference between $\kappa_0^{ver}/\kappa_0^{hor}$ exists with $R^2 < 0.50$ (PTJ, BRJN, MORI and CACV) only horizontal site-specific attenuation value κ_{hor} should be used. In the cases that 1-component vertical instruments are used, estimation of site-

specific value of κ_0 from vertical κ_{ver} model can be allowed (Douglas et al. 2010), otherwise, preferable use of horizontal site-specific value κ_0^{hor} is recommended.

Therefore, for the developed κ models in this chapter and subsequently in the RVT-based site response analysis (Chapter 5), horizontal site-specific attenuation values κ_0^{hor} are used to represent values of near-site attenuation κ_0 below and near each seismological station in Croatia.

4.4. Discussion on the κ in Croatia

4.4.1. Correlation of site-specific attenuation κ_0 and local site parameter V_{S30}

The pioneering κ work by Anderson and Hough (1984) presented first observation of relationship between local site conditions and site-specific attenuation κ_0, (Figure 4.2, right) for which the sites on hard rocks have lower value of κ_0, and sites on soft sediments and rocks have higher κ_0 value. Through years this observation was considerably extended, and numerous studies proposed κ_0–V_{S30} correlations (Figure 4.3). Ktenidou et al. (2014) provided a thorough discussion on the scatter of κ_0–V_{S30} correlations, indicating that the differences between these empirical correlations may depend on the method for calculating or estimating value of site attenuation κ_0 and are also related to how site parameter V_{S30} is measured or estimated for certain local site. These differences increase the complexity when different relations are compared to each other and it is important that measured V_{S30} and calculated κ_0 values are consistently estimated.

The κ_0 has been used in host-to-target adjustment of GMPEs for rock-to-hard rock and site-specific response analysis of critical facilities such as nuclear power plants. Biro and Renault (2012) discussed that when the ground motion dataset of the target region is not available or is inadequate, near-site attenuation κ_0 can be estimated based on the available site parameters, mostly from V_{S30}, using existing κ_0–V_{S30} correlations (e.g., Figure 4.3, Ktenidou et al. 2014). Typically, this negative correlation is modelled by a linear function in log–log space. Again, here needs to be addressed that both variables κ_0 and V_{S30} have some uncertainties. The error in V_{S30} may even be significantly higher than the error in κ_0 (percentage-wise) which is due to several reasons that will be discussed in more detail in Chapter 6.3.2. κ_0–V_{S30} correlations for

regions like Northern California, France, and Switzerland were proposed by Silva et al. (1999), Douglas et al. (2010), Drouet et al. (2010) and Edwards et al. (2011), whereas Chandler et al. (2005) and Van Houtte et al. (2011) derived global relations based on data from California, Japan, and Taiwan (Table 4.3). Most of data are in ranges $620 \text{ m/s} \leq V_{S30} \leq 1500 \text{ m/s}$ and $0.01 \text{ s} \leq \kappa_0 \leq 0.04 \text{ s}$.

Based on the results of the linear regression analysis of $\kappa - R_e$, the estimated site attenuation κ_0 values for Croatia (Figure 4.15, Table 4.3) are typically lower ($\kappa_0 \leq 0.025 \text{ } s$) for stations located on hard rocks ($V_{S30} \geq 1100 \text{ m/s}$) compared to those stations on the soft rocks ($\kappa_0 > 0.025 \text{ s}$ and $V_{S30} = 760-1100 \text{ m/s}$) that are composed of surficial weaker material layers in the top few meters (Figure 4.7). It needs to be underlined that this study lacks the full range of V_{S30} data (i.e., from soft to hard rock soil profiles) to obtain a full-range $\kappa_0 - V_{S30}$ correlation for Croatian seismological network similar to the previously published ones (Figure 4.15). Keeping in mind that station local site values are $V_{S30} > 760 \text{ m/s}$ and HVSR measurements indicate low site amplification for all stations, it can be concluded that near-site attenuation κ_0 values measured in this study are representative for rock sites. Therefore, in Figure 4.15 (update of Figure 4.3. with κ_0 and V_{S30} values for Croatian stations) and in Table 4.3, compiled $\kappa_0 - V_{S30}$ values of rock sites for different global regions for which κ_0 values are calculated based on AH84 method, along with the measured κ_0 and V_{S30} values for Croatian stations, are presented and compared. Figure 4.15 and Table 4.3 shows that the near-site attenuation κ_0 values measured for Croatian stations are quite similar to the global κ_0 values published for rock sites previously.

As mentioned in Ktenidou et al. (2015), in the literature exist only few data for the high values of V_{S30} and very low values of κ_0 and vice versa. At hard rock levels, near-site attenuation κ_0 is mostly determined by the crust nature of the region (i.e., FAS is flat above corner frequency with little decay at higher frequencies with lower attenuation and for which the site amplification effects are negligible). For the bedrock sites with addition of upper soft sedimentary layers, value of κ_0 measured at the surface is increased from hard rock levels because of additional shallow local attenuation and presence of site amplification effects (e.g., Edwards et al. 2011).
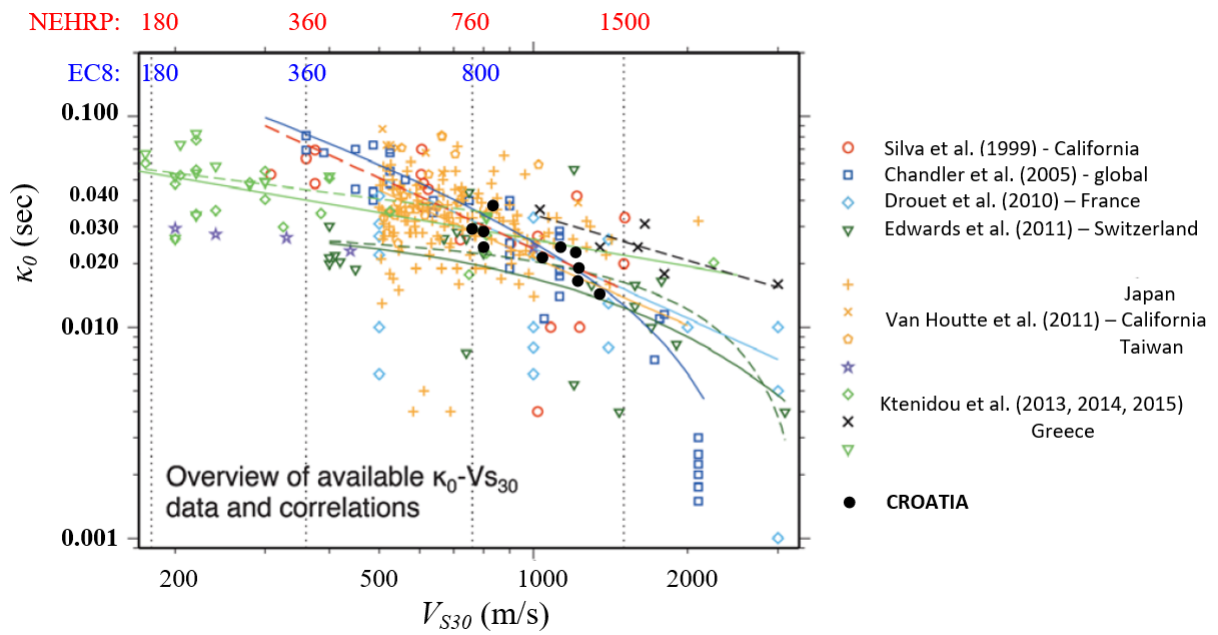
Figure 4.15. Existing $\kappa_0 - V_{S30}$ correlations in the literature (coloured markers and their fit lines for particular regions are shown in legend). Adapted from Ktenidou et al. (2014). κ_0 and V_{S30} values for Croatian stations are shown by black circles. Site V_{S30} classes from NEHRP (see BSSC 2009) (red numbers, dashed lines) and Eurocode 8 (blue numbers) are shown above plot.

Table 4.3. Summarized examples of previously published $\kappa_0 - V_{S30}$ correlations for a range of $V_{S30} = 620-1500$ m/s to compare estimated near-site attenuation κ_0 values for the Croatia with the global ones.

		Region	V_{S30} (m/s)	κ_0 (s)
Silva et al. (1999)		Northern California	760	0.032
			1070	0.022
			1500	0.015
Chandler et al. (2005)		Sino-Korean Paraplatform	1200	0.019-0.039
		South China Fold System	1500	0.014–0.028
		Generic Rock	650–850	0.035–0.040
		Iceland	650	0.040
		NEHRP Site Class C	700–1000	0.040–0.050
		Apennines, Italy Northeastern Italy	620	0.045–0.070
Douglas et al. (2010)		France	Soil sites	0.0270
			Rock sites	0.0207
Drouet et al. (2010)		France	1000	0.008–0.028
			1500	0.005–0.018
Edwards et al. (2011)		Switzerland	760	0.016–0.021
			1070	0.013–0.018
			1500	0.010–0.014
Van Houtte et al. (2011)		Japan/California/Taiwan	760	0.029
			1070	0.020
			1500	0.014
Van Houtte et al. (2014)		New Zealand	800–1100	0.025–0.040
Ktenidou et al. (2013, 2014, 2015)		Northern Greece (EUROSEISTEST)	EC8: A (> 800)	0.016–0.024
Perron et al. (2017)		Provence, France	720–1800	0.025–0.039
CROATIA	**KALN**		**760**	**0.0287**
	PTJ		**EC8–A**	**0.0281**
	OZLJ		**850**	**0.0372**
	RIY		**1190**	**0.0235**
	BRJN		**EC8–A**	**0.0241**
	NVLJ		**1270**	**0.0230**
	MORI		**1290**	**0.0194**
	CACV		**1050**	**0.0217**
	STON		**1390**	**0.0153**
	STA		**1280**	**0.0173**

4.4.2. κ and source dependence

In the previous extensive κ literature it is widely accepted that local site conditions are the dominant contribution to the site specific (near-site) attenuation κ_0 below and near the site. Possible source contributions to the high-frequency spectral parameter κ of the individual ground motion FAS have been discussed among researchers by comparing individual values of κ and M_L (e.g., Kilb et al. 2012).

Figure 4.16 evaluates the contribution of the source parameters on the estimated high-frequency spectral parameter κ by showing the distribution of individual values of κ with magnitude M_L for each station. Even though the scatter of $\kappa-M_L$ is considerably high, no clear trends with magnitude are observed. Because the number of data used in this study is limited, especially in the moderate-to-large magnitude range ($M_L > 4.5$) and because of lack of earthquakes at short epicentral distances ($R_e < 20$ km), this observation does not exclude the possible effect of the source (and near-source effect) on κ.

Anderson and Hough (1984) have chosen magnitude limit $M_L \geq 3.5$ (in this study $M_L \geq 3.0$) and $f_1 \gg f_C$ to exclude source effects on the κ calculation from the high-frequency part of FAS. Therefore, f_1 or f_{max} is always picked higher than f_C (e.g., Edwards et al. 2011; Ktenidou et al. 2013), to avoid any source effects as shown in Figure 4.17. The assumption of a negligible source contribution for κ relies on the validity of the ω-square source model (Brune 1970). Variation from this model, particularly bias between f_C and f_{max}, can affect estimation of the parameter κ. In this study it was estimated under the assumption that stress drop is constant (100 bars). Taking into account proper value of stress drop for each earthquake (or at least for the region), "real" value of f_C (manually chosen in this study) can be determined and bias between f_C and f_{max}, can be checked to avoid any influence of the decaying part of the source spectrum. In this case, lower magnitude limit can be properly determined (e.g., Perron et al. 2017). For the future works, new available data can be used to re-estimate $\kappa-M_L$ dependence and in combination with focal mechanism for each earthquake recording used for κ calculation, as suggested by Purvance and Anderson (2003), strong or negligible source effects on the κ can be determined.
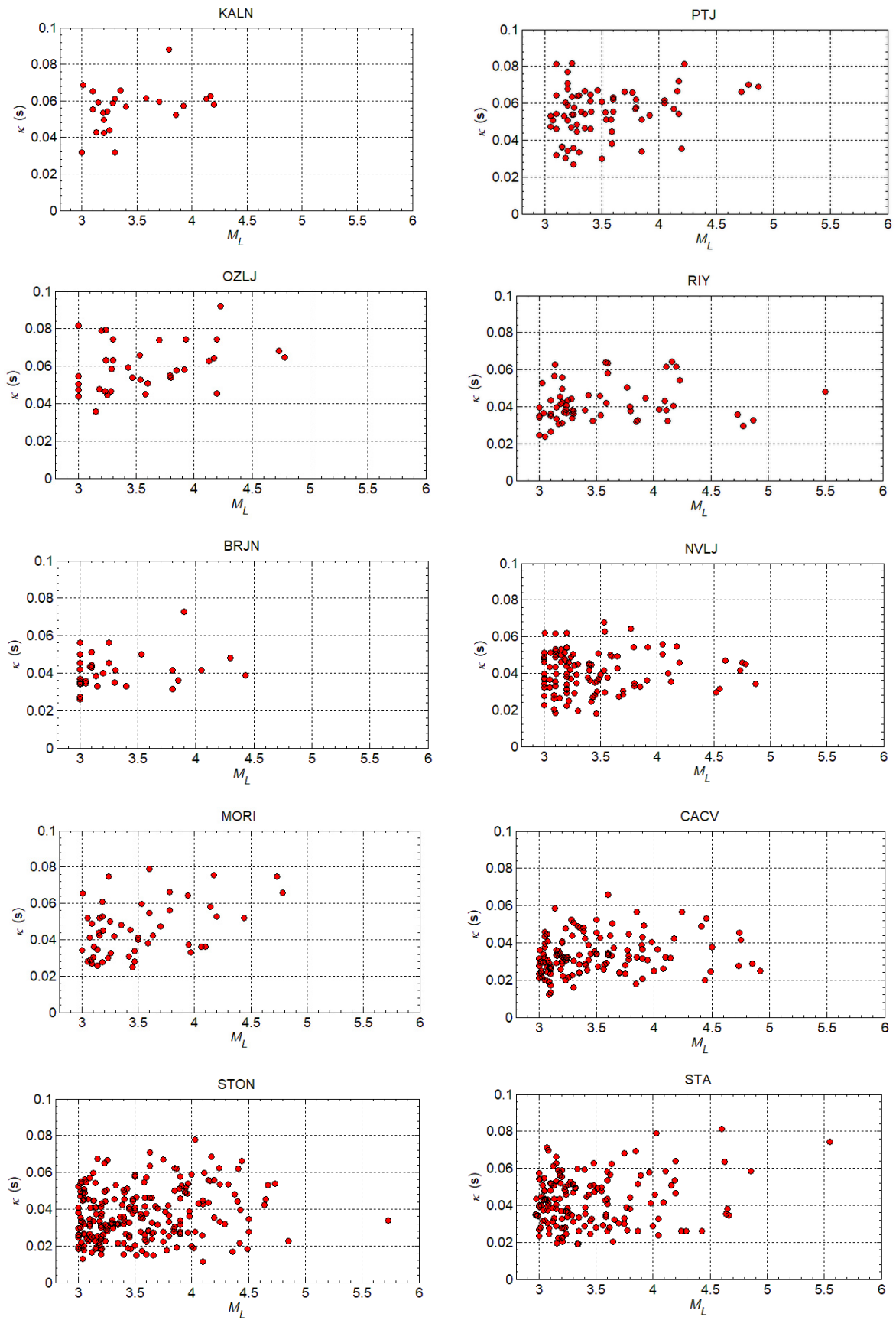
Figure 4.16. Individual horizontal κ dependence on M_L for seismic stations used in this study.
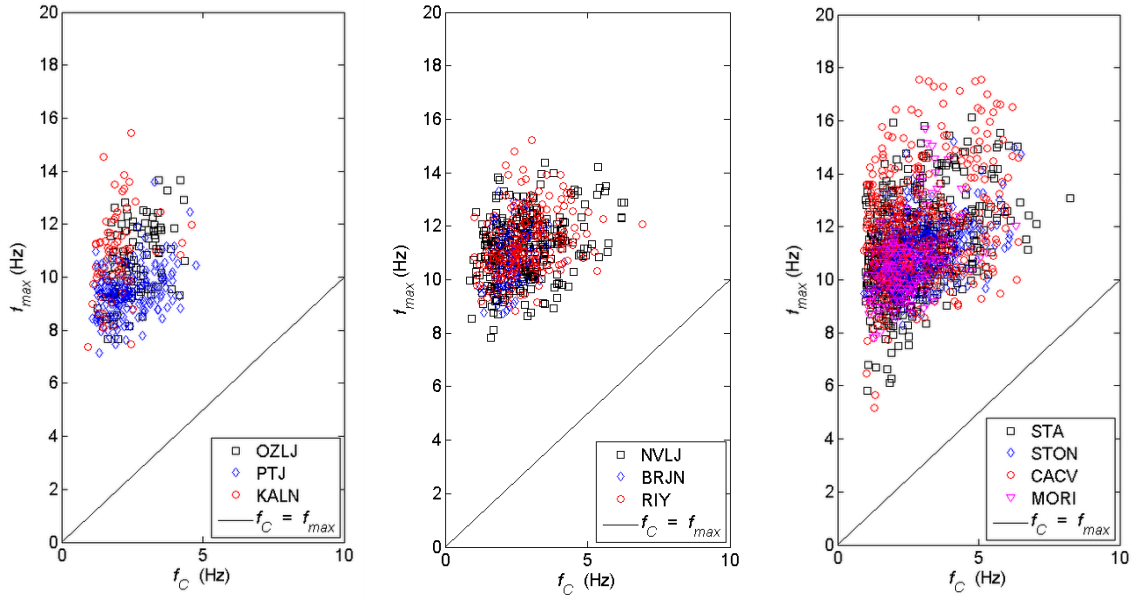
Figure 4.17: Comparison of manually picked f_{max} (or f_1) with f_C for each seismological station. Plots are separated into three groups according to their locations.

4.4.3. κ and regional attenuation

Geographical distribution of data sets used in this study (Figure 4.5) is limited by each station because of the specific geographical distribution of earthquake locations (Figures 4.4) and station operative years (Table 4.1). Question arises if the geographical orientation of data sets (distribution of the epicenters) influence the κ results, local site-specific κ_0 values and regional dependence. Studies of the Gentili and Franceschina (2011), Ktenidou et al. (2013) and Perron et al. (2017) are the only available attempts to include or exclude potential influence of the data set orientation. Castro et al. (2000) attributed κ scatter with distance as the effect of uneven attenuation near the source.

Van Houtte et al. (2014) used recordings from stations which had a wide range of events-to-station azimuths and assumed that any variation in κ with geographical orientation of the data is local effect rather than related to the azimuth. Therefore, to investigate the possible influence of the geographical distribution of the epicentres on the individual κ values and finally on the $\kappa-R_e$ models, the earthquakes are grouped into 30° bins. Note that azimuths were only used to group individual κ values in bins of 30° with respect to azimuthal distribution of R_e (Figure 4.5). Individual κ-groups (bins of 30°) are plotted as a function of epicentral distance R_e and presented in Figure 4.18. κ-groups for different azimuth bins and for similar epicentral distance

show similar κ values despite geographical distribution and variety of source-site paths. Also, for the same azimuthal bin and different epicentral distances, κ values are different. There is no systematic behaviour of certain κ-groups with respect to geographical orientation of epicentre locations. The same conclusion was derived by Ktenidou et al. (2013) and Perron et al. (2017).

Gentili and Franceschina (2011) divided data into eastward and westward azimuth subsets (0°–180° and 180°–360°) to prove regional dependence of κ on the earthquake location. They observed different trends of the high-frequency attenuation between westward and eastward azimuthal area subsets. Data from earthquakes located westward showed weaker attenuation properties with hypothesized S-wave reflections from different parts of the Moho discontinuity under the eastern Po Plain, at about 25–30 km depth. Data from earthquakes located eastward (in western Slovenia), where the Moho deepens up to 45–50 km, showed higher attenuation. These effects were explained by observations that fault zones are often characterized by complex rupture pattern that favour both scattering and generation of trapped waves (within the waveguides) in terms of 10–20 km propagation through low velocity and spatial variation of low intrinsic Q_i near the source, caused by the high level of fracturing that characterizes the fault zones.

The conclusions by Gentili and Franceschina (2011) were derived based on comparison of different values of regression slopes κ_R from stations from different areas. This study presents first ever attempt in κ studies (to the best of author's knowledge) to demonstrate regional κ dependence around each station with spatial distribution of the individual κ values. Individual κ values are plotted using interpolation method (nearest neighbour in the Surfer, Golden Software) to present regional variation of the κ around each station (Figure 4.18, figures below each regression plot). Spatial distribution presents characteristic κ regional variation from each station and for earthquakes occurring within each colour-represented zone. The lowest κ values are spatially distributed within a few kilometres around the stations due to near-site effects. Gradual increase of κ with distance from the stations in the circular-shape distribution confirms that the path effect is attributed to the κ as described by the slope regression κ_R which represents the effects of the regional attenuation (Eq. 4.5). Circular-shape (or close to circular shape) κ distribution is observed for all stations where the dominant near-site attenuation is mainly due to the wave propagation through the shallow crust below and near the site within few kilometres with contribution of the regional attenuation at higher epicentral distances. Deviations from circular/elliptical-shape κ distribution could indicate that beside regional attenuation, other

effects such as local intrinsic attenuation anisotropy (Barton 2007) from different causes (e.g., scattering due to heterogeneity, fracturing, flow of fluids in rocks) could have effect on the κ distribution. Local and regional geological and tectonic characteristics around each station are important to define primary effects on the κ distribution and will be discussed in more detail below Figure 4.18.
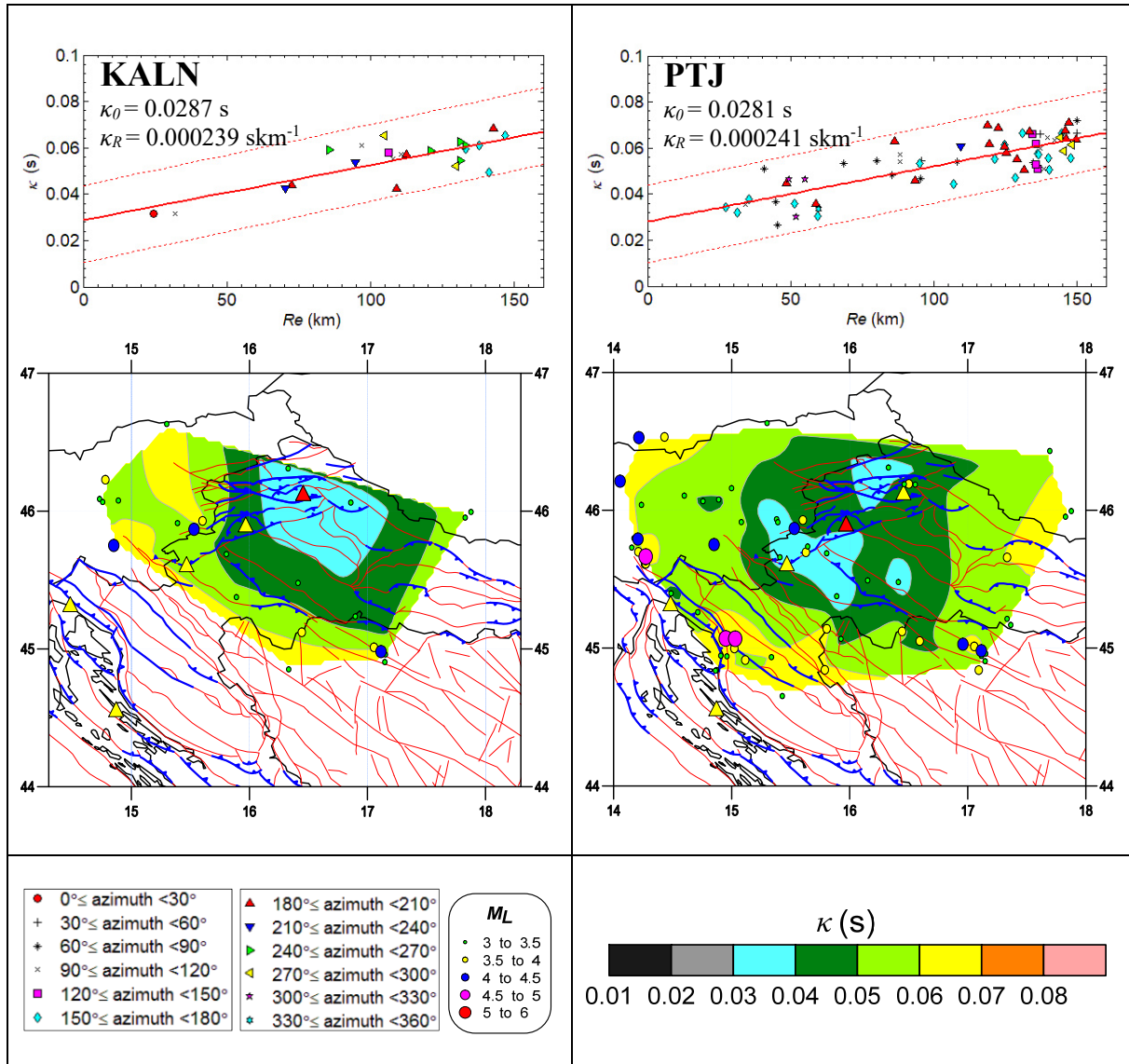
Figure 4.18. Individual κ values plotted as a function of R_e for κ-groups of 30° bins with regression line and 95 % confidence interval for each seismological station (upper figures). Regional κ dependence around each seismological station presented as spatial distribution of the individual κ values plotted using the nearest neighbour interpolation method (bottom figures). Spatial distribution presents characteristic κ regional variation for each station – equally coloured areas indicate κ at respective stations representative for events occurring within those areas. Red lines in bottom figures represent known surface faults and blue lines active faults in Croatia and Bosnia and Hercegovina (Ivančić et al. 2006). Locations of seismic stations are marked with red triangles and neighbouring stations with yellow triangles.

Figure 4.18. ►continued

112
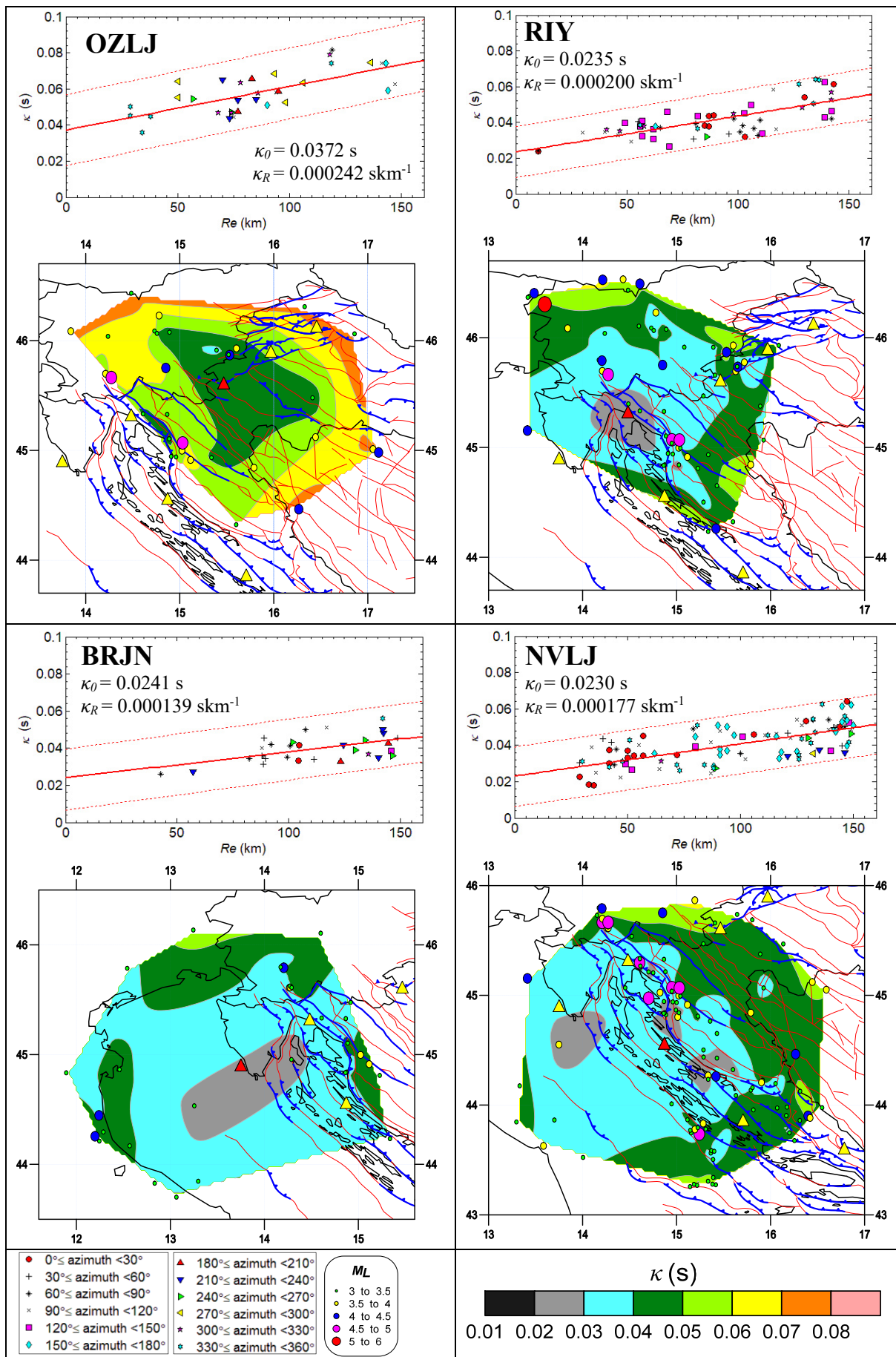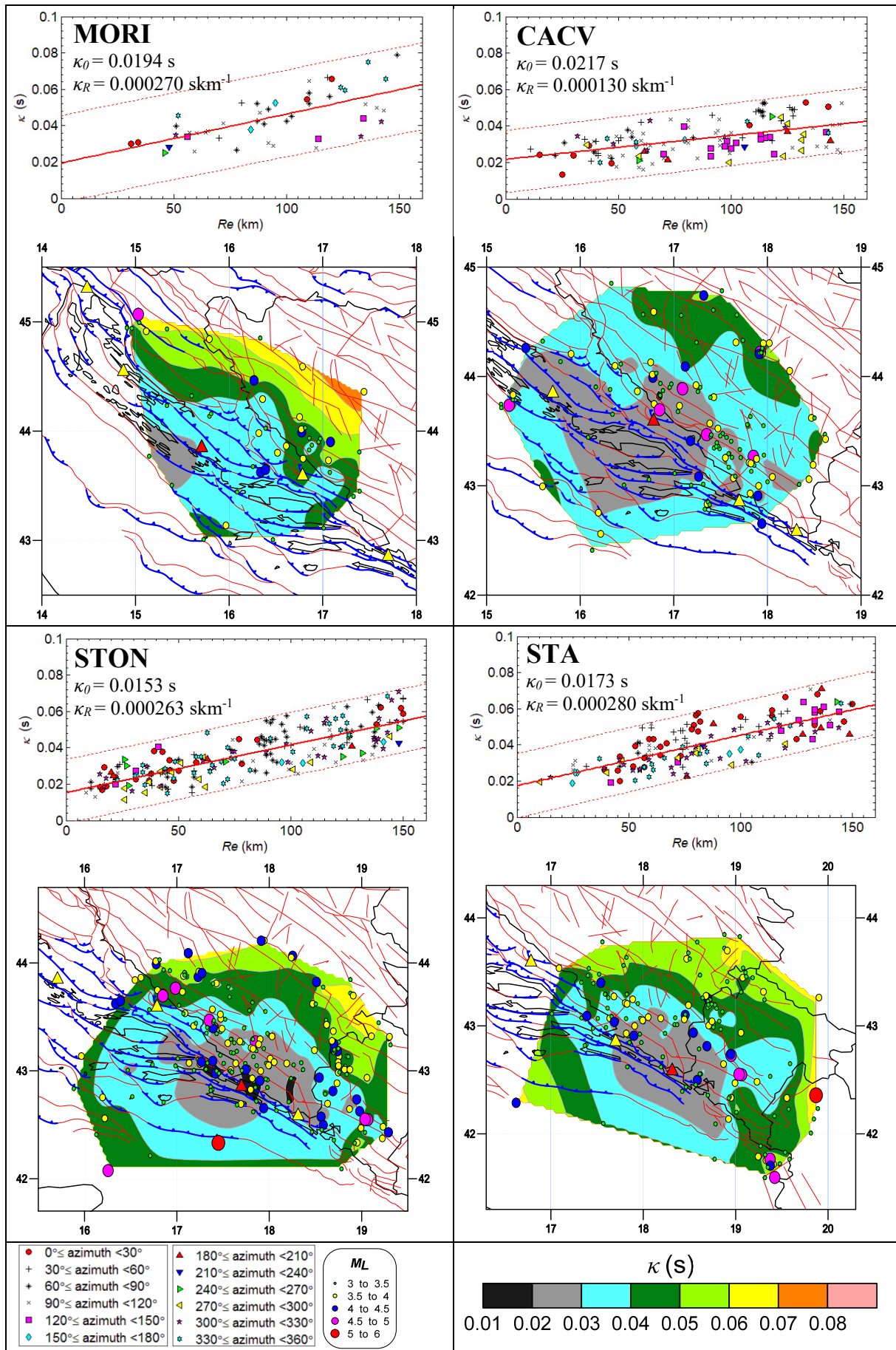
Figure 4.18. ►continued

Stations STA and STON are relatively close to each other (approx. 50 km) with similar local characteristics ($V_{S30} > 1200$ m/s), regional geology (Cretaceous and Palaeogene rocks and High Karst Nappe, Figure 4.6) and tectonic environment (transition from southeastern Dinarides to Albanides). For both stations, values of near-site attenuation κ_0 and regression slope κ_R (regional term of distance dependent attenuation) (Table 4.2) are comparable indicating similar upper crust regional/tectonic contribution to the κ distribution (closely to circular/ellipsoid shape) under influence of fault distribution in the area. Both stations (STON and STA) show anisotropy in regional attenuation: for the same distance, higher κ values are spatially distributed in the direction perpendicular to the strike of the Dinarides than those distributed parallel to it. For the same stations (located in southern Dinarides), anisotropic characteristics of attenuation were observed by Dasović (2015a) by analysis of the azimuthal dependence of Q_P and Q_S.

Observed deviation from the circularly shaped κ distribution for MORI and CACV stations besides the regional upper crust attenuation (significantly different values of κ_R between CACV vs. MORI, STON and STA) could perhaps be explained by the Dinarides transition zone dissected by main active faults in the area (Figure 4.18). These two stations are characterized by different local and regional geology (Figure 4.6): CACV is situated in the hilly area of Jurrasic and Cretaceous carbonate deposits with nearby alluvium of the Cetina river (Figure 4.6), while MORI area is composed of Cretaceous–Palaeogene folded complex (Figure 4.6). Lowest κ values spatially distributed around both stations are attributed to local geology. Most of recorded earthquakes at CACV and MORI are from the area around the international border between Croatia and Bosnia and Herzegovina. CACV is at the one side of active fault zone (marked with blue lines) close to Bosnia and Herzegovina and MORI at the other side close to Adriatic Sea and the active tectonic zone could influence the geometry of the kappa contour lines in this area. Gentili and Franceschina (2011) tried to explain similar differences in weaker/higher κ attenuation zones with S-wave reflections from the Moho discontinuity and with complex fractured fault zone that generates waveguides and trapped waves. The upper crust at the station CACV is up to 28 km thick with carbonate sediments up to 11 km thick and Moho depth at about 58 km, suggest possible overlapping of two tectonic units as the result of the Adria–Dinarides collision and Adria's counterclockwise rotation (model presented in Stipčević et al. 2011). Towards MORI, Moho isobaths from Stipčević et al. (2011) show depth approx. 40 km.

Station NVLJ is situated on the island of Pag composed of Upper Cretaceous limestones and Palaeogene–Neogene limestone breccias and rudist limestones (Figure 4.6). Spatial κ distribution shows that the regional attenuation due to distance from north to southeast tends to be less intense than the one at MORI and more similar to the values at RIY. For both stations, values of κ_0 and κ_R (Table 4.2) are comparable indicating similar upper crust regional attenuation contribution to the κ estimated from earthquake recordings on these stations. The lack of data limits the κ distribution from the part of Adriatic Sea. The problem of coastal stations is that they are affected by few earthquakes from the Adriatic Sea (mostly around Dugi Otok, Palagruža and Jabuka islands). Station RIY is situated in the Rijeka bay area composed mainly of Cretaceous limestones and dolomites (Figure 4.6). κ distribution for RIY is similar as NVLJ, probably due to the similar regional geological and tectonic characteristics around these stations. κ distributions for CACV, MORI, NVLJ and RIY show different anisotropic behaviour than the anisotropic observations by Dasović (2015a). These four stations show similar behaviour as STON and STA, higher κ values spatially distributed in the direction perpendicular to the strike of the Dinarides and lower κ values spatially distributed parallel to it, whereas Dasović (2015a) found for the northern and central External Dinarides weaker Q_P and Q_S attenuation in the direction perpendicular to the Dinarides strike. These effects and comparison between kappa and frequency-dependent $Q(f)$ will be discussed in more detail in next chapter. Station BRJN (Lower Cretaceous limestones and dolomites, Figure 4.6) is close to RIY and NVLJ stations, but due to the limited number of data at larger epicentral distances and fewer data at shorter distances, the interpolation of the κ distribution is very rough, and no concrete conclusions can be drawn. The κ results on these three stations could indicate difference between shallow crustal attenuation properties of the undeformed part of the Adriatic microplate and External Dinarides. More earthquake data are needed to be included in the future for the κ estimation to support and present conclusions on this issue for this area.

Station OZLJ is situated in the transitional zone between External Dinarides and Pannonian Basin in the zone composed mainly of deposits of flysch which transgressively cover Upper Jurassic peri-reefal dolomites and alluvium of river Kupa (Figure 4.6). Higher κ values probably resulted from the higher attenuation zone of alluvium of rivers near Karlovac. The problem of very rough κ distribution presents the limited number of data which is also the case for BRJN and KALN stations. Station PTJ is situated on the top of the Medvednica Mt. as a part of Pannonian Basin–External Dinarides transition zone. The station site area is composed Palaeozoic–Triassic ortometamorphites and parametamorphites, while in the lowland Zagreb

area, Holocene alluvial terraces of the rivers Sava to the south and Krapina are present (Figure 4.6). Observed κ distribution in this zone is clearly divided between lower and higher κ values due to presence of local and regional geological structures; to the north influenced by Ivanščica Mt. and Kalnik Mt., to the south by Žumberak Mt. and Samobor highlands, in its centre by Medvednica Mt. and the Sava river zone. Station KALN also shows very rough κ distribution, with visible trend influenced by Ivanščica Mt. (carbonate rocks) and Kalnik Mt. (Jurassic ophiolitic magmatic rocks and Palaeogene deposits) and nearby rivers alluvium areas (Mura, Drava) (Figure 4.6). Circular or close to circular/elliptical trends in the κ distribution are visible for these three stations. Few deviating cases are probably due to presence of complex geological environments and rough interpolations of κ due to the limited number of data.

4.4.4. κ and frequency-dependent $Q(f)$ function

High-frequency attenuation spectral parameter κ was calculated from the acceleration FAS of the S-waves by assumption that effective quality factor Q in the near-surface rocks (approx. depths up to 2–3 km) is frequency-independent as described by Eq. (4.2). In this case the frequency-independent effective quality factor Q at high frequencies can be estimated from the regression slope of the empirical model, κ_R, using Eqs. (4.2 and 4.3) (e.g., Anderson and Hough 1984; Edwards et al. 2011; Gentili and Franceschina 2011; Ktenidou et al. 2015):

$$Q \approx \frac{1}{\beta_0 \kappa_R} \qquad (4.7)$$

Most κ studies follow classical Anderson and Hough (1984) method to compute κ from high-frequency part of FAS in linear–logarithmic scale without correcting them for frequency-dependent $Q(f)$. Edwards et al. (2011) computed t^* (Eq. 4.3) from κ with correction for the frequency dependent $Q(f)$. Observed differences $\Delta\kappa$ relative to $Q(f)$ models were mostly small with exceptions. Based on this observation, Edwards et al. (2011) concluded that $Q(f)$ correction had small effect on the final estimate of site-specific value κ_0 and that it is better to use the assumption of frequency-independent Q in the κ calculation.

Recently, several attenuation studies of coda waves in Croatia were published by application of Aki and Chouet (1975) single backscattering model to determine Q_C (Dasović 2015a; Dasović et al. 2012, 2013, 2015b; Majstorović et al. 2017). Using the recently published values of Q_0^C

(attenuation of coda waves) and Q_0^S (attenuation of S-waves) and frequency-dependent exponents n_C and n_S in the form $Q_{est}^{C,S}(f) = Q_0^{C,S} f_{C,S}^n$ (Eq. 2.12) , it is possible to compare estimated values of frequency-dependent $Q_{est}^{C,S}(f)$ for the high-frequency range (10–25 Hz) with frequency-independent $Q_{est}(\kappa_R)$ (Eq. 4.7) from two independent attenuation studies (Table 4.4) as some recent studies suggest (e.g., Ktenidou et al. 2015; Perron et al. 2017). Frequency-dependent values Q_0^C and Q_0^S in Table 4.4 corresponds to the values of $Q(f)$ determined for the lapse time of the coda time window $t_L = 30$ s and represents scattering and intrinsic attenuation losses within the crust (crustal events) at depths less than 40 km (Dasović et al. 2015b). Estimated value of $Q_{est}(\kappa_R)$ using Eq. (4.7) was calculated assuming an average crustal shear wave velocity of $\beta_0 = 3.5$ km/s.

Several studies indicated possibility that $Q_{est}^{C,S}(f)$ from the coda waves (or S-waves) estimated for the high-frequency range and $Q_{est}(\kappa_R)$ calculated from κ_R (Eq. 4.7) yield approximately similar values (e.g., Edwards et al. 2011; Gentili and Franceschina 2011; Ktenidou et al. 2013, 2015). Taking into account inherent errors of Q- and κ-measurements, the corresponding values for the Croatian station given in Table 4.4, show that this is mostly also the case here.

Table 4.4: Values of Q_0^C, Q_0^S, n_C and n_S for the lapse time of the coda time window $t_L = 30$ s from *Dasović et al. (2013) and **Dasović (2015a) in the form: $Q_{est}^{C,S}(f) = Q_0^{C,S} f_{C,S}^n$ estimated for the high-frequency range (10–25 Hz) and compared with frequency-independent $Q_{est}(\kappa_R)$ estimated from the regression slope κ_R (Eq. 4.7). ***For BRJN station no published information regarding frequency dependent $Q(f)$ exists.

Station	Q_0^C	n_C	Q_0^S	n_S	Q_{est}^C (10–25 Hz)	Q_{est}^S (10–25 Hz)	$\kappa_R (\text{skm}^{-1})$	$Q_{est}(\kappa_R)$
KALN*	102	0.68	–	–	488–782	–	0.000239	1195
PTJ*	78	0.69	–	–	382–616	–	0.000241	1186
OZLJ**	78	0.69	140	0.68	382–616	670–1074	0.000242	1181
RIY**	84	0.93	80	0.73	715–1362	430–713	0.000200	1429
BRJN***	–	–	–	–	–	–	0.000139	2055
NVLJ**	89	1.16	82	0.65	1286–2875	366–575	0.000177	1614
MORI**	112	0.81	75	0.75	723–1268	422–709	0.000270	1058
CACV**	71	0.88	94	0.65	539–991	420–659	0.000130	2198
STON**	65	0.96	67	0.71	593–1153	344–562	0.000263	1086
STA**	77	0.84	148	0.51	533–954	479–682	0.000280	1020

Direct comparison between two different approaches to represent attenuation (coda waves and κ) for Croatia presented in Table 4.4 is, however, not straightforward, and several issues must be considered. Firstly, the data range in terms of magnitude, epicentral distances and frequencies used in the abovementioned attenuation studies are different than the data ranges used herein. For instance, frequencies considered here are generally larger than those used in coda-Q analyses, thus requiring extrapolations. Secondly, the inherent errors in experimental determinations of Q_C or Q_S and κ_R are substantial (often of the order of $\pm$ 50 %). And thirdly, there is a fundamental difference in one of the basic assumptions, the one of the frequency (in)dependence of Q.

Comparison of Q-values and κ_R was done in numerous studies in other regions of the world. For instance, Perron et al. (2017) compared estimated Q values from κ_R and attenuation studies for the high-frequency range 16–32 Hz in France, and found large discrepancy between two approaches mainly due to inconsistency with the previous attenuation studies and used techniques to evaluate attenuation Q and κ values. In the AH84 method the implicit assumption is that Q is frequency-independent in the shallow upper crust of few hundred meters up to few kilometres for the high-frequency range (f_1-f_2) where κ is calculated. $Q_{est}(\kappa_R)$ values given in Table 4.4 are comparable with values of κ_R and Q values published previously for some regions similar to the Croatia region. Studies of Edwards et al. (2011) (for Switzerland), Drouet et al. (2010) and Douglas et al. (2010) (for France) yield similar frequency-independent $Q = 1000-2000$ estimated from similar κ_R values as this study. Ktenidou et al. (2013, 2015) estimated regional Q of approx. 500–600 between 15–30 Hz for Greece. Gentili and Franceschina (2011) investigated the high-frequency attenuation of S-waves in the southeastern Alps and northern External Dinarides (northeastern Italy). Average frequency-independent $Q = 2140$ was estimated from the κ_R for the corresponding crustal layer between 5 and 15 km depth.

Classical AH84 method is clearly easier to use in the higher seismicity regions as southern California due to large amount of strong motion earthquake data (Anderson and Hough 1984). For this region observed tendency of slow increase of κ (smaller κ_R) with distance implies higher Q values (1000–3000) and the faster increase of κ (higher κ_R) with distance lower Q values (300–1000) which is followed in most kappa studies that used linear $\kappa-R_e$ formulation. Also, the κ_R values that describe regional distance-dependence of κ given in Van Houtte et al. (2011) (for Japan KIK-Net network, California, and Taiwan) are quite similar to the estimated

values of κ_R for some stations in this study. As reported in Gentili and Franceschina (2011) and Ktenidou et al. (2014) it is possible that similar sites exhibit quite large regional differences due to the variability of the underlying Q and V_S structures (e.g., Boore and Joyner 1997; Chandler 2005).

Taking into consideration the issues enumerated above, the results presented in Table 4.4, as well as similar conclusions of other studies, hint to the conclusion that the high-frequency decay of FAS as modelled by κ, has its roots in anelastic (intrinsic) and scattering attenuation properties of the rocks along the path from the source to the receiver.

From the spatial κ distribution presented in Figure 4.18 for each station, it can be concluded that attenuation properties of rocks in the Dinarides are far from isotropic. In general, we observe larger attenuation in directions perpendicular to the mountain chains and to the strike of major regional faults, then parallel to them. The source of this anisotropy is still not confidently determined – the most likely candidates are the preferential orientations of cracks and fractures under the local tectonic stress field, trapping of waves along major faults (waveguides), or attenuation within the fault zones (e.g., Lokmer and Herak 1999; Dasović 2015a).

The values of $Q_{est}(\kappa_R)$ (Table 4.4) that represent the total average regional crustal attenuation around each station, can be tentatively related to the major tectonic units (Figure 4.3). Similar values of $Q_{est}(\kappa_R)$ for KALN, PTJ and OZLJ stations could possibly represent transitional zone between the Pannonian Basin and Internal Dinarides (e.g., Vlahović et al. 2005; Tomljenović et al. 2008). The values of $Q_{est}(\kappa_R)$ could define the transition zone of undeformed Adriatic Microplate (BRJN station) into deformed part of Dinarides (RIY and NVLJ stations) (e.g., Handy et al. 2015). Transitional zone between External Dinarides into Internal Dinarides could explain a large difference between values of $Q_{est}(\kappa_R)$ for MORI and CACV station areas. Also, significant differences between values of $Q_{est}(\kappa_R)$ in the zone NVLJ–MORI–CACV could be explained by strong intrinsic attenuation related to the highly fractured and karstified carbonates and fractures that are expected to be partially or fully filled with fluids in this part of the Dinarides (e.g., Majstorović et al. 2017). In a similar manner, values of $Q_{est}(\kappa_R)$ for MORI, STON and STA stations could represent the regional attenuation of southern External Dinarides. Such conclusions need to be taken cautiously, especially for some stations with small number and narrow azimuthal distribution of data. The main problem in interpreting regional κ

variation/attenuation and its connection with local/regional geological and tectonic environment lies in the proper definition of tectonics (deformed or undeformed plates, fault description) and whether the shallow crustal deposits are thin or thick close to the surface with different geological characteristics at each station area. In this case structural geological and tectonic studies should be incorporated into future κ study for Croatia together with the new available earthquake data from these and other stations.

The solutions to the above-mentioned problems remain open and require extensive future work. Major limitation of the use of Anderson and Hough (1984) classical κ approach in low-to-moderate seismicity areas such as Croatia presents limited quantity and bandwidth of the usable earthquake data for the κ calculation. To overcome problem with data limitation, one possibility is to use displacement FAS from smaller earthquake magnitudes and compare estimated κ values with AH84 method as presented in some studies (e.g., Biasi and Smith 2001; Kilb et al. 2012 and Perron et al. 2017). Also, there is a possibility to remove $Q(f)$ effect from the acceleration FAS to limit possible influence of the $Q(f)$ on the κ, so that the values of two independent attenuation approaches (κ, Q) can be compared (Edwards et al. 2011). The most recent work of Mayor et al. (2018) suggest that AH84 method applied for the S-wave window as in this study can also be applied to coda window. Their results show that Q_C is related to Q from κ_{coda} and show significant regional variation. The relation between κ_{AH} (e.g., this study) and κ_{coda} (and Q_C) needs further studies due to the scarcity of data as presented in this study and also in Mayor et al. (2018) which is a general problem in the much-debated kappa studies.

Results presented in this chapter extend our knowledge on the attenuation of the near-surface crustal layers in Dinarides and provide valuable information on the local source model parameters to be used in host-to-target adjustment of GMPEs and site-specific response analysis in Croatia using RVT-based approaches presented in the next chapter. The main input for the RVT-based site response analysis is the acceleration FAS defined by local and regional seismological parameters (particularly near-site attenuation κ_0) for moderate to strong earthquake scenarios to match target PGA_{ROCK}.

5. Analysis of the local site effects site on the amplification of seismic ground motion in Croatia using EQL RVT-based method

To evaluate local site effects on the strong ground motions, equivalent–linear (EQL) one-dimensional (1-D) site response analysis using RVT-based method is utilized for different sites with measured shear wave velocity profiles around Croatia. The main reason to prefer the relatively new RVT-based method instead of classical TS-approach is the limited or none-existing strong motion database in Croatia as discussed in Chapter 3.3.2. For the 1-D EQL site response analysis RVT-based method, single FAS is sufficient to represent input ground motion; therefore, the recorded strong ground motions are not needed as input. Regional seismological parameters (e.g., magnitude, epicentral distance, focal depth, seismic attenuation, near-site attenuation) are used to define the input rock motion based on the target FAS. In this chapter, 1-D EQL site response analysis is conducted for each site at different input ground motion levels by employing the RVT-based method. The main outcome of 1-D EQL site response analysis is the site-specific amplification factor $AF(T)$ as a function of frequency or period. Selected sites are classified into different categories based on the shear wave velocity profile, the average AFs for each category are presented, and their dependency on the ground shaking level is discussed within this chapter.

5.1. Selection of the earthquake scenarios for the input rock motion for RVT-based analysis

The input rock motion in terms of FAS required for the RVT-based method is developed analytically using the Brune (1970) ω-square point-source stochastic spectrum as a function of the source, propagation path, and site characteristics (here the term "site characteristics" only represents the effect of the near-surface rock layers, not the effect of the overlying soil layers)

as described in Chapter 2. Beyond the earthquake magnitude and the source-to-site distance, most important parameters affecting the shape of the spectrum are the propagation-path attenuation effects: the frequency dependent attenuation $Q(f)$ and the near-site attenuation κ_0. Different combinations of these parameters can be adopted to obtain the FAS that is compatible with the target design spectrum for the bedrock conditions (in this study consistent with values of peak ground accelerations for a return period of the 475-years ground motions in Croatia) as discussed in Boore (2003), Rathje and Ozbey (2006) and Walling et al. (2008).

In each 1-D EQL analysis, some of the seismological parameters are kept unchanged such as the stress drop, focal depth, values of the crustal shear wave velocity, density, $Q(f)$ and κ_0 defined for each station. Stress drop, $\Delta\sigma$, is set to the prescribed constant value of 100 bars (e.g., Hanks and McGuire 1981; Boore 1983, 2003); therefore, the source spectrum depends only on the moment magnitude (or local magnitude). Fictitious focal depth $h = 12$ km as the average value of foci in Croatia is used (Herak et al. 1996). The average values of the crustal shear wave velocity $\beta_0 = 3.5$ km/s and density $\rho_0 = 2800$ kg/m^3 are utilized. Frequency dependent attenuation, $Q(f)$ values, for the coda and S-waves are adopted from Dasović et al. (2013) and Dasović (2015a) (Table 4.4). The near-site attenuation parameter κ_0 was calculated in the previous chapter for each station (Table 4.2) and is used to describe the shape of local/regional FAS at high frequencies.

Other seismological parameters used for the RVT-based site response analysis approach are selected to match the specific target value of the peak ground acceleration (PGA_{ROCK}) for each analysis. To evaluate the soil's behaviour in the linear and non-linear input motion ranges systematically, different input motion intensity levels are defined in terms of PGA_{ROCK}. The earthquake scenarios used to generate different input intensities of PGA_{ROCK} (from very weak 0.03 g to relatively strong 0.37 g that corresponds to return period of 475-years for Ston, see Table 4.1) are given in Table 5.1. In the RVT-based site response analysis, the input motion is characterized by the amplitude of the FAS (Eqs. 3.26 and 3.33) and the ground motion duration (T_{gm}). Ground motion durations for each input motion level are calculated using Eq. (3.28) and provided in Table 5.1.

Eight different magnitude values varying between $M_L = 5.0$ and $M_L = 7.1$ are pre-selected for the analysis. Scenarios with $M_L \leq 5.5$ were chosen as a reference to EC8 Type 2 spectrum (defined for regions where hazard estimates are mostly influenced by earthquakes with the

magnitude $M_S \leq 5.5$) and scenarios with $M_L > 5.5$ with respect to EC8 Type 1 spectrum (defined for regions where earthquakes that contribute most to the hazard have magnitudes $M_S > 5.5$). Some of the historical earthquakes were used as a reference to define the scenarios with $M_L > 6.0$ (e.g., Varaždin 1459, Dubrovnik 1667, Zagreb 1880 and Ston 1996 earthquakes). Empirical relationship between moment magnitude M_W and local magnitude M_L for Croatia (originally from Duni et al., 2010; later updated by Markušić et al. 2016) is used to convert local magnitudes determined for each scenario to moment magnitudes as:

$$M_W = -0.11 + 1.011 \cdot M_L \qquad (5.1)$$

The rupture lengths for the magnitudes used in this study (Table 5.1) are approx. 2 km for lower magnitudes and 30 km for very strong earthquakes according to the Wells and Coppersmith (1994) magnitude-rupture length relation. Although the earthquake source cannot be approximated by the point source model for very strong earthquakes, the extensive literature on RVT-based approach provided the evidence that RVT can provide reasonable estimates and the results are similar to the TS-approach at shorter and larger epicentral distances (from 10 to 100 km as shown by Hanks and McGuire 1981) and for earthquakes $M_W = 5.0-7.7$ (Boore 1983). An equivalent point-source model based on the effective distance concept can successfully predict the average ground motions from $M_W > 6$ earthquakes at a wide distance range, including short distances (< 20 km) (e.g., Yenier and Atkinson 2014) and is incorporated into STRATA program for the EQL–RVT analysis through hypocentral distance definition in the geometrical attenuation spreading function $Z(R) = 1/R$ for shorter distances (Eq. 2.12). Silva et al. (1997) provided one of the most extensive description and thorough validation of stochastic ground motion model with the use of point source FAS model in RVT-based equivalent–linear site response analysis. Their analyses involve modelling of 15 earthquakes in the range of magnitudes $M_W = 5.0-7.5$ and different distance ranges (1 km to 200 km for WNA and 5 km to 450 km for ENA data) at over 500 sites with different generic site characteristics. Results demonstrated that stochastic point source models produce accurate predictions of strong ground motion over the distance range of 0–100 km for magnitudes $M_W = 5.0-7.5$.

Table 5.1. Variable seismological parameters by each station: $M_L, M_W, R_e, Z(R), T_{gm}$ scaled to target $PGA_{ROCK} = $ 0.03 g, 0.06 g, 0.10 g, 0.15 g, 0.20 g, 0.25 g, 0.30 g and 0.37 g. Local magnitudes M_L are converted to moment magnitudes M_W using Eq. (5.1). For a selected earthquake scenario in terms of M_L, epicentral distance R_e was varied manually so that input FAS and response spectrum are compatible with the target value of PGA_{ROCK} ($Sa@0.01$ s in input response spectrum, see Figure 5.1). Geometrical attenuation spreading $Z(R)$ is calculated from hypocentral distance $R = \sqrt{R_e^2 + h^2}$ using Eq. (2.12) for shorter epicentral distances and ground motion duration T_{gm} using Eq. (3.28) as a function of source and path.

	PGA_ROCK = 0.03 g					PGA_ROCK = 0.06 g				
Station	M_L	M_W	R_e(km)	$Z(R)$	T_{gm} (s)	M_L	M_W	R_e(km)	$Z(R)$	T_{gm} (s)
STA			30	0.0309	2.50			24	0.0373	2.60
STON			28	0.0328	2.42			22	0.0399	2.55
CACV			27	0.0338	2.32			21	0.0413	2.47
MORI			28	0.0328	2.41			22	0.0399	2.51
NVLJ	5.0	4.95	24	0.0373	2.23	5.3	5.25	19	0.0445	2.38
BRJN			26	0.0349	2.32			20	0.0429	2.42
RIY			26	0.0349	2.32			21	0.0413	2.42
OZLJ			23	0.0385	2.19			17	0.0481	2.30
PTJ			23	0.0385	2.19			17	0.0481	2.31
KALN			25	0.0361	2.28			19	0.0445	2.34
	PGA_ROCK = 0.10 g					PGA_ROCK = 0.15 g				
Station	M_L	M_W	R_e(km)	$Z(R)$	T_{gm} (s)	M_L	M_W	R_e(km)	$Z(R)$	T_{gm} (s)
STA			18	0.0462	2.66			17	0.0481	3.27
STON			18	0.0462	2.66			16	0.0500	3.23
CACV			15	0.0521	2.54			13	0.0565	3.12
MORI			17	0.0481	2.62			15	0.0521	3.19
NVLJ	5.5	5.45	14	0.0542	2.50	5.8	5.75	12	0.0589	3.08
BRJN			15	0.0521	2.54			13	0.0565	3.12
RIY			16	0.0500	2.58			13	0.0565	3.12
OZLJ			11	0.0614	2.40			8	0.0693	2.98
PTJ			12	0.0589	2.43			10	0.0640	3.01
KALN			13	0.0565	2.47			11	0.0614	3.05
	PGA_ROCK = 0.20 g					PGA_ROCK = 0.25 g				
Station	M_L	M_W	R_e(km)	$Z(R)$	T_{gm} (s)	M_L	M_W	R_e(km)	$Z(R)$	T_{gm} (s)
STA			15	0.0521	3.77			15	0.0521	4.93
STON			14	0.0542	3.73			14	0.0542	4.89
CACV			11	0.0614	3.63			12	0.0589	4.82
MORI			10	0.0640	3.66			12	0.0589	4.86
NVLJ	6.0	5.96	10	0.0640	3.59	6.3	6.26	10	0.0640	4.75
BRJN			11	0.0614	3.63			11	0.0614	4.79
RIY			11	0.0614	3.63			12	0.0589	4.79
OZLJ			7	0.0720	3.51			8	0.0693	4.69
PTJ			8	0.0693	3.53			9	0.0667	4.72
KALN			9	0.0667	3.56			10	0.0640	4.75

Station	$PGA_{ROCK} = 0.30\,g$					$PGA_{ROCK} = 0.37\,g$				
	M_L	M_W	R_e(km)	$Z(R)$	T_{gm}(s)	M_L	M_W	R_e(km)	$Z(R)$	T_{gm}(s)
STA			16	0.0500	6.61			18	0.0462	10.72
STON			15	0.0521	6.61			16	0.0500	10.64
CACV			13	0.0565	6.50			17	0.0481	10.68
MORI			14	0.0542	6.53			17	0.0481	10.68
NVLJ	6.6	6.56	11	0.0614	6.43	7.1	7.07	14	0.0542	10.56
BRJN			12	0.0589	6.46			15	0.0521	10.59
RIY			12	0.0589	6.46			15	0.0521	10.60
OZLJ			9	0.0667	6.36			11	0.0614	10.45
PTJ			10	0.0640	6.39			12	0.0589	10.49
KALN			11	0.0614	6.43			13	0.0565	10.52

The chosen epicentral distances (R_e) were selected to vary from 7 km up to 30 km to define near-site regions so that for different combinations of magnitudes and epicentral distances, the input FAS and response spectrum match target PGA_{ROCK} values from 0.03 g to 0.37 g. Here it needs to be mentioned that some of the scenarios in terms of selected large magnitudes and short epicentral distances provided in Table 5.1 are unrealistic for some stations. One reason to choose the distance ranges up to 30 km is because the nearby recordings constrain κ_0 and the gradual increase of κ begins after 15–20 km as discussed in the previous chapter. In this case the input FAS is compatible with the effect of κ on the shape of local/regional FAS at high frequencies for near-site regions. The other reason for preferring shorter epicentral distances ($R_e < 30$ km), is that large magnitudes can be constrained for the use in RVT-based approach to reach the target PGA_{ROCK} levels. That is to say, when larger epicentral distances are employed in the RVT-based approach, large earthquake magnitudes are required to reach higher values of target PGA_{ROCK} levels, except for lower target PGA_{ROCK} levels. For example, to reach the value of $PGA_{ROCK} = 0.30$ g for $R_e = 50$ km (or more), one would require magnitude larger than 8.0, which is unrealistic for Croatia, and the point source model is not valid. In other way, to reach low level of $PGA_{ROCK} = 0.03$ g with magnitude 7.0, higher value of $R_e \sim 60-80$ km is required which is more realistic scenario.

The problem with the use of short distances to a large fault may be that finite-source effects may dominate, and depending on the site characteristics, the source and site may control different frequency ranges. Silva et al. (1997) showed that point source model from the near-source regions (at short distances, 2 to 15 km) used in vertically propagating shear-wave model in the equivalent–linear site response analysis at both soft rock and deep soil sites, provided

statistically stable site response results comparable with empirical attenuation relations. Different earthquake scenarios scaled to the same input PGA_{ROCK} value defined by different M_W and R_e, yield to different input FAS and response spectrum, but in terms of site amplification factor, differences in median AF were very small, since AF is mainly a function of the local site profile. Therefore, chosen earthquake scenarios for near-site distances are justified in this study (to some points) to see how different input PGA_{ROCK} values for a range of local sites, affects the site amplification factors.

The FAS and the corresponding response spectra (at 5 % of critical damping) for each input PGA_{ROCK} level (Sa at zero period) defined with different M_L values are shown in Figure 5.1. Corresponding FAS for each magnitude is representative for the R_e and other parameters from Table 5.1. It is clearly observed from the figures on the left-hand side that the shape of FAS at high frequencies (> 10 Hz) is affected by the near-site attenuation parameter (κ_0) calculated for each station. The difference in κ_0 for each station influences the shape of the response spectrum (Figure 5.1 – right hand side); the peak of the spectrum shifts to shorter periods as κ_0 decreases (e.g., OZLJ: $\kappa_0 = 0.0372$ s and STON: $\kappa_0 = 0.0153$ s). The other seismological parameters, e.g., $Q(f)$, also affect the shape of FAS but not as much as κ_0 (e.g., Figure 2.5). For site-specific applications of evaluating the seismic response of the local site, definition of earthquake scenarios based on local/regional seismological parameters should be properly defined (realistic magnitudes, epicentral zones with respect to different regions, seismicity, etc.) rather than evaluating the seismic site response based only on previously recorded different strong motions scaled to PGA_{ROCK} (Rathje and Ozbey 2006).

For the purpose of the site response analysis of the selected sites in Croatia using RVT-based approach, the median rock FAS from all stations is used to define target reference PGA_{ROCK} based on different earthquake scenarios combined for different local/regional seismological parameters into FAS (Figure 5.2). Corner frequency (f_C) shifts to lower values with higher magnitude (M_L) values following theoretical Brune (1970) ω-square model (e.g., Figure 2.2). Frequency f_{max} describes site-dependent cut-off frequency where FAS decays rapidly and acts as a soil low-pass filter (e.g, Hanks 1982). For the median rock FAS, f_{max} is constant because seismological station sites are characterized as hard rock sites (similar V_{S30} values) with values of near-site attenuation κ_0 close to zero.
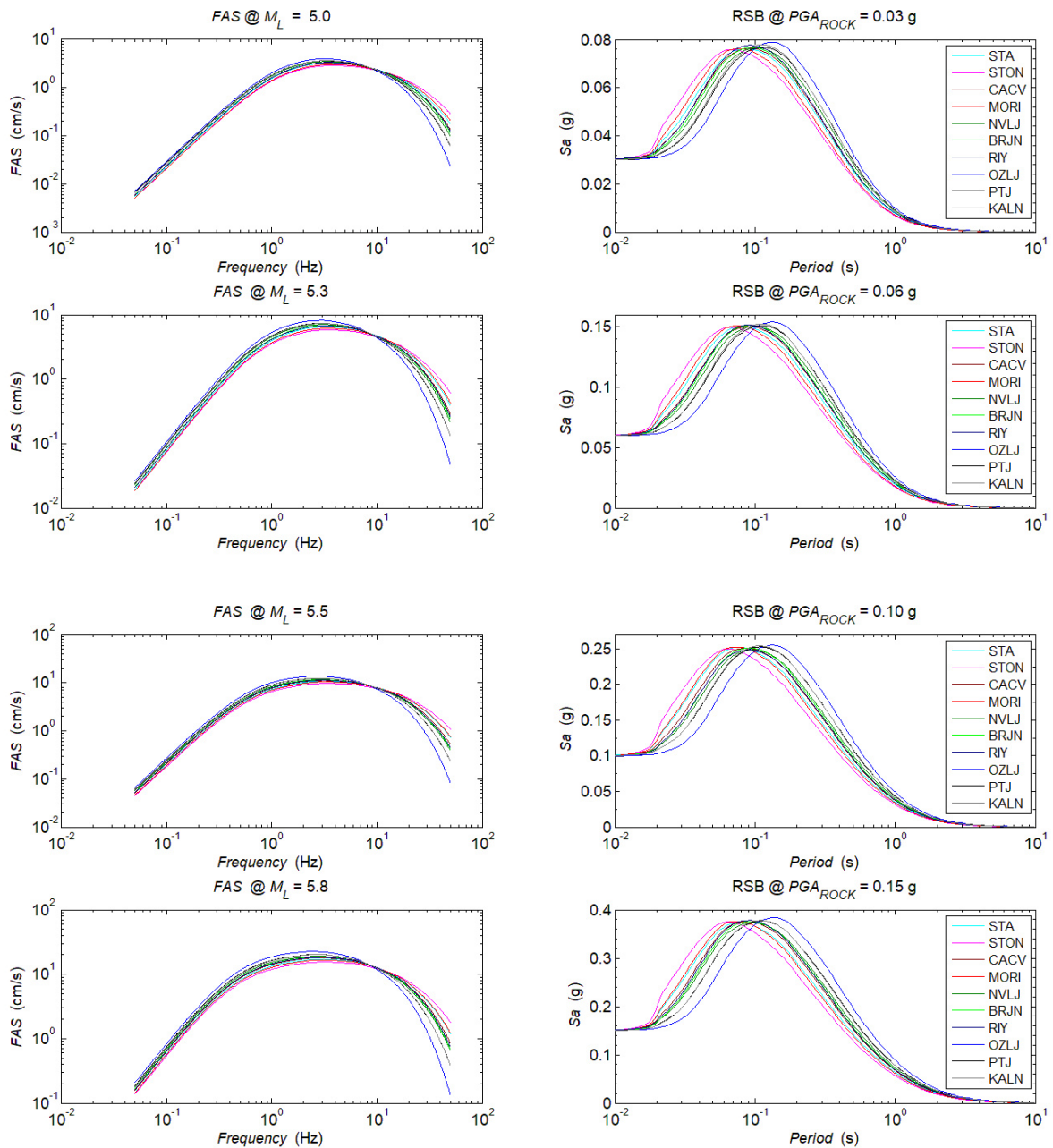
Figure 5.1. Individual Fourier Amplitude Spectra (*FAS*) and Response Spectra (RSB – at 5% of critical damping) for the bedrock condition defined for different earthquake scenarios to match the target PGA_{ROCK} (g) (defined as Sa at zero period value) at each station. See Table 5.1 for other parameters.

127
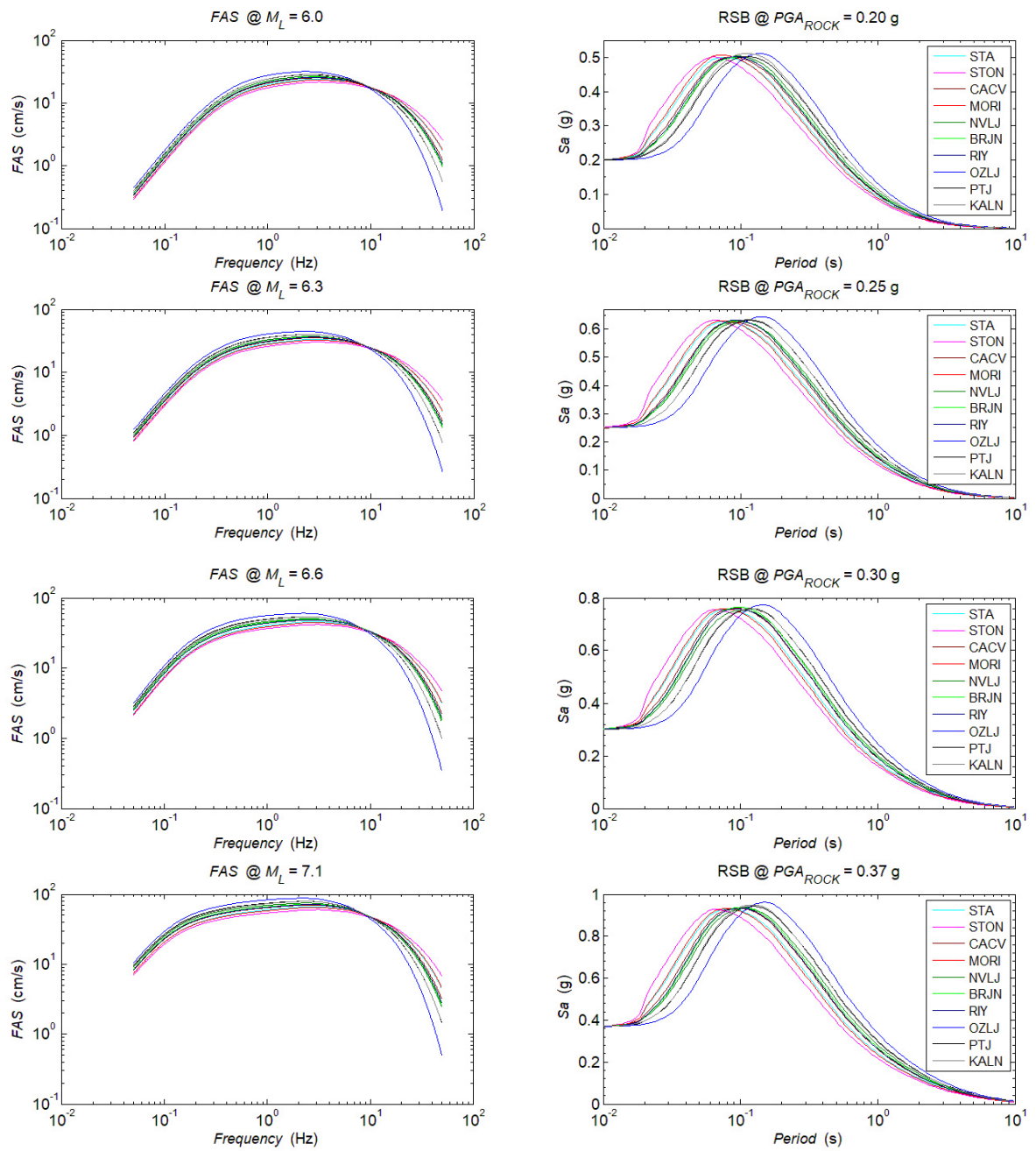
Figure 5.1. ► continued
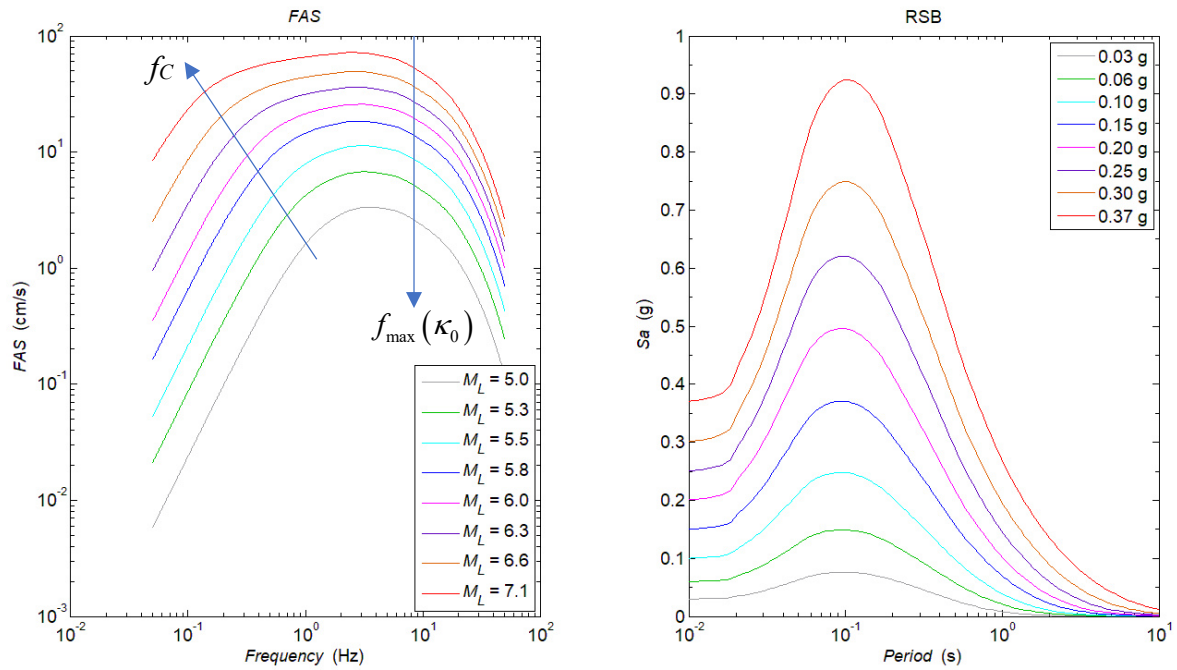
Figure 5.2. Median of Fourier Amplitude Spectra (FAS) and Response Spectra (RSB, 5 % of critical damping) for the bedrock condition defined for different earthquake scenarios to match target PGA_{ROCK} (g) (Sa at zero period value) at each station. The change of corner frequency (f_C) with magnitude (M_L) and cut-off frequency f_{max} that corresponds to the near-site attenuation κ_0 are marked.

5.2. Local soil profiles used in RVT-based site response analysis

The database of local soil profiles selected across Croatia that are employed in the RVT-based site response analysis are compiled from extensive fieldwork that includes the geophysical survey methods and microtremor measurements. Majority of local soil profiles are collected from geophysical measurements from the areas in the vicinity of seismic stations. Some of the shear wave velocity profiles in the northwestern part of Croatia are gathered from the published studies, which were determined with a combination of microtremor HVSR modelling routine and geophysical measurements (e.g., Stanko et al. 2016, 2017; Strelec et al. 2016). Spatial distribution of the selected sites is shown in Figure 5.3. A total of 70 local soil profiles are collected across Croatia with various ranges of V_{S30} and different bedrock depths (from 15 m up to 120 m of depth) (Figure 5.4).
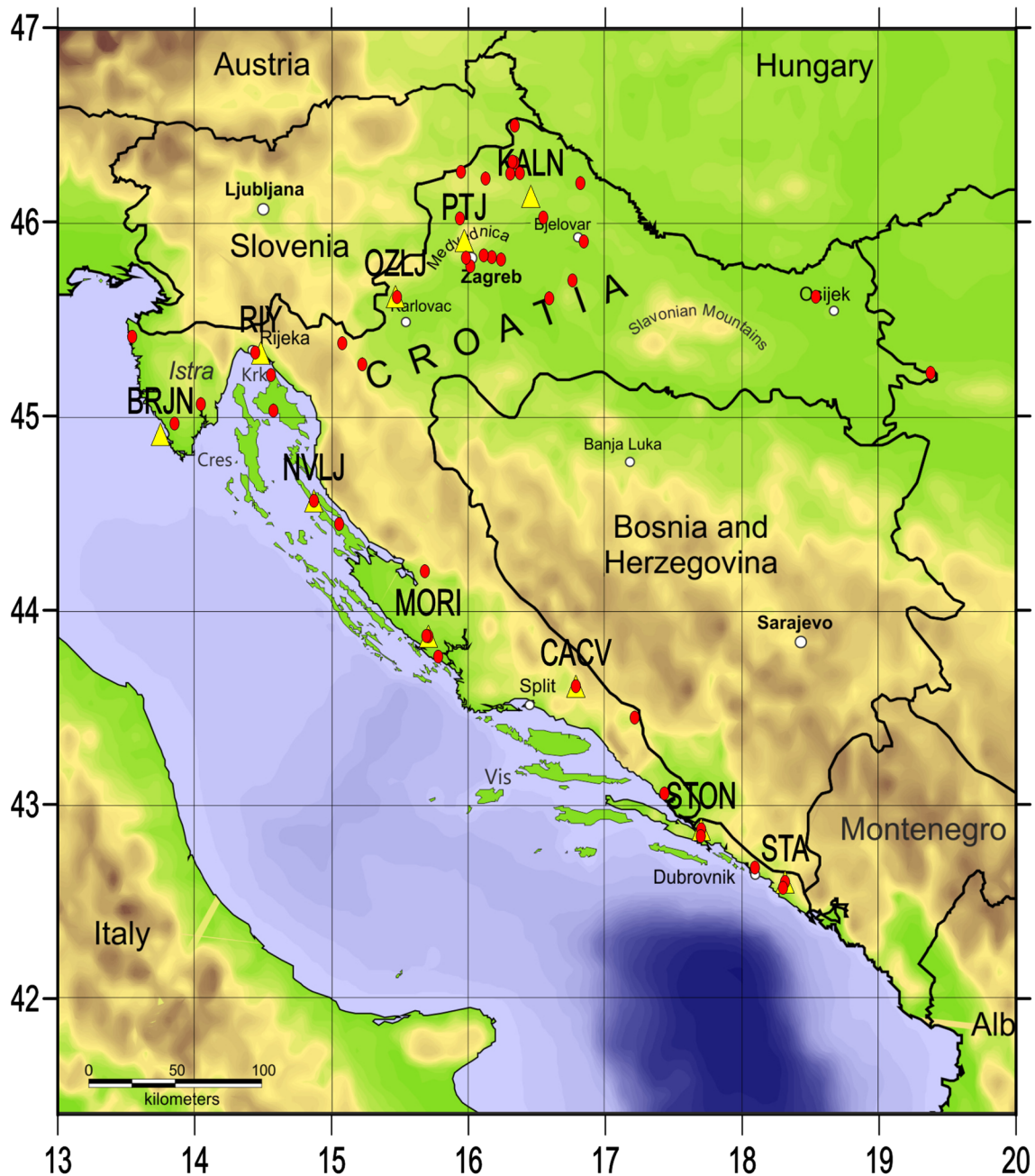
Figure 5.3. Distribution of local soil profiles in Croatia (red points) collected from fieldwork geophysical survey methods and microtremor measurements. Yellow triangles mark locations of seismological stations used in this study.

130
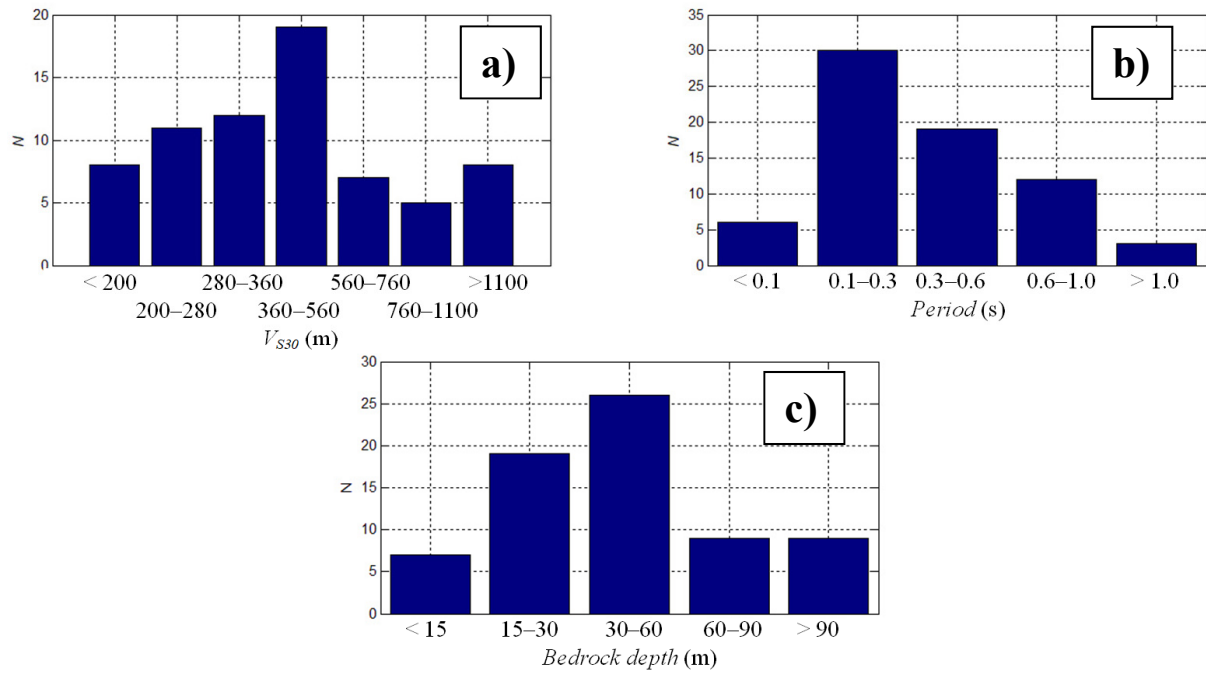
Figure 5.4. Distribution of local soil profiles in terms of site characteristic's: a) V_{S30} (m/s) for set of ranges according to the EC8 soil categories and reference $V_{S30} = 1100$ m/s of the bedrock, b) natural soil period (s), and, c) estimated bedrock depth (m) ranges.

The collected soil profiles are implemented in the STRATA software as explained in Chapter 3.3. In each profile, the soil layers are defined by the corresponding soil properties (shear wave velocity and density). Provided that G_{max} is known from geophysical measurements ($G_{max} = \rho V_S^2$), shear response at various levels of strain can be estimated using soil modulus reduction curves G/G_{max} to represent nonlinear soil behaviour of soils under specific levels of strains from induced ground motions (in this study from 0.03 g to 0.37 g). Equivalent–linear properties of the soil layers, the strain-compatible shear modulus reduction (G/G_{max}) and damping (ξ) curves are selected by considering the widely-used choices in the EQL site response analysis for each soil type that had been published before (Figure 5.5). Under large strains, G/G_{max} decrease strongly for soft soils (lower values of V_S) like clays with low plasticity index (PI < 30), sands or gravels. For these soils, ξ increases more than for the harder soils such as stiff clay with high PI > 100 or rock formations (higher values of V_S) as illustrated with arrows in Figure 5.5. Soil profiles extracted from geophysical measurements do not contain any information about soil's density or the soil classification (the examples from seismic stations shown in Figure 4.7). Drilled boreholes and laboratory sampling tests are required to characterize soil layers in terms of soil type and density. Since the borehole and laboratory data are not available, soil layer types are approximated using the published relation between soil density and shear wave velocity (V_S) (Figure 5.6, Boore 2016).
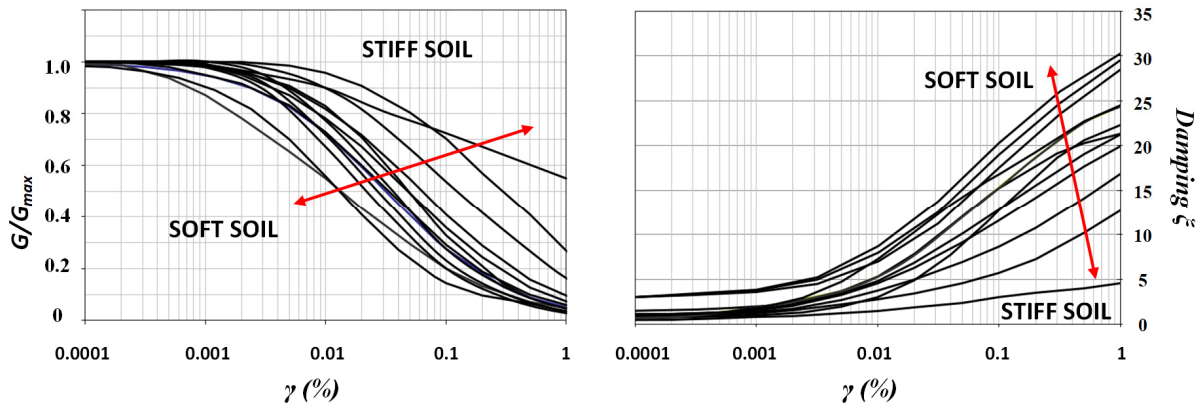
Figure 5.5. Variation of soil shear modulus G/G_{max} and damping ratio ξ curves with strain from the literature used in this study. Soil materials: Rock (Schnabel 1973); Sand and gravel (Seed et al. 1984, 1986); Clay (PI = 10, PI = 15, PI = 30, PI = 50, PI = 100) (Vučetić and Dobry 1991); EPRI sand 6–16 m, 16–37 m, 37–76 m (EPRI 1993); Silt and sand with fines (Darendeli 2001); Gravel (Menq et al. 2003). Softer soils have lower shear wave velocity (V_S) values and vice versa, stiffer clays and rock formations have higher shear wave velocities (see Figure 5.6).
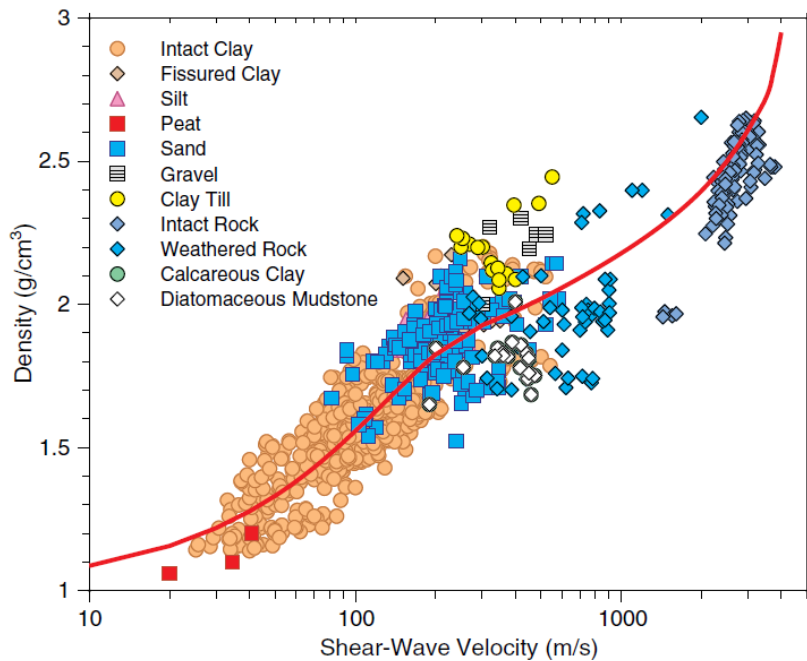
Figure 5.6. The approximated relation (red line) between soil density and shear wave velocity (V_S) of different soil layer types used in this study. Adapted from Boore (2016).

5.3. Results of RVT-based 1-D EQL site response analysis

For the purpose of analysing the local site effects on the AFs, compiled local soil profiles are classified into seven categories according to the V_{S30} parameter (Eq. 4.6) based on EC8 soil classification (Table 5.2).

Soil profiles that consist of loose-to-medium cohesionless soils or soft-to-firm cohesive soils are classified as soil category D ($V_{S30} < 180$ m/s) in EC8. In this study, the limit for this soil category was set up to ($V_{S30} < 200$ m/s) since some of the profiles with thicker soil layers over the bedrock (up to 100 m) contain approx. 10–20 m layers of very soft clays and silts. Main reason why the upper range of V_{S30} for soil category D was moved to 200 m/s instead of 180 m/s can be observed on the examples in Figures 5.7 (a) and (b) for the average V_S distribution for the depths of 20 m—V_{S20}. Small changes in V_S distribution in the first few surficial layers can significantly change the average value of V_{S30} Based on the observations from collected local soil profiles, it was decided to extend the upper limit ($V_{S30} < 200$ m/s) for soil category D. Also, the other soil categories were subdivided based on the observation of the average values of V_{S10} and V_{S20}, in order to provide better insight into the influence upper surficial soil layers have on the amplification of ground motion.

Soil category C in EC8, $V_{S30} = 180-360$ m/s, was subdivided into two sub-categories: $V_{S30} = 200-280$ m/s (deep deposits of clays, sands or gravels of several tens to hundreds of meters of bedrock depth) and $V_{S30} = 280-360$ m/s (dense sands, gravels and stiff clays up to fifty meters of bedrock depth). In EC8, deposits of very dense sand, gravel, very stiff clay or soft rocks from several tens of meters of bedrock are defined in the range of $V_{S30} = 360-800$ m/s. This category is also subdivided into: $V_{S30} = 360-560$ m/s and $V_{S30} = 560-760$ m/s ranges to provide a better insight into the local site effects.

As some nonlinear site amplification models (e.g., Choi and Stewart 2005; Sandikkaya et al. 2013) used the reference $V_{S30} = 760$ m/s to represent the engineering bedrock, the limit for category A in this study was also set up to 760 m/s instead of 800 m/s. Firm to hard rock sites with $V_{S30} \geq 760$ m/s are subdivided into $V_{S30} = 760-1100$ m/s (rock or other rock-like geological formation that includes weaker material at the surface) and $V_{S30} \geq 1100$ m/s categories representing different reference bedrock interpretations.

In Figure 5.4 (b, c) the soil profiles are classified into ranges of natural (or predominant) soil period (T_{pp}) and bedrock depths h (defined for $V_{S30REF} = 1100$ m/s) following the quarter-wave length rule $(\bar{V}_S = 4h/T_{pp})$.

Table 5.2. Soil classification V_{S30} categories according to the seismic design code Eurocode 8 (EC8)

Ground Type	Description of the stratigraphic profile	V_{S30} (m/s)
A	Rock or other rock-like geological formation, including at most of 5 m of weaker material at the surface.	> 800
B	Deposits of very dense sand, gravel, or very stiff clay, at least several tens of metres in thickness, characterised by a gradual increase of mechanical properties with depth.	360–800
C	Deep deposits of dense or medium-dense sand, gravel or stiff clay with thickness from several tens to many hundreds of metres.	180–360
D	Deposits of loose-to-medium cohesionless soil (with or without some soft cohesive layers), or of predominantly soft cohesive soil.	< 180
E	A soil profile consisting of a surface alluvium layer with V_s values of type C and D and thickness varying between about 5 m and 20 m, underlain by stiffer material with $V_S > 800$ m/s.	
S$_1$	Deposits consisting, or containing a layer at least 10 m thick, or soft clays/silts with a high plasticity index (PI>40) and high-water content.	< 100
S$_2$	Deposits of liquefiable soils, of sensitive clays, or any other soil profile not included in type A–E or S$_1$.	

The results of site response analysis using the RVT-based method are presented in terms of the 5 % damped surface response spectrum RSS and the $AF(T)$ at different periods given as ratio of RSS and RSB (Figure 5.2, right). Examples of the analysis for selected local soil profiles in each category are shown in Figures 5.7a–g for a range of input PGA_{ROCK} represented by different line colours. For each example, the variation of the PGA through the soil from the bedrock to the surface is noticeable. Since the input motion is defined at the outcrop (Chapter 3.1.3) the PGA_{ROCK} values given in Figure 5.7 at the bedrock level are 65 % (this is typical value of ratio between the effective strain and maximum strain) of the input PGA_{ROCK} provided in Table 5.1. Bedrock response spectrum (median RSB from all stations in Figure 5.2) matches the target PGA_{ROCK} represented as spectral acceleration Sa at the zero period, in other words, a

full spectral matching procedure is not applied. Peak ground acceleration PGA at the surface in RSS is represented by spectral acceleration Sa at the zero period.

The examples in Figures 5.7a–g are shortly explained in each figure's sub-caption, giving insight about the influence of different local site types (in terms of V_{S30} intra-categories) on the amplification of various seismic ground motion (PGA_{ROCK}).

Main findings from the examples provided in Figures 5.7a–g are:

1) in the linear range ($PGA_{ROCK} < 0.1$ g), the input motion is significantly amplified at the top layers of the profile ($AF@PGA$);

2) AF is most prominent at predominant peak period (response of the soil at the natural soil period T_{pp} for which the resonance is expected) particularly for the softer soils with lower V_{S30} and thicker alluvium layers overlying bedrock;

3) at higher input motion levels ($PGA_{ROCK} > 0.1$ g), softer soils with lower values of V_{S10}, V_{S20}, and V_{S30} undergo the non-linear behaviour for which $AF < 1$ due to degradation of shear modulus under large deformations (G decrease and ξ increase with large strains, Figure 5.5);

4) under nonlinearity, $AF@PGA$ decreases significantly below the $AF = 1$ line at shorter spectral periods and at the predominant peak, the spectral peak period is prolonged (increased) with decreasing $AF@PP$;

5) for stiffer soils (rock formations) with higher V_{S10}, V_{S20}, and V_{S30} values, $AF@PGA$ and $AF@PP$ are "stabilized" at all spectral periods regardless of large values of PGA_{ROCK} showing "little to no" amplification, particularly above 0.10 s.

6) observed significant amplifications $AF@PGA$ and $AF@PP$ for stiffer soils and hard rock formations with $V_{S30} > 560$ m/s at shorter periods (< 0.20 s) are mainly due to the response of hard bedrock interaction with surficial few meters of shallow weaker material.

Some of the above-mentioned observations regarding soil non-linearity behaviour under different input motions PGA_{ROCK} for certain local sites are comparable with the extensive site response analysis literature and will be discussed in more detail in Chapter 5.4 (e.g., Vučetić 1992; Beresnev and Wen 1996; Walling et al. 2008; Dhakal et al. 2013; Kottke and Rathje 2013; Bolisetti et al. 2014).
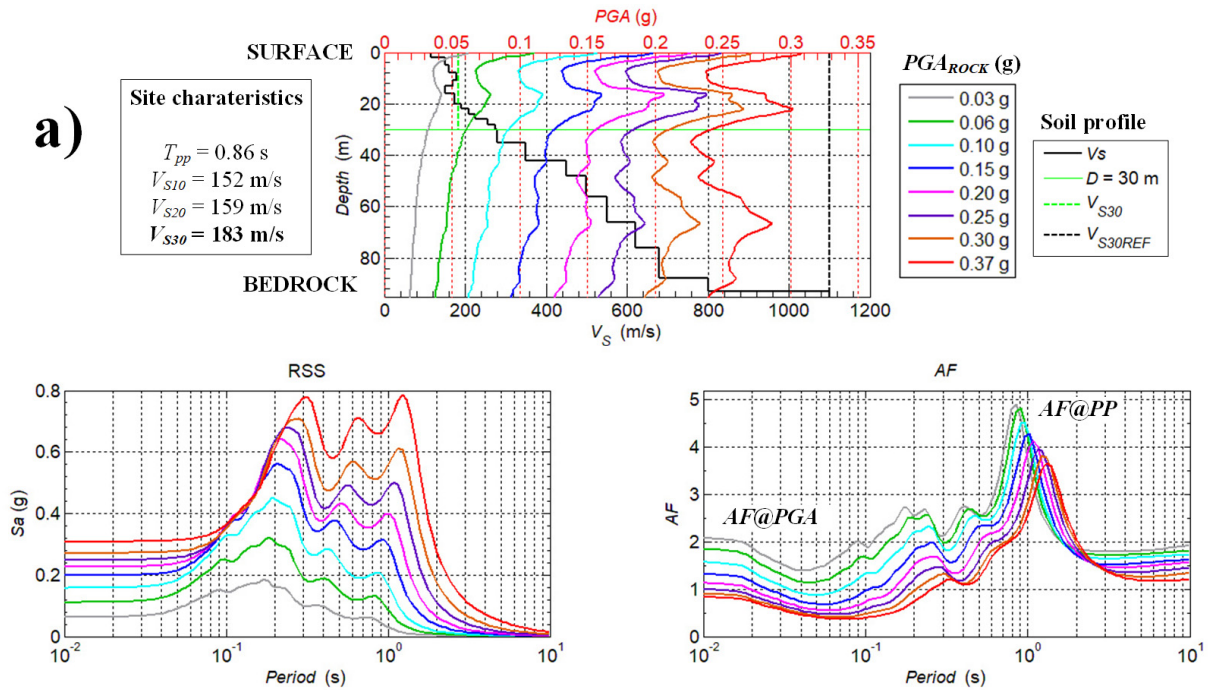
Figure 5.7a. Example of *AF* for soil category $V_{S30} < 200$ m/s. In the linear range for which $PGA_{ROCK} < 0.1$ g, *AF@PGA* is approx. 2, and *AF@PP* is higher than 4. With higher levels of $PGA_{ROCK} > 0.1$ g, top soil layers (< 20 m) with $V_S < 200$ m/s undergoes into de-amplification at lower periods for which *AF*<1 due to non-linear soil response (soil degradation under large deformations; *G* decrease and ξ increase with large strains) and predominant period T_{pp} is shifted to higher values with decreasing *AF@PP*.
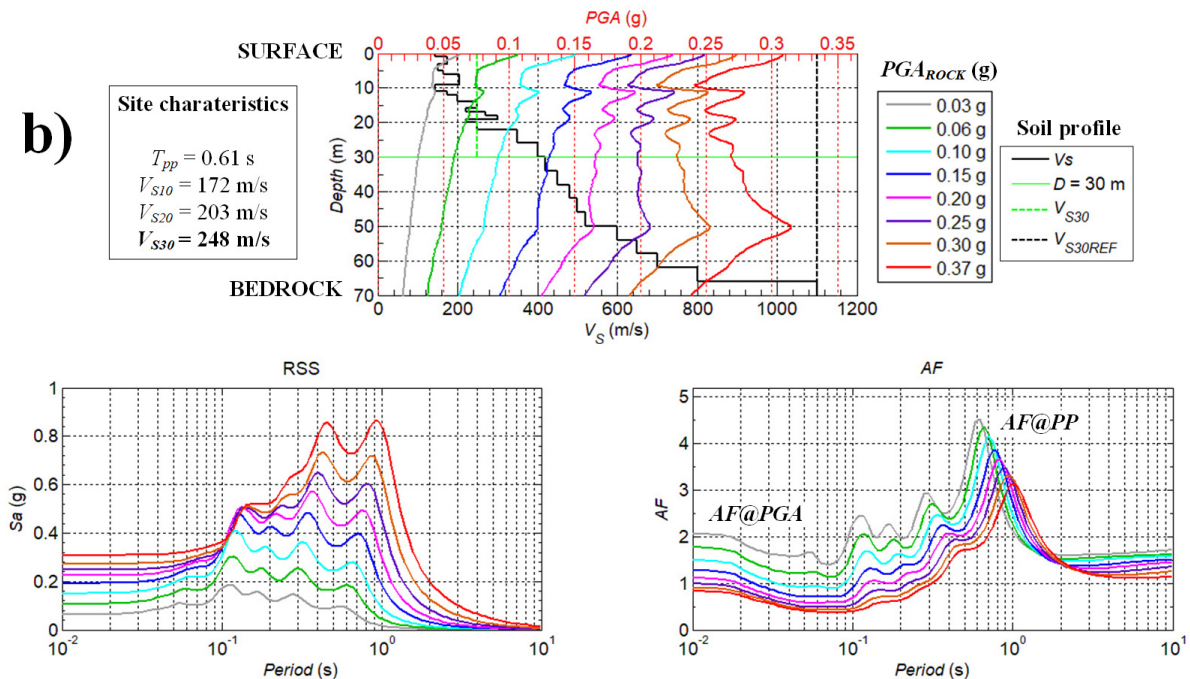
Figure 5.7b. Example of *AF* for soil category $200 \leq V_{S30} < 280$ m/s. *AF@PGA* are similar to the example in Figure 5.7a due to similar values of V_{S10}, and *AF@PP* are slightly lower due to higher value of V_{S30} compared to the example in Figure 5.7a. Similar non-linear behaviour *AF* < 1 at shorter periods is observed as in Figure 5.7a, particularly due to the response of very soft top layers (< 20 m) with lower V_S values to the input ground motion.

136
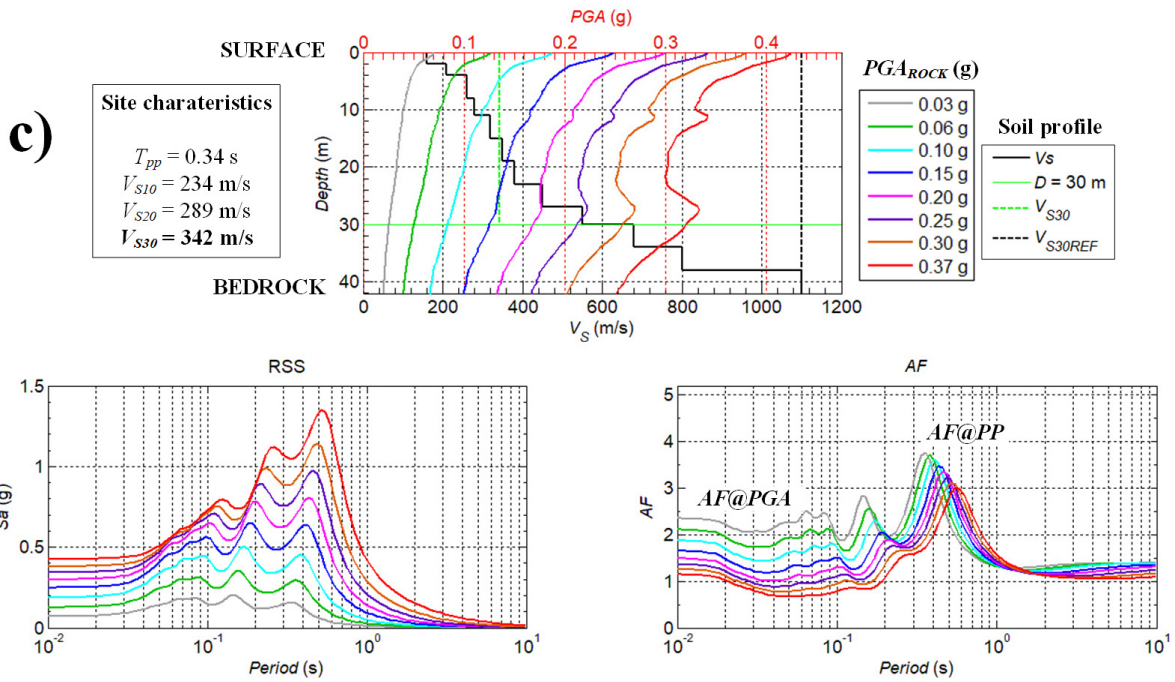
Figure 5.7c. Example of *AF* for soil category $280 \leq V_{S30} < 360$ m/s. *AF@PGA* and *AF@PP* are slightly lower compared to the examples in Figure 5.7 (a, b) with similar non-linear behaviour showing less de-amplification, particularly due to higher values of $V_{S10}, V_{S20}, V_{S20}$. Other characteristic *AF* peaks at shorter period are observed. With higher input motions, *AF* peaks at shorter period are flattened due to the nonlinear deamplification effect. Similar behaviour is observed in previous examples (a–c).
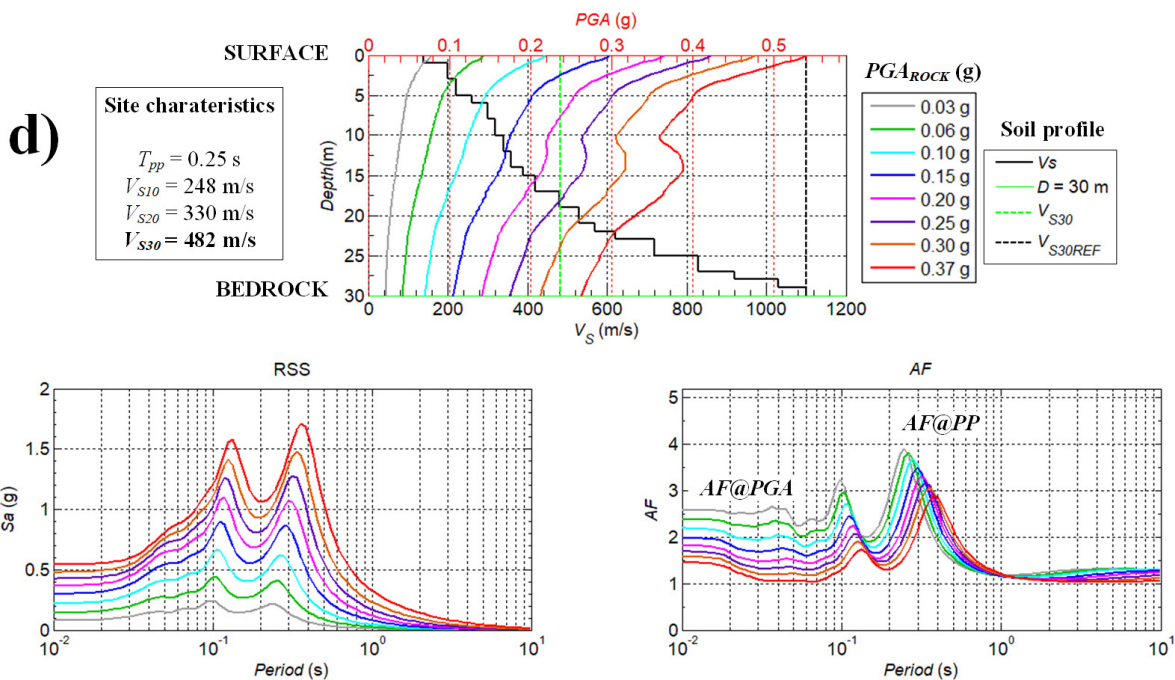
Figure 5.7d. Example of *AF* for soil category $360 \leq V_{S30} < 560$ m/s. *AF@PGA* and *AF@PP* are similar to the example in Figure 5.7c mostly due to top few meters of weaker material (similar value of V_{S10}) without significant non-linear effects at shorter periods due to slightly higher values of V_{S30}). Decrease of *AF@PP* and predominant period lengthening with higher PGA_{ROCK} is similar to the example in Figure 5.7c but with less impact as in Figure 5.7 (a, b). Non-linear effects in this range of V_{S30} are not excluded particularly due to the variation of the upper softer soil layers, depth of the bedrock and the intensity of input ground motion.
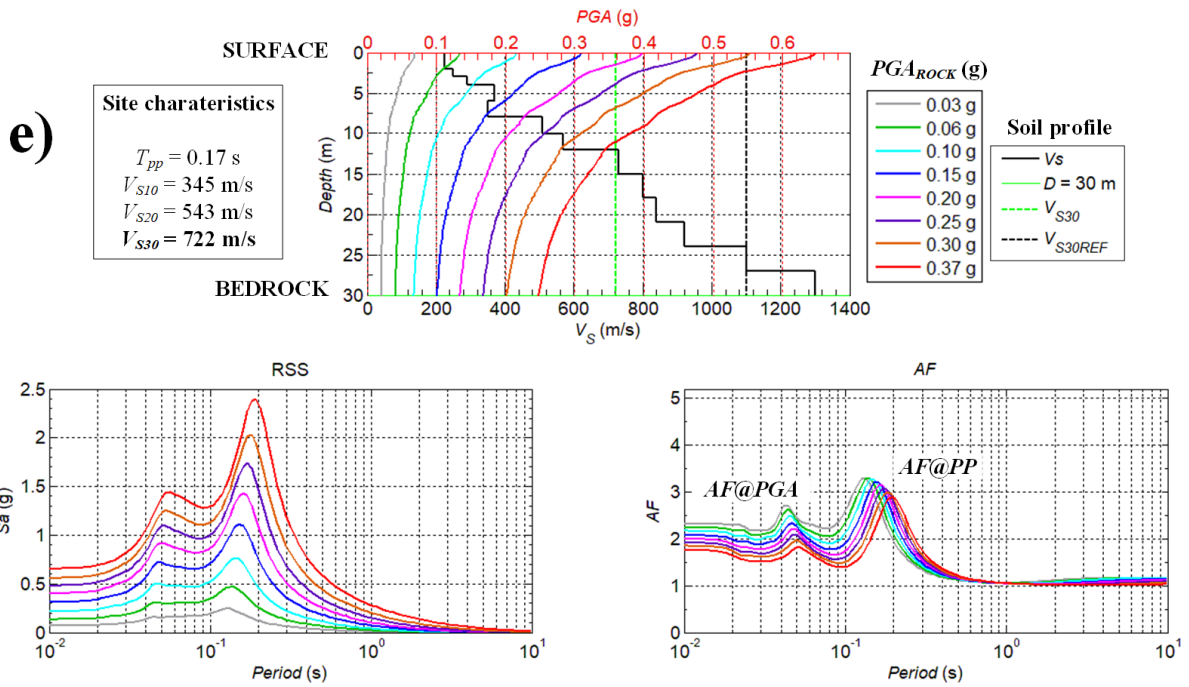
Figure 5.7e. Example of *AF* for soil category $560 \leq V_{S30} < 760$ m/s. For stiffer soils with higher V_{S30} values, *AF@PGA* and *AF@PP* "become more stable" with the change of input PGA_{ROCK} and values are approx. 2 *@PGA* and 3 *@PP* compare to example in Figure 5.7d.
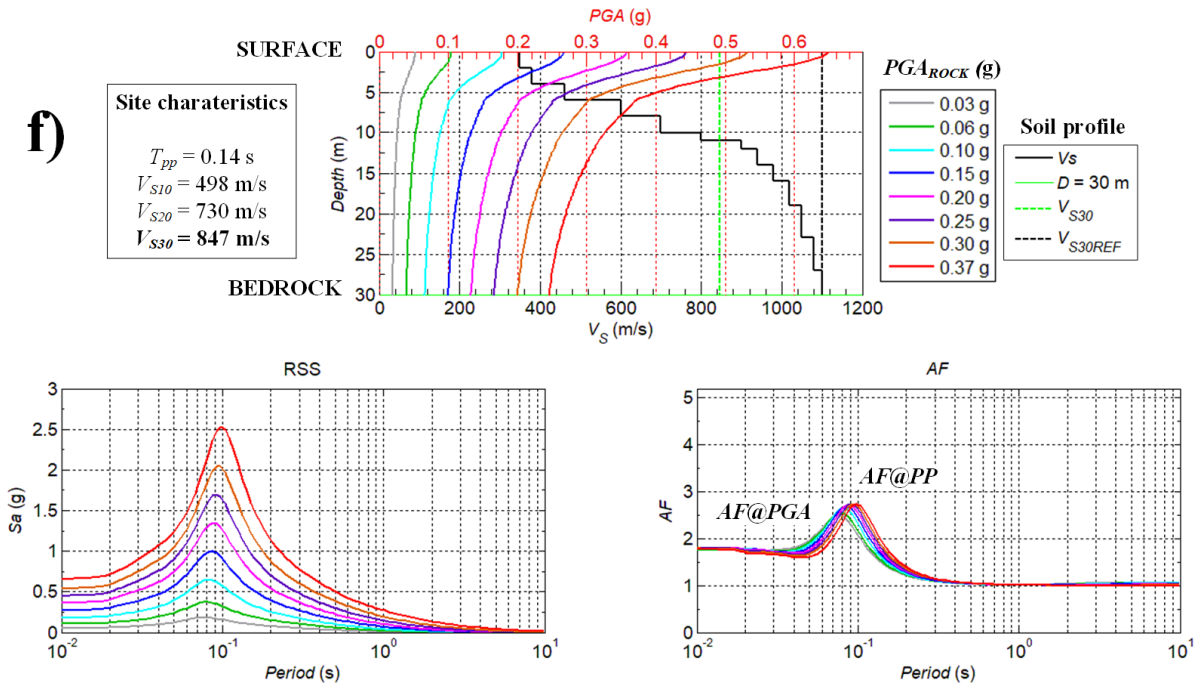
Figure 5.7f. Example of *AF* for soil category $760 \leq V_{S30} < 1100$ m/s. This is the profile at OZLJ station (Figure 4.6). *AF@PGA* and *AF@PP* almost "stabilize" with the change of input PGA_{ROCK} at all periods for rock-like formations with higher values of V_{S30} with top few meters of weaker material. *AF* represents the response of bedrock's interaction with few meters of shallow weaker material at the surface without non-linear effects which resulted in observed *AF@PP* at lower periods.
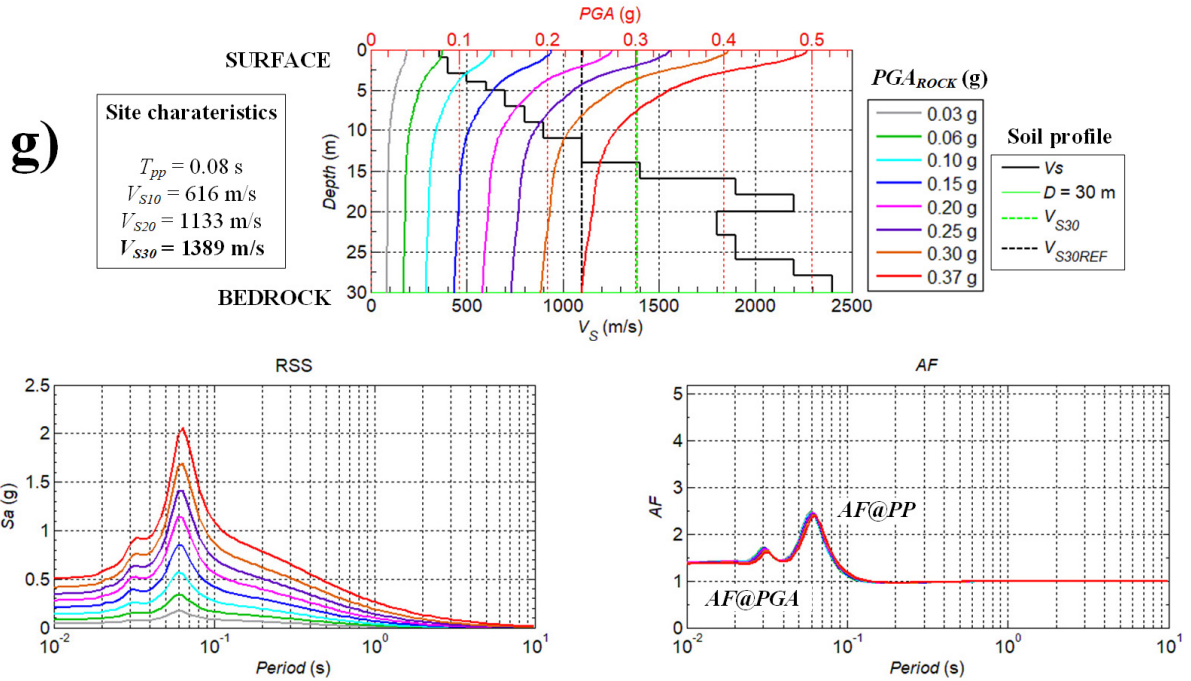
Figure 5.7g. Example of AF for reference bedrock conditions $V_{S30} \geq 1100$ m/s. This is the profile at STON station (Figure 4.6). $AF@PGA$ and $AF@PP$ are constant regardless of input PGA_{ROCK}. Hard rock formations with higher values of $V_{S30} \geq 1100$ m/s show little to no amplification at all periods, particularly above 0.10 s. Observed peaks $AF@PP$ at shorter periods (< 0.10 s) are mainly due to the response of bedrock's interaction with few meters of shallow weaker material at the surface.

5.4. Discussion of the local site effects on the site amplification factors

Figure 5.7 presented the AFs as a function of the spectral period, site characteristics (natural soil period, shear wave velocity of each soil layer and average values of shear wave velocity in top 30 m, V_{S30}) and input ground motion. The deviation of the peak periods of the AFs from the natural period of the profile is very significant, especially when $PGA_{ROCK} > 0.2$ g as observed from examples in Figure 5.7 (a–d), consistent with the observations of Beresnev and Wen (1996) on the effects of soil non-linearity. The reduction observed at surface PGA (for $AF@PGA$) relative to PGA_{ROCK} for $PGA_{ROCK} > 0.2$ g in soft soil sites were attributed to the soil's non-linearity by Seed et al. (1976) and Seed and Idriss (1983). To compare the results from this study with previous studies, PGA at surface ($Sa@0.01$ s) were plotted as a function of PGA_{ROCK} for selected soil V_{S30} intra-categories as shown in Figure 5.8.

Figure 5.8 shows that the soil non-linearity effects tend to dominate for soft site profiles with V_{S30} lower than 280 m/s at larger values of $PGA_{ROCK} > 0.2$ g: for these cases the values of surface PGA are below the $AF = 1$ line (similar to the examples shown in Figure 5.7 (a–c). For the cases for which $360 \leq V_{S30} < 760$ m/s, some sites can have significant amplification mostly due to the effects of upper weaker soil materials and very shallow bedrock (lower V_S values or velocity inversion layers) as presented in Figures 5.7 (d–e) and trends of PGA at surface are in-between non-linear and linear response for different values of PGA_{ROCK}. For stiffer soils with $V_{S30} > 760$ m/s, variation of PGA at the surface is linear with PGA_{ROCK} and significant amplifications (up to 1.8) are present due to upper soft soil layers above bedrock (similar observations are reported in Walling et al. (2008) and Kamai et al. (2014) for sites with $V_{S30} = 760, 850$ and 900 m/s). This issue is important to be addressed and will be discussed in more detail in Chapter 6.3.3, particularly for the Eurocode 8, for which the amplification for harder sites with $V_{S30} > 800$ m/s is neglected.
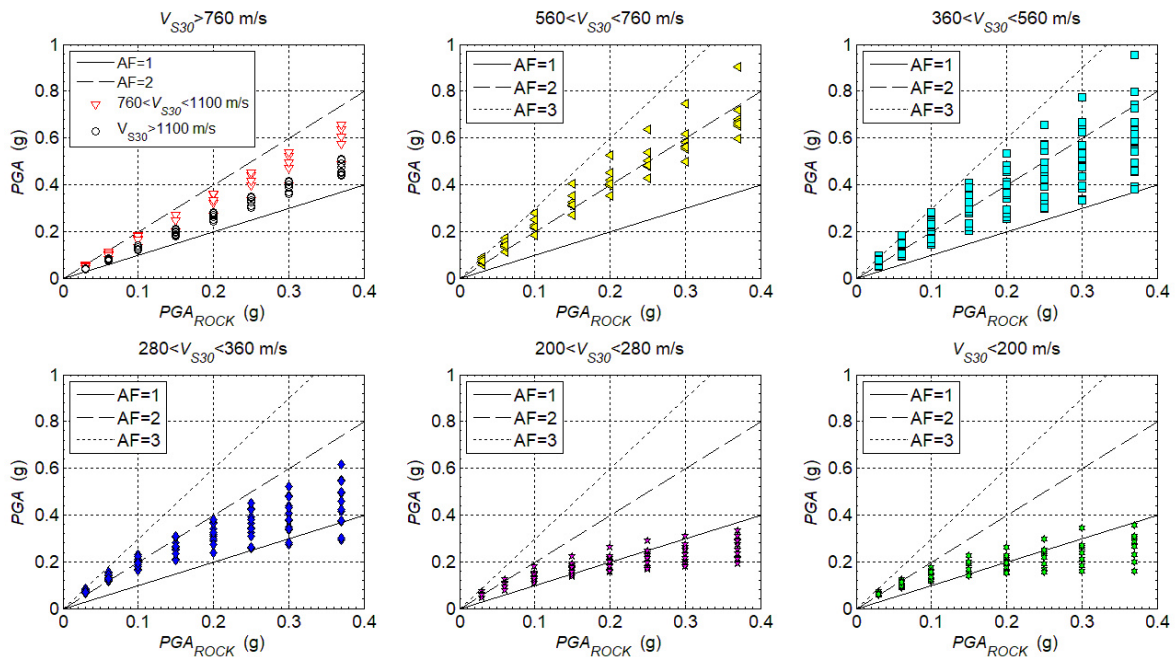
Figure 5.8. Variation of peak ground accelerations PGA at surface ($Sa@0.01$ s) as a function of PGA_{ROCK} for selected soil categories: $V_{S30} < 200$ m/s; $V_{S30} = 200–280$ m/s; $V_{S30} = 280–360$ m/s; $V_{S30} = 360–560$ m/s; $V_{S30} = 560–760$ m/s; $V_{S30} = 760–1100$ m/s; $V_{S30} \geq 1100$ m/s.

It is important to understand how AFs at different spectral periods are influenced by the seismic response of local site for certain earthquake scenarios. The dominant period/frequency of the ground motion and the natural period/frequency of the soil are especially critical for possible resonance effects during earthquakes which can result in heavy destruction (e.g., 1985 Mexico

City earthquake damage). Figure 5.9 presents the variation of $AF@PP$ as a function of average shear wave velocity in top 10 m (V_{S10}), 20 m (V_{S20}) and 30 m (V_{S30}) for different input PGA_{ROCK} levels (0.03 g, 0.1 g and 0.3 g). Although the average shear wave velocity in the upper 30 m (V_{S30}) is used in last decades as a primary indicator of local site effects, the upper 10 m (V_{S10}) and 20 m (V_{S20}) values of shallow soft layers above the bedrock, can provide valuable and important information of the local site effects on the site amplifications. As it is known for years in earthquake engineering literature (e.g., Reiter 1990; Kramer 1996), soft sites with lower values of V_S amplify the ground motions the most at resonant period of soil. From the introduction of soil categories in terms of V_{S30} in 90's (e.g., Boore et al. 1997, NEHRP, EC8), it is generally accepted that the sites with lower values of V_{S30} amplify seismic ground motions more than sites with higher values of V_{S30}. The examples in Figure 5.7 show that top few meters of soil play a very important role in the amplification of ground motion propagated from the bedrock to the surface. Harder sites with $V_{S30} > 1100$ m/s and $AF(@PP) \approx 2$ still show some amplification mostly due to the response of shallow few meters of soft soil layers overlying hard bedrock. For the approx. values of $V_{S10} = 400$ m/s, $V_{S20} = 500$ m/s and $V_{S30} = 760$ m/s, "constant amplification" $AF(@PP) \approx 2$ is observed regardless of the intensity of input PGA_{ROCK}. Highest "resonant" amplifications $AF(@PP) > 3$ occur for sites with very soft top layers of soil profiles $V_{S10} < 400$ m/s, $V_{S20} < 500$ m/s and $V_{S30} < 760$ m/s with the change of input PGA_{ROCK}.

Figure 5.10 presents the variation of AFs at four spectral periods (0.01 s, 0.1 s, 0.3 s and 1.0 s) with different site charateristics parameters ($V_{S10}, V_{S20}, V_{S30}$) for different input PGA_{ROCK} levels (0.03 g, 0.1 g and 0.3 g). At shorter periods, nonlinear soil amplification means that less amplification occurs for larger input intensities because of the increased levels of induced strain and damping for stiffer soils. At mid-to-long periods, nonlinear soil amplification means that more amplification occurs for larger input intensities because of increased levels of induced strain and period lengthening effect for softer soils. Low-intensity input ground motion allows the soil to respond more in the linear range, significantly reducing the stiffness degradation, which consequently results in the greater surface-to-bedrock acceleration ratio. On the contrary, high-intensity input ground motions induce large strains and therefore consequential nonlinear behaviour. This, in turn, reduces the stiffness and increases the hysteretic damping, reducing the ability of the soil to transmit force to the surface and structure above (e.g., Rathje et al. 2006, 2010; Dhakal et al. 2013; Boliseti et al. 2014). Site AFs at longer spectral period are approaching to unity for firm-to-hard sites with higher values of ($V_{S10}, V_{S20}, V_{S30}$) and at lower

spectral periods soil non-linearity is exhibited for softer sites with higher intensity of input ground motion. Variation of the AF for cases a), b) and c) in Figure 5.10 show very similar behaviour with respect to $V_{S10}, V_{S20}, V_{S30}$, mainly because soil profiles are defined from geophysical measurements and V_S distribution with depth in most cases is linear (see Figure 5.7), except for few V_S inversions (Figure 4.6, example for CACV station).
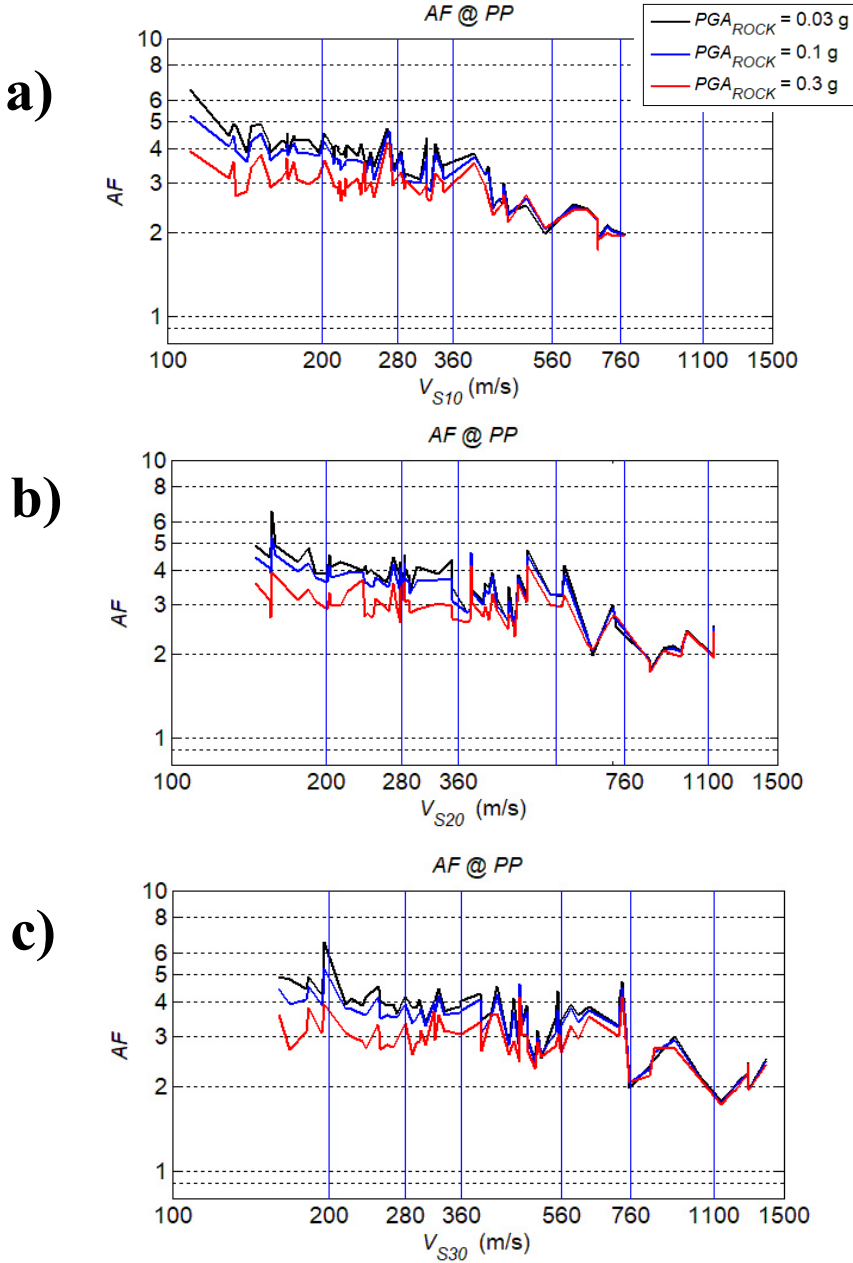
Figure 5.9. Variation of the amplification factor at predominant peak period ($AF@PP$) with the average shear wave velocity in top: a) 10 m (V_{S10}), b) 20 m (V_{S20}) and c) 30 m (V_{S30}) for different input PGA_{ROCK} levels (0.03 g, 0.1 g and 0.3 g).

a) $AF-V_{S10}$
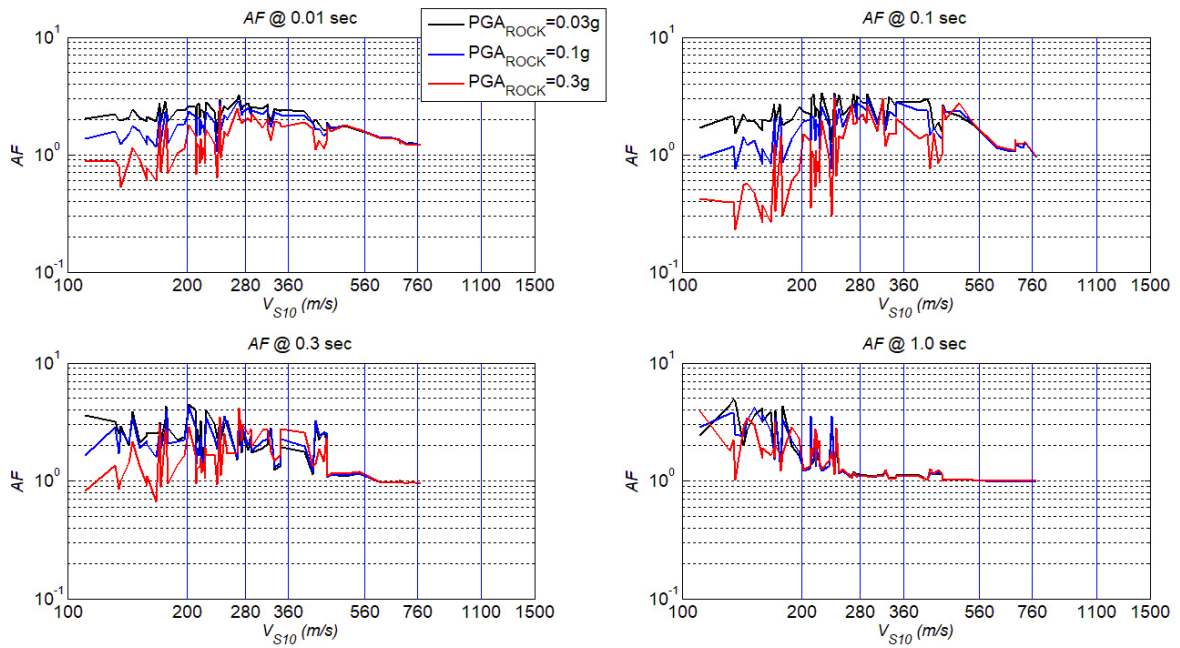
b) $AF-V_{S20}$
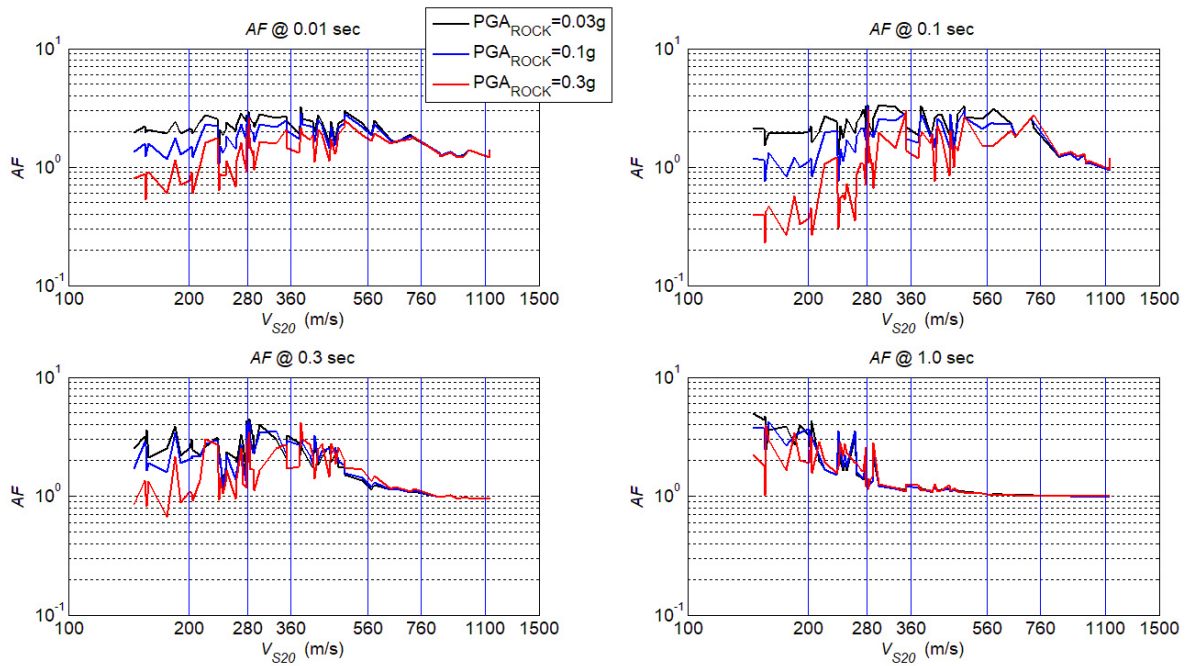
Figure 5.10. Variation of the amplification factors (AFs) for four spectral periods with the average shear wave velocity in the top: a) 10 m (V_{S10}), b) 20 m (V_{S20}) and c) 30 m (V_{S30}) for different input PGA_{ROCK} levels (0.03 g, 0.1 g and 0.3 g).

c) $AF-V_{S30}$
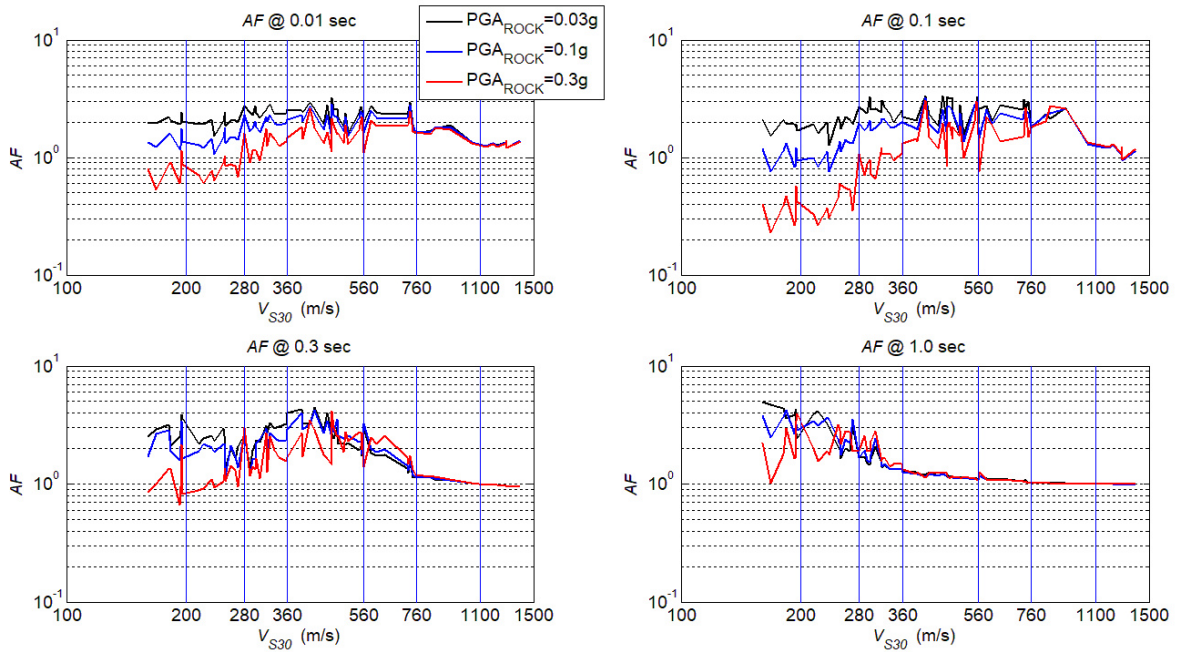
Figure 5.10. ► continued

Knowing AF at a particular spectral period helps us to design earthquake-resistant structures to avoid potential resonance with seismic ground motion, or in the case of already existing structures to reinforce them to improve their seismic resistance (e.g., Elnashai and Di Sarno 2008; Celebi at al. 2010). Figure 5.10 presented variation of the AFs at four spectral periods of typical reinforced concrete (RC) structures (e.g., Gallipoli et al. 2010): a) 0.01 s or for the PGA at the surface of the soil profile, b) 0.1 s or 10 Hz which is typical for normal houses, c) 0.3 s or 3.33 Hz which is typical for structures from 2 to 6 stories, and d) 1.0 s or 1.0 Hz typical for taller structures from 10 to 20 stories. For different range of input ground motion (PGA_{ROCK}), AF varies significantly with chosen spectral period for different site characteristics parameters ($V_{S10}, V_{S20}, V_{S30}$). Knowing these variations, new structures on particular local site can be constructed to avoid potential resonance at natural soil period taking into account nonlinear effects at shorter spectral periods. Simply said, if one wants to construct building with 10 stories (natural period approx. 0.5–1.0 s) or 4 stories (natural period approx. 0.2–0.4 s) on a local site with $V_{S30} = 300$ m/s, particular care needs to be taken to account for different behaviour of amplification factor with period for smaller intensity earthquakes, or for larger earthquakes where the nonlinear effects can play important role (soil degradation or rupture) (e.g., Kramer 1996; Elnashi and Di Sarno 2008).

Site amplification factors for different ranges of local site conditions and different input ground motions (Figures 5.7–5.10) show that amplification decreases with increasing PGA_{ROCK} for lower values of V_{S30} where de-amplification is the strongest for the soft sites with small V_{S30}. Generally speaking, breaking point where amplification at the surface ($AF@0.01$ s) starts to be "constant" with respect to intensity of input ground motion, can be set to approx. $V_{S10} = 400$ m/s, $V_{S20} = 500$ m/s and $V_{S30} = 760$ m/s, whereas "little to no" amplification is observed for $V_{S30} > V_{S30REF} = 1100$ m/s as can be seen in Figure 5.10.

Presented variation of the AFs upon different intensity of input ground motion at particular spectral period for different local V_{S30} sites is comparable with the site-amplification models (3.42–3.46) shown in Figure 3.12 (Choi and Stewart 2005; Boore and Atkinson 2008) and Figure 3.14 (Sandikkaya et al. 2013). In a similar way, using empirically developed site AFs presented in this chapter, a nonlinear site-amplification model depending on the assumed PGA_{ROCK} for Croatian local soil profile datasets (in terms of V_{S30}) will be proposed.

6. Empirical nonlinear site amplification model for Croatia

In this chapter, the RVT-based site response analysis results for a range of local soil profiles ($160 < V_{S30} < 1389$ m/s) – profiles presented in Chapter 5) are used to develop a nonlinear site amplification model for Croatia in a way similar to the recently proposed nonlinear site amplification models (e.g., Choi and Stewart 2005; Walling et al. 2008; Sandikkaya et al. 2013; Kamai et al. 2014). Proposed nonlinear site amplification model for Croatia is developed using a simple functional form based on the site parameter (V_{S30}) and intensity of input rock motion (PGA_{ROCK}). A short overview of the previous AF models is provided in this chapter to be able to discuss the selected functional form. Then, the model predictions are compared with the median predictions of the previous models to evaluate the consistencies and discrepancies with the previous attempts.

6.1. Short summary of the recently developed nonlinear site amplification models

In Chapter 3.4, state-of-the-art nonlinear site amplification models that predict the site amplification factors (AFs) are presented and their databases, utilized soil profiles and ground motions, advantages and disadvantages of the applied methods are thoroughly discussed. Therefore, only a short summary will be provided here. All previous models follow the general functional form as the sum of the linear (f_{LIN}) and nonlinear (f_{NL}) terms:

$$\ln(AF) = f_{LIN}(V_{S30}) + f_{NL}(PGA_{ROCK}, V_{S30}) \qquad (6.1)$$

Models given in Eq. (6.2) (proposed by Choi and Stewart 2005) and Eq. (6.3) (by Walling et al. 2008) were developed within the framework of the NGA projects. Latter model was updated and extended by Kamai et al. (2014) using the same functional form. Model given in Eq. (6.4)

was proposed by Sandikkaya et al. (2013), explicitly using the Pan-European strong motion database. One of the clear distinctions among these models is the applied methodology: Choi and Stewart (2005) and Sandikkaya et al. (2013) models depend on the calculated AFs from the empirical datasets; whereas, the Walling et al. (2008) and Kamai et al. (2014) models were developed by performing RVT-based site response analysis on random/generic soil profiles.

Choi and Stewart (2005) AF model:

$$\ln(AF) = a(T)ln\left(\frac{V_{S30}}{V_{REF}}\right) + b(T, V_{S30})ln\left(\frac{PGA_{ROCK}}{0.1}\right) \qquad (6.2)\text{-}(3.45)$$

Walling et al. (2008) and Kamai et al. (2014) AF model:

$$\ln(AF) = a(T)ln\left(\frac{V_{S30}}{V_{LIN}(T)}\right) - b(T)ln(PGA_{ROCK} + c)$$

$$+ b(T)ln\left[PGA_{ROCK} + c\left(\frac{V_{S30}}{V_{LIN}(T)}\right)^n\right]; \quad V_{S30} < V_{LIN}(T) \qquad (6.3\text{a})\text{-}(3.46\text{a})$$

$$\ln(AF) = [a(T) + b(T)]ln\left(\frac{V_{S30}}{V_{LIN}(T)}\right) + d; \ V_{S30} \geq V_{LIN}(T) \qquad (6.3\text{b})\text{-}(3.46\text{b})$$

Sandikkaya et al. (2013) AF model:

$$\ln(AF) = a(T)ln\left(\frac{V_{S30}}{V_{REF}}\right) + b(T)ln\left[\frac{PGA_{REF} + c\left(\frac{V_{S30}}{V_{REF}}\right)^n}{(PGA_{REF} + c)\left(\frac{V_{S30}}{V_{REF}}\right)^n}\right]; V_{S30} < V_{REF} \quad (6.4\text{a})\text{-}(3.42\text{a})$$

$$\ln(AF) = a(T)ln\left(\frac{\min(V_{S30}, V_{CON})}{V_{REF}}\right); V_{S30} \geq V_{REF} \qquad (6.4\text{b})\text{-}(3.42\text{b})$$

In all three models, PGA_{REF} or PGA_{ROCK} is the peak ground acceleration at the reference rock conditions, V_{REF} is shear wave velocity of the reference rock (750, 1100 or 1180 m/s depending on the study), V_{CON} stands for the limiting V_{S30} after which the site amplification is constant, $V_{LIN}(T)$ represents the cut-off V_{S30} value representing the end of nonlinear site amplification zone at each period, c and n are the period-independent regression parameters. Coefficient c defines the transition between the higher and lower ground motion amplitudes, coefficient n captures the soil non-linearity at lower V_{S30} values, and coefficient d implicitly relates the linear

transition between $V_{LIN}(T)$ and V_{REF}. Period-dependent coefficient $a(T)$ describes the linear change in AF with V_{S30} up to V_{REF} and $b(T)$ controls the nonlinear soil behaviour based on PGA_{REF}. In all models, the nonlinear coefficient $b(T) = 0.0$ for sites with $V_{S30} > V_{REF}$.

6.2. Proposed nonlinear site amplification model for Croatia

None of the functional forms given above is directly adopted for developing the AF model for Croatia based on the AF dataset presented in Chapter 5. Instead, the functional form given in Eqs. (6.5) is preferred because:

a) **the strong motion dataset of Croatia is limited.** Choi and Stewart (2005) used 209 strong motion stations with available borehole information and geophysical measurements. Their nonlinear site amplification model was developed based on 209 pairs of V_{S30} site classifications and different values of PGA for 1828 recordings from 154 earthquakes based on Eq. (6.2). Similarly, Sandikkaya et al. (2013) utilized the strong motion dataset that was developed within the framework of the SHARE project (http://www.share-eu.org/), which includes 5530 three-component accelerograms from 414 earthquakes at 1616 sites to develop nonlinear site amplification model based on Eq. (6.4). For Croatia, developing the nonlinear site amplification model based on the empirical strong motion database is not possible due to limited strong motion database, especially for high ground shaking levels (only a few records from Croatia exist in the BSHAP database as presented in Šalić et al. 2017).

b) **the soil profiles used in this study are measured.** Walling et al. (2008) and Kamai et al. (2014) developed analytical models based on the 1D site response simulations for the purpose of providing nonlinear AF to be used in GMPE development to overcome the scarcity of strong ground motion data required to constrain the nonlinear site response. The AFs were estimated using the RVT-based equivalent linear site response analysis based on six generic soil profiles (V_{S30} =190, 270, 400, 560, 760 and 900 m/s) using an algorithm to randomize the shear-wave velocity profiles, layer thicknesses, bedrock depth, and nonlinear soil properties. On the other hand, the shear wave velocity profiles collected for purpose of this study are "real" soil profiles as explained in Chapter 5.

Therefore, the range of uncertainty covered in the AFs calculated in the proposed model is significantly different than that of Walling et al. (2008) and Kamai et al. (2014).

c) **the applicability range of the proposed model is different.** The range of input ground motions utilized in this study is $0.03 \leq PGA_{ROCK} \leq 0.37$ g to be consistent with the return period of 475-years ground motions in Croatia, while other studies covered a larger range of PGA_{ROCK} from 0.01 g up to 1.5 g.

Choi and Stewart (2005) proposed discrete AF models for V_{S30} ranges defined by NEHRP site categories while Walling et al. (2008), Sandikkaya et al. (2013) and Kamai et al. (2014) developed continuous nonlinear-site amplification models covering a large range of V_{S30} values. In this study, an approach similar to Choi and Stewart (2005) is preferred and discrete AF models for V_{S30} categories presented in Figure 5.7 (D: $V_{S30} < 200$ m/s; C1: $200 \leq V_{S30} < 280$ m/s; C2: $280 \leq V_{S30} < 360$ m/s; B1: $360 \leq V_{S30} < 560$ m/s; B2: $560 \leq V_{S30} < 760$ m/s; A: $760 \leq V_{S30} < 1100$ m/s; A0: $V_{S30} \geq 1100$ m/s) are developed. The main reason behind this preference is the soil profiles: since real (measured) soil profiles are used in this study, number of data in each category varies significantly and a stable continuous functional form is hard to achieve. Number of studied soil profiles within each V_{S30} category is shown in Figure 5.4a above.

Proposed functional form for each V_{S30} category follows the general form given in Eq. (6.1) and the model proposed by Choi and Stewart (2005) (Eq. 6.2) with slight modifications as given below:

a) $160 \leq V_{S30} < 760$ m/s:

$$\ln(AF) = a(T)\ln\left(\frac{V_{S30}}{V_{REF}}\right) + b_1(T)\ln\left(\frac{PGA_{ROCK}}{0.1 \text{ g}}\right) + b_2(T)\left[\ln\left(\frac{PGA_{ROCK}}{0.1 \text{ g}}\right)\right]^2 \qquad (6.5a)$$

b) $760 \leq V_{S30} < 1100$ m/s:

$$\ln(AF) = a(T)\ln\left(\frac{V_{S30}}{V_{REF}}\right) + b_1(T)\ln\left(\frac{PGA_{ROCK}}{0.1 \text{ g}}\right) \qquad (6.5b)$$

c) $V_{S30} \geq V_{REF} = 1100$ m/s:

$$\ln(AF) = a(T)\ln\left(\frac{V_{S30}}{V_{REF}}\right) \qquad (6.5c)$$

Site amplification factor AF as a function of PGA_{ROCK} for soil V_{S30} intra-categories with median amplification regression function following the proposed AF model (functional form of Eqs. 6.5) at different spectral periods is presented in Figures 6.1 to 6.7 based on the AF dataset presented in Chapter 5. Figures 6.1 to 6.7 show that the distribution of AFs with PGA_{ROCK} is generally flat at PGA_{ROCK} values up to about 0.1 g, representing linear site response. After 0.1 g, AFs decrease as PGA_{ROCK} increases, showing the effect of soil's non-linearity. The term "0.1 g" is added as a pivot point that represents the transition between the linear and nonlinear behaviour of AFs with increasing PGA_{ROCK}. On the other hand, the linear form as proposed by Choi and Stewart (2005) is not adequate to describe the significant non-linearity at larger PGA_{ROCK} levels. Trends from Figures 6.1–6.7 indicate that the AFs are proportional to $ln(V_{S30}/V_{REF})$ in the linear range (low input ground motions): when the profile is softer it has stronger linear amplification. As intensity of input ground motion increases, the amplification at short-to-middle periods decreases as a manifestation of increased damping. At longer periods, the amplification is not dependent on PGA_{ROCK} for stiffer profiles, but increases with PGA_{ROCK} for the softer profiles, as a result of the shift in the predominant peak to longer periods. When a single linear function for PGA_{ROCK} is used, the decrease in AF with large PGA_{ROCK} values pulls the tail of the regression line up, artificially increasing AF at smaller PGA_{ROCK} values, therefore quadratic term is added in Eq. (6.5a). The regression coefficients in Eq. (6.5), $a(T)$, $b_1(T)$ and $b_2(T)$ are period-dependent. For $V_{S30} \geq V_{REF} = 1100$ m/s (reference soil category A0), there is no dependence on the PGA_{ROCK} (e.g., Abrahamson and Silva 2008) and $b_1(T)$ and $b_2(T)$ are set to zero value. Full list of the regression coefficients with standard errors from the regression for each soil category are listed in Tables 6.1–6.7.

Figures 6.8 and 6.9 show variation of the nonlinear site coefficients $b_1(T)$ and $b_2(T)$ as a function of spectral period for each V_{S30} category. Negative values of $b_1(T)$ and $b_2(T)$ describe the decrease in AF at shorter periods due to non-linearity. High negative values are estimated for softer sites with lower values of V_{S30} for which the non-linearity is the strongest in terms of de-amplification, i.e., decrease of AF with PGA_{ROCK}. For stiffer sites with higher values of V_{S30}, $b_1(T)$ and $b_2(T)$ values are lower and closer to zero value indicating that nonlinear effects are low or can be neglected. For site category A ($760 \leq V_{S30} < 1100$ m/s), coefficient $b_1(T)$ at longer spectral periods shows very low value (close to zero) and amplification becomes insensitive to input rock motion, whereas at shorter periods (< 0.1 sec) small $b_1(T)$ values represent the variation of the amplification of the bedrock motion due to thin soft surface layers

above shallow bedrock (peak of the response spectra of bedrock motion is at approx. 0.1 s, Figure 5.2).

A closer look at Figures 5.7a–g would show that the soft site profiles with lower values of V_{S30} (and long predominant periods) are generally deeper soil profiles; bedrock depth ranging between 65–85 m. On the other hand, soil profiles with higher values of V_{S30} (and shorter predominant periods) generally have shallow bedrock depths and thin soil cover (< 10 m). In Figures 6.8 and 6.9, the period at which the values of $b_1(T)$ and $b_2(T)$ becomes positive is strongly correlated with the predominant period of the soil profile. The shift from negative to positive values is related to the amplification due to elongation of the predominant period (shift of the peak into longer periods) as observed in Figures 5.7a–d. Similar variations in nonlinear site amplification coefficient $b(T)$ were also observed in Choi and Stewart (2005); Walling et al. (2008); Sandikkaya et al. (2013) and Kamai et al. (2014) (e.g., Figure 3.12, right). In this study, the nonlinear site amplification parameters are not smoothed as in the example given in Figure 3.12, since the site amplification model proposed here is not currently adopted in a GMPE.

Figure 6.1: Site amplification factor AF as a function of PGA_{ROCK} for soil intra-category D with median amplification regression function (blue thick line) for different spectral periods. Circles represent individual AFs for each studied soil profile presented in Chapter 5 within soil intra-category D. Regression coefficients $a(T), b_1(T)$ and $b_2(T)$ are listed in Table 6.1.

C1: 200 ≤ V_{S30} < 280 m/s
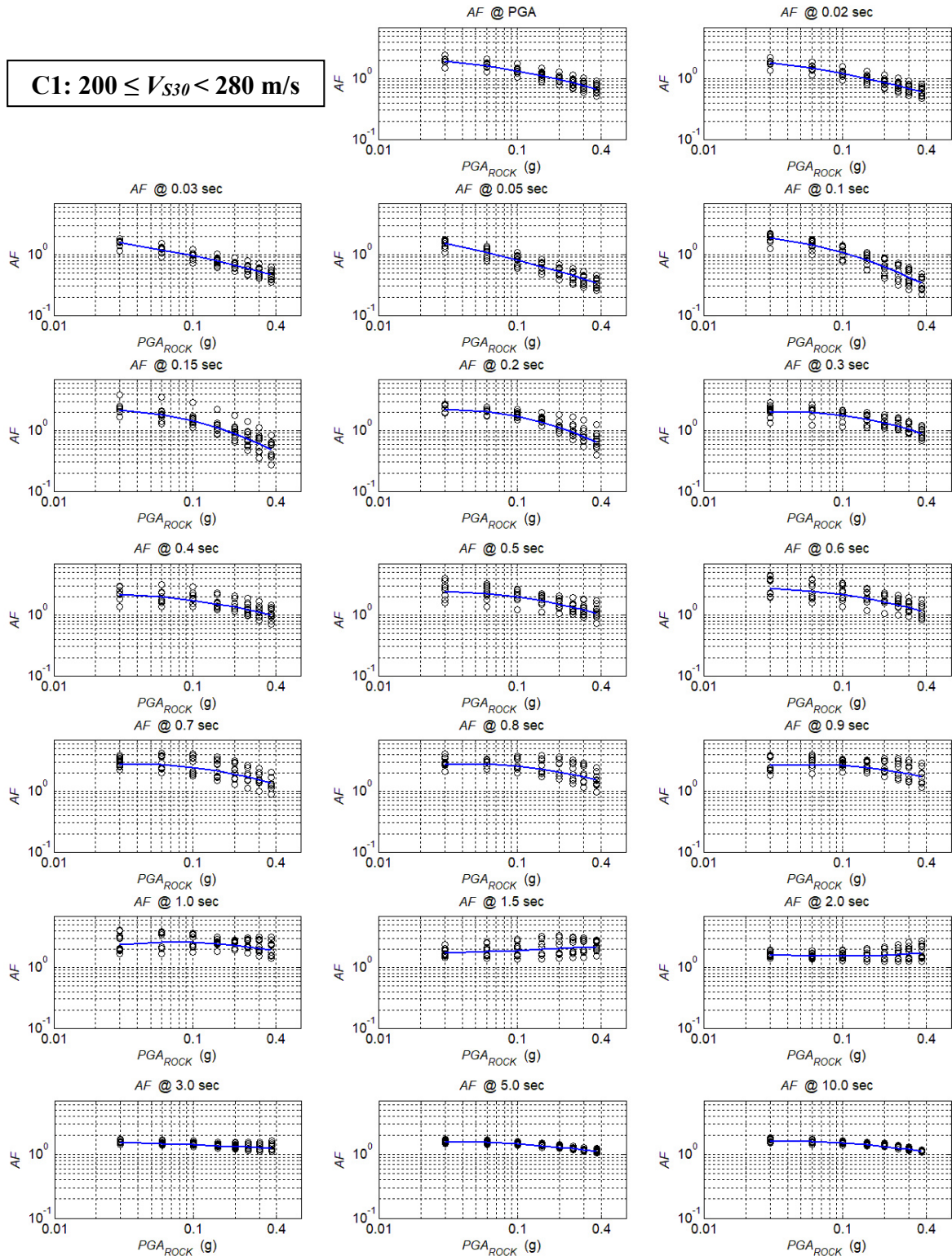
Figure 6.2: Site amplification factor AF as a function of PGA_{ROCK} for soil intra-category C1 with median amplification regression function (blue thick line) for different spectral periods. Circles represent individual AFs for each studied soil profile presented in Chapter 5 within soil intra-category C1. Regression coefficients $a(T), b_1(T)$ and $b_2(T)$ are listed in Table 6.2.
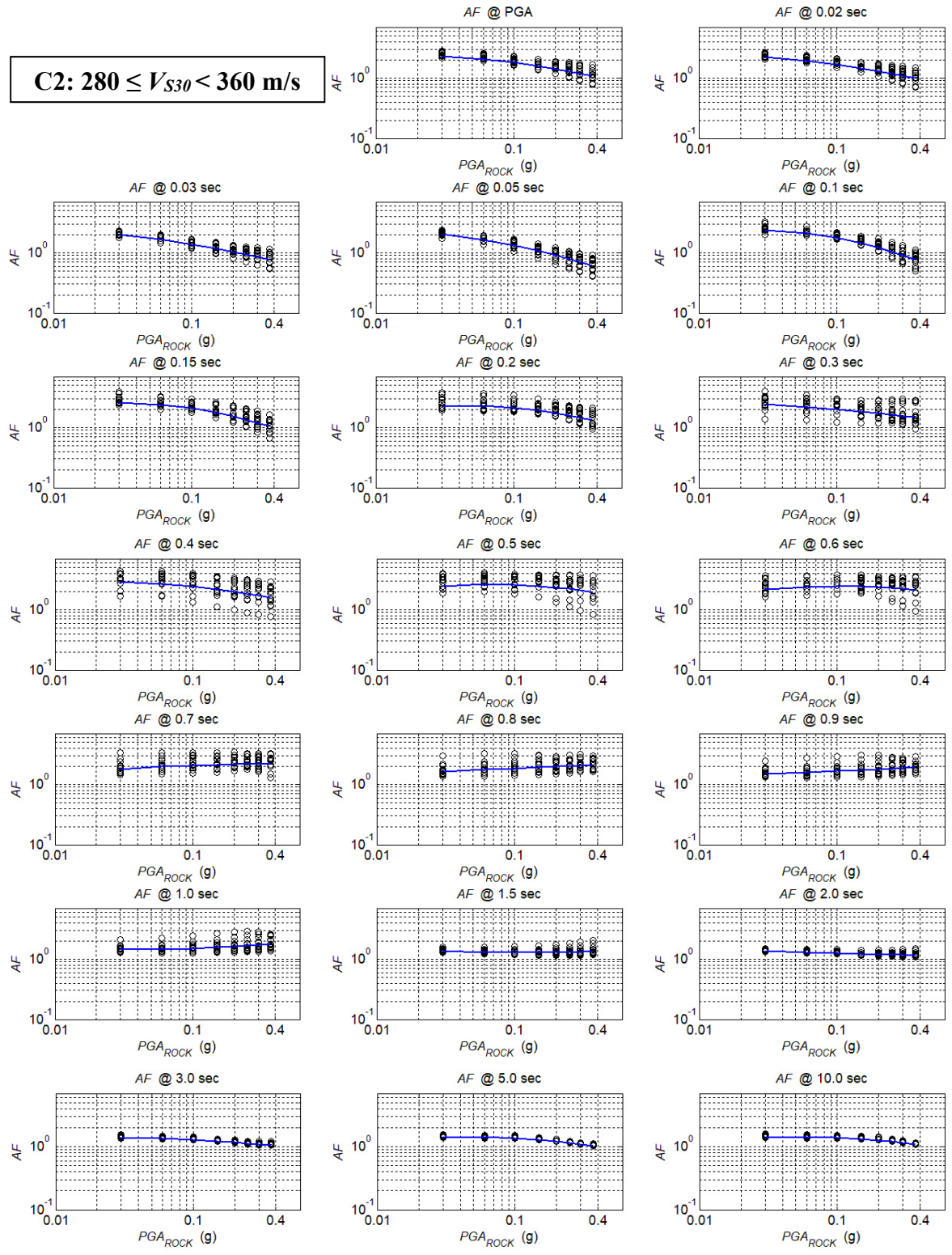
Figure 6.3: Site amplification factor AF as a function of PGA_{ROCK} for soil intra-category C2 with median amplification regression function (blue thick line) for different spectral periods. Circles represent individual AFs for each studied soil profile presented in Chapter 5 within soil intra-category C2. Regression coefficients $a(T), b_1(T)$ and $b_2(T)$ are listed in Table 6.3.
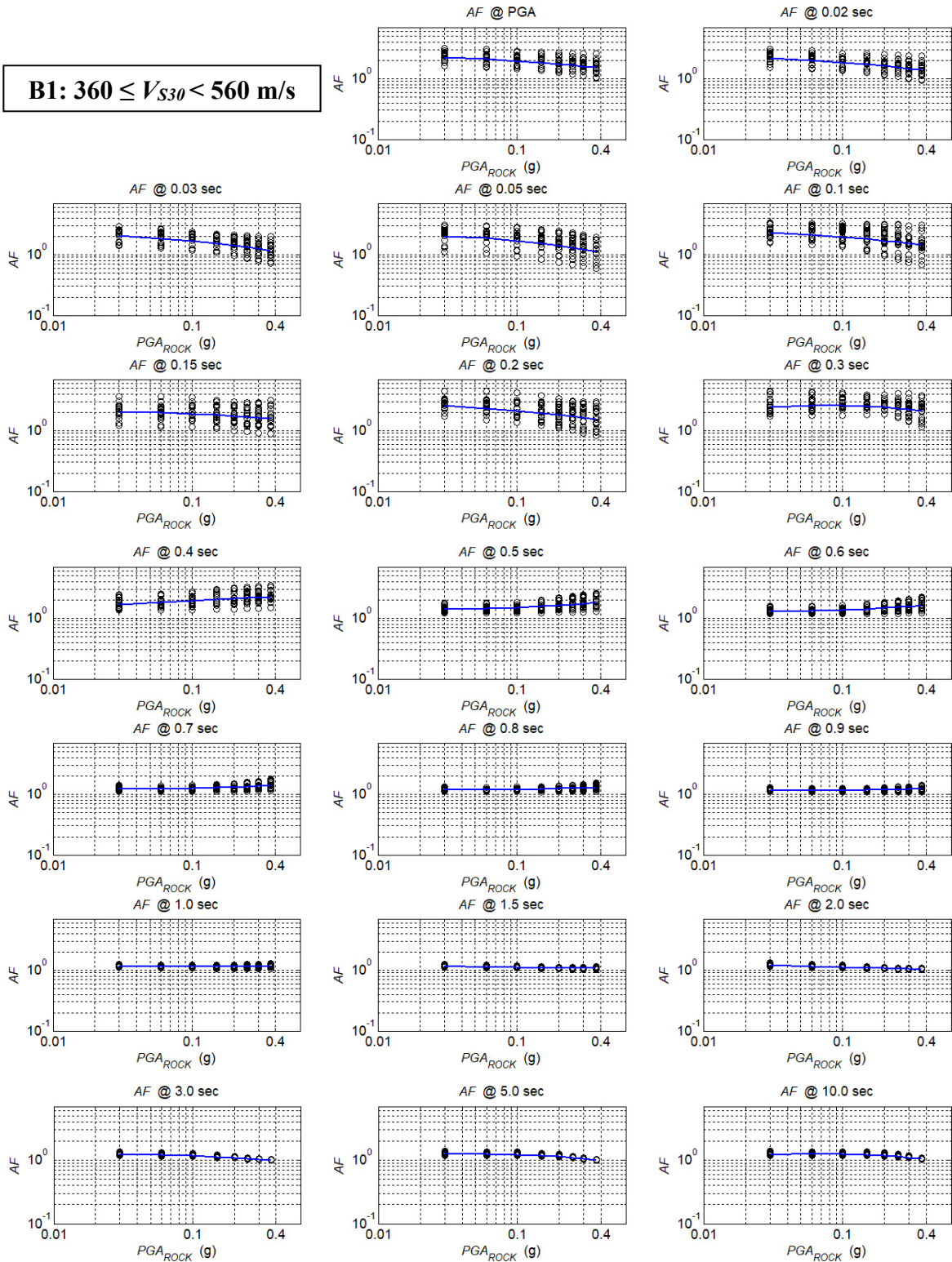
Figure 6.4: Site amplification factor AF as a function of PGA_{ROCK} for soil intra-category B1 with median amplification regression function (blue thick line) for different spectral periods. Circles represent individual AFs for each studied soil profile presented in Chapter 5 within soil intra-category B1. Regression coefficients $a(T)$, $b_1(T)$ and $b_2(T)$ are listed in Table 6.4.

B2: $560 \leq V_{S30} < 760$ m/s
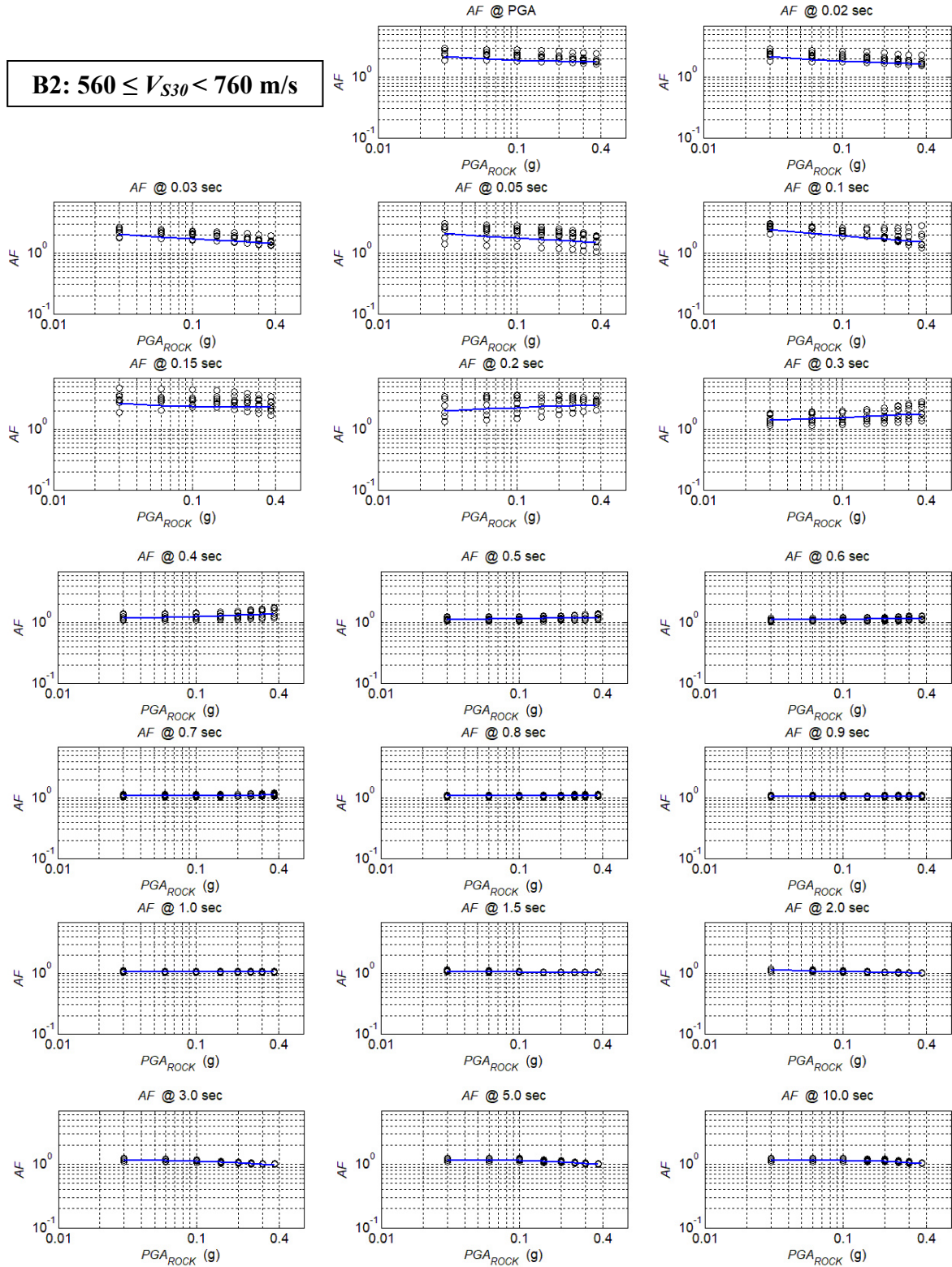
Figure 6.5: Site amplification factor AF as a function of PGA_{ROCK} for soil intra-category B2 with median amplification regression function (blue thick line) for different spectral periods. Circles represent individual AFs for each studied soil profile presented in Chapter 5 within soil intra-category B2. Regression coefficients $a(T)$, $b_1(T)$ and $b_2(T)$ are listed in Table 6.5.
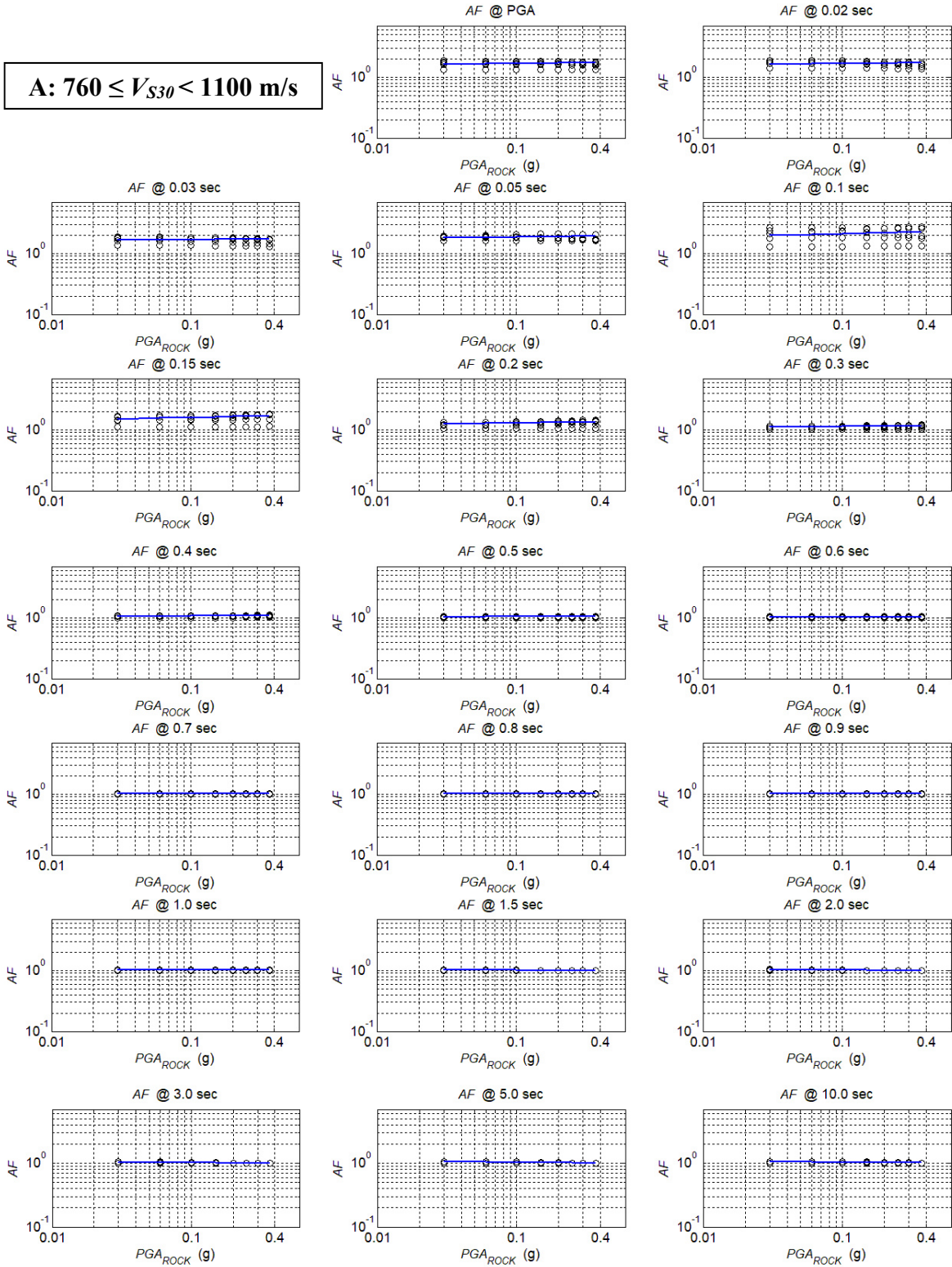
Figure 6.6: Site amplification factor AF as a function of PGA_{ROCK} for soil intra-category A with median amplification regression function (blue thick line) for different spectral periods. Circles represent individual AFs for each studied soil profile presented in Chapter 5 within soil intra-category A. Regression coefficients $a(T)$ and $b_1(T)$ are listed in Table 6.6.
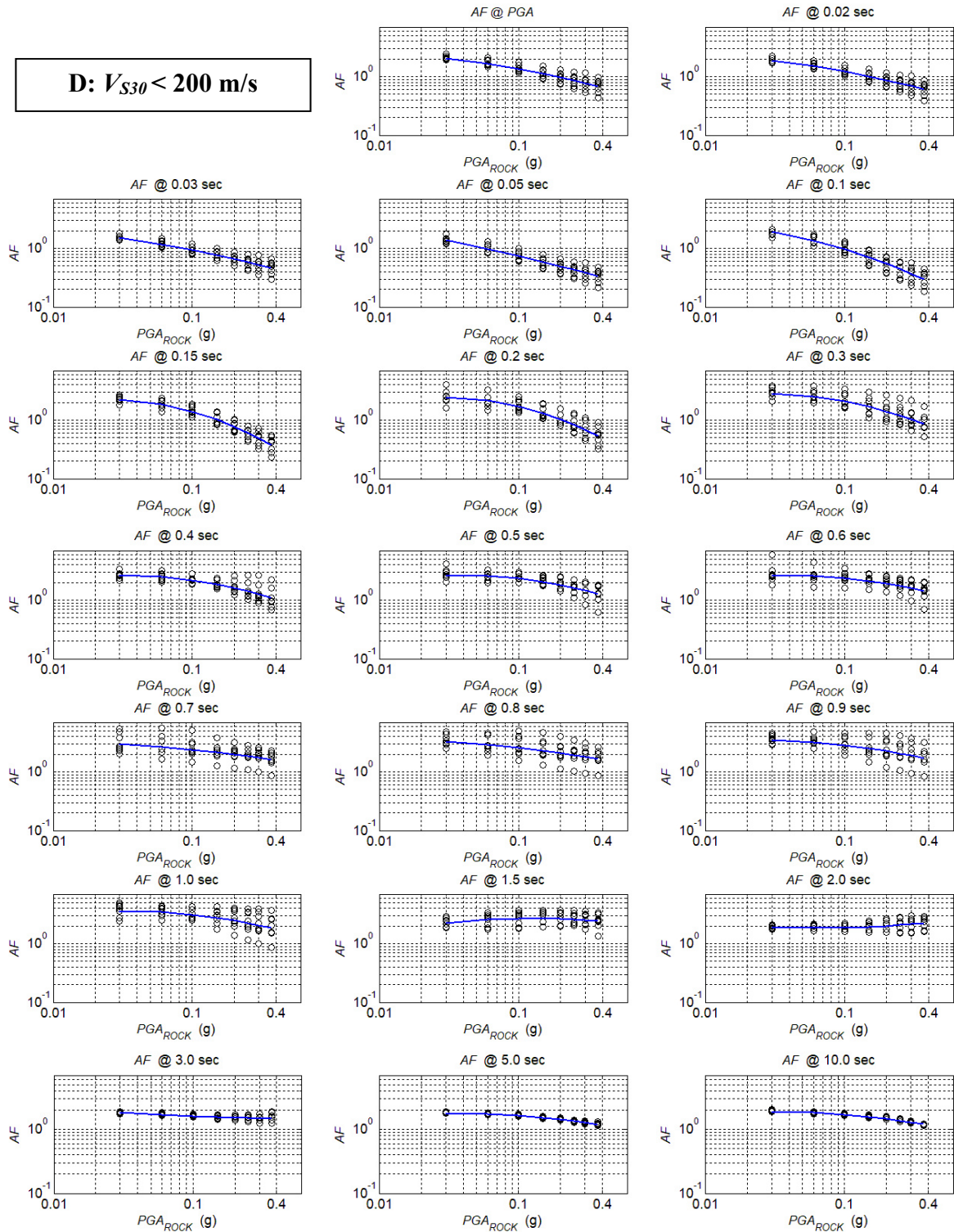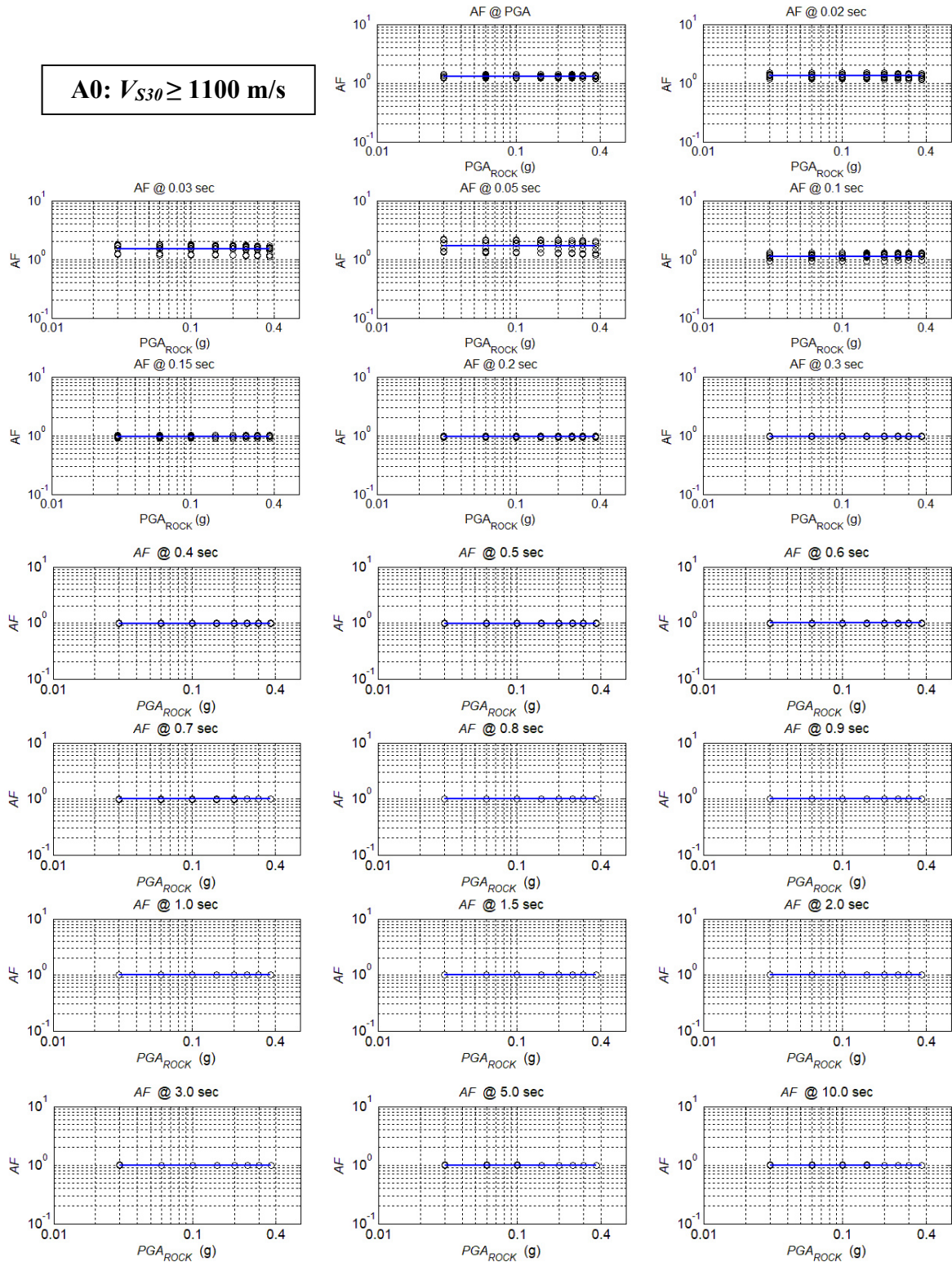
Figure 6.7: Site amplification factor AF as a function of PGA_{ROCK} for soil intra-category A0 with median amplification regression function (blue thick line) for different spectral periods. Circles represent individual AFs for each studied soil profile presented in Chapter 5 within soil intra-category A0. Regression coefficient $a(T)$ is listed in Table 6.7.

Table 6.1: Regression coefficients $a(T)$, $b_1(T)$ and $b_2(T)$ with their standard errors for soil intra-category D: $V_{S30} < 200$ m/s.

T (s)	a	b_1	b_2	$SE\text{-}a$	$SE\text{-}b_1$	$SE\text{-}b_2$
0.01	-0.1778	-0.4324	-0.0763	0.0210	0.0292	0.0394
0.02	-0.1129	-0.4417	-0.0679	0.0209	0.0291	0.0392
0.03	0.0394	-0.4702	-0.0492	0.0208	0.0290	0.0392
0.05	0.1747	-0.5667	-0.0288	0.0222	0.0309	0.0416
0.10	0.0144	-0.7291	-0.1462	0.0263	0.0366	0.0494
0.15	-0.1926	-0.6891	-0.2402	0.0240	0.0335	0.0452
0.20	-0.3065	-0.5723	-0.2338	0.0308	0.0429	0.0579
0.30	-0.4219	-0.4501	-0.1667	0.0352	0.0491	0.0662
0.40	-0.4463	-0.3339	-0.1449	0.0292	0.0406	0.0548
0.50	-0.4967	-0.2728	-0.1517	0.0269	0.0375	0.0506
0.60	-0.4940	-0.2314	-0.1075	0.0304	0.0424	0.0572
0.70	-0.5039	-0.2394	-0.0436	0.0376	0.0523	0.0706
0.80	-0.5474	-0.2630	-0.0583	0.0404	0.0562	0.0759
0.90	-0.6053	-0.2734	-0.0863	0.0408	0.0568	0.0767
1.00	-0.6555	-0.2517	-0.1119	0.0383	0.0533	0.0719
1.50	-0.5685	0.0425	-0.0862	0.0258	0.0359	0.0484
2.00	-0.3634	0.0512	0.0619	0.0194	0.0270	0.0364
3.00	-0.2762	-0.0912	0.0090	0.0090	0.0126	0.0170
5.00	-0.2819	-0.1568	-0.0611	0.0035	0.0049	0.0066
10.00	-0.3056	-0.1738	-0.0677	0.0040	0.0055	0.0075

Table 6.2: Regression coefficients $a(T)$, $b_1(T)$ and $b_2(T)$ with standard errors for soil intra-category C1: $200 \leq V_{S30} < 280$ m/s.

T (s)	a	b₁	b₂	SE-a	SE-b₁	SE-b₂
0.01	-0.2065	-0.4147	-0.0840	0.0190	0.0222	0.0299
0.02	-0.1329	-0.4284	-0.0747	0.0188	0.0220	0.0297
0.03	0.0340	-0.4750	-0.0541	0.0187	0.0219	0.0295
0.05	0.1442	-0.5967	-0.0531	0.0219	0.0257	0.0346
0.10	-0.0536	-0.6618	-0.1730	0.0301	0.0352	0.0475
0.15	-0.2669	-0.5726	-0.2072	0.0365	0.0427	0.0576
0.20	-0.3920	-0.4676	-0.2194	0.0269	0.0314	0.0424
0.30	-0.4065	-0.3018	-0.1653	0.0241	0.0282	0.0381
0.40	-0.3908	-0.2958	-0.0935	0.0263	0.0307	0.0415
0.50	-0.4860	-0.3232	-0.1177	0.0293	0.0343	0.0463
0.60	-0.5476	-0.3261	-0.1159	0.0335	0.0392	0.0528
0.70	-0.6391	-0.2724	-0.1393	0.0356	0.0417	0.0563
0.80	-0.6742	-0.2160	-0.1355	0.0342	0.0401	0.0540
0.90	-0.6871	-0.1511	-0.1233	0.0320	0.0375	0.0505
1.00	-0.6746	-0.0706	-0.1172	0.0296	0.0347	0.0468
1.50	-0.4539	0.0934	0.0112	0.0276	0.0323	0.0436
2.00	-0.3000	0.0188	0.0540	0.0206	0.0241	0.0325
3.00	-0.2535	-0.0913	-0.0087	0.0092	0.0108	0.0146
5.00	-0.2706	-0.1307	-0.0623	0.0048	0.0056	0.0076
10.00	-0.2947	-0.1348	-0.0662	0.0049	0.0057	0.0077

Table 6.3: Regression coefficients $a(T)$, $b_1(T)$ and $b_2(T)$ with their standard errors for soil intra-category C2: $280 \leq V_{S30} < 360$ m/s.

T (s)	a	b_1	b_2	SE-a	SE-b_1	SE-b_2
0.01	-0.5286	-0.2946	-0.0701	0.0214	0.0208	0.0280
0.02	-0.4511	-0.3148	-0.0620	0.0212	0.0206	0.0278
0.03	-0.2890	-0.3775	-0.0532	0.0212	0.0206	0.0278
0.05	-0.2509	-0.4789	-0.0942	0.0238	0.0231	0.0312
0.10	-0.5122	-0.4309	-0.1671	0.0226	0.0220	0.0296
0.15	-0.6557	-0.3512	-0.1361	0.0263	0.0255	0.0344
0.20	-0.6764	-0.1963	-0.1322	0.0269	0.0261	0.0352
0.30	-0.6097	-0.1970	-0.0214	0.0385	0.0374	0.0503
0.40	-0.7949	-0.2317	-0.0794	0.0483	0.0469	0.0632
0.50	-0.8510	-0.0786	-0.1042	0.0421	0.0408	0.0550
0.60	-0.7963	0.0041	-0.0831	0.0345	0.0335	0.0452
0.70	-0.6546	0.0807	-0.0358	0.0262	0.0255	0.0343
0.80	-0.5501	0.0991	-0.0080	0.0246	0.0239	0.0322
0.90	-0.4512	0.0974	0.0154	0.0240	0.0233	0.0314
1.00	-0.3661	0.0802	0.0322	0.0229	0.0222	0.0299
1.50	-0.2245	-0.0085	0.0310	0.0133	0.0130	0.0175
2.00	-0.1999	-0.0708	0.0084	0.0071	0.0069	0.0093
3.00	-0.2302	-0.1147	-0.0374	0.0037	0.0036	0.0048
5.00	-0.2744	-0.1161	-0.0760	0.0033	0.0032	0.0043
10.00	-0.2958	-0.0953	-0.0713	0.0044	0.0043	0.0057

Table 6.4: Regression coefficients $a(T), b_1(T)$ and $b_2(T)$ with their standard errors for soil intra-category B1: $360 \leq V_{S30} < 560$ m/s.

T (s)	a	b_1	b_2	$SE\text{-}a$	$SE\text{-}b_1$	$SE\text{-}b_2$
0.01	-0.8516	-0.1489	-0.0327	0.0346	0.0229	0.0305
0.02	-0.7775	-0.1712	-0.0328	0.0353	0.0233	0.0311
0.03	-0.6554	-0.2233	-0.0439	0.0388	0.0256	0.0342
0.05	-0.6737	-0.2276	-0.0703	0.0503	0.0332	0.0443
0.10	-0.8614	-0.1846	-0.0359	0.0552	0.0364	0.0486
0.15	-0.8134	-0.0978	-0.0353	0.0471	0.0311	0.0414
0.20	-0.9565	-0.1990	-0.0310	0.0527	0.0348	0.0464
0.30	-1.2260	-0.0472	-0.0873	0.0364	0.0240	0.0320
0.40	-0.8390	0.1190	-0.0012	0.0245	0.0161	0.0215
0.50	-0.5127	0.1015	0.0358	0.0202	0.0134	0.0178
0.60	-0.4026	0.0786	0.0332	0.0165	0.0109	0.0146
0.70	-0.2857	0.0481	0.0248	0.0115	0.0076	0.0101
0.80	-0.2314	0.0315	0.0201	0.0090	0.0059	0.0079
0.90	-0.1912	0.0170	0.0166	0.0071	0.0047	0.0062
1.00	-0.1624	0.0037	0.0141	0.0056	0.0037	0.0050
1.50	-0.1287	-0.0343	0.0096	0.0035	0.0023	0.0031
2.00	-0.1466	-0.0637	0.0008	0.0035	0.0023	0.0031
3.00	-0.2066	-0.0850	-0.0269	0.0043	0.0028	0.0038
5.00	-0.2640	-0.0788	-0.0550	0.0048	0.0032	0.0043
10.00	-0.2860	-0.0538	-0.0571	0.0053	0.0035	0.0047

Table 6.5: Regression coefficients $a(T), b_1(T)$ and $b_2(T)$ with their standard errors for soil intra-category B2: $560 \leq V_{S30} < 760$ m/s.

T (s)	a	b_1	b_2	SE-a	SE-b_1	SE-b_2
0.01	-1.5295	-0.0916	0.0211	0.0806	0.0319	0.0420
0.02	-1.4285	-0.1079	0.0217	0.0816	0.0324	0.0426
0.03	-1.2709	-0.1343	0.0072	0.0821	0.0325	0.0428
0.05	-1.3491	-0.1320	0.0062	0.1346	0.0533	0.0702
0.10	-1.5532	-0.1785	0.0097	0.1009	0.0400	0.0526
0.15	-2.0209	-0.0652	0.0400	0.1588	0.0629	0.0829
0.20	-1.9413	0.0817	-0.0157	0.0825	0.0327	0.0430
0.30	-1.0398	0.0991	0.0092	0.0579	0.0229	0.0302
0.40	-0.5594	0.0518	0.0063	0.0326	0.0129	0.0170
0.50	-0.3481	0.0282	0.0037	0.0201	0.0080	0.0105
0.60	-0.2776	0.0198	0.0029	0.0159	0.0063	0.0083
0.70	-0.2018	0.0096	0.0023	0.0113	0.0045	0.0059
0.80	-0.1668	0.0037	0.0024	0.0092	0.0037	0.0048
0.90	-0.1416	-0.0021	0.0027	0.0077	0.0030	0.0040
1.00	-0.1247	-0.0081	0.0033	0.0066	0.0026	0.0035
1.50	-0.1168	-0.0302	0.0053	0.0062	0.0025	0.0032
2.00	-0.1532	-0.0508	0.0019	0.0079	0.0031	0.0041
3.00	-0.2390	-0.0666	-0.0167	0.0106	0.0042	0.0055
5.00	-0.3163	-0.0612	-0.0381	0.0122	0.0048	0.0064
10.00	-0.3457	-0.0396	-0.0424	0.0130	0.0051	0.0068

Table 6.6: Regression coefficients $a(T)$ and $b_1(T)$ with their standard errors for soil intra-category A: $760 \leq V_{S30} < 1100$ m/s. Nonlinear site coefficient $b_2(T) = 0.0$.

T (s)	a	b_1	SE-a	SE-b_1
0.01	-1.8083	0.0216	0.1212	0.0351
0.02	-1.8097	0.0167	0.1291	0.0374
0.03	-1.8539	0.0010	0.1183	0.0343
0.05	-2.1864	0.0252	0.1378	0.0399
0.10	-2.6093	0.0551	0.2118	0.0613
0.15	-1.6471	0.0477	0.0489	0.0142
0.20	-0.9261	0.0269	0.0171	0.0049
0.30	-0.4418	0.0122	0.0066	0.0019
0.40	-0.2379	0.0060	0.0035	0.0010
0.50	-0.1454	0.0032	0.0024	0.0007
0.60	-0.1140	0.0021	0.0020	0.0006
0.70	-0.0797	0.0008	0.0016	0.0005
0.80	-0.0635	0.0000	0.0015	0.0004
0.90	-0.0518	-0.0008	0.0014	0.0004
1.00	-0.0438	-0.0018	0.0015	0.0004
1.50	-0.0401	-0.0067	0.0025	0.0007
2.00	-0.0572	-0.0129	0.0041	0.0012
3.00	-0.0932	-0.0199	0.0060	0.0017
5.00	-0.1236	-0.0208	0.0077	0.0022
10.00	-0.1401	-0.0153	0.0082	0.0024

Table 6.7: Regression coefficients $a(T)$ with standard errors for soil intra-category reference bedrock: $V_{S30} > V_{S30REF} = 1100$ m/s. Nonlinear site coefficients $b_1(T) = 0.0$ and $b_2(T) = 0.0$.

T (s)	a	SE-a
0.01	1.6878	0.0821
0.02	1.8025	0.1054
0.03	2.6688	0.1702
0.05	3.4235	0.1688
0.10	0.7561	0.1110
0.15	-0.2601	0.0288
0.20	-0.3240	0.0163
0.30	-0.2421	0.0104
0.40	-0.1658	0.0070
0.50	-0.1192	0.0051
0.60	-0.1010	0.0043
0.70	-0.0798	0.0034
0.80	-0.0690	0.0030
0.90	-0.0607	0.0027
1.00	-0.0544	0.0025
1.50	-0.0446	0.0023
2.00	-0.0421	0.0024
3.00	-0.0401	0.0025
5.00	-0.0375	0.0025
10.00	-0.0337	0.0025
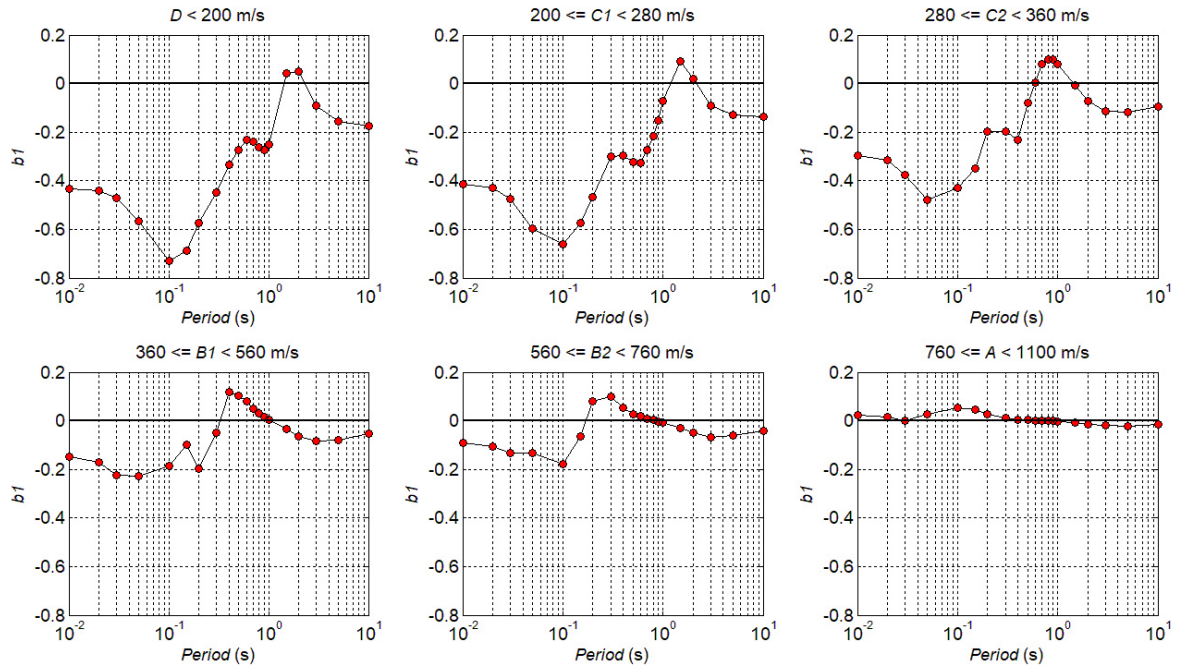
Figure 6.8. Variation of regression coefficient $b_1(T)$ with spectral period. For soil category A0 nonlinear coefficient $b_2(T) = 0.0$.
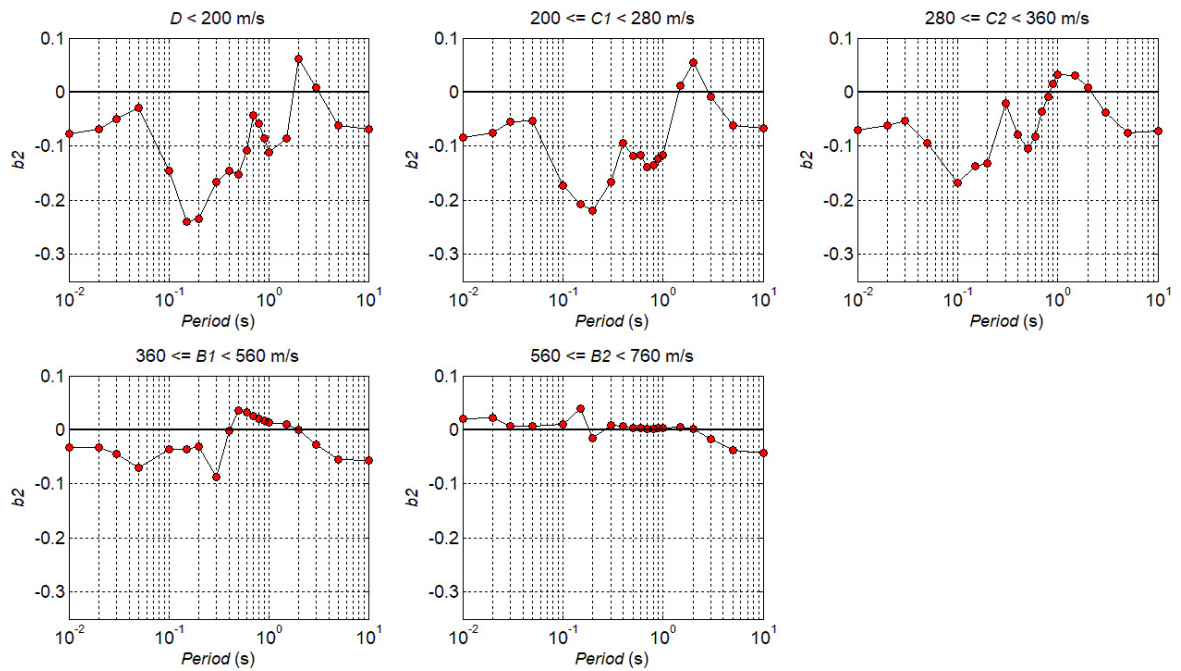
Figure 6.9. Variation of regression coefficient $b_2(T)$ with spectral period. For soil categories A and A0 nonlinear coefficient $b_2(T) = 0.0$.

166

6.3. Evaluation and discussion of the proposed nonlinear site amplification model for Croatia

In this section, the proposed nonlinear site amplification models for Croatia are evaluated by comparing the median predictions with the AFs given in Eurocode 8 (EC8) and the median predictions of Sandikkaya et al. (2013) and Kamai et al. (2014) site amplification models. There are several reasons for choosing these two AF models for comparison. First of all, Sandikkaya et al. (2013) model was developed after Choi and Stewart (2005) and Walling et al. (2008) models and the modellers showed that their new model was comparable with the site amplification factors given in Abrahamson and Silva (2008) and Boore and Atkinson (2008) GMPEs (e.g., Figures 3.14–15). Sandikkaya et al. (2013) model was developed for Pan-European region which is closely related to the seismological source models for the Western Balkan Region (Mihaljević et al. 2017), while the other AF models were developed for the Western US. Although the models are intended to be applicable in other shallow crustal and active tectonic regions around the world, local models developed from the regional datasets are expected to reflect the regional tectonic characteristics better than the others. Additionally, Sandikkaya et al. (2013) model was compared with Eurocode 8 for Type 1 ($M_S > 5.5$) and Type 2 ($M_S \leq 5.5$) response spectra (Figure 3.15) and the authors emphasized the importance of period dependence of site amplification for different PGA_{ROCK} levels. Sandikkaya et al. (2013, 2018) showed that soil nonlinearity as well as period-dependent amplification site factors are poorly constrained in the current EC8 provisions regardless of variations in reference rock spectral amplitudes. On the other hand, the work of Kamai et al. (2014) was based on the RVT-based site response analysis results as this study; therefore the Kamai et al. (2014) AF model is expected to be consistent with the results of this study.

Figures 6.11–6.16 compare the median predictions of the proposed model with the median predictions of Sandikkaya et al. (2013) and Kamai et al. (2014) site amplification models for each site category. Figure 6.10 presents the elastic response spectra defined in EC8 for each site category (E, D, C, B and A). In this study, the Type-2 response spectra is represented with $PGA_{ROCK} = 0.05$ g and 0.10 g, and Type-1 with $PGA_{ROCK} = 0.20$ g and 0.30 g. Amplification factors from EC8 are calculated following the same expression used for site response analysis amplification factors (Eq. 1.1) as the ratio of the response spectrum at the surface and at the bedrock (soil category A) and added to Figures 6.11 to 6.16 for comparison.
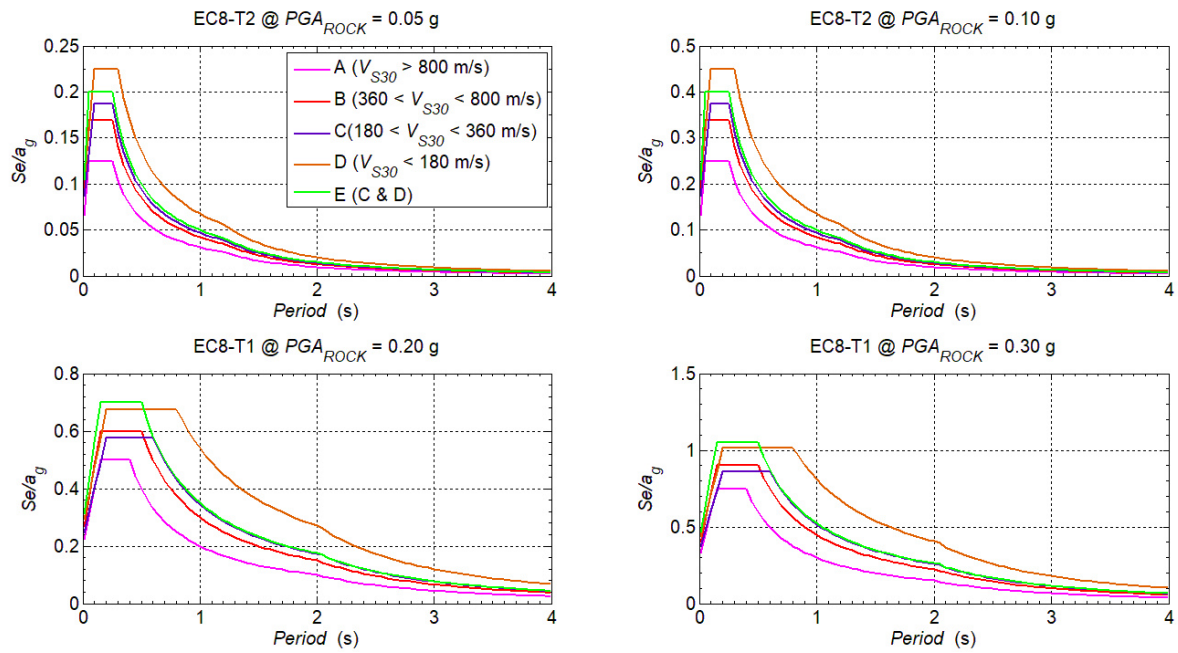
Figure 6.10. Elastic response spectra defined by building seismic design code Eurocode 8 for each ground type (A, B, C, D, E) and for spectra of Type 2 (top row) and Type 1 (bottom row). Note that soil category E represent soil profile consisting of a surface alluvium layers with V_S values of type C and D varying between 5 m and 20 m underlain by stiffer material with $V_S > 800$ m/s.
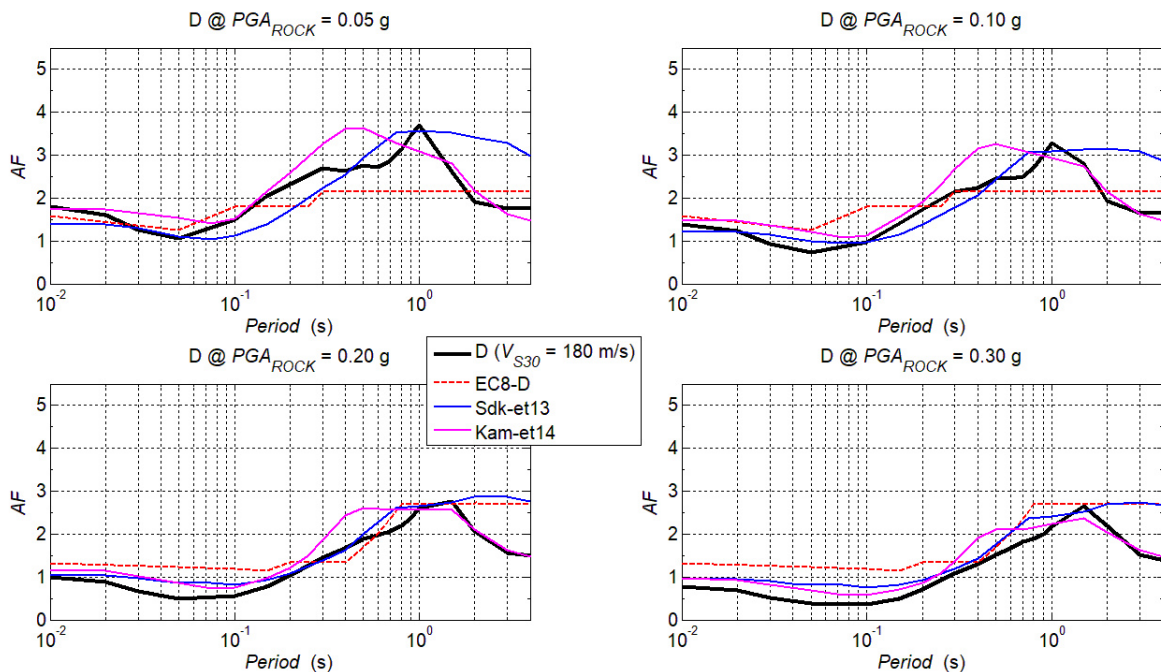
Figure 6.11: Comparison of proposed nonlinear site amplification period-dependent model for $V_{S30} = 180$ m/s within soil intra-category D: $V_{S30} < 200$ m/s (thick black line). AF–EC8 soil category D is represented with red dashed line, Sandikkaya et al. (2013) and Kamai et al. (2014) models with blue and magenta lines for different input $PGA_{ROCK} = 0.05$ g and 0.10 g (EC8-Type 2) and $PGA_{ROCK} = 0.20$ g and 0.30 g (EC8-Type 1).
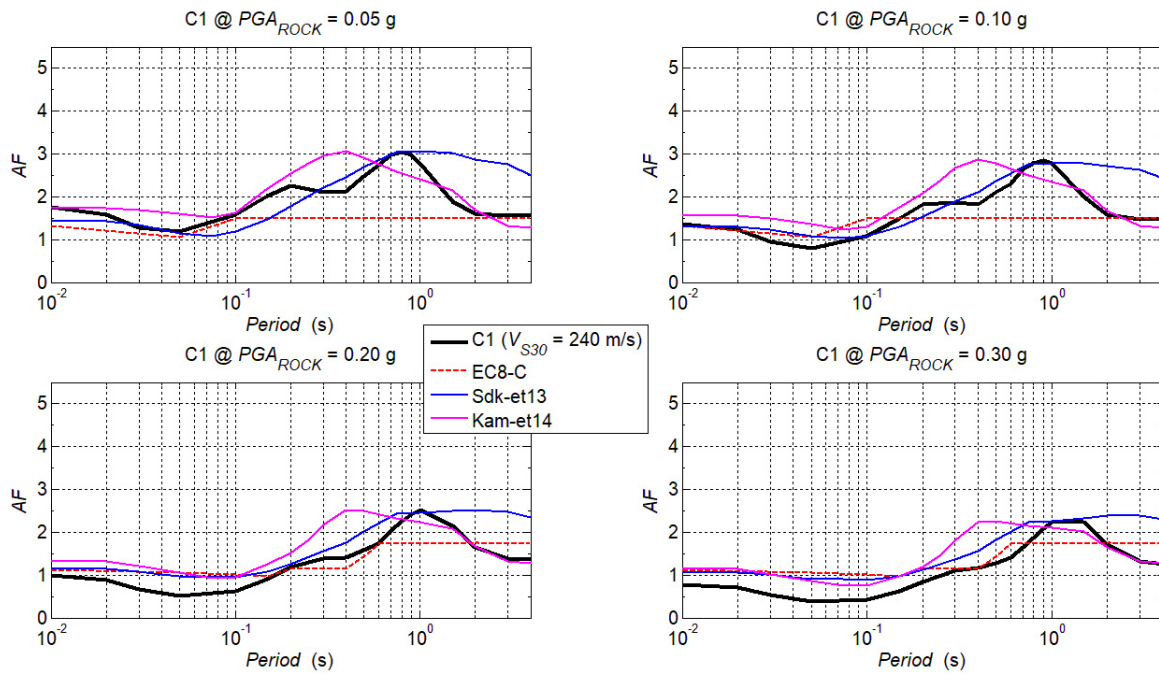
Figure 6.12: Comparison of proposed nonlinear site amplification period-dependent model for $V_{S30} = 240$ m/s within soil intra-category C1: $200 \leq V_{S30} = 280$ m/s (thick black lines). AF–EC8 soil category C is represented with red dashed line, Sandikkaya et al. (2013) and Kamai et al. (2014) models with blue and magenta lines for different input $PGA_{ROCK} = 0.05$ g and 0.10 g (EC8-Type 2) and $PGA_{ROCK} = 0.20$ g and 0.30 g (EC8-Type 1).
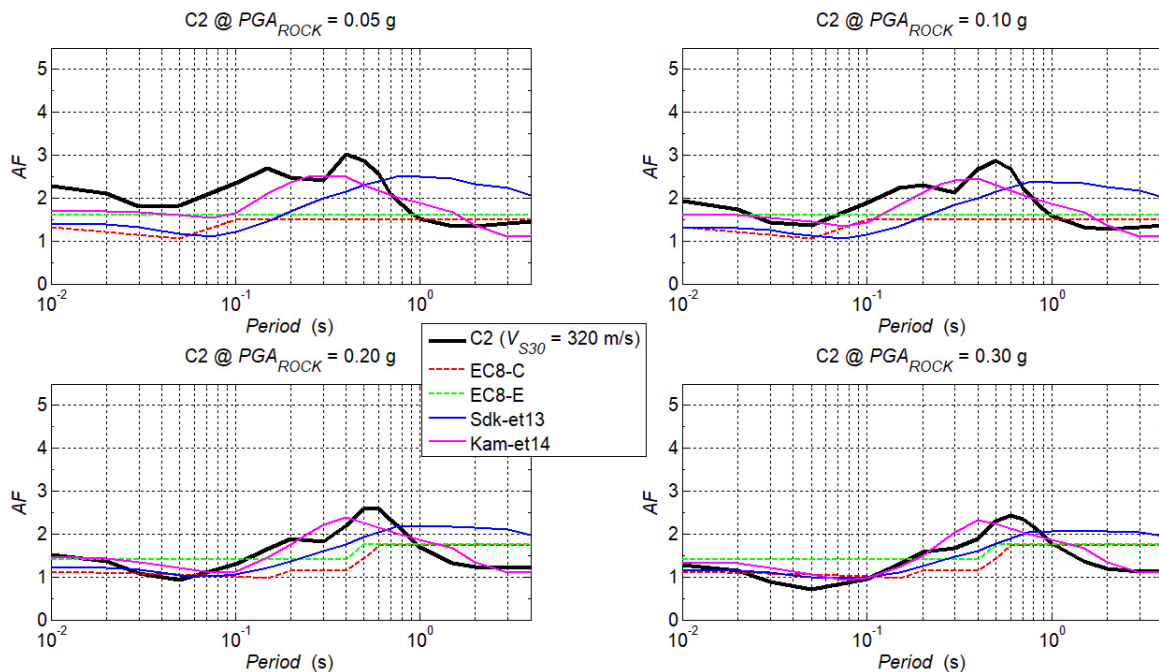
Figure 6.13: Comparison of proposed nonlinear site amplification period-dependent model for $V_{S30} = 320$ m/s within soil intra-category C2: $280 \leq V_{S30} = 360$ m/s (thick black lines). AF–EC8 soil categories C and E are represented with red and green dashed lines, Sandikkaya et al. (2013) and Kamai et al. (2014) models with blue and magenta lines for different input $PGA_{ROCK} = 0.05$ g and 0.10 g (EC8-Type 2) and $PGA_{ROCK} = 0.20$ g and 0.30 g (EC8-Type 1).

169
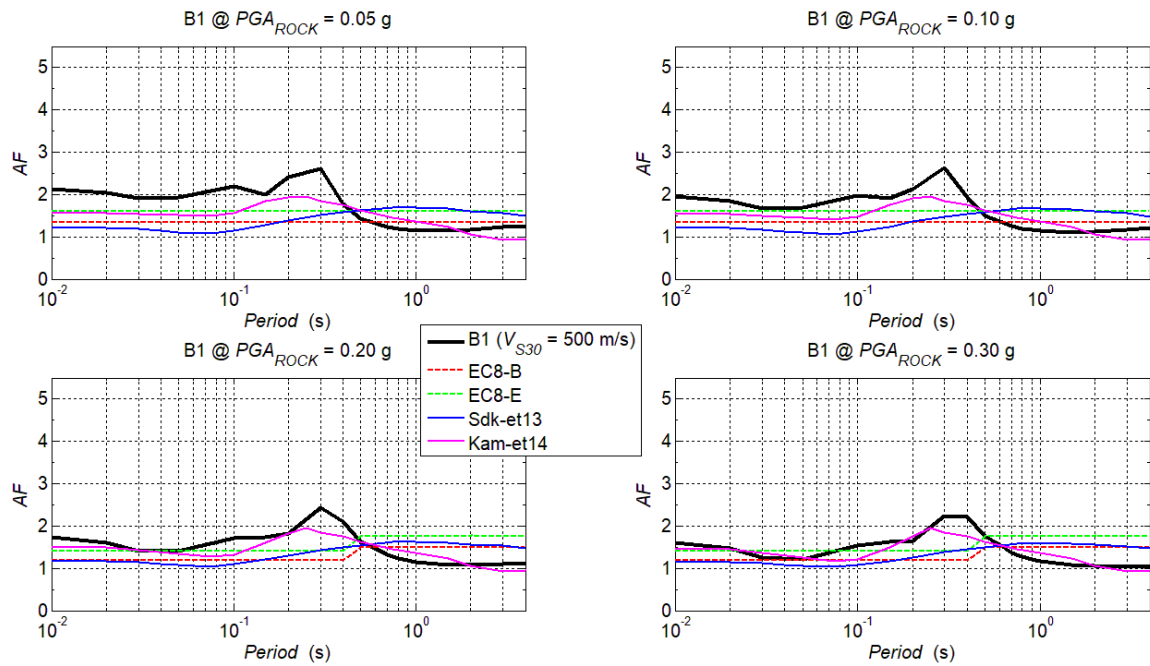
Figure 6.14: Comparison of proposed nonlinear site amplification period-dependent model for $V_{S30} = 500$ m/s within soil intra-category B1: $360 \leq V_{S30} = 560$ m/s (thick black lines). AF–EC8 soil categories B and E are represented with red and green dashed lines, Sandikkaya et al. (2013) and Kamai et al. (2014) models with blue and magenta lines for different input $PGA_{ROCK} = 0.05$ g and 0.10 g (EC8-Type 2) and $PGA_{ROCK} = 0.20$ g and 0.30 g (EC8-Type 1).
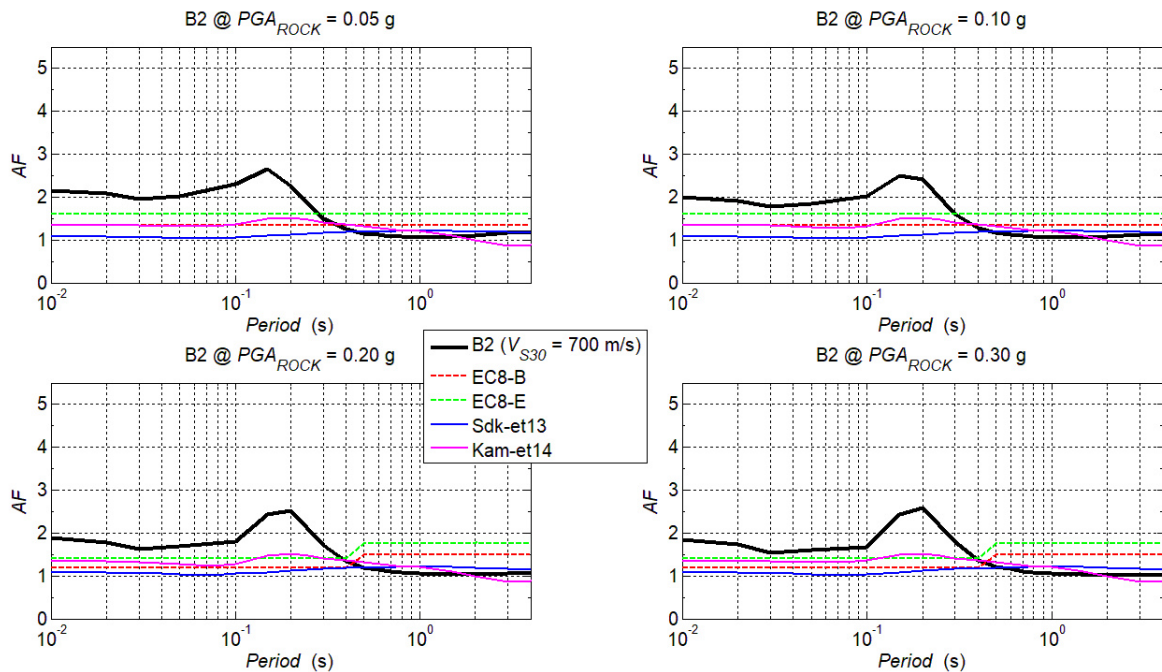
Figure 6.15: Comparison of proposed nonlinear site amplification period-dependent model for $V_{S30} = 700$ m/s within soil intra-category B2: $560 \leq V_{S30} = 760$ m/s (thick black lines). AF–EC8 soil categories B and E are represented with red and green dashed lines, Sandikkaya et al. (2013) and Kamai et al. (2014) models blue and magenta lines for different input $PGA_{ROCK} = 0.05$ g and 0.10 g (EC8-Type 2) and $PGA_{ROCK} = 0.20$ g and 0.30 g (EC8-Type 1).

170
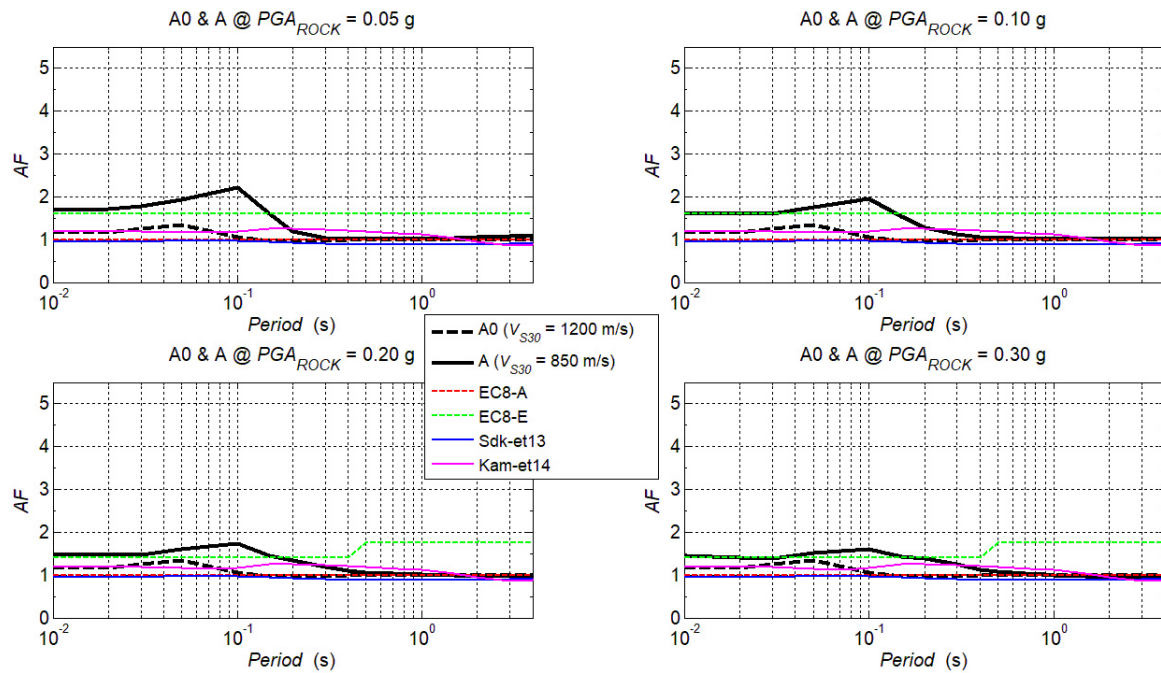
Figure 6.16: Comparison of proposed nonlinear site amplification period-dependent model for $V_{S30} = 850$ m/s within soil intra-category A: $760 \leq V_{S30} = 1100$ m/s (thick black lines) and for $V_{S30} = 1200$ m/s within A0: $V_{S30} \geq V_{REF}$ (thick dashed black lines). AF–EC8 soil categories A and E are represented with red and green dashed lines, Sandikkaya et al. (2013) and Kamai et al. (2014) models with blue and magenta lines for different input $PGA_{ROCK} = 0.05$ g and 0.10 g (EC8-Type 2) and $PGA_{ROCK} = 0.20$ g and 0.30 g (EC8-Type 1).

6.3.1. Comparison with previous empirical site amplification models

Based on the trends in Figures 6.11–6.16, proposed model's median predictions can be compared to the median predictions of Sandikkaya et al. (2013) and Kamai et al. (2014) models in three main site categories:

a) **Medium to hard soil–Soft rock: 200 m/s $\leq V_{S30} < 560$ m/s range (Figures 6.12, 6.13, 6.14):** In this range, median predictions of the proposed AF model for Croatia are in good agreement with the median predictions of previous empirical AF models. Proposed model's predictions at short periods (up to 0.3 s) are slightly lower than the predictions of previous models for $200 \leq V_{S30} < 280$ m/s (Figure 6.12) for $PGA_{ROCK} = 0.20$ g and $PGA_{ROCK} = 0.30$ g, indicating that the nonlinear term in the proposed model is stronger than in the previous models. This slightly stronger nonlinear effect may be related to different equivalent linear soil properties utilized in this study and by Kamai et al. (2014). Since Sandikkaya et al. (2013) did not use site amplification

171

simulations but an empirical database in model development, a weaker nonlinear term is expected. For $280 \le V_{S30} < 360$ m/s range (Figure 6.13), all models are in good agreement for $PGA_{ROCK} > 0.05$ g; while, proposed AFs are higher than the others for $PGA_{ROCK} = 0.05$ g where differences are most prominent at short periods. Behaviour is similar in $360 \le V_{S30} < 560$ m/s range (Figure 6.14), however, the agreement with the previous models is observed when $PGA_{ROCK} > 0.10$ g. It is notable that the site amplification for $PGA_{ROCK} = 0.05$ g (and for $PGA_{ROCK} < 0.10$ g) for hard soils with $V_{S30} > 360$ m/s is linear and significantly different compared to Sandikkaya et al. (2013) model; therefore, predictions of the previous models were not directly adopted in GMPEs. Instead, the linear site amplification terms were re-regressed during GMPE building stage. Different behaviour of the two models may stem from the sparse V_{S30} recordings in the ground-motion databases as well as the differences in the implemented modelling approach in each functional form. In mid-to-long periods (> 0.4 s), trends in the proposed model's predictions and Kamai et al. (2014) model are similar due to the same methodology adopted; however, the peak of AFs in the proposed model is shifted to longer periods. This difference might be related to the definition of the soil profiles (real/measured soil profiles in this study vs. generic randomized soil profiles in Kamai et al. 2014).

b) **Rock sites: 560 m/s $\le V_{S30} < 1100$ m/s range (Figures 6.15, 6.16):** In this range, the site amplifications tend to get smaller, reaching to $AF = 1$ at the reference rock conditions (reference bedrock is defined as $V_{S30} = 750$ m/s by Sandikkaya et al. 2013, $V_{S30} = 1180$ m/s by Kamai et al. 2014 and $V_{S30} = 1100$ m/s in this study). Additionally, the site amplification behaviour is presumably linear for stiff sites; therefore, the AFs tend to be independent of the input PGA_{ROCK}. In mid-to-long spectral periods (> 0.4 s), all three models (including the proposed model) show the expected behaviour. On the other hand, proposed AFs at short periods are significantly higher than the predictions of Sandikkaya et al. (2013) and Kamai et al. (2014) models. There are several reasons for this. A closer look at Figures 6.15 and 6.16 would show that the AFs provided by Sandikkaya et al. (2013) model is almost constant and equal to 1; mainly because the reference bedrock was defined at $V_{S30} = 750$ m/s and the AFs were calculated using an empirical database with very limited data over $V_{S30} > 700$ m/s. On the other hand, predictions of Kamai et al. (2014) model are higher than the predictions

of Sandikkaya et al. (2013) model (also higher than 1) but smaller than the AFs proposed in this study, especially in short periods. It is worth to notice that the bedrock depths of the soil profiles used in this study are less than 30 m for most sites with $V_{S30} > 360$ m/s (Figure 5.4c). The generic soil profiles utilized in Kamai et al. (2014) are generally deeper soil profiles (bedrock depth > 30m). Pehlivan et al. (2017) presented that significant short period amplifications are experienced when the input rock motions with low intensity, short duration and high frequency content are applied in the site response analysis through shallow sites with high impedance contrast. A similar response of shallow soil-bedrock interface is observed in this study at the predominant period due to the high impedance contrast in the considered soil profiles (Figures 5.7d–f). Anbazhagan et al. (2013) noticed that the AFs in site response analysis are slightly different when the input ground motion is applied at 30 m depth (with different bedrock V_{REF}) or at engineering bedrock (same V_{REF} for all profiles) when soil profile is less than 30 m. Therefore, Kamai et al. (2014) model may not accurately capture the expected short period amplifications when low-to-moderate input ground motions are applied as in this study. For the reference bedrock conditions, $V_{S30} \geq 1100$ m/s (A0), predicted amplifications at short periods are higher, and at mid-to-long periods they are comparable to those from Sandikkaya et al. (2013) and Kamai et al. (2014) (Figure 6.16).

c) **Soft sites: 200 m/s $< V_{S30}$ (Figure 6.11):** This range represents the sites located on very soft soil deposits; therefore, the site amplifications are strongly nonlinear and the estimated AFs are closely correlated to the spatial distribution of soil layers and equivalent linear dynamic soil properties. Almost all of the AFs models include significant uncertainty in estimating the soft soil response; uncertainty is due to the lack of data to constrain data-driven models (e.g., Sandikkaya et al. 2013) and due to the sensitivity of simulation-driven models (e.g., Kamai et al. 2014 and this study) to the choice of soil properties. Figure 6.11 shows that the AFs estimated by all three models have similar trends with period, but the AFs vary significantly. Figure 6.11 indicates that the strong nonlinear term in the proposed model tends to decrease the AF below 1, especially for high input motions. A strong interaction between linear and nonlinear terms is also noticeable; proposed model scales very strongly with input PGA_{ROCK}. Kamai et al. (2014) noted that the AF models must not replace the site-specific analysis

(especially for soft soil range); however, the AF models should be extrapolated to these soft soil ranges to be able to provide a full AF model to be used in GMPE development. Because the scope of this thesis does not include the implementation of the proposed model in GMPE development, the current form of the model is not applicable for $200 \text{ m/s} < V_{S30}$ until the number of simulations is increased to properly model this uncertainty in the future (see Section 6.3.3).

6.3.2. Comparison with Eurocode 8 site factors

Sandikkaya et al. (2013) compared the period-dependent AFs with the AF recommended in NEHRP (BSSC 2009) and EC8, observing that the poor period-dependent AFs in EC8 are incompatible with the AF model predictions. Most recent work by Sandikkaya et al. (2018) pointed out the shortcomings of EC8 site factors as the improper representation of nonlinear soil response and poor period-dependent variations. In Figures 6.11–16, proposed AF model for Croatia is compared with site amplification factors given in EC8 for each soil category. For this comparison, EC8–AFs are defined with the reference to the EC8 soil category A for different input target spectra scaled to $PGA_{ROCK} = 0.05 \text{ g}, 0.10 \text{ g}, 0.20 \text{ g}$ and 0.30 g.

Results of this study also show that the median predictions of the proposed AF models are different than the AFs given in EC8: AFs proposed in this study are strongly nonlinear and heavily dependent on the period. Figures 6.11–6.12 show that proposed AFs are similar to the EC8-AFs in short periods but smaller than EC8–AFs at longer periods for soil categories with $V_{S30} < 280 \text{ m/s}$ for $PGA_{ROCK} < 0.10 \text{ g}$. For larger input ground motion amplitudes (for $PGA_{ROCK} > 0.10 \text{ g}$), AFs from EC8 fail to follow the expected nonlinear trend at shorter periods and only slightly capture the peak of the amplifications at the predominant period for site categories D and C1. The EC8 site factors disregard nonlinear soil behaviour that generally results in higher spectral ordinates as site conditions change from rock to softer soils, consistent with observations from papers by Sandikkaya et al. (2013, 2018).

For stiffer sites with $V_{S30} > 360 \text{ m/s}$, AFs from EC8 are generally close to unity (EC8-A and EC8–B), whereas the proposed model shows significant amplification with respect to site classes B1, B2 and A. Figures 6.14–6.16 show that the proposed AFs are significantly higher (up to two times) than EC8–AFs at short periods. Anbazhagan et al. (2009) observed that site

class categories based on V_{S30} may lead to overestimation of V_{S30} for sites that have engineering bedrock shallower than 25–30 m, as in some presented cases in this study, particularly in B1, B2 and A soil categories. It is worth to notice that significant amplifications experienced by the presence of shallow weaker materials above hard bedrock are not taken into consideration within EC8 soil category classes described by the parameter V_{S30}. In EC8, these sites are described as soil category E which represents soil profile consisting of a surface alluvium layers with V_S values of type C and D varying between 5 m and 20 m underlain by stiffer material with $V_S > 800$ m/s (Figure 6.10, Table 5.2). Example of such profiles which contain presence of soft surface layers with low V_S values and shallow bedrock can be seen in Figure 5.7e, f. For the soil intra-categories C2, B1, B2 and A for which shallow bedrock is present, predicted AFs are more comparable to some points with EC8–E site amplification factors (Figures 6.13–16) than the AFs given for that site class. It should be mentioned that soil categories in this study were classified into discrete V_{S30} intervals mainly for the purpose of developing nonlinear site amplification model for Croatia in the functional form in Eq. (6.5). The problem of soil category E in EC8 is that it is represented without the corresponding V_{S30} value, therefore similar category was not used in this study, and profiles were classified only by V_{S30}. Similar problem also persists in the recent models by Sandikkaya et al. (2013) and Kamai et al. (2014), and others.

Site parameter V_{S30} is used for years to describe local site characteristics and is heavily incorporated into site response analysis methods, seismic design building codes (EC8, NEHRP) and into recent nonlinear site amplification models. The incorporation of parameter V_{S30} into site response analysis and nonlinear site amplification models can present serious problems due to numerous reasons as it can lead to wrong conclusions. Firstly, EC8 soil category classes based on V_{S30} may misrepresent local site amplifications when used in site response analysis. This is particularly a problem if soil profile is defined solely based on V_{S30} of the soil layer above the bedrock without consideration of real soil profiles divided into multilayer soil column, e.g., generic soil profile used by Walling et al. (2008) and Kamai et al. (2014). Secondly, there is a problem of potentially improper definition of V_{S30} based on measured soil profiles and the exploration depths from geophysical measurements. Some of the geophysical methods using S-wave techniques (e.g., MASW, SASW, S-wave Seismic Refraction) rarely reach the last layer below 20–30 m of depth which can result in a wrong value of parameter V_{S30} for the site profile. This can be improved with a combination of Refraction Microtremor (ReMi) methods or with HVSR modelling to extract bedrock depths, or at least shear wave

velocity layers close to bedrock depths. Also, in analysis of geophysical measurements using forward modelling of horizontally layered soil model, assumption is that shear wave velocity increases with depth. In reality, soil is heterogeneous, soil layers are not horizontal and velocity inversions are present which are rarely "captured" by geophysical methods. Thirdly, site classes in EC8 are defined not only based on V_{S30}, but also based on in-situ tests such as Standard Penetration Test (SPT) and Cone Penetration Test (CPT). Correlations between geophysical measurements and in-situ tests can significantly improve value of V_{S30} and, therefore site class type can be properly defined. The problem with in-situ tests is that they are not applicable in stiff soils. Also, such tests are expensive and are used only for critical projects. For site response analysis, definition of the input soil model is critical. It is best to combine geophysical methods to extract V_S values of multi-layered soil profile with borehole drilling and in-situ tests, so that representative soil model will be a realistic and representative one. Also, it is important to properly define the bedrock depth of the soil profile, particularly since geophysical methods can rarely reach below 30 m of depths, and borehole drilling is often prohibitively expensive.

Recent site amplification models indicate that amplification for the stiffer sites ($V_{S30} > 800$ m/s) are constant and close or equal to unity regardless of input ground motion amplitudes. This study shows that significant amplifications can be experienced due to the presence of shallow weaker material above the bedrock, even though the local soil V_{S30} parameter corresponds to stiffer site classes A and B of EC8. The observations imply significant deviations from the site factors computed from the site response models in this study and the recent models, as well as those provided in the EC8 guidelines. Definition of "realistic" soil profiles with proper site characteristics (V_{S30}, bedrock depth, site period, soil layers type) is important for site response analysis, and they should be included into nonlinear site amplification models, as models based solely on a single "questionable" site parameter V_{S30} can lead to wrong conclusions. Also, one should remember that presented AF models must not replace the site-specific analysis (especially for soft soil range) due to numerous reasons discussed in Chapter 5 and 6.

6.3.3. Implementation of the proposed site amplification models in GMPEs

The site amplification models for Croatia presented here might be used to update GMPEs (peak acceleration attenuation relations) developed for Croatia (Herak et al. 2001 and Markušić et al. 2002). Proposed nonlinear site amplification for the reference-rock can be taken into account in a similar manner as ground motion predictive model given by Akkar et al. (2014) (Eq. 3.40). In future, updated attenuation relations (GMPEs) for Croatia are expected to be developed based on new recordings and updated earthquake catalogues, taking into consideration attenuation effects $(Q(f), \kappa_0)$ and nonlinear site amplifications that considers linear and nonlinear local site conditions expressed by V_{S30} as proposed in this study. Also, it is important to extend accelerometric network in Croatia so that accelerograms from strong earthquakes are recorded. Strong motion data of certain region present the most important and invaluable information for developing of GMPE for that area.

One needs to keep in mind that proposed nonlinear site amplification models presented in this study are only developed for the range of $0.03 \text{ g} \leq PGA_{ROCK} \leq 0.37 \text{ g}$ due to the use of RVT-based site response analysis approach with seismological point source model. Future RVT-modelling approaches using PGA_{ROCK} needs to be extended to higher values considering many more realistic soil profiles with proper site characterization (V_{S30}, bedrock depth, site period, soil layers type) then has been done in this study, following the examples of some of the recent nonlinear site amplification models that used RVT based approach (e.g., Walling et al. 2008 and Kamai et al. 2014). In this way full range of PGA_{ROCK} can be covered to develop nonlinear site amplification model that can be embedded into future GMPEs for Croatia.

7. Conclusions

This dissertation presents analyses of local site effects on the amplification of seismic ground motion using 1-D EQL site response analysis based on the stochastic Random Vibration Theory (the RVT-based method). In seismically active regions where a large strong motion database exists, the well-known and straightforward site response analysis based on time series approach (the TS-approach) may be preferred to estimate the site amplification factors (AFs). The main reason for choosing the relatively new 1-D EQL site response analysis with RVT-based method for this study is the limited existing strong motion database in Croatia. In the RVT-based method, single theoretical point source Fourier Amplitude Spectrum (FAS) defined by the local and regional seismological parameters is adequate to represent the input ground motion. Therefore, the recorded (or empirical) strong ground motions are not needed as input. It is important to keep in mind that for very large earthquakes their source cannot be approximated by a point source model, the directivity effects play a significant role, and the epicentral distance isn't the representative distance. The earthquake scenarios thus need to be carefully defined to maintain the necessary realism in such cases.

Beyond the earthquake magnitude and the source-to-site distance, the choice of seismological parameters, particularly the parameters which describe the high-frequency part of FAS, play an important role in estimating the AFs for RVT-based method. Therefore, the scope of this thesis covers the calculation of the high-frequency attenuation parameter κ for the earthquakes recorded by the Croatian Seismological Network, and estimation of the local site-specific attenuation parameter κ_0 for each station.

The conclusions of this research will be presented based on the three major sections of the dissertation: i) calculation of the high-frequency parameter κ for the Croatian Seismological Network and estimation of κ_0 for each station (Chapter 4), ii) analysis of the local site effects on the amplification of seismic ground motion by the 1-D EQL site response analysis using the RVT-based method (Chapter 5), and iii) development of the empirical nonlinear site amplification model for Croatia (Chapter 6).

7.1. Summary and conclusions on the high-frequency attenuation parameter kappa (κ) for Croatian Seismological Network

- This portion of the study presents the calculation of κ for recordings from ten seismological stations of the Croatian network for earthquakes with $3.0 \leq M_L \leq 5.7$ at $R_e \leq 150$ km in the period of 2002–2016, using Anderson and Hough (1984) approach.

- For each station, κ_0 parameter is estimated using the linear $\kappa-R_e$ dependence by least-squares regression with the rejection of outliers (points out of the 95% confidence interval) for horizontal and vertical ground motion components (κ_{hor} and κ_{ver}). Possible errors in R_e could have impact on the inferred value of κ_0 and slope κ_R. Differences between standard linear least-squares regression and error-in-variables regression are less than 5 % when standard error for $R_e = \pm 3-5$ km, but can be significantly higher if uncertainties in R_e are much higher. In these cases, the use of error-in-variable regression is preferable.

- Comparison between κ_{hor} and κ_{ver} models is performed by evaluating the zero-distance kappa ($\kappa_0^{ver}/\kappa_0^{hor}$) and the slope of the regression model ($\kappa_R^{ver}/\kappa_R^{hor}$). Observed differences between κ_0^{hor} and κ_0^{ver} are attributed to the local effects, whereas, the similarity between κ_R^{ver} and κ_R^{hor} values are related to the regional contributions.

- Estimated horizontal κ_0 values for Croatian seismological stations are typically lower ($\kappa_0 \leq 0.025\ s$) for the stations located on hard rocks ($V_{S30} \geq 1100$ m/s) compared to the stations on the soft rocks ($\kappa_0 > 0.025$ s and $V_{S30} = 760-1100$ m/s). Findings are consistent with the previously published global κ_0 values for rock sites.

- The scatter of κ with M_L is considerably high and no clear trends with respect to the magnitude are observed since κ is calculated for frequencies above the corner frequency; therefore, the source effects on the value of κ can be neglected. Due to lack of earthquakes at short epicentral distances ($R_e < 20$ km), this observation should be taken with caution for possible near-source effects on κ.

- κ-groups for different azimuth bins and for similar epicentral distance show similar κ values despite geographical distribution and variety of source-site paths. Also, for the same azimuthal bin and different epicentral distances, κ values are different. There is no systematic behaviour of certain κ-groups with respect to geographical orientation of epicentre locations.

- An attempt was made to estimate the $\kappa's$ regional dependence by providing the spatial distribution of the κ values based on interpolation by the nearest neighbour method. The lowest κ values are spatially distributed within a few kilometres around the stations due to near-site effects and gradual increase of κ with distance from the stations in the circular-shape distribution represents the effects of the regional attenuation. Deviations (or scatter) from circular/ellipsoid-shape of κ distribution could indicate that beside isotropic local and regional attenuation as primary contributions, other effects such as attenuation anisotropy from different causes (e.g., preferential orientations of cracks and fractures under the local tectonic stress field, trapping of waves along major faults-waveguides, or attenuation within the fault zones) possibly have effect on the κ distribution.

- Attenuation values calculated by two different approaches, the frequency-dependent quality factor $Q(f)$ from the attenuation of coda waves in the Dinarides (Dasović 2015a; Dasović et al. 2012, 2013, 2015b) and the frequency-independent $Q_{est}(\kappa_R)$ derived from the slope (κ_R) are compared for the high-frequency range (10–25 Hz) to verify the accuracy of the regression slope κ_R of the $\kappa - R_e$ models in this study. Observed discrepancies between two Q contributions are mostly within the respective confidence limits, and can be attributed mainly to different techniques to estimate $Q(f)$ and κ, and complexity and variability in the whole-path attenuation contributions to κ.

- Horizontal site-specific attenuation values κ_0^{hor} calculated in this chapter are used to represent values of near-site attenuation κ_0 below and near each seismological station in Croatia and subsequently in the RVT-based site response analysis to define high-frequency shape of the input FAS as explained in Chapter 5.

- Results presented in this part of study are significant especially because the κ and κ_0 values for the Croatian seismological network were not calculated before and the findings provide valuable information to be used in host-to-target adjustment of future GMPEs in hard rock sites and site-specific response analysis based on random vibration theory approach.

7.2. Summary and conclusions on the local site effects on the amplification of seismic ground motion using EQL RVT-based method

- 1-D EQL site response analysis using RVT-based method is utilized for different sites with measured shear wave velocity profiles around Croatia for different input ground motion levels (in terms of PGA_{ROCK}). For the purpose of analysing the effect of soil profile on AFs, compiled local soil profiles are classified into seven categories according to the V_{S30} parameter based on EC8 soil classifications.

- Eight different magnitude values varying between $M_L = 5.0$ and $M_L = 7.1$ are pre-selected to develop input FAS for the analysis. The chosen epicentral distances (R_e) were selected to vary from 7 km up to 30 km to define near-site regions so that for different combinations of magnitudes and epicentral distances, the input FAS and response spectrum match target PGA_{ROCK} values from 0.03 g to 0.37 g. One reason to choose this distance range is because the nearby recordings constrain κ_0. The other reason for preferring shorter epicentral distances $(R_e < 30$ km), is that large magnitudes can be constrained for the use in RVT-based approach to reach the higher target PGA_{ROCK} levels.

- Input PGA_{ROCK} level is defined as spectral acceleration Sa at the zero period in response spectra for bedrock condition (RSB). The results of site response analyses are presented in terms of the 5 % damped surface response spectra RSS (response spectra give valuable information about the period at which max acceleration can be expected if an earthquake is used to excite SDOF system) and the $AF(T)$ at different periods calculated by Eq. (1.1). Peak ground acceleration PGA at the surface in RSS is represented by the corresponding Sa at zero period.

- For low-intensity input ground motions $(PGA_{ROCK} < 0.1$ g), the input motion is significantly amplified in the top layers of the profile ($AF@PGA$) and AF is most prominent at predominant peak period particularly for the softer soils with lower V_{S30} and thicker alluvium layers overlying bedrock.

- At higher input motion levels $(PGA_{ROCK} > 0.1$ g), softer soils with lower values of $V_{S10}, V_{S20},$ and V_{S30} show non-linear behaviour; therefore, $AF@PGA$ decreases

significantly below the $AF = 1$ line at shorter spectral periods, and at the predominant peak, the spectral peak period increases with decreasing $AF@PP$.

- For stiffer soils (or soft rock formations) with higher V_{S10}, V_{S20}, and V_{S30} values, $AF@PGA$ and $AF@PP$ are "stabilized" at all spectral periods regardless of large values of PGA_{ROCK} showing "little to no" amplification, particularly above 0.10 s; whereas observed significant amplifications $AF@PGA$ and $AF@PP$ for stiffer soils and hard rock formations at shorter periods (< 0.20 s) are mainly due to the response of bedrock's interaction with few meters of shallow weaker material at the surface.

- It is important to understand how AFs at different spectral periods are influenced by the seismic response of a site for certain earthquake scenarios for possible resonance effects during earthquakes which can result in heavy destruction. For different levels of input ground motion (PGA_{ROCK}), AF varies significantly with chosen spectral period for different site characteristics parameters ($V_{S10}, V_{S20}, V_{S30}$). Knowing these variations, new structures (or older) on particular local site can be constructed (or reinforced) to avoid potential resonance at natural soil period taking into account nonlinear effects at shorter spectral periods which is important in local earthquake engineering problems.

7.3. Summary and conclusions on the empirical nonlinear site amplification model for Croatia

- The RVT-based site response analysis results for a range of local soil profiles ($160 < V_{S30} < 1389$ m/s) are used to develop a nonlinear site amplification model for Croatia in a way similar to the recently proposed nonlinear site amplification models as a function of the local site parameter (V_{S30}) and intensity of input rock motion (PGA_{ROCK}).

- Functional form given in Eq. (6.5) is slightly different when compared to the functional forms of the recently proposed nonlinear site amplification models because: a) the strong motion dataset of Croatia is limited, b) the soil profiles used in this study are actually measured and, c) the applicability range $0.03 \leq PGA_{ROCK} \leq 0.37$ g of the proposed model is different than in other models. The term "0.1 g" is added as a pivot point that represents the transition between the linear and nonlinear behaviour of AFs with increasing PGA_{ROCK}.

- The distribution of AFs with PGA_{ROCK} is generally flat at PGA_{ROCK} values up to 0.1 g, representing linear site response. After 0.1 g, AFs decrease as PGA_{ROCK} increases, showing the effect of soil nonlinearity at shorter periods for the softer profiles. At longer periods, the amplification is not dependent on PGA_{ROCK} for stiffer profiles, but increases with PGA_{ROCK} for the softer profiles, as a result of the shift in the predominant peak to longer periods.

- Negative values of regression coefficients $b_1(T)$ and $b_2(T)$ describe the decrease in AF at shorter periods due to non-linearity. High negative values are estimated for softer sites with lower values of V_{S30} for which the non-linearity is the strongest in terms of de-amplification, i.e., decrease of AF with PGA_{ROCK}. For stiffer sites with higher values of V_{S30}, $b_1(T)$ and $b_2(T)$ values are lower and closer to zero, indicating that nonlinear effects are low or can be neglected.

- Proposed nonlinear site amplification models for Croatia are evaluated by comparing the median predictions with the AFs given in Eurocode 8 (EC8) and the median predictions of Sandikkaya et al. (2013) and Kamai et al. (2014) site amplification models.

- For medium to hard soils and soft rocks defined by $200 \, \text{m/s} \leq V_{S30} < 560 \, \text{m/s}$, median predictions of the proposed AF model for Croatia are in good agreement with the median predictions of Sandikkaya et al. (2013) and Kamai et al. (2014) empirical AF models. Observed differences may be related to different equivalent linear soil properties utilized in RVT site response methods, developed site amplifications based on empirical database or definition of the soil profiles (real/measured soil profiles in this study vs. generic randomized soil profiles in others).

- For rock sites for which $560 \, \text{m/s} \leq V_{S30} < 1100 \, \text{m/s}$, generally the site amplifications tend to get smaller, reaching $AF = 1$ at the reference rock conditions (reference bedrock is defined as $V_{S30} = 1100 \, \text{m/s}$ in this study). In medium-to-long spectral periods (> 0.4 s), all three models (including the proposed model) show similar expected behaviour, reaching $AF = 1$. On the other hand, proposed AFs at short periods (< 0.3 s) are significantly higher than the predictions of Sandikkaya et al. (2013) and Kamai et al. (2014) models. Short period amplifications can be experienced when the input rock motions of small amplitudes, short duration and high frequency content are applied in the site response analysis through shallow sites with high impedance contrast as is the case in this study.

- For soft sites, $200 \text{ m/s} < V_{S30}$, the site amplifications are strongly nonlinear and the estimated AFs by all three models have similar trends with period, but the AFs vary significantly. Almost all of the AFs models include significant uncertainty in estimating the soft soil response; uncertainty is due to lack of data to constrain the data-driven models and due to the sensitivity of simulation-driven models to the choice of soil properties.

- Sandikkaya et al. (2013, 2018) showed that soil nonlinearity as well as period-dependent amplification site factors are poorly constrained in the current EC8 provisions regardless of variations in reference rock spectral amplitudes. Results of this study also show that the median predictions of the proposed AF model are different than the AF given in EC8: AFs proposed here are strongly nonlinear for soft sites and heavily dependent on the period. Significant amplifications were observed for the sites with presence of shallow weaker materials above hard bedrock, even though the local soil V_{S30} parameter correspond to stiffer site classes B and A in EC8 where amplifications are neglected.

- Definition of "realistic" soil profiles with proper site characteristics (V_{S30}, bedrock depth, site period, soil layers type) is important for site response analysis, and they should be included into nonlinear site amplification models, as models based solely on a single "questionable" site parameter V_{S30}, can lead to wrong conclusions.

7.4. Future recommendations

The findings of this study regarding the high-frequency attenuation parameter κ and proposed nonlinear site amplification model for Croatia can be expanded in the future to address some of the issues revealed during this study.

One of the significant shortcomings of the database used here is the lack of recordings at short epicentral distances for almost all of the stations. Even if the trend of κ with distance is clearly visible for all cases, more data that will be collected in the future may provide more evidence and resolution for the shortest distances, especially for stations where the lack of data is most prominent. When the database is updated, κ_0 may be re-estimated to provide better insight into some issues regarding horizontal and vertical κ models, their comparison, regional κ variation/attenuation and connection with local/regional geological and tectonic environment.

Estimation of κ from displacement FAS from smaller earthquakes and comparison with estimated κ values from this study using AH84 method can also provide valuable information about abovementioned issues. Finally, observed discrepancy between two attenuation approaches, $Q(f)$ and $Q_{est}(\kappa_R)$ can be overcome with comparison between κ_{AH} (this study) and κ_{coda} (and Q_C) as some of the most recent studies suggest (e.g., Mayor et al. 2018).

Proposed nonlinear AF model can be used to provide an initial estimate of AFs for the cases when no site-specific ground response analysis is available, but should not be used as a replacement for the site-specific analysis (especially for soft soil profiles). However, the AF model should be extrapolated to these soft soil ranges to be able to provide a full AF model to be used in GMPE development. Future RVT-modelling approaches using PGA_{ROCK} needs to be extended to higher values of PGA_{ROCK} on many more considered V_{S30} soil profiles as the number of data in each category varies significantly. In this way full range of PGA_{ROCK} can be covered to develop proper statistical nonlinear site amplification model that can be embedded into future GMPEs relations for Croatia. New and updated peak acceleration attenuation relations (GMPEs) for Croatia are expected to be developed based on a new recorded data and updated earthquake catalogue taking into consideration attenuation effects ($Q(f)$ and κ_0) and nonlinear site amplification as proposed in this study. It is of paramount importance to enlarge the accelerometric network in Croatia so that accelerograms from future strong earthquakes will be recorded. Strong motion data of certain region present the most important and invaluable information for developing of GMPE relations for that area, and such recordings can also be used for estimation of high-frequency attenuation parameter κ for strong earthquakes.

Prošireni sažetak na hrvatskom jeziku

1. Uvod

1.1. Lokalni uvjeti tla i amplifikacija seizmičkoga gibanja

Na oštećenja nastala na nekoj lokaciji osim magnitude potresa i epicentralne udaljenosti, znatan utjecaj imaju lokalni uvjeti tla, pri čemu dolazi do amplifikacije (ili de-amplifikacije) zbog promjena značajki upadnog seizmičkoga gibanja (amplituda, frekvencija, duljina trajanja) od osnovne stijene do površine tla. U posljednja tri desetljeća razorni potresi velikih magnituda ($M_W \geq 6.0$) diljem svijeta, npr. Italija (L'Aquila 2009., Amatrice i Norcia 2016.), Meksiko (1985., 2017.), Novi Zeland (Christchurch 2011., Canterbury 2010., Kaikoura 2016.) Nepal (2015.), Japan (Kobe 1995., Tohoku 2011.) Čile (2010., 2015.), Kina (Sichuan 2008.), Tajvan (Chi-Chi 1999.), Turska (Kocaeli 1999.), SAD (Whittier Narrows 1987., Loma Prieta 1989., Northridge 1994.) potvrdili su da je i utjecaj lokalnoga tla bitan faktor u distribuciji oštećenja od potresa uz posljedice koje dolaze od samog žarišta potresa i propagacije potresnih valova (npr. Reiter 1990; Kramer 1996; Meunier i sur. 2008; Aki i Richards 2009; Panzera i sur. 2013). Utjecaj lokalnoga tla na efekte potresa prvi je znanstveno objasnio Stur (1871) na osnovi proučavanja oštećenja nastalih nakon potresa u Klani 1870. godine.

Amplifikacijski faktor kao funkcija perioda (ili frekvencije), definira se kao omjer akceleracijskih spektara odziva na površini i na osnovnoj stijeni (izraz 1.1). U seizmički aktivnijim područjima, klasična jednodimenzionalna (1-D) ekvivalentno-linearna (EQL) analiza seizmičkoga odziva lokalnoga tla korištenjem zabilježenih akceleracija jakih potresa, tzv. *„Time-Series"* (TS) metoda, bazira se na propagaciji potresnog gibanja od osnovne stijene kroz potpovršinske slojeve do same površine tla (npr. Idriss i Seed 1968; Schnabel i sur. 1972; Seed i sur. 1984; Idriss i Sun 1992; Kramer 1996; Rathje i sur. 2010; Hashash i sur. 2011). Glavna prednost klasične EQL analize primjenom ulaznog gibanja u vremenskoj

domeni jest korištenje malog broja parametara tla (npr. brzine transverzalnih valova, gustoće tla, krivulje modula smicanja i prigušenja tla) i relativno kratko vrijeme računanja.

Glavni nedostatak korištenja klasične EQL–TS metode vidljiv je u područjima umjerene seizmičnosti, kao što je Hrvatska, gdje ima malo zabilježenih akcelerograma jakih potresa. Analiza seizmičkoga odziva lokalnoga tla na temelju tzv. teorije nasumičnog titranja (engl. *Random Vibration Theory* – RVT) je proširenje postupka stohastičkog simuliranja gibanja tla razvijenog od strane seizmologa radi predviđanja parametara gibanja tla (npr. Brune 1970; Hanks i McGuire 1981; Boore 1983, 2003). RVT metoda pokazala se dobrom EQL alternativom za predviđanje spektara odziva na površini bez potrebe za ulaznim vremenskim zapisima akceleracija (npr. Boore 1983, 2003; Silva i Lee 1987; Silva i sur. 1997; Rathje i Ozbey 2006; Kottke i Rathje 2013). Ulazno gibanje za EQL–RVT analizu definirano je preko Fourierovog amplitudnog spektra (FAS) seizmičkoga gibanja na temelju lokalnih i regionalnih seizmoloških parametara za određeni potresni scenarij, bez potrebe za vremenskim zapisima akceleracija jakih potresa.

Nelinearni amplifikacijski modeli, kao sastavni dio atenuacijskih relacija predviđanja potresnog gibanja tla (GMPE), predstavljaju alternativu klasičnoj EQL analizi seizmičkoga odziva lokalnoga tla. Takvi modeli obično su razvijeni na temelju velike baze podataka amplifikacijskih faktora kao funkcije lokalnih uvjeta tla (iskazanih preko parametra lokalnoga tla V_{S30}, prosječna brzina transverzalnih S-valova u gornjih 30 m) za određena ulazna gibanja (PGA_{ROCK} – referentna vršna akceleracija definirana za osnovnu stijenu) korištenjem određenih statističkih modela (npr. Choi i Stewart 2005; Walling i sur. 2008; Sandikkaya i sur. 2013).

1.2. Cilj i hipoteza istraživanja

Cilj ovog istraživanja bio je razviti sistematičnu analizu utjecaja lokalnih uvjeta tla na amplifikaciju seizmičkoga površinskoga gibanja u Hrvatskoj na temelju 1-D ekvivalentno-linearne (EQL) analize i teorije nasumičnog titranja (RVT). Određenim kombinacijama seizmoloških parametara (npr. magnitude, hipocentralne udaljenost, seizmičke atenuacije, lokalne atenuacije) definira se ulazno gibanje u EQL–RVT analizi preko FAS-a za niz potresnih scenarija, a kako bi odgovaralo vršnoj akceleraciji za osnovnu stijenu definiranoj

prema seizmičkom hazardu za Hrvatsku. Visokofrekventni atenuacijski parametar "kapa" (κ) znatno utječe na amplitude FAS-a na višim frekvencijama (npr. Anderson i Hough 1984; Ktenidou i sur. 2013, 2014) i kao takav, osim magnitude potresa i udaljenosti, predstavlja važan parametar za definiranje ulaznog FAS-a u EQL–RVT analizi. U Hrvatskoj dosad nije određena vrijednost parametra κ, te će jedan dio istraživanja biti usmjeren u tom smjeru, a kako bi se pokušali definirati svi lokalni i regionalni seizmološki parametri potrebni za definiranje FAS-a za EQL–RVT analizu.

Istraživanje je podijeljeno u tri dijela. Prvi dio istraživanja odnosi se na određivanje visokofrekventnog atenuacijskog parametra (κ) iz zabilježenih potresa te pripadnih lokalnih atenuacija (κ_0) na odabranim seizmološkim postajama u Hrvatskoj na temelju metode koju su predložili Anderson i Hough (1984) (Poglavlje 4). Drugi dio istraživanja odnosi se na procjenu amplifikacije seizmičkoga gibanja tla za niz odabranih lokalnih uvjeta tla u Hrvatskoj upotrebom EQL–RVT analize definiranih preko FAS-a za niz potresnih scenarija na temelju lokalnih i regionalnih seizmoloških parametara (Poglavlje 5). Za potrebe analize i diskusije lokalne atenuacije i veze s lokalnim tlom te za ulazne modele tla u EQL–RVT analizi u Poglavljima 4 i 5, provedena su geofizička istraživanja na seizmološkim postajama i na raznim lokacijama diljem Hrvatske. Zadnji dio istraživanja (Poglavlje 6) odnosi se na razvijanje empirijskoga nelinearnog amplifikacijskog modela za Hrvatsku na temelju procijenjenih amplifikacijskih faktora kao funkcije lokalnih uvjeta tla (V_{S30}) za određena referentna ulazna gibanja definirana na osnovnoj stijeni (PGA_{ROCK}).

2. Spektar seizmičkoga potresnog gibanja tla

Fourierov amplitudni spektar gibanja tla $FAS(M_0, R, f)$ definiran je izrazom (2.1) kao funkcija položaja i procesa u žarištu potresa, atenuacijskih efekata zbog rasprostiranja i raspršenja valova u sredstvu te utjecaja lokalnoga tla. Najčešće se koristi Fourierov akceleracijski spektar gibanja tla, a mogu se koristiti i spektri pomaka ili brzine (npr. Hanks i McGuire 1981; Boore 1983, 2003). Općenito, lokalna geologija i oblik terena najviše utječu na mijenjanje karakteristika upadnog seizmičkoga gibanja (amplituda, frekvencija, duljina trajanja) te na intenzitet površinskoga seizmičkog gibanja na nekoj lokaciji, što direktno utječe i na oštećenja nastala uslijed potresa (slika 2.1).

Za potrebe stohastičkog predviđanja gibanja tla, spektar žarišta potresa definiran je pomoću jednostavnog modela teorijskog spektra točkastog izvora, tzv. ω^2 spektar (Brune 1970), kao funkcija seizmičkoga momenta i frekvencije (izraz 2.7). Spektar samog žarišta potresa najviše ovisi o jakosti potresa (magnitudi), a manjim dijelom o padu napetosti u izvoru potresa (prema izrazu 2.10), što se manifestira u promjeni granične frekvencije (f_C – frekvencija do koje spektar akceleracije raste kao kvadrat frekvencije, a nakon toga je relativno konstantan). Potresi većih magnituda imaju manje granične frekvencije i obrnuto (slika 2.2). Parametar koji opisuje pad napetosti u žarištu (engl. *stress drop*) teško je odrediti za područje Hrvatske s obzirom da se taj parametar najčešće određuje na temelju jačih potresa ($M_W > 5.5$). Iz tog razloga je u ovom radu uzeta konstantna vrijednost navedenog parametra, $\Delta\sigma = 100$ bar, što odgovara prosječnim vrijednostima određenima za dio jugoistočne Europe (npr. Allman i Shearer 2009).

Fourierov amplitudni spektar modificira se na višim frekvencijama zbog atenuacijskih efekata uslijed geometrijskog rasprostiranja, unutrašnjeg trenja te raspršenja seizmičkih valova na nehomogenostima u sredstvu (izraz 2.11) (npr. Boore 2003). Geometrijsko rasprostiranje definira se kao funkcija udaljenosti pri čemu amplituda prostornih valova opada obrnuto proporcionalno udaljenosti (izraz 2.12, slika 2.3). Ukupna atenuacija koda valova, $1/Q_C$, (atenuacija je obrnuto proporcionalna faktoru dobrote) definirana je kao zbroj doprinosa intrinzične atenuacije i atenuacije zbog raspršenja (izraz 2.13) te je frekvencijski ovisna (izraz 2.14) (npr. Giampiccolo i sur. 2004). Atenuacijski efekti znatno utječu na oblik spektra na višim frekvencijama u odnosu na sam spektar žarišta potresa (slika 2.4 prema izrazu 2.15).

Utjecaj lokalnoga tla na FAS opisan je preko amplifikacijske funkcije (izraz 2.17, tablica 2.1, Boore i Joyner 1997) te funkcije opadanja koja opisuje smanjivanje spektralnih amplituda na višim frekvencijama (izraz 2.20). Pokazalo se da iznad određene frekvencije (f_{max}), FAS značajno opada (eksponencijalno, izraz 2.20b) (npr. Hanks 1982; Anderson i Hough 1984). Parametar koji opisuje eksponencijalni pad spektra na višim frekvencijama naziva se spektralni parametar „kapa" i ovisan je najvećim dijelom o lokalnim uvjetima tla, te opisuje utjecaj lokalne atenuacije (parametar κ_0 za udaljenosti $R \approx 0$ km) ispod i oko same postaje na oblik FAS-a (slika 2.6, izraz 2.21). Što je lokalna atenuacija veća, veća je i vrijednost κ_0, te FAS znatnije opada na višim frekvencijama u odnosu na isti spektar definiran preko frekvencijski ovisnog faktora dobrote $Q(f)$.

3. Metode za procjenu utjecaja lokalnih uvjeta tla na amplifikaciju seizmičkoga površinskog gibanja

Procjena utjecaja lokalnih uvjeta tla na seizmičko gibanje predstavlja značajan problem u području potresnog inženjerstva. Najveći problem predstavlja procjena odziva lokalnoga tla radi predviđanja amplifikacije površinskoga gibanja za slučajeve potencijalnih potresa za potrebe protupotresne gradnje ili rekonstrukcije postojećih građevina kako bi se u slučaju potresa smanjile nastale materijalne štete i spasili ljudski životi.

Već dugi niz godina jednodimenzionalna (1-D) ekvivalentno–linearna (EQL) analiza seizmičkoga odziva lokalnoga tla se koristi za procjenu utjecaja lokalnih uvjeta tla na amplifikaciju seizmičkoga površinskog gibanja. Prvi put je predstavljena 1968. godine (Idriss i Seed 1968), zatim je implementirana u programe SHAKE (Schnabel i sur. 1972) i SHAKE 91 (Idriss i Sun 1992) te nedavno u program DEEPSOIL (Hashash 2012). Stohastičko modeliranje seizmičkoga gibanja preko RVT metode korištenjem EQL analize implementirano je u program RASCAL (Silva i Lee 1987) te u program STRATA (Kottke i Rathje 2009) koji je upotrijebljen korišten za potrebe ovog istraživanja. Nelinearni amplifikacijski modeli kao funkcije V_{S30} i PGA_{ROCK} mogu predstavljati alternativu klasičnoj EQL analizi seizmičkoga odziva lokalnog tla (npr. Choi i Stewart 2005; Walling i sur. 2008; Sandikkaya i sur. 2013; Kamai i sur. 2014).

3.1. Ekvivalentno–linearna analiza odziva lokalnoga tla

(1-D) ekvivalentno–linearna (EQL) analiza seizmičkoga odziva lokalnoga tla bazira se na linearno–elastičnoj vertikalnoj propagaciji horizontalno polariziranih valova kroz slojevito sredstvo, pri čemu je nelinearnost tla uključena kroz odgovarajuća svojstva naprezanja slojeva tla (npr. modul smicanja i faktor prigušenja) (slika 3.2). EQL analiza seizmičkog odziva lokalnoga tla sastoji se od tri koraka: 1) definiranja slojeva tla preko brzina S valova, 2) odabira dinamičkih svojstava za određenu vrstu tla preko krivulja modula smicanja G/G_{max} i prigušenja ξ, te 3) definiranja ulaznoga seizmičkog gibanja PGA_{ROCK}.

Ekvivalentno–linearni model tla bazira se na linearno–viskoznom Kelvin-Voightovom modelu (slika 3.3). U slučaju određene potresne pobude na tlo (prirodne ili umjetne), elastička

energija se gubi zbog prigušenja prema krivulji histereze (slika 3.4a). Kod malih napetosti τ, deformacija γ je mala i modul smicanja je najveći (G_{max}). Općenito, modul smicanja kod malih deformacija $G_{max} = \rho V_S^2$ definira se prema vrijednostima brzina V_S dobivenih geofizičkim metodama. S većim napetostima i većim deformacijama do granične vrijednosti τ_c, modul smicanja G se smanjuje i dostiže vrijednost koja se naziva sekantni modul smicanja $G_{sec} = \tau_c/\gamma_c$, a koji aproksimira ekvivalentno–linearni modul smicanja tla. Općenito, tla manje krutosti (modula smicanja) će se više degradirati pri većim deformacijama, pri čemu G opada, a ξ raste s povećanjem deformacije γ (slika 3.4b,c). U EQL analizi seizmičkoga odziva lokalnog tla, ekvivalentno-linearna aproksimacija nelinearnoga ponašanja tla bazira se na iteracijskom postupku. On se izvodi tako da se početne vrijednosti $G_0(G_{max})$ i ξ_0 koje odgovaraju malim deformacijama, iteracijski prilagođavaju efektivnim vrijednostima sve većih deformacija (slika 3.5). Iteracije se izvode dok se ne postigne dovoljno mala razlika između predviđenih i efektivnih vrijednosti.

Odziv ekvivalentno-linearnog modela tla za određeno seizmičko gibanje temelji se na rješavanju 1-D valne jednadžbe (izraz 3.7) za vertikalnu propagaciju SH valova kroz slojevito tlo od osnovne stijene (engl. *bedrock*) do površine. Rješenje jednadžbe prikazano je u obliku prijenosne funkcije (engl. *transfer function*) (izraz 3.20) koja opisuje amplifikaciju seizmičkoga površinskog gibanja u odnosu na ulazno seizmičko gibanje definirano za osnovnu stijenu. Polazište za analizu rasprostiranja valova kroz poluprostor (slojevito tlo i stijena) je definiranje ulaznog gibanja s osnovne stijene te odnosa između amplituda gibanja na osnovnoj stijeni (engl. *bedrock motion*) s gibanjima na površinskim izdancima osnovne stijene (engl. *outcrop motion*) te gibanjima na slobodnoj površini (engl. *free surface motion*) (slike 3.6a). U EQL analizi, ulazno gibanje najčešće je definirano za izdanak osnovne stijene (engl. *outcrop*) s obzirom da je većina zabilježenih akceleracija snimljena na površinskim izdancima stijene. U takvom slučaju povećanje amplitude od izdanka osnovne stijene prema slobodnoj površini $(T_{1,o})$ iznosi otprilike 65 % povećanja amplitude od osnovne stijene prema slobodnoj površini $(T_{1,b})$ (izrazi 3.21a, b, c, slika 3.6b) (npr. Kramer 1996; Bardet i sur. 2000; Hashash 2012).

3.2. EQL analiza odziva lokalnoga tla korištenjem vremenskih nizova akceleracija (engl. *Time Series*)

Postoji nekoliko problema prilikom korištenja zapisa akceleracija jakih potresa. Prvo, odabir zabilježenih akceleracija jakih potresa na izdancima stijena $(V_{S30} > 800 \text{ m/s})$ u odnosu na one zabilježene na mekanijim tlima, igra veliku ulogu zbog lokalne amplifikacije. Drugo, veliki problem predstavljaju područja tzv. srednje do slabe seizmičnosti kao što je Hrvatska, gdje ima malo zabilježenih akceleracija jakih potresa. I, treće, svaki zapis potresa ima različita svojstva te je potrebno koristiti veliki broj takvih zapisa (najmanje deset i više), kako bi se dobio statistički stabilan prosjek odziva lokalnoga tla, tj. prosječna amplifikacija svih individualnih ulaznih gibanja. Takav primjer prikazan je slici 3.8 za niz ulaznih gibanja skaliranih na $PGA_{ROCK} = 0.05$ g. Samim time takav pristup povećava i vrijeme potrebno za računanje odziva lokalnoga tla.

3.3. EQL analiza odziva lokalnoga tla pomoću teorije nasumičnog titranja (engl. *Random Vibration Theory*)

Nedostatak zabilježenih akceleracija jakih potresa može se riješiti na dva načina: a) korištenjem neke od baza podataka jakih seizmičkih gibanja (u ovom radu korištena je globalna baza podataka NGA-W2: http://ngawest2.berkeley.edu/) ili b) korištenjem stohastičkog modeliranja gibanja tla pomoću teorije nasumičnog titranja (engl. *Random Vibration Theory*) (npr. Hanks i McGuire 1981; Boore 1983, 2003).

Teorijsko predviđanje seizmičkoga gibanja pomoću RVT metode predstavljeno je prvi puta u radu Hanks i McGuire (1981), a temelji se na činjenici da se visokofrekventno gibanje tla jakih potresa može aproksimirati kao gibanje ograničenog trajanja unutar vremenskog prozora S valova $(0 \leq t - R/\beta_0 \leq T_{gm})$ za stacionarni gaussovski pojasno ograničen bijeli šum $(f_C \leq f \leq f_{max})$ definiran svojstvima izvora i atenuacijskim efektima rasprostiranja seizmičkih valova kroz unutrašnjost Zemlje (izraz 3.25a). Glavna prednost stohastičkog modeliranja gibanja tla pomoću RVT metode jest određivanje vršne vrijednosti akceleracije tla i trajanja snažnog gibanja tla iz FAS-a korištenjem Parsevalova teorema i statistike ekstremnih vrijednosti (npr. Vanmarcke i Lai 1980; Boore 1983, 2003; Rathje i Ozbey 2006). Vršna akceleracija (a_{max}) definirana je preko vršnog faktora (PF) (izraz 3.32, Cartwright i

Longuet-Higgins 1956), u odnosu na efektivnu akceleraciju (a_{rms}) definiranu preko FAS-a (izraz 3.27) i trajanje snažnog gibanja tla T_{gm}, kao funkcija izvora i rasprostiranja potresnih valova (izraz 3.28). Spektar odziva u RVT metodi definiran je izrazom 3.33, pri čemu se FAS množi transfer funkcijom jednostavnog harmoničkog oscilatora (SDOF) (izraz 3.34) za odabrane prirodne frekvencije i prigušenje. Ulazna vrijednost akceleracije PGA_{ROCK} definirana je kao vrijednost spektralne akceleracije Sa za nulti period na spektru odziva (izraz 3.35).

Glavna prednost RVT metode u odnosu na TS u EQL analizi bazira se na definiranju ulaznog gibanja samo preko FAS-a za određeni potresni scenarij bez potrebe za vremenskim zapisima akceleracija jakih potresa (npr. slika 3.9). Prijenosna funkcija (izraz 3.20) definira odnos između ulaznog FAS-a na osnovnoj stijeni i FAS-a na površini (slika 3.10). Kottke i Rathje (2009) implementirali su RVT metodu u program STRATA za EQL analizu lokalnoga odziva tla (slika 3.11a), koja predviđa statistički stabilan spektar odziva na površini za određeni potresni scenarij kao i TS metoda. Pokazalo se da je amplifikacijski faktor (AF) određen iz jedne EQL–RVT analize sličan prosječnoj vrijednosti amplifikacijskih faktora određenih iz mnoštva zapisa jakih potresa u EQL–TS analizi (Rathje i Ozbey 2006; Kottke i Rathje 2009, 2013; Kottke 2010; Rathje i sur. 2010). Razlike između te dvije EQL metode (RVT i TS) su općenito manje od 10 % za cijeli raspon spektralnih perioda, dok su najveće razlike između dva pristupa (do 25 %) opažene na osnovnom periodu tla (slika 3.11b) (npr. Kottke i Rathje 2013).

S obzirom da je ulazno gibanje kod RVT metode definirano preko FAS-a za određeni potresni scenarij (ili niz potresnih scenarija) na temelju teorijskog spektra točkastog izvora, postavlja se pitanje vrijedi li aproksimacija i za potrese većih magnituda. Pokazalo se da RVT metoda za raspon magnituda $M_W = 5.0–7.7$ daje rezultate koji su usporedivi sa zapisima jakih potresa (npr. Boore 1983, 2003; McGuire i sur. 1984; Silva i Lee 1987; Silva i sur. 1997; Rathje i Ozbey 2006; Kottke i Rathe 2013). Ekvivalentno-točkasti model izvora direktno je implementiran u RVT metodu preko hipocentralne udaljenosti $R = \sqrt{(R_e^2 + h^2)}$ (Yenier i Atkinson 2014) što omogućuje da su dobiveni rezultati u prosjeku usporedivi s mnogo kompleksnijim modelima izvora za potrese s magnitudama $M_W > 6.0$. Korištenjem lokalnih i regionalnih seizmoloških parametara u odnosu na teorijske seizmološke parametre, predviđeni seizmčki odziv i gibanje lokalnoga tla iz RVT metode daje rezultate koji su usporedivi s rezultatima iz TS metode (npr. Rathje i Ozbey 2006; Kottke i Rathje 2013). Samim time

EQL–RVT metoda za procjenu lokalne amplifikacije može u područjima slabe do umjerene seizmičnosti zamijeniti klasičnu TS metodu i potrebu za mnoštvom zapisa akceleracija jakih potresa.

3.4. Nelinearni amplifikacijski modeli kao sastavni dio atenuacijskih relacija predviđanja potresnog gibanja tla (GMPE)

Jednadžbe predviđanja potresnog gibanja tla ili atenuacijske relacije omogućavaju procjenu iznosa maksimalnog horizontalnog ubrzanja, na temelju poznavanja magnitude potresa, udaljenosti od žarišta potresa, tipa tla, te vrste i geometrije rasjeda (npr. Atkinson i Boore 2006; Akkar i Bommer 2010; Bommer i Akkar 2012; Akkar i sur. 2014). Dobivene su statističkom analizom velikog broja zapisa jakih potresa za određena područja. Općenito, vrijede samo za područja za koja su izvedene jer u sebi implicitno sadrže regionalna geološka i tektonska svojstva. Određenim modifikacijama izvedene GMPE relacije mogu se prilagoditi i za neka lokalna područja ili se mogu odabrati najprikladnije relacije koje najbolje opisuju određeno područje (npr. Šalić i sur. 2016). 20-ak godina nakon američkih GMPE relacija izvedene su i prve GMPE relacije za Europu. Atenuacijske relacije za Hrvatsku izveli su Herak i sur. (2001) (izraz 3.38) i Markušić i sur. (2002) (izraz 3.39). Te relacije izvedene su kao funkcije lokalne magnitude M_L i epicentralne udaljenosti s pretpostavkom da je lokalno tlo seizmoloških postaja stjenovito odnosno čvrsto tlo. Nedavno, Akkar i sur. (2014) su izveli empirijsku GMPE relaciju (izrazi 3.40 i 3.41) za dio Europe (Italija, Grčka, Turska). Prvi dio navedene relacije opisuje referentni model gibanja tla $Y_{REF}(M_W, R, SoF)$ kao funkciju magnitude, udaljenosti te vrste rasjedanja (izraz 3.41). Drugi dio relacije opisuje nelinearni amplifikacijski model za linearno i nelinearno ponašanje tla izraženo preko V_{S30} i PGA_{REF} izveden u radu Sandikkaya i sur. (2013). Nelinearni AF model (izraz 3.42) prvi je izvedeni empirijski amplifikacijski model u Europi dobiven statističkom regresijskom analizom na temelju pan-Europske baze zapisa gibanja tla uslijed jakih potresa. Regresijski koeficijent $a(T)$ opisuje linearnu promjenu AF s V_{S30} do referentne vrijednosti V_{REF} koja opisuje svojstva osnovne stijene, dok koeficijent $b(T)$ opisuje nelinearno ponašanje ovisno o PGA_{REF} (ili PGA_{ROCK}).

Boore i sur. (1997) prvi su predložili jednostavni amplifikacijski model kao funkciju parametra V_{S30} (izraz 3.43), dok su Abrahamson i Silva (1997) dodali nelinearni član kao

funkciju ulaznog gibanja definiranog za osnovnu stijenu (PGA_{ROCK}) (izraz 3.44). Kasnije su Choi i Stewart (2005) na temelju baze podataka za jake potrese razvili empirijski amplifikacijski model koji uključuje linearne i nelinearne lokalne efekte (izraz 3.45) za određene V_{S30} kategorije tla. Modificirani Choi i Stewart (2005) AF model prikazan na slici 3.12 implementiran je u atenuacijske relacije predviđanja gibanja tla u sklopu NGA-West1 (Boore i Atkinson 2008; Chiou i Youngs 2008). Kompleksniji model (izraz 3.46) razvili su Walling i sur. (2008) na temelju stohastičke EQL–RVT metode na generički definiranim V_{S30} profilima tla. AF model (Walling i sur. 2008) prikazan na slici 3.13 implementiran je u također u atenuacijske relacije predviđanja gibanja tla u sklopu NGA-West1 (Abrahamson i Silva 2008 i Campbell i Bozorgnia 2008). Nelinearni amplifikacijski model Sandikkaya i sur. (2013) direktno je usporediv (slike 3.14 i 3.15) s AF modelima kao sastavni dio GMPE relacija Abrahamson i Silva (2008) te Boore i Atkinson (2008). Važno je napomenuti da je u svim AF modelima (izrazi 3.42–3.46) nelinearno ponašanje tla ovisno o dva parametra: V_{S30} i PGA_{ROCK}. Općenito, amplifikacijski faktor AF se smanjuje s povećanjem vrijednosti PGA_{ROCK} za mekša tla s manjim vrijednostima V_{S30}, pri čemu dolazi do izražaja nelinearno ponašanje tla. Za čvršća tla s većim vrijednostima V_{S30}, amplifikacijski faktor je neovisan o PGA_{ROCK} i nelinearni efekti postaju zanemarivi. Amplifikacijski faktor definiran je kao funkcija perioda te ovisi o nelinearnom ponašanju tla s obzirom na maksimalnu amplitudu pobudnoga gibanja tla PGA_{ROCK}, dok norma Eurokod 8 (EC8) propisuje amplifikacijski faktor koji slabo ovisi o periodu (slika 3.15, Sandikkaya i sur. 2013, 2018).

4. Određivanje visokofrekventnog atenuacijskog parametra kapa (κ) u Hrvatskoj

4.1. Teorijski pregled metode za određivanje parametra κ

Spektralni parametar κ predložen je 80-ih godina prošlog stoljeća za opisivanje visokofrekventne atenuacije S valova s obzirom da tadašnji atenuacijski modeli nisu bili dovoljno dobri da objasne odstupanje između stvarnog i teorijskog Bruneovog (1970) spektra S valova. Hanks (1982) je na temelju velikog broja zabilježenih akceleracija jakih potresa opazio značajno opadanje FAS-a na određenoj frekvenciji te uveo pojam granične frekvencije f_{max} kao prethodnik parametru κ. Na temelju tih opažanja, Hanks (1982) zaključuje da je f_{max} prvenstveno rezultat utjecaja lokalnih uvjeta tla. Parametar f_{max} definiran je kao

nisko-propusni filter lokalnoga tla te je kasnije uključen u stohastičko modeliranje gibanja tla (npr. Boore 1983, 2003; Hanks i McGuire 1981). Empirijski spektralni parametar κ uveden je u radu Anderson i Hough (1984) kao proširenje eksponencijalne formulacije opisivanja atenuacije S valova kroz unutrašnjost Zemlje (izraz 4.2). Prema Anderson i Hough (1984), spektralni parametar κ pojedinog zapisa potresa sadrži dva atenuacijska doprinosa (izraz 4.3): frekvencijski ovisan parametar $Q(f)$ za opisivanje atenuacije S valova prilikom širenja kroz Zemljino sredstvo, te frekvencijski neovisan parametar κ_0 za opisivanje tzv. plitke lokalne atenuacije ispod i neposredno oko same postaje (za udaljenosti $R \approx 0$ km).

Metoda opisana u radu Andersona i Hough (1984) (skraćeno AH84) određivanja spektralnog parametra κ bazira se na opažanju eksponencijalnog opadanja Fourierovog spektra akceleracijskih zapisa S valova za potrese raspona magnituda $M_L = 3.5-6.8$ na visokim frekvencijama. Sastoji se od dva koraka (slika 4.1), od kojih je prvi Fourierova transformacija akceleracijskog gibanja S valova, a drugi određivanje parametra κ iz nagiba (izraz 4.4) visokofrekventnog dijela FAS-a u linearno–logaritamskoj skali iznad određene frekvencije f_{max} (ili f_1), nakon koje spektar naglo počinje padati do razine šuma (f_2). Na ovaj način određuje se spektralni parametar κ pojedinog zapisa potresa na određenoj epicentralnoj udaljenosti (R_e). Anderson i Hough (1984) su predložili linearnu ovisnost između pojedinačno određenih vrijednosti κ svakog akcelerograma i pripadnih epicentralnih udaljenosti (izraz 4.5, slika 4.2). U izrazu (4.5) parametar κ_0 opisuje atenuacijski doprinos potpovršinskih plitkih geoloških struktura ispod i neposredno oko same postaje (ili lokacije) te se naziva lokalna atenuacija postaje ili lokacije. Nagib (κ_R) linearne ovisnosti $\kappa-R_e$ povezan je s regionalnom atenuacijom (izrazi 4.2 i 4.3), zbog rasprostiranja S valova kroz Zemljinu koru ispod i blizu postaje unutar nekoliko kilometara oko žarišta.

Posljednjih nekoliko godina, parametar lokalne atenuacije κ_0 koreliran je s parametrom lokalnoga tla V_{S30} (slika 4.3, Ktenidou i sur. 2014), pri čemu se navodi zaključak da manje vrijednosti κ_0 odgovaraju većim vrijednostima V_{S30} (tvrđa tla) i obrnuto. Također, nekoliko istraživanja potkrepljuje opažanje da plitki površinski slojevi (tla i stijena) (do dubine od 1–2 km) na manjim epicentralnim udaljenostima (< 50 km) najviše doprinose disipaciji energije i samim time najviše utječu na visokofrekventni dio FAS-a. Doprinos izvora na parametar κ još nije detaljno istražen u postojećoj literaturi, međutim nekoliko istraživanja ne isključuju mogućnost utjecaja izvora na iznose κ (npr. Kilb i sur. 2012; Ktenidou i sur. 2013; Perron i sur. 2017).

4.2. Područje istraživanja i baza zapisa potresa

Područje istraživanja (slika 4.4) obuhvaća krško područje Dinarida između Jadranske mikroploče i Panonskog bazena kao dijela Euroazijske ploče (npr. Tomljenović i sur. 2008; Schmidt i sur. 2008; Handy i sur. 2015). Dinaridi su borano-navlačni pojas koji je nastao deformacijom Jadranske mikroploče tijekom kolizije i interakcije s Euroazijskom pločom. Pružaju se SZ–JI, od Južnih Alpa na sjeverozapadu do Albanida i Helenida jugoistočno. Dijele se na dva dijela: Vanjske ili Krške Dinaride koji se protežu duž Jadranske obale te na Unutarnje Dinaride koji se protežu kroz središnji i sjeverni dio Bosne i Hercegovine prema Savskoj suturnoj zoni koja Dinaride dijeli od Panonskog bazena (npr. Vlahović i sur. 2005; Tomljenović i sur. 2008; Handy i sur. 2015). Panonski bazen je dio pretežito nizinskog područja koje se rasprostire između planinskih lanaca Alpa, Karpata i Dinarida. Jugozapadni dio Panonskog bazena omeđen je rijekama Kupom i Savom na jugu i Dravom na sjeveru (npr., Šumanovac i sur. 2015). Seizmički najaktivniji dio Republike Hrvatske je jugoistočni dio oko Stona i Dubrovnika (npr. Markušić i sur. 2017), područje Rijeke (npr. Ivančić i sur. 2006) te u kontinentalnom dijelu Hrvatske područje oko Zagreba te dio oko gorja u sjeverozapadnoj Hrvatskoj (Ivanščica, Kalnik) (npr. Herak i sur. 2009).

Za potrebe određivanja spektralnog parametra κ, odabrano je deset seizmoloških postaja (prikazanih na slici 4.4 crvenim trokutima): Kalnik (KALN), Puntijarka (PTJ), Ozalj (OZLJ), Rijeka (RIY), Brijuni (BRJN), Novalja (NVLJ), Morići (MORI), Čačvina (CACV), Ston (STON) i Stravča (STA). Korišteni su zapisi potresa u razdoblju 2002.–2016., magnituda $3.0 \leq M_L \leq 5.7$, epicentralnih udaljenosti $R_e \leq 150$ km te dubina žarišta $h < 30$ km. Odabir donje granice lokalne magnitude i gornje granice epicentralnih udaljenosti igra značajnu ulogu kod određivanje κ pojedinačnih potresa, a sve s ciljem smanjivanja doprinosa izvora (npr. Anderson i Hough 1984; Drouet i sur. 2010; Ktenidou i sur. 2013). Broj zapisa potresa za svaku seizmološku postaju je različit (tablica 4.1) s obzirom na različitu seizmičnost područja unutar kojeg se nalaze. Takav izbor utječe i na azimutalnu razdiobu potresa oko pojedinih postaja (slika 4.5) te na raspon epicentralnih udaljenosti. Za neke postaje (npr. STA, STON) zapisi potresa pokrivaju raspon od najmanjih epicentralnih udaljenosti pa sve do gornje granice, dok kod nekih postoji problem malog broja podataka (npr. KALN, BRJN).

Slika 4.6 prikazuje lokalne geološke karakteristike užeg područja oko svake seizmološke postaje (Geološka karta Republike Hrvatske, 1:300 000; Tumač geološke karte HGI 2009). Postaja KALN nalazi se na području gorja Kalnik gdje lokalno dominiraju jurske ofiolitne magmatske stijene. Lokalno područje oko postaje PTJ smještene na vrhu Medvednice izgrađeno je pretežito od paleozojskih parametamorfnih i ortometamorfnih stijena. Seizmološka postaja OZLJ nalazi se na klisuri iznad rijeke Kupe izgrađenoj pretežito od senonskih flišnih naslaga. Za postaje RIY i BRJN, lokalno područje pretežito je izgrađeno od naslaga donjokrednih vapnenaca i dolomita. Seizmološka postaja NVLJ nalazi se na otoku Pagu na području kojim dominiraju naslage foraminiferskih vapnenaca paleocensko–eocenske starosti i tercijarnih karbonatnih breča paleogensko–neogenske starosti. Rudistni vapnenci gornjokredne starosti izgrađuju najveću površinu oko postaje MORI. Seizmološka postaja CACV smještena je jugoistočno od Sinjskog polja, u karbonatnim naslagama (vapnenci i dolomiti) jurske starosti koje su navučene na kompaktan karbonatni kompleks krednih naslaga. Seizmološka postaja STON smještena je u zaljevu Bistrina nedaleko od Stona na gornjokrednim vapnencima. Postaja STA smještena je u Konavoskim brdima na kontaktu karbonata gornjojurske i donjokredne starosti.

Terenska geofizička istraživanja (refrakcijska S tomografija i mjerenje mikroseizmičkoga nemira) su provedena na lokacijama seizmoloških postaja kako bi se odredili parametri lokalnoga tla: V_{S30} – prosječna brzina S valova u gornjih 30 m (izraz 4.6), te f_{res} – rezonantna ili osnovna frekvencija tla i HVSR amplituda kao indikacija potencijalne lokalne amplifikacije (npr. SESAME 2004). Geofizički profili tla na lokacijama seizmoloških postaja (slika 4.7) ukazuju na prisutnost čvrstih tala i stijena s $V_{S30} > 800$ m/s (prema Eurokodu 8 radi se o kategoriji tla A), što je usporedivo s lokalnim geološkim kartama. Mjerenje mikroseizmičkoga nemira na većini je postaja u skladu s geološkim kartama i geofizičkim mjerenjima te ukazuje na referentnu spektralnu krivulju s amplitudama HVSR < 2 bez izraženih značajnih vrhova. Prisutnost amplituda HVSR > 2 (do maks. 3) pridružena je topografskim efektima na lokacijama nekih seizmoloških postaja (KALN, PTJ i OZLJ) (npr. slični efekti su viđeni u radu Stanko i sur. 2016). S obzirom na izmjerene vrijednosti V_{S30}, prisutnost površinskih mekih slojeva tla s manjim vrijednostima V_S, te s obzirom na izmjerene HVSR krivulje, kao referentna vrijednost za izdanak osnovne stijene do dubine 30 m uzeta je $V_{S30REF} = 1100$ m/s.

4.3. Rezultati procjene visokofrekventnog parametra κ za Hrvatsku

Parametar κ određen je za svaki zapis potresa i pripadni FAS pomoću AH84 metode (dva primjera prikazana na slikama 4.9 i 4.10). Korišteni su trokomponentni seizmogrami (horizontalne NS i EW komponente te vertikalna Z komponenta) akceleracija gibanja tla lokalnih potresa, frekvencije uzorkovanja 50 Hz. Seizmogrami su filtrirani pojasno-ograničenim filtrom 0.5–25 Hz kako bi se uklonili neželjeni šumovi. Odabran je prozor S valova minimalnog trajanja 3 s, no u nekim slučajevima dio kode se nije mogao izbjeći. Akceleracijski prozor S valova transformiran je brzom Fourierovom transformacijom (FFT) u FAS gibanja tla. Vrijednost κ određena je iz nagiba visokofrekventnog dijela spektra prema izrazu (4.4). Na taj način izračunate su vrijednosti κ pojedinačnih zapisa potresa na odabranim postajama.

Svaki akcelerogram potresa i pripadni FAS vizualno su provjereni kako bi se izbjegli slučajevi prisutnosti rezonantnih vrhova ili ravni spektri, te su sve odabrane frekvencije (f_C, f_1, f_{max}, f_2) određene ručno. Te su frekvencije prikazane ovisno o lokalnoj magnitudi (M_L) i epicentralnoj udaljenosti (R_e) na slici 4.11 kako bi se provjerilo postoje li određena odstupanja trendova od teorijskih. Granična frekvencija f_C ovisi o svojstvima izvora te očekivano opada s povećanjem M_L (npr. Boore 2003). Određeno raspršenje f_C koje se uočava kod manjih magnituda može ukazivati na utjecaj izvora kod manjih epicentralnih udaljenosti ($R_e < 60$ km) (npr. Kilb i sur. 2012). Trendovi frekvencija f_{max} (ili f_1) i f_2 su uniformni s M_L i R_e. f_{max} je određena lokalnom geologijom oko same postaje, dok je f_2 gornja granična frekvencija šuma (ili Nyqvistova frekvencija). Horizontalne κ vrijednosti (NS, EW) usrednjene su u prosječnu horizontalnu vrijednost κ_{hor}. Slučajevi u kojima se dvije vrijednosti κ horizontalnih komponenti razlikuju za više od 25 % su odbačeni.

Većina istraživanja vezanih uz κ (npr. Douglas i sur. 2010; Van Houtte i sur. 2011, 2014; Ktenidou i sur. 2013, 2015; Perron i sur. 2017) koristi samo horizontalne komponente. Neka istraživanja su pokazala da su određene vertikalne κ_{ver} vrijednosti sustavno manje od horizontalnih κ_{hor} vrijednosti (npr. Douglas i sur. 2010; Ktenidou i sur. 2013). Slika 4.12 pokazuje usporedbu omjera vertikalnih i horizontalnih iznosa (κ_{ver}/κ_{EW}, κ_{ver}/κ_{NS} i $\kappa_{ver}/\kappa_{hor}$) te su opažene male razlike između omjera κ_{EW} i κ_{NS} s κ_{ver} u odnosu na $\kappa_{ver}/\kappa_{hor}$. Za većinu seizmoloških postaja omjer $\kappa_{ver}/\kappa_{hor}$ blizak je jedinici. Kod nekih postaja (MORI, CACV i STON) omjer $\kappa_{ver}/\kappa_{hor}$ znatno je manji od

0.90, dok je kod nekih postaja omjer $\kappa_{ver}/\kappa_{hor}$ veći od 1.20 (KALN i BRJN). Odstupanja su vrlo vjerojatno posljedica kompleksne lokalne geologije i topografije koja može direktno utjecati na vertikalnu komponentnu gibanja tla na tim postajama.

Prema Andersonu i Hough (1984), linearna ovisnost $\kappa-R_e$ (izraz 4.5) povezuje individualne κ vrijednosti s epicentralnim udaljenostima R_e, kako bi se razvio κ model te odredio parametar lokalne atenuacije κ_0 pojedinih postaja (slike 4.13–14). Parametar κ_0 određen je iz linearne regresije za epicentralne udaljenosti $R_e = 0$ km. U ovom istraživanju κ modeli za obje komponente (horizontalna i vertikalna) su promatrani kako bi se odredili parametri lokalne atenuacije κ_0^{hor} i κ_0^{ver} iz linearne ovisnosti, te usporedile dobivene vrijednosti. U linearnoj regresiji odbačene su točke koje znatno odstupaju (izvan 95 % intervala pouzdanosti). Nezanemarive individualne pogreške epicentralnih udaljenosti (R_e) mogu utjecati na primjenljivost obične linearne regresije najmanjih kvadrata, pa tako i na konačnu vrijednost κ_0 i nagiba κ_R. Zato je napravljen test ortogonalne regresije (York i sur. 2004) uzimajući u obzir standardne pogreške R_e i κ, te se pokazalo da su razlike manje od 5 % u odnosu na standardnu linearnu regresiju za pogreške u $R_e = \pm\, 2-5$ km, dok razlike mogu biti znatne ako su i pogreške kod R_e veće, te ako su pogreške tih dviju varijabli jako korelirane. U tablici 4.2 prikazani su dobiveni parametri standardne linearne regresije $\kappa-R_e$ (prema izrazu 4.5) za horizontalne i vertikalne κ modele po pojedinim postajama te njihovi omjeri.

Nagib linearne regresije κ_R pokazuje postupno povećanje vrijednosti κ s R_e na svim postajama (npr. Anderson i Hough 1984; Ktenidou i sur. 2013, 2015). Na manjim udaljenostima prosječna κ vrijednost može se aproksimirati konstantom koja odgovara približnoj vrijednosti κ_0 te je rezultat utjecaja lokalnih uvjeta tla u relativno plitkoj kori ispod i neposredno oko postaje. Postupno povećanje nagiba pravca regresije počinje na udaljenostima većim od 15–20 km što navodi na zaključak o utjecaju regionalne atenuacije (npr. Van Houtte i sur. 2014; Ktenidou i sur. 2015). Na nekim postajama postoji problem malog broja podataka što može utjecati na konačni rezultat, ali se u svim $\kappa-R_e$ modelima može uočiti linearna ovisnost.

Specifičan pokazatelj reprezentativnosti linearne regresije jest koeficijent determinacije R^2 (tablica 4.2) te je model to reprezentativniji što je on bliže vrijednosti 1. Međutim, s obzirom da je relativno veliko raspršenje κ s R_e tipično za ovakva istraživanja (slike 4.13–14), u literaturi se navodi da vrijednost $R^2 > 0.60$ predstavlja dovoljno jaku linearnu $\kappa-R_e$ ovisnost

(npr. Ktenidou i sur. 2013, 2014). Za vrijednosti $0.40 < R^2 < 0.60$ linearna $\kappa - R_e$ ovisnost je prihvatljiva, međutim određeni faktori mogu utjecati na konačnu κ_0 vrijednost (npr. utjecaj izvora, azimutalna distribucija, Perron i sur. 2017). Linearne $\kappa - R_e$ ovisnosti koje imaju $0.20 < R^2 < 0.40$ su upitne te mogu biti rezultat prvenstveno nereprezentativno malog broja podataka.

Dosad u literaturi nisu zabilježeni pokušaji određivanja parametra lokalne atenuacije za vertikalnu komponentu κ_0^{ver} iz linearne $\kappa - R_e$ ovisnosti. Douglas i sur. (2010) i Ktenidou i sur. (2013) odredili su κ vrijednosti iz vertikalnih gibanja tla, međutim κ_{ver} modeli s udaljenošću nisu razmatrani. Omjeri $\kappa_0^{ver}/\kappa_0^{hor}$ i $\kappa_R^{ver}/\kappa_R^{hor}$ su razmatrani kako bi se dobio uvid u utjecaj lokalne i regionalne geologije i tektonike na $\kappa - R_e$ modele na pojedinim postajama. Omjeri $\kappa_0^{ver}/\kappa_0^{hor} > 1$ tipični su za postaje koje se nalaze na povišenim područjima (KALN, PTJ, OZLJ, BRJN) pri čemu topografija terena može utjecati na spektar gibanja tla (npr. Perron i sur. 2017). Omjeri $\kappa_0^{ver}/\kappa_0^{hor} < 0.74$ za postaje CACV i MORI mogu ukazivati na utjecaj određenih geomorfoloških i geoloških karakteristika terena te na potencijalno lokalno raspršenje s obzirom na tektoniku. Za postaje STA, STON, NVLJ i RIY omjeri $\kappa_0^{ver}/\kappa_0^{hor}$ su blizu i oko jedinice (0.82–0.95) te prate usporedbu individualnih $\kappa_{ver}/\kappa_{hor}$. Zanimljivo je da su omjeri $\kappa_R^{ver}/\kappa_R^{hor}$ za sve postaje 0.87–1.12 (tablica 4.2) što navodi na zaključak da je za κ_{hor} i κ_{ver} modele doprinos regionalne atenuacije sličan. Takav zaključak je logičan s obzirom na povećanje nagiba pravca regresije za udaljenosti 15–20 km, dok je dominantni utjecaj na vrijednosti lokalnih atenuacija κ_0^{hor} i κ_0^{ver} lokalno tlo ispod i oko samih postaja, a koje utječe na različite komponente gibanja tla (NS, EW i Z) (npr. Ktenidou i sur. 2013, 2014, 2015). Općenito, vrijednosti κ_{ver} s R_e su više raspršene od κ_{hor} te su vrijednosti R^2 za κ_{ver} modele znatno manje od R^2 za κ_{hor} modele. S obzirom na prethodnu diskusiju, horizontalne vrijednosti lokalne atenuacije κ_0^{hor} (tablica 4.2) uzete su kao reprezentativne vrijednosti lokalne atenuacije κ_0 u okolici seizmoloških postaja u Hrvatskoj.

4.4. Diskusija parametra κ za Hrvatsku

U literaturi je općenito prihvaćeno da manje vrijednosti lokalne atenuacije κ_0 odgovaraju čvrstim stijenama koje imaju veće vrijednosti V_{S30}, dok mekše stijene s manjim V_{S30} imaju veće vrijednosti κ_0 (npr. Anderson i Hough 1984; Ktenidou i sur. 2014). U tablici 4.3 uspoređene su vrijednosti lokalne atenuacije κ_0 seizmoloških postaja s određenim

vrijednostima V_{S30} na temelju geofizičkih istraživanja. Za postaje na čvrstim stijenama ($V_{S30} \geq 1100\,\text{m/s}$) vrijednosti lokalne atenuacije su manje ($\kappa_0 \leq 0.025\,s$) nego za postaje na mekšim stijenama ($V_{S30} = 760\text{–}1100\,\text{m/s}, \kappa_0 > 0.025\,s$), a kod kojih su prisutni površinski meki slojevi. Općenito, na svim postajama vrijednosti $V_{S30} > 760\,\text{m/s}$ uz zanemarivu HVSR amplifikaciju, ukazuju da se radi lokacijama na čvrstim stijenama. Samim time, može se zaključiti da vrijednosti lokalne atenuacije κ_0 odgovaraju pretežito čvrstim stijenama na kojim se nalaze seizmološke postaje. Uspoređujući iznose $\kappa_0\text{–}V_{S30}$ iz tablice 4.3 i slike 4.15 sa vrijednostima iz svijeta, može se uočiti da su iznosi κ_0 za hrvatske seizmološke postaje slični vrijednostima $\kappa_0\text{–}V_{S30}$ iz različitih dijelova svijeta, prvenstveno za čvrste stijene (npr. Silva i sur. 1999; Chandler i sur. 2005; Douglas i sur. 2010; Drouet i sur. 2010; Edwards i sur. 2011; Van Houtte i sur. 2011; Ktenidou i sur. 2013, 2014, 2015; Perron i sur. 2017).

Utjecaj izvora na određivanje visokofrekventnog parametra κ iz individualnog gibanja tla i pripadnog FAS-a predmet je rasprave među istraživačima. Mogući doprinos izvora na κ prikazan je usporedbom s lokalnim magnitudama M_L za svaku postaju (slika 4.16). Raspršenje $\kappa\text{–}M_L$ je dosta veliko pa se može zaključiti da je utjecaj izvora na κ zanemariv. Međutim, s obzirom na broj podataka u određenom rasponu magnituda ($M_L > 4.5$) te nedostatak zapisa potresa na manjim udaljenostima ($R_e < 20\,\text{km}$), ne može se isključiti potencijalni doprinos izvora na κ (pogotovo bliskog izvora) (npr. Edwards i sur. 2011; Kilb i sur. 2012; Ktenidou i sur. 2013; Perron i sur. 2017). Zato je, prema Andersonu i Hough (1984), frekvencija f_1 ili f_{max} uvijek je veća odf_C (slika 4.17), kako bi se izbjegli potencijalni utjecaji izvora na κ.

Castro i sur. (2000) navode da je raspršenje κ s udaljenošću posljedica utjecaja nejednolike atenuacije blizu izvora. S obzirom na geografsku razdiobu podataka u ovom istraživanju (slika 4.5), postavlja se pitanje utječe li geografska orijentacija izvora potresa na iznose κ. Na slici 4.18 individualne vrijednosti κ sortirane su te prikazane kao funkcija epicentralne udaljenosti R_e. S obzirom na veliko raspršenje grupa unutar prozora azimuta od 30° u $\kappa\text{–}R_e$ ovisnosti, može se zaključiti da geografska orijentacija epicentara ne utječe na konačne vrijednosti κ i pripadne lokalne atenuacije κ_0 iz $\kappa\text{–}R_e$ ovisnosti (npr. Ktenidou i sur. 2013; Van Houte i sur. 2014; Perron i sur. 2017).

Gentili i Franceschina (2011) opazili su različite nagibe κ_R na stanicama ovisno o potresima s različitih područja. Regionalnu ovisnost opisali su većom atenuacijom duž rasjeda zbog efekata valovoda u razlomljenoj zoni, a manju atenuaciju kao posljedicu različitih refleksija S

valova u plitkim zonama Mohorovičećeva diskontinuiteta. Usporedno s $\kappa - R_e$ modelima ovisno o geografskoj orijentaciji podataka, na slici 4.18 prikazane su prostorne razdiobe individualnih κ vrijednosti kako bi se dobila slika regionalne atenuacije oko svake postaje. Interpolacijskom metodom najbližih susjeda nacrtane su regionalne promjene vrijednosti κ oko svake postaje. Očekivano, najniže κ vrijednosti prostorno su raspoređene oko same postaje unutar nekoliko kilometara gdje je doprinos lokalne atenuacije κ_0 najveći. Postupno povećanje s udaljenošću od postaje potvrđuje da su propagacijski efekti izraženi preko nagiba linearne regresije κ_R dominantni te opisuju doprinos regionalne atenuacije na većim udaljenostima.

Prostorna razdioba κ za pojedine postaje (slika 4.18) ukazuje da su atenuacijska svojstva stijena u Dinaridima daleko od izotropnih. Općenito se može uočiti veća atenuacija poprečno na pružanje planinskih lanaca i regionalnih rasjednih sustava, nego duž njihovog pružanja. Uzrok ove anizotropnosti još nije moguće jednoznačno utvrditi, a najizgledniji uzroci za to su preferencijska orijentacija pukotina pod utjecajem lokalnih i regionalnih polja napetosti, usmjeravanje valnog polja duž geoloških struktura (valovodi), te veća atenuacija unutar rasjednih zona (npr. Lokmer i Herak 1999; Dasović 2015a).

Neki istraživači povezuju frekvencijski ovisan $Q(f)$ s frekvencijski neovisnim Q određenim iz nagiba linearne regresije κ_R (izraz 4.7) (npr. Anderson i Hough 1984; Edwards i sur. 2011; Gentili i Franceschina 2011; Ktenidou i sur. 2015; Perron i sur. 2017). Na taj način mogu se međusobno usporediti dva nezavisna istraživanja atenuacije. Tablica 4.4 prikazuje vrijednosti $Q_{est}^{C,S}(f)$ iz nedavnih istraživanja kode i S valova (Dasović 2015a; Dasović i sur. 2012, 2013, 2015b;) s vrijednostima $Q_{est}(\kappa_R)$ određenih iz κ_R za visokofrekventni dio (10–25 Hz). Prvo, u oba istraživanja nije korišten isti skup podataka (jednakog raspona magnituda i epicentralnih udaljenosti). Drugo, standardne pogreške Q_C, Q_S i κ_R su u pravilu znatne (često i veće od ± 50 %). I treće, postoji fundamentalna razlika u pretpostavci o frekvencijskoj (ne)ovisnosti faktora Q. Uzevši sve to u obzir, kao i rezultate sličnih istraživanja koja su spomenuta ranije, rezultati u tablici 4.4 ukazuju da su korijeni opadanja FAS na visokim frekvencijama vjerojatno u intrinzičnim anelastičnim svojstvima stijena te raspršenju energije na putu od izvora do prijemnika.

Kao što je ranije pokazano, prostorna raspodjela parametra κ vezana je uz lokalna i regionalna stratigrafska i tektonska svojstva. Vrijednosti $Q_{est}(\kappa_R)$ između pojedine postaje i okolnog

područja mogu ukazivati na regionalni atenuacijski doprinos. Slične $Q_{est}(\kappa_R)$ vrijednosti za KALN, PTJ i OZLJ mogu definirati prijelaznu zonu između dijela Panonskog bazena i Unutarnjih Dinarida, $Q_{est}(\kappa_R)$ vrijednosti za BRJN, RIY i NVLJ mogu definirati dio zone između nedeformiranog dijela Jadranske mikropločе u deformirani dio Dinarida, $Q_{est}(\kappa_R)$ vrijednosti za MORI i CACV mogu ukazivati na prijelaznu zonu između Vanjskih i Unutarnjih Dinarida te $Q_{est}(\kappa_R)$ vrijednosti za STON i STA mogu definirati regionalni atenuacijski doprinos jugoistočnog dijela Vanjskih Dinarida prema Albanidima. Također, dobivene vrijednosti $Q_{est}(\kappa_R)$ iz ovog istraživanja mogu se usporediti sa sličnim κ_R i Q regionalnim vrijednostima (npr. Švicarska, Francuska $Q = 1000–2000$; Grčka $Q = 500–600$; sjeveroistočna Italija $Q = 2140$). Lokalne i regionalne razlike u atenuacijskim doprinosima najviše su posljedica potpovršinskih Q i V_S struktura te rasjednih i pukotinskih krških struktura (npr. Boore i Joyner 1997; Gentili i Franceschina 2011; Ktenidou i sur. 2014) kao što je slučaj u Dinaridima. Buduća istraživanja bi svakako trebala koristiti veći broj potresa i postaja, što će pomoći da se izvedu pouzdaniji zaključci o vezi $Q_{est}^{C,S}(f)$ i $Q_{est}(\kappa_R)$ s regionalnom atenuacijom i geološkom građom.

5. Analiza utjecaja lokalnih uvjeta tla na amplifikaciju seizmičkoga površinskoga gibanja u Hrvatskoj pomoću EQL–RVT metode

5.1. Odabir potresnih scenarija za definiranje ulaznog gibanja u RVT analizi

Pri proračunima, neki su seizmološki parametri držani konstantnima: pad napetosti u žarištu $\Delta\sigma = 100$ bar (npr. Hanks i McGuire 1981; Boore 1983, 2003), fiktivna dubina žarišta $h = 12$ km (Herak i sur. 1996), prosječne vrijednosti brzine rasprostiranja transverzalnih valova u kori ($\beta_0 = 3.5$ km/s) i gustoće ($\rho_0 = 2800$ kg/m^3), a neki su bili specifični za svaku postaju: $Q(f)$ (tablica 4.4, Dasović 2015a) i κ_0 (Poglavlje 4, tablica 4.2).

Ostali seizmološki parametri (lokalne magnitude i epicentralne udaljenosti) mijenjani su za svaku postaju kako bi FAS definirao ulazno gibanje za osnovnu stijenu (PGA_{ROCK}) za

određenu vrijednost horizontalne vršne akceleracije definirane prema seizmičkom hazardu (za povratni period 475 godina). Ulazno gibanje definirano je za vršne vrijednosti akceleracije $PGA_{ROCK} = 0.03$ g, 0.06 g, 0.10 g, 0.15 g, 0.20 g, 0.25 g, 0.30 g i 0.37 g (tablica 5.1). Različite vrijednosti lokalne magnitude između $M_L = 5.0$ i $M_L = 7.1$ (momentna magnituda M_W izračuna se prema izrazu 5.1) su odabrane prema EC8 tipovima spektra ($M_s \leq 5.5$ i $M_s > 5.5$) te prema jačim potresima $M_L > 6.0$ (iz povijesti i nedavno) za određena područja (npr. Varaždin 1459., Dubrovnik 1667., Zagreb 1880. i Ston 1996.). Ekvivalentna udaljenost izražena je preko hipocentralne udaljenosti kako bi se u RVT analizi definirao ekvivalentno-točkasti model izvora za potresne scenarije s velikim magnitudama ($M_W > 6.0$) (npr. Yenier i Atkinson 2014). Epicentralne udaljenosti R_e odabrane su u rasponu između 7 km i 30 km. Takav odabir udaljenosti omogućuje definiranje visokofrekventnog dijela FAS-a preko lokalne atenuacije κ_0 za bliske potrese. Također, manje epicentralne udaljenosti zahtijevaju manje magnitude potresa za definiranje određene veće vrijednosti PGA_{ROCK}. Za veće epicentralne udaljenosti, potrebne su i veće magnitude potresa kako bi se definirala veća vrijednost PGA_{ROCK}, što dovodi u pitanje smisao korištenja teorijskog modela točkastog izvora za definiranje ulaznog FAS-a u RVT analizi.

Na temelju odabranih potresnih scenarija, definirani su Fourierovi amplitudni spektri (FAS) za svaku seizmološku postaju (slika 5.1, lijevo). Lokalna atenuacija κ_0, kao lokalni parametar postaje, najviše utječe na oblik FAS-a na višim frekvencijama i na pripadne spektre odziva (RSB) definirane za osnovnu stijenu (slika 5.1, desno). Vrijednost ulaznog gibanja PGA_{ROCK} definirana je za spektralnu akceleraciju Sa nultog perioda u spektru ulaznog odziva RSB. Za potrebe EQL–RVT analize seizmičkoga odziva lokalnoga tla u Hrvatskoj, srednjak FAS-a i spektra odziva (slika 5.2) je korišten kako bi se definirala pojedina vrijednost PGA_{ROCK} za osnovnu stijenu. Za veće magnitude (M_L) granična frekvencija (f_C) pomiče se prema nižim frekvencijama (točkasti Brune (1970) ω^2 model). Frekvencija f_{max} definira frekvenciju nakon koje amplituda FAS-a počinje naglo opadati. S obzirom da je lokalno tlo na lokacijama seizmoloških postaja definirano kao čvrsta stijena sa sličnim vrijednostima V_{S30}, f_{max} je prikazana kao konstantna vrijednost (slike 5.1 i 5.2).

5.2. Lokalni profili tla korišteni za EQL–RVT analizu

Lokalni profili tla prikupljeni su s raznih lokacija diljem Hrvatske (slika 5.3) na temelju terenskih geofizičkih istraživanja, mjerenja mikroseizmičkoga nemira te iz objavljenih radova (npr. Stanko i sur. 2016, 2017; Strelec i sur. 2016). Ukupno je prikupljeno 70 lokalnih profila tla diljem Hrvatske s različitim vrijednostima V_{S30}, dubinama osnovne stijene i osnovnog perioda tla (slika 5.4). Modeli lokalnih tala korišteni su u programu STRATA za EQL–RVT analizu. Slojevi tla u svakom modelu definirani su njegovim svojstvima: brzinama S valova (V_S), gustoćama, krivuljama modula smicanja (G/G_{max}) i prigušenja (ξ) (slike 5.5 i 5.6). Općenito, kod velikih deformacija, mekanija tla (npr. gline niske plastičnosti PI < 30) jače degradiraju, tj. krivulja G/G_{max} brže pada, a ξ raste, dok je kod tvrđih tala (npr. stijena i slične formacije tla) situacija obrnuta (slika 5.5). U EQL analizi, krivulje modula smicanja (G/G_{max}) i prigušenja (ξ) tla definiraju nelinearno ponašanje tla za određena ulazna gibanja.

5.3. Rezultati 1-D EQL–RVT analize seizmičkoga odziva lokalnoga tla

Za potrebe analize utjecaja lokalnih uvjeta tla na amplifikaciju seizmičkoga površinskog gibanja u Hrvatskoj, lokalni profili tla razvrstani su na temelju parametra V_{S30} prema kategorizaciji tla u Eurokodu 8 (tablica 5.2). Dodatno, EC8 kategorije su podijeljene u sedam V_{S30} kategorija (slika 5.4) kako bi se mogli detaljnije opisati lokalni uvjeti tla. Također, treba naglasiti da je u EC8 osnovna stijena definirana za $V_{S30} = 800$ m/s, dok je u ovom istraživanju referentna osnovna stijena definirana za $V_{S30REF} = 1100$ m/s.

Rezultati 1-D EQL analize seizmičkoga odziva lokalnoga tla pomoću RVT metode prikazani su u obliku 5 % prigušenog akceleracijskog spektra odziva na površini (RSS) i amplifikacijskog faktora $AF(T)$ (izraz 1.1) kao funkcije perioda (slika 5.7). Spektar odziva prikazuje odziv sustava s jednim stupnjem slobode za spektralne periode na kojima se može očekivati najveća akceleracija za određeno ulazno potresno gibanje. Na slici 5.7 prikazane su promjene ulaznog gibanja PGA_{ROCK} od osnovne stijene kroz različita lokalna tla do površine. Najvažniji zaključci iz primjera na slici 5.7a–g su: 1) tlo se ponaša linearno za slabija ulazna gibanja ($PGA_{ROCK} < 0.1$ g), te je ulazno gibanje najviše amplificirano u gornjim mekim slojevima tla $AF@PGA$ (vrijednost amplifikacijskog faktora za vršno gibanje tla); 2) vrijednost AF-a ($AF@PP$) je najizraženija na vlastitom (ili rezonantnom) periodu tla T_{pp},

pogotovo za tla s manjim vrijednostima V_{S30} i debelim aluvijalnim slojevima iznad osnovne stijene; 3) za ulazna gibanja veće amplitude ($PGA_{ROCK} > 0.1$ g) tlo se ponaša nelinearno pri čemu je $AF < 1$ zbog degradacije tla, pogotovo kod tala s malim vrijednostima V_{S10}, V_{S20} i V_{S30}; 4) zbog nelinearnosti se $AF@PGA$ drastično smanjuje ispod $AF < 1$ na kraćim spektralnim periodima, dok na vlastitom periodu dolazi do pomaka vrha $AF@PP$ prema duljim spektralnim periodima sa smanjenjem amplitude; 5) kod čvrstih tala, s većim vrijednostima V_{S10}, V_{S20}, i V_{S30}, $AF@PGA$ i $AF@PP$ su uravnoteženi kroz cijeli raspon spektralnih perioda, pogotovo iznad 0.10 s i ne pokazuju ovisnost o PGA_{ROCK}; 6) opažene amplifikacije $AF@PGA$ i $AF@PP$ za čvrsta tla i stijene s $V_{S30} > 560$ m/s kod kraćih spektralnih perioda (< 0.20 s) rezultat su interakcije plitke osnovne stijene i mekih površinskih slojeva tla (npr. Vučetić 1992; Beresnev i Wen 1996; Walling i sur. 2008; Dhakal i sur. 2013; Kottke i Rathje 2013; Bolisetti i sur. 2014).

5.4. Diskusija utjecaja lokalnih uvjeta tla na amplifikacijski faktor

Općenito, amplifikacija površinskoga gibanja iz EQL–RVT analize ovisi o svojstvima lokalnoga tla (osnovni period tla, V_S pojedinačnih slojeva, V_{S30}) i ulaznom gibanju PGA_{ROCK}. Za ulazna gibanja definirana za slabije potrese, opažena amplifikacija je veća za lokalna tla s manjim V_{S30} vrijednostima nego za ulazna gibanja definirana za jake potrese. Opaženo smanjenje amplifikacije vršnog gibanja tla (za $AF@PGA$, period od 0.01 s) u odnosu na PGA_{ROCK} i odstupanje spektralnog vrha (smanjenje amplitude, pomak u periodu) od osnovnog perioda tla značajno je za $PGA_{ROCK} > 0.2$ g zbog nelinearnog ponašanja lokalnoga tla (slike 5.7 a–d) (npr. Seed i sur. 1976; Seed i Idriss 1983; Beresnev i Wen 1996). Nelinearni utjecaji na vršnu akceleraciju ($PGA@0.01$ s) najviše dominiraju za lokalna tla s $V_{S30} < 280$ m/s (slika 5.8), gdje su opažene vrijednosti PGA na površini ispod linije $AF = 1$ u odnosu na PGA_{ROCK}, pogotovo za ulazna gibanja s $PGA_{ROCK} > 0.2$ g. Također, meki površinski slojevi tla najviše utječu na amplifikaciju gibanja tla kod lokalnih tala s $360 \leq V_{S30} < 760$ m/s. Za tla s $V_{S30} > 760$ m/s PGA na površini raste linearno s PGA_{ROCK}, a značajna amplifikacija (do 1.8) rezultat je interakcije osnovne stijene s plitkim pokrovom mekih slojeva tla (slika 5.8) te je amplifikacija PGA neovisna o PGA_{ROCK}.

U potresnom inženjerstvu važno je poznavati ponašanje amplifikacijskih faktora na osnovnim ili rezonantnim periodima tla zbog moguće pojave opasne rezonancije tlo–građevina prilikom

potresa. Utjecaj lokalnoga tla na amplifikaciju površinskoga gibanja tla opisan je preko parametra lokalnoga tla u gornjih 30 m (V_{S30}). Međutim, s obzirom na opaženi utjecaj gornjih mekih slojeva tla na amplifikaciju gibanja tla (slika 5.7), na slici 5.9 prikazana je ovisnost amplifikacijskog faktora na rezonantnom periodu ($AF@PP$) o brzini u gornjih 10 m (V_{S10}), 20 m (V_{S20}) i 30 m (V_{S30}) tla. Slika 5.10 prikazuje ponašanje $AF(T)$ s obzirom na vezu visine armirano-betonske građevine i spektralnog perioda (npr. Gallipoli i sur. 2010): a) amplifikacija gibanja tla na površini (0.01 s), b) 0.1 s (10 Hz) za tipične kuće, c) 0.3 s (3.33 Hz) za građevine visine 2 do 6 katova, d) 1.0 s (1.0 Hz) za građevine visine 10 do 20 katova. Nelinearno ponašanje mekih tala (manje vrijednosti $V_{S10}, V_{S20}, V_{S30}$) tipično je kod kratkih spektralnih perioda, pri čemu dolazi do smanjenja amplifikacije (de-amplifikacije) za veće vrijednosti PGA_{ROCK}. Kod srednjih do duljih spektralnih perioda nelinearno ponašanje je izraženo preko značajne amplifikacije s pomakom rezonantnih perioda. Kod čvrstih tala (s većim vrijednostima $V_{S10}, V_{S20}, V_{S30}$), vrijednosti $AF(T)$ s obzirom na određeni spektralni period mogu se smatrati konstantnim za $V_{S10} = 400$ m/s, $V_{S20} = 500$ m/s i $V_{S30} = 760$ m/s ovisno o povećanju PGA_{ROCK}, te se približavaju jedinici za vrijednosti $V_{S30} \geq V_{S30REF} = 1100$ m/s. Ponašanje amplifikacijskih faktora ovisno o spektralnom periodu za određenu vrstu građevine i seizmičko gibanje na osnovnoj stijeni PGA_{ROCK} važno je kod projektiranja protupotresnih građevina, kako bi se izbjegla moguća rezonancija tlo–građevina, ili za protupotresnu rekonstrukciju postojećih građevina u slučaju budućih potresa (npr. Elnashi i Di Sarno 2008; Celebi i sur. 2010).

6. Empirijski nelinearni amplifikacijski model za Hrvatsku

Empirijski nelinearni amplifikacijski model za Hrvatsku razvijen je na temelju dobivenih amplifikacijskih faktora iz Poglavlja 5 dobivenih pomoću EQL–RVT metode za određeni raspon lokalnih uvjeta tla ($160 < V_{S30} < 1389$ m/s) kao funkcija lokalnih uvjeta tla (V_{S30}) za određena referentna ulazna gibanja na osnovnoj stijeni (PGA_{ROCK}) te je detaljnije uspoređen s novijim amplifikacijskim modelima (Sandikkaya i sur. 2013; Kamai i sur. 2014).

6.1. Kratki pregled novijih nelinearnih amplifikacijskih modela

Nelinearni amplifikacijski modeli za linearno i nelinearno ponašanje tla (izraz 6.1) uslijed određenog potresnog gibanja izraženi su kao funkcije parametara V_{S30} i PGA_{REF} (Poglavlje 3.4). Za potrebe usporedbe i diskusije izvedenog AF modela za Hrvatsku s novijim AF modelima, prikazan je kratki pregled statističkih modela (izrazi 6.2–6.4): Choi i Stewart (2005), Walling i sur. (2008) i Kamai i sur. (2014) te Sandikkaya i sur. (2013).

6.2. Predloženi nelinearni amplifikacijski model za Hrvatsku

Predloženi nelinearni amplifikacijski model za Hrvatsku (izraz 6.5) sličan je AF modelu koji su predložili Choi i Stewart (2005) (izraz 6.2) s manjim modifikacijama koje su uvedene zbog nekoliko razloga: a) broj zapisa akceleracija uslijed jakih potresa za Hrvatsku je jako mali dok su Choi i Stewart (2005) i Sandikkaya i sur. (2013) za razvoj svojeg AF modela koristili empirijsku bazu podatka s više od 1600 zapisa akceleracija tla; b) lokalni profili tla za Hrvatsku su izmjereni na temelju geofizičkih istraživanja te predstavljaju stvarne V_{S30} modele, dok su Walling i sur. (2008) i Kamai i sur. (2014) razvili AF modele na temelju generiranih V_{S30} modela u EQL–RVT analizu što direktno utječe na rezultate; c) raspon ulaznih gibanja za Hrvatsku je definiran prema povratnom periodu od 475 godina ($0.03 \leq PGA_{ROCK} \leq 0.37$ g) te je znatno različit u odnosu na novije AF modele koji imaju veći raspon PGA_{ROCK} (0.01 g do 1.5 g).

Nelinearni amplifikacijski model za Hrvatsku razvijen je za određene kategorije V_{S30} lokalnoga tla (prema Poglavlju 5, slika 5.4a): D: $V_{S30} < 200$ m/s; C1: $200 \leq V_{S30} < 280$ m/s; C2: $280 \leq V_{S30} < 360$ m/s; B1: $360 \leq V_{S30} < 560$ m/s; B2: $560 \leq V_{S30} < 760$ m/s; A: $760 \leq V_{S30} < 1100$ m/s; A0: $V_{S30} \geq 1100$ m/s. Razlog tome leži u činjenici da su to izmjereni profili tla pri čemu je broj podataka ograničen za svaku kategoriju i samim time je teško dobiti jedinstveni statistički model kao kod gore navedenih modela. U predloženom AF modelu za Hrvatsku (izraz 6.5) koeficijent $a(T)$ opisuje linearnu promjenu AF s V_{S30} do referentne vrijednosti V_{REF}, dok koeficijenti $b_1(T)$ i $b_2(T)$ opisuju nelinearno ponašanje AF ovisno o PGA_{ROCK}.

Slike 6.1–7 prikazuju nelinearnu regresiju (prema izrazu 6.5) dobivenih AF-a i PGA_{ROCK} ovisno o V_{S30} i odabranim spektralnim periodima. Općenito, vrijednosti AF-a su slične kod slabijih ulaznih gibanja do otprilike $PGA_{ROCK} = 0.1$ g i ponašaju se linearno-proporcionalno kao $ln(V_{S30}/V_{REF})$. S povećanjem $PGA_{ROCK} > 0.1$ g vrijednosti AF-a počinju značajno opadati zbog nelinearnosti tla, pogotovo kod tala s manjim vrijednostima V_{S30} (mekanija tla). Iz tog razloga je u predloženi model dodan član „0.1 g" kao prijelazna točka između linearnog i nelinearnog ponašanja AF-a s obzirom na PGA_{ROCK}. Opažena nelinearnost AF-a kod mekanijih tala je izražena na kraćim do srednjim spektralnim periodima kao značajno opadanje AF-a, dok na rezonantnom periodu dolazi do pomaka vrha AF-a prema duljim periodima s povećanjem PGA_{ROCK}. Kvadratni član je u predloženi AF model za mekanija tla (izraz 6.5a) dodan jer linearna funkcija PGA_{ROCK} umjetno povećava regresijsku krivulju AF-a kod manjih vrijednosti PGA_{ROCK}.

Slike 6.8 i 6.9 prikazuju promjenu nelinearnih koeficijenata $b_1(T)$ i $b_2(T)$ kao funkcije spektralnih perioda za V_{S30} kategorije tla. Negativne vrijednosti tih koeficijenata na nižim periodima opisuju opadanje AF-a kod mekanijih tala (manje vrijednosti V_{S30}). Kod čvrstih tala s većim vrijednostima V_{S30}, koeficijenti $b_1(T)$ i $b_2(T)$ su manji i približavaju se nuli što označava da je nelinearnost zanemariva. Period na kojem koeficijenti $b_1(T)$ i $b_2(T)$ prelaze iz negativnih u pozitivne vrijednosti povezan je s rezonantnim periodom AF i pomakom šiljka prema većim periodima zbog nelinearnosti. Za čvrsta tla ($760 \leq V_{S30} < 1100$ m/s) na temelju opažanja je odabran koeficijent $b_2(T) = 0.0$, dok su za stijene ($V_{S30} > V_{REF}$) oba koeficijenta $b_1(T) = 0.0$ i $b_2(T) = 0.0$. Kod čvrstih tala, AF nije ovisan o PGA_{ROCK}, pogotovo na višim spektralnim periodima, dok je određena opažena amplifikacija na nižim spektralnim periodima posljedica interakcije mekih površinskih slojeva s plitkom osnovnom stijenom.

6.3. Evaluacija i diskusija predloženog nelinearnog amplifikacijskog modela za Hrvatsku

Nelinearni amplifikacijski modeli za lokalne kategorije V_{S30} evaluirani su usporedbom predviđenog AF-a za Hrvatsku s amplifikacijskim faktorima iz Eurokoda 8 (slika 6.10) i najnovijim AF modelima (Sandikkaya i sur. 2013; Kamai i sur. 2014) za četiri ulazna gibanja definirana s $PGA_{ROCK} = 0.05$ g, 0.10 g, 0.20 g i 0.30 g (slike 6.11–6.16).

Usporedba AF modela za Hrvatsku s AF modelima Sandikkaye i sur. (2013) i Kamaia i sur. (2014) može se izdvojitiu tri opažena slučaja. Za srednja do čvrsta tla i mekanije stijene (slike 6.12, 6.13 i 6.14), **200 m/s ≤ V_{S30} < 560 m/s,** predviđeni AF model za Hrvatsku usporediv je s novijim AF modelima. AF model za Hrvatsku kod nižih perioda (do 0.3 s) pokazuje značajne nelinearne efekte u AF-u u odnosu na prijašnje modele za jača ulazna gibanja (PGA_{ROCK} > 0.20 g). Prvenstveno, razlika u odnosu na model iz rada Sandikkaya i sur. (2013) leži u činjenici da je njihov AF model razvijen na temelju empirijske baze akceleracija jakih potresa (Italija, Grčka, Turska) modificiranjem modela iz radova Choi i Stewart (2005) i Walling i sur. (2008) za tzv. pan-Europsku regiju za koju se može uzeti da je seizmološki slična zapadnom Balkanu (npr. Mihaljević i sur. 2017), a ne na temelju EQL analize. Slabiji nelinearni efekti su u takvim modelima očekivani. S druge strane, model iz Kamai i sur. (2014) razvijen je na temelju RVT analize za skup generiranih modela tla čime se direktno može usporediti s rezultatima dobivenim ovim istraživanjem. Dio razlika u odnosu na taj model potječe od definiranja ekvivalentno–linearnih svojstava lokalnih tala preko krivulja modula smicanja i prigušenja u RVT analizi. Za čvršća tla V_{S30} > 280 m/s i PGA_{ROCK} < 0.10 g ponašanje AF modela je linearno i predloženi AF model za Hrvatsku pokazuje veća predviđanja u odnosu na druge modele, dok su modeli usporedivi za PGA_{ROCK} > 0.10 g. Na višim periodima (> 0.4 s), predloženi AF model za Hrvatsku usporediv je s onim Kamaia i sur. (2014) zbog jednake RVT metodologije. Razlike opažene između dva modela su uzrokovane od definiranja ulaznih modela lokalnoga tla (izmjereni modeli za Hrvatsku nasuprot generiranim modelima u Kamai i sur. (2014)). Za stijene, **560 m/s ≤ V_{S30} < 1100 m/s** (slike 6.15 i 6.16), ponašanje AF modela za Hrvatsku je linearno i neovisno o PGA_{ROCK}. Kod srednjih do duljih perioda (> 0.4 s) sva tri modela pokazuju očekivano ponašanje $AF \cong 1$. Kod kraćih perioda (< 0.3 s), AF model za Hrvatsku predviđa značajno veće amplifikacije u odnosu na modele Sandikkaya i sur. (2013) i Kamai i sur. (2014). Prvi od njih je razvijen na temelju empirijske baze podataka za model referentne osnovne stijene V_{S30} = 750 m/s. S druge strane, Kamai i sur. (2014) su model razvili za referentnu osnovnu stijenu s V_{S30} = 1180 m/s za niz generiranih profila tala s većim dubinama osnovne stijene. Model referentne osnovne stijene u ovom istraživanju definiran je za V_{S30} = 1100 m/s na izmjerenim profilima tla, pri čemu većina profila s V_{S30} > 360 m/s ima relativno plitku osnovnu stijenu (< 30 m). Kod nižih perioda, opažene amplifikacije rezultat su razlike u impedanciji između plitke osnovne stijene i mekih slojeva tla, pogotovo kod slabijih ulaznih gibanja (npr. Anbazhagan i sur. 2013; Pehlivan i sur. 2017). Za mekana

tla, $\mathbf{200\ m/s} < \boldsymbol{V_{S30}}$ (slika 6.11), sva tri modela pokazuju nelinearno ponašanje ($AF < 1$) ovisno o PGA_{ROCK} kod kraćih perioda, dok kod duljih perioda postoji razlika u AF-u između tri modela. Neodređenost kod sva tri AF modela postoji prvenstveno zbog manjka analiziranih profila mekanih tala, odabira dinamičkih svojstava tla (krivulje modula smicanja i prigušenja) te u konačnici osjetljivosti samih metoda analize odziva tla na linearno i nelinearno ponašanje uslijed jakih ulaznih gibanja.

Sandikkaya i sur. (2013, 2018) navode važnost varijacije amplifikacijskog faktora kao funkcije perioda ovisno o amplitudi PGA_{ROCK} ulaznog gibanja i lokalnom tlu (V_{S30}) u usporedbi s normom Eurokod 8 (EC8) u kojoj je amplifikacijski faktor za određene kategorije tla slabo ovisan o periodu. AF model za Hrvatsku usporediv je s EC8 kod nižih perioda, dok je na višim periodima znatno veći za lokalna tla s $V_{S30} < 280$ m/s i $PGA_{ROCK} < 0.10$ g. Kod jačih ulaznih gibanja ($PGA_{ROCK} > 0.10$ g), AF–EC8 na nižim periodima ne slijedi nelinearni trend kao AF model, dok je kod viših perioda, pogotovo na osnovnom periodu, AF–EC8 djelomično usporediv s predloženim AF modelom. Amplifikacijski faktor u Eurokodu 8 daje neprikladan nelinearni odziv tla za jača seizmička gibanja na temelju slabo o periodu ovisnog AF-a za određenu kategoriju tla. Kod čvršćih tala, $V_{S30} > 360$ m/s, AF–EC8 se generalno približavaju jedinici, dok je AF model za Hrvatsku periodno ovisan te pokazuje znatne amplifikacije u odnosu na EC8. Lokalna tla s mekim površinskim slojevima i plitkom osnovnom stijenom nisu uzeta u obzir u EC8 preko parametra V_{S30}, već su definirana kao posebna kategorija E bez reference na iznose V_{S30}. Usporedbom među kategorija tla C2, B1, B2 i A može se uočiti da su predviđeni AF-i djelomično usporedivi s kategorijom EC8–E. Općenito, noviji AF modeli i propisi (EC8, NEHRP) predviđaju konstantne AF-e bliske ili jednake jedinici za tla s $V_{S30} > 800$ m/s, dok se ovdje pokazalo da i u takvim tlima mogu postojati znatne amplifikacije zbog prisutnosti površinskih mekih slojeva iznad plitke osnovne stijene. To je posebno važno jer parametar lokalnog tla V_{S30} igra važnu ulogu u amplifikacijskim modelima, pri čemu postoje određene nepouzdanosti (određivanje iz geofizičkih istraživanja, korelacija s in-situ bušotinskim ispitivanjima, dubina osnovne stijene) koje bi svakako trebalo detaljnije razmotriti u budućim istraživanjima.

7. Zaključak

Zaključci ovog istraživanja izdvojeni su zasebno za tri glavna dijela disertacije: 1) Određivanje visokofrekventnog atenuacijskog parametra kapa (κ) u Hrvatskoj, 2) Analiza utjecaja lokalnih uvjeta tla na amplifikaciju seizmičkoga površinskoga gibanja u Hrvatskoj pomoću EQL–RVT metode, i 3) Empirijski nelinearni amplifikacijski model za Hrvatsku.

7.1. Određivanje visokofrekventnog atenuacijskog parametra kapa (κ) u Hrvatskoj

- Visokofrekventni atenuacijski parametar kapa (κ) i pripadna lokalna atenuacija κ_0 pomoću metode Andersona i Hough (1984) određeni su za odabrane seizmološke postaje u Hrvatskoj na temelju zapisa potresa u razdoblju 2002.–2016. magnituda $3.0 \leq M_L \leq 5.7$, epicentralnih udaljenosti $R_e \leq 150$ km te dubina žarišta $h < 30$ km.

- Parametar lokalne atenuacije κ_0 određen je iz linearne ovisnosti $\kappa-R_e$ za epicentralne udaljenosti $R_e = 0$ km za svaku postaju i komponente (κ_{hor} i κ_{ver}) parametra κ. Nezanemarive individualne pogreške epicentralnih udaljenosti (R_e) mogu utjecati na primjenljivost obične linearne regresije najmanjih kvadrata, pa tako i na konačnu vrijednost κ_0 i nagiba κ_R. Uzimajući u obzir standardne pogreške R_e i κ u ortogonalnoj regresiji (York i sur. 2004), pokazalo se da su razlike manje od 5 % u odnosu na standardnu linearnu regresiju za pogreške u R_e od 2–5 km, dok razlike mogu biti znatne ako su pogreške kod R_e veće i ako su pogreške tih dviju varijabli jako korelirane, te se preporuča koristiti ortogonalnu regresiju u takvim slučajevima.

- Usporedbom modela za κ_{hor} i κ_{ver} utvrđeno je da su opažene razlike između $\kappa_0^{ver}/\kappa_0^{hor}$ posljedica lokalnih utjecaja tla, dok sličnosti u vrijednostima κ_R^{ver} i κ_R^{hor} dolaze od doprinosa regionalne atenuacije.

- Za postaje na čvrstim stijenama ($V_{S30} \geq 1100$ m/s) lokalna atenuacija je manja ($\kappa_0 \leq 0.025\ s$) nego za postaje na mekšim stijenama ($V_{S30} = 760-1100$ m/s, $\kappa_0 > 0.025\ s$) te su vrijednosti usporedive s globalnim korelacijama κ_0-V_{S30} za čvrste stijene.

- Raspršenje $\kappa-M_L$ je dosta veliko i može se zaključiti da je doprinos izvora na vrijednost κ zanemariv, iako s obzirom na nedostatak podataka na manjim

epicentralnim udaljenostima, ne može se skroz isključiti potencijalni doprinos izvora na κ.

- S obzirom na veliko raspršenje grupa unutar prozora azimuta od 30° u ovisnosti κ o R_e, može se zaključiti da geografska orijentacija epicentara ne utječe na konačne vrijednosti κ i pripadne lokalne atenuacije κ_0.

- Regionalne promjene individualnih vrijednosti κ oko svake postaje promatrane su preko njihovih prostornih raspodjela. Najniže κ vrijednosti prostorno su raspoređene oko same postaje unutar nekoliko kilometara gdje je doprinos lokalne atenuacije κ_0 najveći. Postupno povećanje s udaljenošću od postaje potvrđuje da su propagacijski efekti izraženi preko nagiba linearne regresije κ_R dominantni te opisuju doprinos regionalne atenuacije na većim udaljenostima. Opažena odstupanja prostornih raspodjela parametra κ na pojedinim postajama ukazuju da osim izotropne lokalne i regionalne atenuacije, efekti anizotropije atenuacije zbog različitih uzroka (npr. preferencijske orijentacije pukotina pod utjecajem lokalnih i regionalnih polja napetosti te usmjeravanja valnog polja duž geoloških struktura (valovodi) te atenuacija unutar rasjednih zona) igraju važnu ulogu u prostornoj raspodjeli κ oko samih postaja.

- Rezultati dva nezavisna atenuacijska istraživanja – frekvencijski ovisnog $Q(f)$ određen za atenuaciju koda valova u Dinaridima (Dasović 2015a; Dasović i sur. 2012, 2013, 2015b) i frekvencijski neovisan $Q_{est}(\kappa_R)$ određen iz nagiba linearne regresije κ_R za visokofrekventni dio spektra (10–25 Hz) – su uspoređeni kako bi se provjerio regionalni doprinos atenuacije κ_R u $\kappa{-}R_e$ modelu. Opažena odstupanja između dva pristupa uglavnom su unutar intervala pouzdanosti pojedinih mjerenja, te se mogu pripisati različitim osnovnim pretpostavkama i postupcima njihova određivanja, kao i kompleksnostima i varijabilnostima atenuacijskih doprinosa na realnim stazama valova (npr. Anderson i Hough 1984; Edwards i sur. 2011; Gentili i Franceschina 2011; Ktenidou i sur. 2015; Perron i sur. 2017).

- Horizontalne vrijednosti lokalne atenuacije κ_0^{hor} uzete su kao reprezentativne vrijednosti lokalne atenuacije κ_0 u okolici seizmoloških postaja u Hrvatskoj i za definiranje visokofrekventnog oblika FAS-a ulaznog gibanja u EQL–RVT analizi utjecaja lokalnih uvjeta tla na amplifikaciju seizmičkoga površinskoga gibanja

- Parametri κ i κ_0 određeni po prvi put za seizmološke postaje u Hrvatskoj i mogu se koristiti u budućim istraživanjima vezano uz razvoj atenuacijskih relacija (GMPE), kao i za potrebe EQL–RVT analize seizmičkog odziva lokalnoga tla.

7.2. Analiza utjecaja lokalnih uvjeta tla na amplifikaciju seizmičkoga površinskoga gibanja u Hrvatskoj pomoću EQL–RVT metode

- Jednodimenzionalna (1-D) ekvivalentno-linearna (EQL) analiza seizmičkoga odziva lokalnoga tla na temelju RVT metode na različitim izmjerenim lokalnim profilima tla kategoriziranim u sedam kategorija V_{S30}, korištena je za analizu utjecaja lokalnih uvjeta tla na amplifikaciju seizmičkoga površinskoga gibanja u Hrvatskoj.

- Potresni scenariji definirani su na temelju određenih kombinacija lokalnih i regionalnih seizmoloških parametara za magnitude potresa između $M_L = 5.0$ i $M_L = 7.1$ i epicentralnih udaljenosti između 7 i 30 km kako bi se definirao FAS ulaznog gibanja u RVT metodi za zadanu vršnu akceleraciju PGA_{ROCK} u rasponu od 0.03 g do 0.37 g. Manje epicentralne udaljenosti su odabrane kako bi se definirao visokofrekventni dio FAS-a opisan preko lokalne atenuacije κ_0 za bliske potrese.

- Rezultati 1-D EQL analize seizmičkoga odziva lokalnoga tla pomoću RVT metode prikazani su u obliku 5 % prigušenog akceleracijskog spektra odziva na površini (RSS) i amplifikacijskog faktora $AF(T)$. Spektar odziva prikazuje odziv sustava s jednim stupnjem slobode za spektralne periode na kojima se može očekivati najveća akceleracija za određeno ulazno potresno gibanje. Vrijednost ulaznog gibanja PGA_{ROCK} definirana je za spektralnu akceleraciju Sa nultog perioda u spektru ulaznog odziva (RSB).

- Za pobudna gibanja manje amplitude ($PGA_{ROCK} < 0.1$ g), gibanje je najviše amplificirano u gornjim mekim slojevima tla, i vrijednost AF-a je najveća na vlastitom (ili rezonantnom) periodu tla, pogotovo za tla s manjim vrijednostima V_{S30} i debelim aluvijalnim slojevima iznad osnovne stijene.

- Za jača pobudna gibanja ($PGA_{ROCK} > 0.1$ g), tla s malim vrijednostima $V_{S10}, V_{S20},$ i V_{S30} se ponašaju nelinearno, pri čemu se zbog nelinearnosti AF drastično smanjuje ispod $AF < 1$ na kratkim spektralnim periodima (uključujući $AF@PGA$), dok na vlastitom periodu dolazi do pomaka vrha $AF@PP$ prema većim spektralnim periodima.

- Kod čvrstih tala s većim iznosima $V_{S10}, V_{S20},$ i V_{S30}, $AF@PGA$ i $AF@PP$ su uravnoteženi kroz cijeli raspon spektralnih perioda, i ne pokazuju ovisnost o PGA_{ROCK}, pogotovo iznad 0.10 s. Opažene manje amplifikacije $AF@PGA$ i $AF@PP$

za čvrsta tla i stijene s $V_{S30} > 560$ m/s kod kraćih spektralnih perioda (< 0.20 s), rezultat su interakcije plitke osnovne stijene i mekih površinskih slojeva tla.

- Pokazalo se da za male i velike vrijednosti PGA_{ROCK} tj. slabe ili jake potresne scenarije, $AF(T)$ znatno varira kao funkcija spektralnog perioda s obzirom na vrstu lokalnoga tla $(V_{S10}, V_{S20}, V_{S30})$. Linearno ili nelinearno ponašanje amplifikacijskih faktora ovisno o spektralnom periodu za određenu vrstu građevine i seizmičko gibanje na osnovnoj stijeni PGA_{ROCK} važno je kod projektiranja protupotresnih građevina kako bi se potencijalno izbjegla rezonancija tlo–građevina ili za protupotresnu rekonstrukciju postojećih građevina za buduće potrese.

7.3. Empirijski nelinearni amplifikacijski model za Hrvatsku

- Predloženi nelinearni amplifikacijski model za Hrvatsku (izraz 6.5) manjim je dijelom izmijenjen u odnosu na novije AF modele (Choi i Stewart 2005; Sandikkaya i sur. 2013; Kamai i sur. 2014) iz nekoliko razloga: a) broj zapisa akceleracija uslijed jakih potresa za Hrvatsku je vrlo malen, b) lokalni profili tla $(160 < V_{S30} < 1389$ m/s) za Hrvatsku su izmjereni na temelju geofizičkih istraživanja te predstavljaju stvarne V_{S30} modele, i c) raspon ulaznih gibanja $0.03 \leq PGA_{ROCK} \leq 0.37$ g za Hrvatsku je različit u odnosu na druge modele. U predloženi model dodan je član „0.1 g" kao prijelazna točka između linearnog i nelinearnog ponašanja AF s obzirom na PGA_{ROCK}.

- Ponašanje AF je slično kod slabijih ulaznih gibanja do $PGA_{ROCK} = 0.1$ g i predstavlja linearni odziv tla. Povećanjem PGA_{ROCK} na iznose veće od 0.1 g, vrijednosti AF počinju značajno opadati zbog nelinearnosti tla na kraćim periodima, pogotovo kod tla s manjim vrijednostima V_{S30} (mekanija tla). Opažena nelinearnost AF kod mekanijih tala je izražena na kratkim i srednjim spektralnim periodima kao značajno opadanje AF-a, dok na rezonantnom periodu s povećanjem PGA_{ROCK} dolazi do pomaka maksimuma AF prema većim periodima.

- Negativne vrijednosti regresijskih koeficijenata $b_1(T)$ i $b_2(T)$ na kraćim periodima opisuju opadanje AF kod mekanijih tala (manje vrijednosti V_{S30}). Kod čvrstih tala s većim vrijednostima V_{S30}, koeficijenti $b_1(T)$ i $b_2(T)$ su manji i približavaju se nuli pa je nelinearnost zanemariva.

- Predloženi nelinearni amplifikacijski modeli za lokalne kategorije V_{S30} evaluirani su usporedbom predviđenih AF za Hrvatsku s amplifikacijskim faktorima iz Eurokoda 8 i najnovijim AF-modelima koje su objavili Sandikkaya i sur. (2013) i Kamai i sur. (2014).

- Za srednja do čvrsta tla i mekanije stijene (200 m/s $\leq V_{S30} < 560$ m/s) predloženi model AF za Hrvatsku usporediv je s novijim AF-modelima. Opažene razlike mogu se pripisati različitim definicijama ekvivalentno-linearnih svojstava tla preko krivulja modula smicanja i prigušenja, razvoju AF-modela na temelju empirijske baze akceleracija jakih potresa ili razlike između izmjerenih i generiranih modela tla.

- Za stijene (560 m/s $\leq V_{S30} < 1100$ m/s) ponašanje modela AF za Hrvatsku je linearno i neovisno o PGA_{ROCK}. Kod srednjih do duljih perioda (> 0.4 s) sva tri modela pokazuju očekivano ponašanje, $AF \cong 1$. Kod nižih perioda (< 0.3 s), AF model za Hrvatsku predviđa značajno veću amplifikaciju u odnosu na rezultate Sandikkaye i sur. (2013) i Kamaia i sur. (2014). Kod kraćih perioda i za pobudna gibanja male amplitude, opažene amplifikacije rezultat su razlike u impedanciji između plitke osnovne stijene i mekih slojeva tla.

- Za mekana tla (200 m/s $< V_{S30}$) sva tri modela pokazuju nelinearno ponašanje ($AF < 1$) ovisno o PGA_{ROCK} kod kratkih perioda, dok kod dugih perioda postoji razlika u AF-u između ta tri modela. Neodređenost kod sva tri AF modela postoji zbog manjka mekanih profila tla, odabira dinamičkih svojstava tla (krivulje modula smicanja i prigušenja) te u konačnici osjetljivosti samih metoda analize odziva tla za linearno i nelinearno ponašanje uslijed jakih ulaznih gibanja.

- Amplifikacijski faktor u normi Eurokod 8 predviđa za određene kategorije tla nepriličan nelinearni odziv tla za jača seizmička gibanja na temelju slabe ovisnosti AF o periodu (Sandikkaya i sur. 2013, 2018). U ovom je istraživanju utvrđeno da je predloženi AF model za Hrvatsku periodno ovisan te pokazuje znatne amplifikacije u odnosu na AF u EC8.

- Definiranje realnih profila tla s određenim lokalnim parametrima tla (V_{S30}, dubina osnovne stijene, osnovni period tla, vrsta slojeva tla) vrlo je važno u analizi seizmičkog odziva i ti parametri trebali bi se uvesti u nelinearne amplifikacijske modele. To je posebno važno jer amplifikacijski modeli ovisni samo o jednom parametru V_{S30} lokalnog tla, za koji postoji mnogo nepouzdanosti, mogu navesti na krive zaključke.

7.4. Buduća istraživanja

Istraživanje je pokazalo da je unatoč tome što postoji nedostatak zapisa potresa na manjim epicentralnim udaljenostima ovisnost κ o R_e vidljiva na svim postajama. Novi podaci o iznosima κ mogu pomoći da se riješe nedoumice i izvedu konkretni zaključci oko usporedbe κ_{hor} i κ_{ver} i veze lokalnih i regionalnih varijacija κ s obzirom na geološku građu promatranih područja. Također, parametar κ može se odrediti iz FAS-a pomaka i usporediti s vrijednostima κ iz AH84 metode, čime se navedeni problem malog broja podataka za neke postaje može djelomično riješiti. I konačno, opažene razlike između dva atenuacijska pristupa $Q(f)$ i $Q_{est}(\kappa_R)$ moći će riješiti usporedbom dobivenih vrijednosti κ_{AH} iz ovog istraživanja i budućih istraživanja κ_{coda} (i Q_C) kao što su utvrdili neki autori (npr. Mayor i sur. 2018).

Predloženi nelinearni amplifikacijski model za Hrvatsku kao funkcija lokalnih uvjeta tla izraženih preko parametra V_{S30} i vršnih akceleracija PGA_{ROCK} može predstavljati alternativu klasičnoj EQL analizi seizmičkoga odziva lokalnoga tla. Treba, međutim, biti oprezan, pogotovo kod mekanih tala u kojima dominiraju nelinearni efekti u slučaju jakih potresnih gibanja. Buduća istraživanja potrebno je provesti za što veći raspon amplituda pobudnih gibanja (PGA_{ROCK}), te na većem broju lokalnih profila za EQL–RVT analizu, čime bi se broj AF-a za svaku kategoriju V_{S30} znatno povećao. Time bi i predloženi nelinearni AF model za Hrvatsku bio statistički stabilniji za korištenje pri razvoju budućih atenuacijskih relacija predviđanja gibanja tla za Hrvatsku (ili ažuriranje postojećih) na temelju novih akcelerograma i ažuriranog kataloga potresa uzimajući u obzir atenuacijske efekte ($Q(f)$ i κ_0), kao i utjecaj lokalnoga tla. Također je iznimno važno da se poveća mreža akcelerometara kako bi se zapisali akcelerogrami budućih jakih potresa. Zapisi jakih potresa su *conditio sine qua non* kvalitetno izvedenih seizmoloških parametara potrebnih za stohastičko modeliranje i u konačnici za izvod atenuacijskih relacija za predviđanje gibanja tla kao i određivanje visokofrekventnog atenuacijskog parametra κ za jake potrese.

References

Abrahamson, N.A., Silva, W.J., 1997. Empirical response spectral attenuation relationships for shallow crustal earthquakes. Seismological Research Letters 68, 94–127. Doi:10.1785/gssrl.68.1.94

Abrahamson, N., Silva, W., 2008. Summary of the Abrahamson & Silva NGA ground-motion relations. Earthq. Spectra 24, 67–97. Doi:10.1193/1.2924360

Allmann, B.P., Shearer, P.M., 2009. Global variations of stress drop for moderate to large earthquakes. Journal of Geophysical Research: Solid Earth 114. Doi:10.1029/2008JB005821

Aki, K., Chouet, B., 1975. Origin of coda waves: Source, attenuation, and scattering effects. Journal of Geophysical Research 80, 3322–3342. Doi:10.1029/JB080i023p03322

Aki, K., Richards, P.G., 2009. Quantitative seismology, 2nd ed, University Science Books. Doi:10.1016/S0065-230X(09)04001-9

Akkar, S., Bommer, J.J., 2010. Empirical Equations for the Prediction of PGA, PGV, and Spectral Accelerations in Europe, the Mediterranean Region, and the Middle East. Seismological Research Letters 81, 195–206. Doi:10.1785/gssrl.81.2.195

Akkar, S., Sandikkaya, M.A., Bommer, J.J., 2014. Empirical ground-motion models for point- and extended-source crustal earthquake scenarios in Europe and the Middle East. Bulletin of Earthquake Engineering 12, 359–387. Doi:10.1007/s10518-013-9461-4

Ambraseys, N.N., 1995. The prediction of earthquake peak ground acceleration in Europe. Earthquake Engineering & Structural Dynamics 24, 467–490. Doi:10.1002/eqe.4290240402

Anbazhagan, P., Sitharam, T.G., Vipin, K.S., 2009. Site classification and estimation of surface level seismic hazard using geophysical data and probabilistic approach. Journal of Applied Geophysics 68, 219–230. Doi:10.1016/j.jappgeo.2008.11.001

Anbazhagan, P., Neaz Sheikh, M., Parihar, A., 2013. Technical Paper : influence of rock depth on seismic site classification for shallow bedrock regions. Natural Hazards Review 14, 108–121. Doi:10.1061/(ASCE)NH.1527-6996.0000088.

Anderson, J.G., Hough, S.E., 1984. A model for the shape of the Fourier amplitude spectrum of acceleration at high frequencies. Bulletin of the Seismological Society of America 74, 1969–1993.

Atkinson, G.M., Boore, D.M., 1995. Ground-motion relations for eastern north America. Bulletin of the Seismological Society of America 85, 17–30. Doi:10.1785/0120050245

Atkinson, G.M., Boore, D.M., 2006. Earthquake ground-motion prediction equations for eastern North America. Bulletin of the Seismological Society of America 96, 2181–2205. Doi:10.1785/0120050245

Atkinson, G.M., Silva, W., 1997. An empirical study of earthquake source spectra for California earthquakes. Bulletin of the Seismological Society of America 87, 97–113.

Bardet, J.P., Ichii, K., Lin, C.H. 2000. EERA: A Computer program for Equivalent-linear Earthquake Site Response Analysis of Layered Soil Deposits. University of Southern California, Los Angeles (available at: http://www.ce.memphis.edu/7137/eera.htm)

Barton, N., 2007. Rock quality, seismic velocity, attenuation and anisotropy. 1st ed. Taylor & Francis Group, London

Beresnev, I., Wen, K., 1996. Nonlinear Soil Response-A Reality ? Bulletin of the Seismological Society of America 86, 1964–1978. Doi:10.1061/(ASCE)0733-9410(1996)122:9(725)

Biasi G.P., Smith K. D. 2001. Site effects for seismic monitoring stations in the vicinity of Yucca Mountain, Nevada, MOL20011204.0045, a report prepared for the US DOE/University and Community College System of Nevada (UCCSN) Cooperative Agreement.

Bindi, D., Massa, M., Luzi, L., Ameri, G., Pacor, F., Puglia, R., Augliera, P., 2014. Pan-European ground-motion prediction equations for the average horizontal component of PGA, PGV, and 5%-damped PSA at spectral periods up to 3.0 s using the RESORCE dataset. Bulletin of Earthquake Engineering 12, 391–430. doi:10.1007/s10518-013-9525-5

Biro, Y., and Renault, P., 2012. Importance and impact of host-to-target conversions for ground motion prediction equations in PSHA, in 15th World Conference on Earthquake Engineering, Lisbon, Portugal, 24–28 September 2012.

Bolisetti, C., Whittaker, A.S., Mason, H.B., Almufti, I., Willford, M., 2014. Equivalent linear and nonlinear site response analysis for design and risk assessment of safety-related nuclear structures. Nuclear Engineering and Design 275, 107–121. Doi:10.1016/j.nucengdes.2014.04.033

Bommer, J.J., Akkar, S., 2012. Consistent source-to-site distance metrics in ground-motion prediction equations and seismic source models for PSHA. Earthquake Spectra 28, 1–15. Doi:10.1193/1.3672994

Boore, D.M., 1983. Stochastic simulation of high-frequency ground motions based on seismological models of the radiated spectra. Bulletin of the Seismological Society of America 73, 1865–1894.

Boore, D.M., 2003. Simulation of Ground Motion Using the Stochastic Method. Pure and Applied Geophysics. 160: 635–676. Doi:10.1007/PL00012553

Boore, D.M., 2004. Can site response be predicted? Journal of Earthquake Engineering 8, 1–41. Doi:10.1080/13632460409350520

Boore, D.M., 2016. Determining generic velocity and density models for crustal amplification calculations, with an update of the Boore and Joyner (1997) generic site amplification for Vs(Z)=760 m/s. Bulletin of the Seismological Society of America. Doi:10.1785/0120150229

Boore, D.M., Atkinson, G.M., 2008. Ground-motion prediction equations for the average horizontal component of PGA, PGV, and 5%-damped PSA at spectral periods between 0.01 s and 10.0 s. Earthquake Spectra 24, 99–138. Doi:10.1193/1.2830434

Boore, D.M., Boatwright, J., 1984. Average body-wave radiation coefficients. Bulletin of the Seismological Society of America 74, 1615–1621.

Boore D.M., Thompson E.M., 2012. Empirical Improvements for Estimating Earthquake Response Spectra with Random-Vibration Theory. Bulletin of the Seismological Society of America 102 (2), 761-772.

Boore D.M., Thompson E.M., 2015. Revisions to some parameters used in stochastic-method simulations of ground motion. Bulletin of the Seismological Society of America 105 (2A), 1029-1041.

Boore, D.M., Joyner, W.B., 1984. A note on the use of random vibration theory to predict peak amplitudes of transient signals. Bulletin of the Seismological Society of America 74, 2035–2039.

Boore, D.M., Joyner, W.B., 1997. Site amplifications for generic rock sites. Bulletin of the Seismological Society of America 87, 327–341.

Boore, D.M., Joyner, W.B., Fumal, T.E., 1997. Equations for Estimating Horizontal Response Spectra and Peak Acceleration from Western North American Earthquakes: A Summary of Recent Work. Seismological Research Letters 68, 128–153. Doi:10.1785/gssrl.76.3.368

Boore, D.M., Stewart, J.P., Seyhan, E., Atkinson, G.M., 2014. NGA-West 2 Equations for Predicting PGA , PGV , and 5 % Damped PSA for Shallow Crustal Earthquakes. Earthquake Spectra 30 (3), 1–38. Doi:10.1193/070113EQS184M

Bozorgnia, Y., Abrahamson, N.A., Al Atik, L., Ancheta, T.D., Atkinson, G.M., Baker, J.W., Baltay, A., Boore, D.M., Campbell, K.W., Chiou, B.S.J., Darragh, R., Day, S., Donahue,

J., Graves, R.W., Gregor, N., Hanks, T., Idriss, I.M., Kamai, R., Kishida, T., Kottke, A., Mahin, S.A., Rezaeian, S., Rowshandel, B., Seyhan, E., Shahi, S., Shantz, T., Silva, W., Spudich, P., Stewart, J.P., Watson-Lamprey, J., Wooddell, K., Youngs, R., 2014. NGA-West2 research project. Earthquake Spectra 30, 973–987. doi:10.1193/072113EQS209M

Brune, J.N., 1970. Tectonic stress and the spectra of seismic shear waves from earthquakes. Journal of Geophysical Research 75, 4997–5009. Doi:10.1029/JB075i026p04997

Building Seismic Safety Council (BSSC). 2009. NEHRP Recommended Seismic Provisions For New Buildings and Other Structures: Part 1, Provisions, Federal Emergency Management Agency (P-750), Washington, D.C.

Campbell, K. W., 2003. Prediction of strong ground motion using the hybrid empirical method and its use in the development of ground motion (attenuation) relations in eastern North America, Bull. Seismol. Soc. Am. 93, 1012–1033.

Campbell, K.W., Bozorgnia, Y., 2008. NGA ground motion model for the geometric mean horizontal component of PGA, PGV, PGD and 5% damped linear elastic response spectra for periods ranging from 0.01 to 10 s. Earthquake Spectra 24, 139–171. Doi:10.1193/1.2857546

Campbell, K.W., Hashash, Y. M. A., Kim, B., Kottke, A. R., Rathje, E. M., Silva, W. J., Stewarr, J. P., 2014. Reference-Rock Site Conditions for Central and Eastern North America : Part II - Attenuation (Kappa) Definition. Peer Report 2014/11, (August 2014).

Cartwright, D.E., Longuet-Higgins, M.S., 1956. The Statistical Distribution of the Maxima of a Random Function. Proc. R. Soc. A Math. Phys. Eng. Sci. 237, 212–232. Doi:10.1098/rspa.1956.0173

Castro, R. R., Trojani, L., Monachesi, G., Mucciarelli, M., Cattaneo, M., 2000. The spectral decay parameter κ in the region of Umbria-Marche, Italy. J. Geophys. Res. 105(B10), 23811–23823, Doi:10.1029/2000JB900236.

Celebi, M., Bazzurro, P., Chiaraluce, L., Clemente, P., Decanini, L., Desortis, A., Ellsworth, W., Gorini, A., Kalkan, E., Marcucci, S., Milana, G., Mollaioli, F., Olivieri, M., Paolucci, R., Rinaldis, D., Rovelli, A., Sabetta, F., Stephens, C., 2010. Recorded motions of the 6 April 2009 Mw 6.3 L'Aquila, Italy, earthquake and implications for building structural damage: Overview. Earthquake Spectra 26, 651–684. Doi:10.1193/1.3450317

Chandler, a. M., Lam, N.T.K., Tsang, H.H., Sheikh, M.N., 2005. Estimation of near-surface attenuation in bedrock for analysis of intraplate seismic hazard. Journal of Seismology and Earthquake Engineering 7, 159–173.

Chi-Miranda, M.A., Montejo, L.A., 2017. A numerical comparison of random vibration theory and time histories based methods for equivalent-linear site response analyses. International Journal of Geo-Engineering 8, 22. Doi:10.1186/s40703-017-0059-6

Chiou, B. S.J., Youngs, R., 2008. An NGA model for the average horizontal component of peak ground motion and response spectra, Earthq. Spectra 24, 173–215. Doi: 10.1193/1.2894832

Chiou, B.S.J., Youngs, R.R., 2014. Update of the Chiou and Youngs NGA model for the average horizontal component of peak ground motion and response spectra. Earthquake Spectra 30, 1117–1153. doi:10.1193/072813EQS219M

Choi, Y., Stewart, J.P., 2005. Nonlinear site amplification as function of 30 m shear wave velocity. Earthq. Spectra 21, 1–30. Doi:10.1193/1.1856535

Cormier, V.F., 1982. The Effect of Attenuation on Seismic Body Waves. Bulletin of the Seismological Society of America 72, 169–200.

Croatian Geological Survey – Hrvatski geološki institut, 2009a. Geological Map of Republic of the Republic of Croatia at the 1:300,000 scale.. Available at: http://webgis.hgi-cgs.hr/gk300/default.aspx

Croatian Geological Survey – Hrvatski geološki institute, 2009b. Explanatory notes of the Geological Map of the Republic of Croatia 1:300,000. p.147

Dainty, A.M., 1981. A scattering model to explain seismic Q observations in the lithosphere between 1 and 30 Hz. Geophys. Res. Lett. 8, 1126–1128. Doi: 10.1029/GL008i011p01126

Darendeli M., 2001. Development of a New Family of Normalized Modulus Reduction and Material Damping Curves (Ph.D. dissertation). University of Texas at Austin, USA

Dasović, I., 2015a. Attenuation of seismic waves beneath the Dinarides. (PhD dissertation). University of Zagreb, Faculty of Science. Croatia

Dasović, I., Herak, M., Herak, D., 2012. Attenuation of coda waves in the contact zone between the Dinarides and the Adriatic Microplate. Studia Geophysica et Geodaetica 56, 231–247. Doi:10.1007/s11200-010-0077-8

Dasović, I., Herak, M., Herak, D., 2013. Coda-Q and its lapse time dependence analysis in the interaction zone of the Dinarides, the Alps and the Pannonian basin. Physics and Chemistry of the Earth 63, 47–54. Doi:10.1016/j.pce.2013.03.001

Dasović, I., Ruščić, M., Herak, D., Herak, M., 2015b. Attenuation of high-frequency body waves in the crust of the Central External Dinarides. Journal of Seismology 19, 849–860. Doi:10.1007/s10950-015-9498-8

Delavaud, E., Cotton, F., Akkar, S., Scherbaum, F., Danciu, L., Beauval, C., Drouet, S., Douglas, J., Basili, R., Sandikkaya, M.A., Segou, M., Faccioli, E., Theodoulidis, N., 2012. Toward a ground-motion logic tree for probabilistic seismic hazard assessment in Europe. Journal of Seismology 16, 451–473. Doi:10.1007/s10950-012-9281-z

Del Monaco, F., Tallini, M., De Rose, C., Durante, F., 2013. HVNSR survey in historical downtown L'Aquila (central Italy): Site resonance properties vs. subsoil model. Engineering Geology 158, 34–47. Doi:10.1016/j.enggeo.2013.03.008

Dhakal, R.P., Lin, S.L., Loye, A.K., Evans S.J., 2013. Seismic design spectra for different soil classes. Bulletin-New Zealand Society for Earthquake Engineering 46(2): 79-87.

Di Giacomo, D., Gallipoli, M.R., Mucciarelli, M., Parolai, S., Richwalski, S.M., 2005. Analysis and modelling of HVSR in the presence of a velocity inversion: The case of Venosa, Italy. Bulletin of the Seismological Society of America 95, 2364–2372. Doi:10.1785/0120040242

Douglas, J., 2017. Ground motion prediction equations 1964–2017. http://peer.berkeley.edu/globalgmpe/

Douglas, J., Gehl, P., Bonilla, L.F., Ǵlis, C., 2010. A κ model for mainland France. Pure and Applied Geophysics 167, 1303–1315. Doi:10.1007/s00024-010-0146-5

Drouet, S., Cotton, F., Guéguen, P., 2010. VS30, κ, regional attenuation and Mw from accelerograms: Application to magnitude 3-5 French earthquakes. Geophysical Journal International 182, 880–898. Doi:10.1111/j.1365-246X.2010.04626.x

Duni, L., Kuka, S., Kuka, N., 2010. Local relations for converting M L to M W in Southern-Western Balkan region. Acta Geodaetica et Geophysica Hungarica 45, 317–323. Doi:10.1556/AGeod.45.2010.3.6

Edwards, B., Fäh, D., 2013. Measurements of stress parameter and site attenuation from recordings of moderate to large earthquakes in Europe and the Middle East. Geophysical Journal International 194, 1190–1202. doi:10.1093/gji/ggt158

Edwards, B., Fäh, D., Giardini, D., 2011. Attenuation of seismic shear wave energy in Switzerland. Geophysical Journal International 185, 967–984. Doi:10.1111/j.1365-246X.2011.04987.x

Electric Power Research Institute (EPRI), 1993. Guidelines for determining desing Basis Ground Motions. Technical Report EPRI TR-102293. Palo Alto, California.

Elgamal, A., He, L., 2004. Vertical Earthquake Ground Motion Records: An Overview, Journal of Earthquake Engineering, 8 (5), 663-697.

Elnashai, A.S., Di Sarno, L., 2008. Fundamentals of Earthquake Engineering, Fundamentals of Earthquake Engineering. John Wiley and Sons. Doi:10.1002/9780470024867

Eurocode 8 (EC8), 2004. Design of structures for earthquake resistance - Part 1 : General rules, seismic actions and rules for buildings, European Committee for Standardization, Brussels. Doi:10.3403/0324437

Futterman, W.I., 1962. Dispersive body waves. Journal of Geophysical Research 67, 5279. Doi:10.1029/JZ067i013p05279

Gallipoli, M.R., Mucciarelli, M., Šket-Motnikar, B., Zupanćić, P., Gosar, A., Prevolnik, S., Herak, M., Stipčević, J., Herak, D., Milutinović, Z., Olumćeva, T., 2010. Empirical estimates of dynamic parameters on a large set of European buildings. Bulletin of Earthquake Engineering 8, 593–607. Doi:10.1007/s10518-009-9133-6

Gentili, S., Franceschina, G., 2011. High frequency attenuation of shear waves in the southeastern Alps and northern Dinarides. Geophysical Journal International 185, 1393–1416. Doi:10.1111/j.1365-246X.2011.05016.x

Gosar, A., 2007. Microtremor HVSR study for assessing site effects in the Bovec basin (NW Slovenia) related to 1998 Mw5.6 and 2004 Mw5.2 earthquakes. Engineering Geology 91, 178–193. Doi:10.1016/j.enggeo.2007.01.008

Gosar, A., Martinec, M., 2009. Microtremor HVSR study of site effects in the Ilirska Bistrica town area (S.Slovenia). Journal of Earthquake Engineering 30, 13–50. Doi:10.1080/13632460802212956

Gosar, A., Rošer, J., Šket-Mošnikar, B., Zupančić, P., 2010. Microtremor study of site effects and soil-structure resonance in the city of Ljubljana (central Slovenia). Bulletin of Earthquake Engineering 8, 571–592. Doi:10.1007/s10518-009-9113-x

Giampiccolo, E., Gresta, S., Rasconà, F., 2004. Intrinsic and scattering attenuation from observed seismic codas in Southeastern Sicily (Italy). Physics of the Earth and Planetary Interiors 145, 55–66. Doi:10.1016/j.pepi.2004.02.004

Gülerce, Z., Kargioğlu, B., Abrahamson, N.A., 2016. Turkey-adjusted NGA-W1 horizontal ground motion prediction models. Earthquake Spectra 32, 75–100. doi:10.1193/022714EQS034M

Handy, M. R., Ustaszewski, K., Kissling, E., 2015. Reconstructing the Alps-Carpathians-Dinarides as a key to understanding switches in the subduction polarity, slab gaps and surface motion. Int. J. Earth Sci. (Geol Rundsch) 104, 1–26. Doi:10.1007/s00531-014-1060-3

Hanks, T.C., 1982. Fmax. Bulletin of the Seismological Society of America 72, 1867–1879.

Hanks, T.C., Kanamori, H., 1979. A moment magnitude scale, in: Journal of Geophysical Research B: Solid Earth. pp. 2348–2350. Doi:10.1029/JB084iB05p02348

Hanks, T.C., McGuire, R.K., 1981. The character of high-frequency strong ground motion. Bulletin of the Seismological Society of America 71, 2071–2095.

Hashash, Y.M.A, Groholski, D.R., Phillips, C.A., Park, D., Musgrove, M., 2011. DEEPSOIL 5.0, user Manual and Tutorial. Champaign, IL:University of Illinois at Urbana-Champaign.

Herak, D., Herak, M., Tomljenović, B., 2009. Seismicity and earthquake focal mechanisms in North-Western Croatia. Tectonophysics 465, 212–220. Doi:10.1016/j.tecto.2008.12.005

Herak, M., 2011a. Overview of recent ambient noise measurements in Croatia in free-field and in buildings. Geofizika, vol. 28, pp. 21-40

Herak, M., Herak, D., Markušić, S., 1996. Revision of the earthquake catalogue and seismicity of Croatia, 1908-1992. Terra Nova. Doi:10.1111/j.1365-3121.1996.tb00728.x

Herak, M., Markušić, S., Ivančić, I., 2001. Attenuation of Peak Horizontal and Vertical Acceleration in the Dinarides Area. Studia geoph. et geod. 45, 383–394.

Herak, M., Allegretti, I., Herak, D., Kuk, K., Kuk, V., Marić, K., Markušić, S., Stipčević, J., 2010. HVSR of ambient noise in Ston (Croatia): Comparison with theoretical spectra and with the damage distribution after the 1996 Ston-Slano earthquake. Bulletin of Earthquake Engineering 8, 483–499. Doi:10.1007/s10518-009-9121-x

Herak, M., Allegretti, I., Herak, D., Ivančić, I., Kuk, V., Marić, K., Markušić, S., Sović, I., 2011b. Seismic hazard map of Croatia for a return period of 475-years (http://seizkarta.gfz.hr/)

Herak, M., Živčić, M., Sović, I., Cecić, I., Dasović, I., Stipčević, J., Herak, D., 2018. Historical Seismicity of the Rijeka Region (Northwest External Dinarides, Croatia)—Part II: The Klana Earthquakes of 1870. Seismological Research Letters 89 (4), 1524-1536. Doi: 10.1785/0220180064

Idriss, I.M., Seed, H.B., 1968. Seismic Response of Horizontal Soil Layers. Journal of the Soil Mechanics and Foundations Division 94, 1003–1034.

Idriss, I. M., Sun, J. I., 1992. Shake91, A Computer Program for Conducting Equivalent Linear Seismic Response Analysis of Horizontally Layered Soil Deposits, Modified based on the original SHAKE program by Schnabel, Lysmer and Seed, 1972 94.

Ivančić, I., Herak, D., Markušić, S., Sović, I., Herak, M., 2006. Seismicity of Croatia in the period 2002-2005. Geofizika 23, 87–103.

Joyner, W.B., Warrick, R.E., Fumal, T.E., 1981. the Effect of Quaternary Alluvium on Strong Ground Motion in the Coyote Lake, California, Earthquake of 1979. Bull. Seismol. Soc. Am. 71, 1333–1349. Doi:10.1007/s13398-014-0173-7.2

Leyton, F., Ruiz, S., Sepúlveda, S.A., Contreras, J.P., Rebolledo, S., Astroza, M., 2013. Microtremors' HVSR and its correlation with surface geology and damage observed after the 2010 Maule earthquake (Mw 8.8) at Talca and Curico, Central Chile. Engineering Geology 161, 26–33. Doi:10.1016/j.enggeo.2013.04.009

Liu, L., Pezeshk, S., 1999. An improvement on the estimation of pseudoresponse spectral velocity using RVT method. Bulletin of the Seismological Society of America 89, 1384–1389.

Lokmer, I., Herak, M., 1999. Anisotropy of P-wave Velocity in the Upper Crust of the Central External Dinarides. Studia Geophysica et Geodaetica 43(4), 345–356. Doi: /10.1023/A:102322691

Kamai, R., Abrahamson, N.A., Silva, W.J., 2014. Nonlinear horizontal site amplification for constraining the NGA-West2 GMPEs. Earthq. Spectra. Doi:10.1193/070113EQS187M

Kilb, D., Biasi, G., Anderson, J., Brune, J., Peng, Z., Vernon, F.L., 2012. A comparison of spectral parameter kappa from small and moderate earthquakes using southern California ANZA seismic network data. Bulletin of the Seismological Society of America 102, 284–300. Doi:10.1785/0120100309

Kottke, A.R., 2010. A Comparison of Seismic Site Response Methods. (Ph.D. dissertation). The University of Texas at Austin.

Kottke, A.R., Rathje, E.M., 2009. Technical Manual for Strata. PEER Report 2008/10. Pacific Earthquake Engineering Research Center College of Engineering University of California, Berkeley. p. 100

Kottke, A.R., Rathje, E.M., 2013. Comparison of time series and random-vibration theory site-response methods. Bull. Seismol. Soc. Am. 103, 2111–2127. Doi:10.1785/0120120254

Ktenidou, O.J., Gélis, C., Bonilla, L.F., 2013. A study on the variability of Kappa (κ) in a Borehole: Implications of the computation process. Bulletin of the Seismological Society of America 103, 1048–1068. Doi:10.1785/0120120093

Ktenidou, O.-J., Cotton, F., Abrahamson, N.A., Anderson, J.G., 2014. Taxonomy of κ: a review of definitions and estimation approaches targeted to applications. Seismological Research Letters 85, 135–146. Doi:10.1785/0220130027

Ktenidou, O.J., Abrahamson, N.A., Drouet, S., Cotton, F., 2015. Understanding the physics of kappa (κ): Insights from a downhole array. Geophysical Journal International 203, 678–691. Doi:10.1093/gji/ggv315

Kramer, S. L., 1996. Geotechnical Earthquake Engineering. 1st ed. Prentice-Hall. New Jersey. p.654

Majstorović, J., Belinić, T., Namjesnik, D., Dasović, I., Herak, D., Herak, M., 2017. Intrinsic and scattering attenuation of high-frequency S-waves in the central part of the External Dinarides. Physics of the Earth and Planetary Interiors 270, 73–83. Doi:10.1016/j.pepi.2017.06.005

Markušić, S., Herak, M., Herak, D., Ivančić, I., 2002. Peak Horizontal-to-Vertical Acceleration Ratio and Local Amplification of Strong Ground Motion. Studia Geophysica et Geodaetica 46, 83. Doi:10.1023/A:1019889600531

Markušić, S., Gülerce, Z., Kuka, N., Duni, L., Ivančić, I., Radovanović, S., Glavatović, B., Milutinović, Z., Akkar, S., Kovačević, S., Mihaljević, J., Šalić, R., 2016. An updated and unified earthquake catalogue for the Western Balkan Region. Bulletin of Earthquake Engineering 14, 321–343. Doi:10.1007/s10518-015-9833-z

Markušić, S., Ivančić, I., Sović, I., 2017. The 1667 Dubrovnik earthquake–some new insights. Studia Geophysica et Geodaetica, 61, 1–14. http://link.springer.com/10.1007/s11200-016-1065-4.

Mayor, J., Bora, S.S., Cotton, F., 2018. Capturing regional variations of hard-rock $\kappa 0$ from coda analysis. Bulletin of the Seismological Society of America 108, 399–408. doi:10.1785/0120170153

McGuire, R.K., Hanks, T.C., 1980. RMS accelerations and spectral amplitudes of strong ground motion during the San Fernando, California earthquake. Bulletin of the Seismological Society of America 70, 1907–1919. Doi:10.1002/bdrb.20340

McGuire, R.K., Becker, A.M., Donovan, N.C., 1984. Spectral estimates of seismic shear waves. Bulletin of the Seismological Society of America 74, 1427–1440.

Menq F.-Y., 2003. Dynamic Properties of Sandy and Gravelly Soils (Ph.D. dissertation). University of Texas, Austin, USA.

Meunier, P., Hovius, N., Haines, J.A., 2008. Topographic site effects and the location of earthquake induced landslides. Earth and Planetary Science Letters 275, 221–232. Doi:10.1016/j.epsl.2008.07.020

Mihaljević, J., Zupančič, P., Kuka, N., Kaluđerović, N., Koçi, R., Markušić, S., Šalić, R., Dushi, E., Begu, E., Duni, L., Živčić, M., Kovačević, S., Ivančić, I., Kovačević, V., Milutinović, Z., Vakilinezhad, M., Fiket, T., Gülerce, Z., 2017. BSHAP seismic source characterization models for the Western Balkan region. Bulletin of Earthquake Engineering 15, 3963–3985. Doi:10.1007/s10518-017-0143-5

Mucciarelli, M., Gallipoli M.R., 2001. A critical review of 10 years of microtremor HVSR technique. Bolletino di geofisica teorica es applicate, vol. 42, n. 3-4, pp. 255-266

Nakamura, Y., 1989. Method for Dynamic Characteristics Estimation of Subsurface using Microtremor on the Ground Surface. Quarterly Report of RTRI (Railway Technical Research Institute) (Japan), 30(1), 25-33.

Ordonez, G. A., 2009. User's manual SHAKE2000: A computer program for the 1-D analysis of geotechnical earthquake engineering problems. GeoMotions, LLC. 258 p. (available at http://www.geomotions.com/Download/SHAKE2000Manual.pdf)

Panzera, F., Lombardo, G., D'Amico, S., Galea, P., 2013. Speedy Techniques to Evaluate Seismic Site Effects in Particular Geomorphologic Conditions: Faults, Cavities, Landslides and Topographic Irregularities (Chapter 5). InTech, 102-138

Paolucci, E., Albarello, D., D'Amico, S., Lunedei, E., Martelli, L., Mucciarelli, M., Pileggi, D., 2015. A large scale ambient vibration survey in the area damaged by May-June 2012 seismic sequence in Emilia Romagna, Italy. Bulletin of Earthquake Engineering 13, 3187–3206. Doi:10.1007/s10518-015-9767-5

Pehlivan, M., Park, D., Sadiq, S., Hashash, Y.M.A., 2017. Seismic site response of shallow sites in moderate seismicity regions. Proceedings of the 19th International Conference on Soil Mechanics and Geotechnical Engineering, Seoul., p.1569-1572

Perron, V., Hollender, F., Bard, P.Y., Gélis, C., Guyonnet-Benaize, C., Hernandez, B., Ktenidou, O.J., 2017. Robustness of kappa (κ) measurement in low-to-moderate seismicity areas: Insight from a site-specific study in provence, France. Bulletin of the Seismological Society of America 107, 2272–2292. Doi:10.1785/0120160374

Pischiutta, M., Rovelli, A., Salvini, F., Di Giulio, G., Ben-Zion, Y., 2013. Directional resonance variations across the pernicana fault, Mt Etna, in relation to brittle deformation fields. Geophysical Journal International 193, 986–996. doi:10.1093/gji/ggt031

Power, M., Chiou, B., Abrahamson, N., Bozorgnia, Y., Shantz, T., Roblee, C., 2008. An overview of the NGA project. Earthquake Spectra 24, 3–21. doi:10.1193/1.2894833

Purvance, M.D., Anderson, J.G., 2003. A comprehensive study of the observed spectral decay in strong-motion accelerations recorded in Guerrero, Mexico. Bulletin of the Seismological Society of America 93, 600–611. Doi:10.1785/0120020065

Rathje, E.M., Ozbey, M.C., 2006. Site-Specific Validation of Random Vibration Theory-Based Seismic Site Response Analysis. J. Geotech. Geoenvironmental Eng. 132, 911–922. Doi:10.1061/_ASCE_1090-0241_2006_132:7_911

Rathje, E.M., Kottke, A.R., Trent, W.L., 2010. Influence of Input Motion and Site Property Variabilities on Seismic Site Response Analysis. Journal of Geotechnical and Geoenvironmental Engineering 136(4), 607–619. Doi:.org/10.1061/(ASCE)GT.1943-5606.0000255

Reiter, L., 1990. Earthquake Hazard Analysis: Issues and insights. Columbia University Press. p.254

Sandikkaya, M.A., Akkar, S., Bard, P.Y., 2013. A nonlinear site-amplification model for the next pan-European ground-motion prediction equations. Bull. Seismol. Soc. Am. 103, 19–32. Doi:10.1785/0120120008

Sandikkaya M. A., Akkar S., Bard, P.Y., 2018. A probabilistic procedure to describe site amplification factors for seismic design codes. Soil Dynamics and Earthquake Engineering. Available online 17 February 2018. Doi: 10.1016/j.soildyn.2018.01.050

Schmid, S.M., Bernoulli, D., Fügenschuh, B., Matenco, L., Schefer, S., Schuster, R., Tischler, M., Ustaszewski, K., 2008. The Alpine-Carpathian-Dinaridic orogenic system: Correlation and evolution of tectonic units. Swiss Journal of Geosciences 101, 139–183. Doi:10.1007/s00015-008-1247-3

Schnabel, P.B., 1973. Effects of local geology and distance from source on earthquake ground motions. (Ph.D. dissertation), University of California, Berkeley

Schnabel, P.B., Lysmer, J., Seed, H.B., 1972. SHAKE: a computer program for earthquake response analysis of horizontally layered sites, Earthquake Engineering Research Center. Doi:U.CB/EERC-72/12.

Seed, H.B., Idriss, I.M., 1983. Ground Motions and Soil Liquefaction During Earthquakes, EERI Monograph, Earthquake Engineering Research Institute, Oakland, CA.

Seed, H.B., Muraka, R., Lysmer, J., Idriss, I.M., 1976. Relationships of maximum acceleration, maximum velocity, distance from source, and local site conditions for moderately strong earthquakes. Bulletin of the Seismological Society of America 66, 1323–1342.

Seed, B.H., Tokimatsu, K., Harder, L.F., Chung, R.M., 1984. Influence of SPT Procedures in Soil Liquefaction Resistance Evaluations. Journal of Geotechnical Engineering 111, 1425–1445. Doi:10.1061/(ASCE)0733-9410(1985)111:12(1425)

Seed, H.B., Wong, R.T., Idriss, I.M., Tokimatsu, K., 1986. Moduli and Damping Factors for Dynamic Analyses of Cohesionless Soils. Journal of Geotechnical Engineering 112, 1016–1032. Doi:10.1061/(ASCE)0733-9410(1986)112:11(1016)

Seht, M.I.V., Wohlenberg, J., 1999. Microtremor Measurements Used to Map Thickness of Soft Sediments. Bulletin of the Seismological Society of America 89, 250–259.

SESAME: Bard, P., Duval, A., Koehler, A., Rao, S., 2004. SESAME H/V User Guidelines, in: Guidelines for the Implementation of the H/V Spectral Ratio Technique on Ambient Vibrations Measurements, Processing and Interpretation. pp. 1–62. Doi: 10.1111/j.1365-246X.2006.03282.x

Silva, W.J., Lee, K., 1987. WES RASCAL code for synthesizing earthquake ground motions, Rep. No. 24. U.S. Army Eng. Waterw. Exp. Stn. 121.

Silva, W.J., Abrahamson, N., Toro, G., Constantino, C., 1997. Description and validation of the stochastic ground motion model, Final report. Brookhaven Natl. Lab. Assoc. Univ. Inc. Upt. 1176.

Silva, W., Darragh, R., Gregor, N., 1999. Reassessment of Site Coefficients and Near-Fault Factors for Building Code Provisions. Technical Report Program Element II: 98-HQGR-1010, 98-NaN-NaN-1, p.116.

Stein, S., Wysession, M., 2003. An Introduction to Seismology, Earthquakes, and Earth Structure. Blackwell Publishing Ltd. P.512

Stanko, D., Markušić, S., Strelec, S., Gazdek, M., 2016. Seismic response and vulnerability of historical Trakošćan Castle using HVSR method. Environ Earth Sci 75: 368. Doi:10.1007/s12665-015-5185-x

Stanko, D., Markušić, S., Strelec, S., Gazdek, M., 2017. HVSR analysis of seismic site effects and soil-structure resonance in Varaždin city (North Croatia). Soil Dynamics and Earthquake Engineering 92, 666–677. Doi:10.1016/j.soildyn.2016.10.022

Strelec, S., Stanko, D., Gazdek, M., 2016. Empirical correlation between the shear-wave velocity and the dynamic probing heavy test: Case study, Varaždin, Croatia. Acta Geotechnica Slovenica 13, 3–15.

Stipčević, J., Tkalčić, H., Herak, M., Markušić, S., Herak, D., 2011. Crustal and uppermost mantle structure beneath the External Dinarides, Croatia, determined from teleseismic receiver functions. Geophysical Journal International 185, 1103–1119. doi:10.1111/j.1365-246X.2011.05004.x

Stur, D. (1871). Das Erdbeben von Klana im Jahre 1870, Jahrbuch des Kaiserlich-Königlichen Geologischen Reichsanstalt, XXI band, Vienna, Austria, 231–264 (in German).

Šalić, R., Sandıkkaya, M.A., Milutinović, Z., Gülerce, Z., Duni, Ll., Kovačević, V., Markušić, S., Mihaljević, J., Kuka, N., Kaludjerović, N., Kotur, N., Krmpotić, S., Kuk, K., and Stanko, D., 2016. BSHAP Project Strong Ground Motion Database and Selection of Suitable Ground Motion Models for the Western Balkan Region, Bulletin of Earthquake Engineering. 15: 1319. Doi: 10.1007/s10518-016-9950-3.

Šumanovac, F., 2012. Osnove geofizičkih istraživanja (Basics of geophysical investigations). Faculty of Mining, Geology and Petroleum Engineering, Zagreb. p.356

Šumanovac, F., Orešković, J., Grad, M. 2009. Crustal structure at the contact of the Dinarides and Pannonian basin based on 2-D seismic and gravity interpretation of the Alp07 profile in the ALP 2002 experiment. Geophysical Journal International,179(1), 615–633. Doi:10.1111/j.1365-246X.2009.04288.x

Tomljenović, B., Csontos, L., Marton, E., Marton, P., 2008. Tectonic evolution of the northwestern Internal Dinarides as constrained by structures and rotation of Medvednica Mountains, North Croatia. Geological Society, London, Special Publications 298, 145–167. Doi:10.1144/SP298.8

Udias, A., Madariaga, R., Bufron, E., 2014. Source Mechanism of Earthquakes: Theory and Practice. Cambridge University Press. p.301

Ustaszewski, K., Schmid, S.M., Fügenschuh, B., Tischler, M., Kissling, E., Spakman, W., 2008. A map-view restoration of the alpine-carpathian-dinaridic system for the early miocene, in: Swiss Journal of Geosciences. doi:10.1007/s00015-008-1288-7

Vanmarcke E.H., 1975. On the distribution of the first-passage time for normal stationary random processes. Journal of Applied Mechanics; 42 (1): 215-220.

Vanmarcke, E.H., Lai, S.-S.P., 1980. Strong-motion duration and RMS amplitude of earthquake records. Bulletin of the Seismological Society of America 70, 1293–1307.

Van Houtte, C., Drouet, S., Cotton, F., 2011. Analysis of the origins of κ (kappa) to compute hard rock to rock adjustment factors for GMPEs. Bulletin of the Seismological Society of America 101, 2926–2941. Doi:10.1785/0120100345

Van Houtte, C., Ktenidou, O.J., Larkin, T., Holden, C., 2014. Hard-site $\kappa 0$ (kappa) calculations for Christchurch, New Zealand, and comparison with local ground-motion prediction models. Bulletin of the Seismological Society of America 104, 1899–1913. Doi:10.1785/0120130271

Vlahović, I., Tišljar, J., Velić, I., Matičec, D., 2005. Evolution of the Adriatic Carbonate Platform: Palaeogeography, main events and depositional dynamics. Palaeogeography, Palaeoclimatology, Palaeoecology 220, 333–360. doi:10.1016/j.palaeo.2005.01.011

Vučetić, M., 1992. Soil Properties and seismic response. 10 World Conf. on Earthquake Engineering, 1199–1204.

Vučetić, M., Dobry, R., 1991. Effect of Soil Plasticity on Cyclic Response. Journal of Geotechnical Engineering 117, 89–107. Doi:10.1061/(ASCE)0733-9410(1991)117:1(89)

Walling, M., Silva, W., Abrahamson, N., Kramer, S.L., 2008. Nonlinear site amplification factors for constraining the NGA models. Earthq. Spectra 24, 243–255. Doi:10.1193/1.2934350

Wang, X., Rathje, E.M., 2016. Influence of peak factors on site amplification from random vibration theory based site-response analysis. Bulletin of the Seismological Society of America 106, 1733–1746. Doi:10.1785/0120150328

Wells, D.L., Coppersmith, K.J., 1994. New Empirical Relationships among Magnitude, Rupture Length, Rupture Width, Rupture Area, and Surface Displacement. Bulletin of the Seismological Society of America 84, 974–1002.

Yenier, E., Atkinson, G.M., 2014. Equivalent point-source modeling of moderate-to-large magnitude earthquakes and associated ground-motion saturation effects. Bulletin of the Seismological Society of America 104, 1458–1478. doi:10.1785/0120130147

York, D., Evenson, N., Martinez, M., Delgado, J., 2004. Unified equations for the slope, intercept, and standard errors of the best straight line. American Journal of Physics 72, 367–375.

Zhao, J.X., Zhang, J., Asano, A., Ohno, Y., Oouchi, T., Takahashi, T., Ogawa, H., Irikura, K., Thio, H.K., Somerville, P.G., Fukushima, Yasuhiro, Fukushima, Yoshimitsu, 2006. Attenuation relations of strong ground motion in Japan using site classification based on predominant period. Bulletin of the Seismological Society of America 96, 898–913. doi:10.1785/0120050122

Curriculum Vitae

DAVOR STANKO

University of Zagreb, Faculty of Geotechnical Engineering, Department of Geotechnics

Hallerova aleja 7, Varaždin, HR-42000

e-mail: davor.stanko@gfv.hr; stankodavor@gmail.com

EDUCATION

2005–2011: Master of Science in Physics (mag.phys) at Department of Physics, Faculty of Science, University of Zagreb

2001–2005: Computer technician at Technical Middle School Čakovec

PROFESSIONAL TRAINING

August/September 2015: Visiting scientist at Department for Risk, Disaster Management and Strategic Planning, Institute of Earthquake Engineering and Engineering Seismology, Skopje, Republic of Macedonia

June 2015: Visiting Ph.D study stay at Middle East Technical University (METU), Civil Engineering Department, Ankara, Turkey

January – July 2011: Master thesis visit (student exchange) at Istituto Nazionale Fisica Nucleare Laboratori Nazionali del Sud INFN LNS, Nuclear Physics Laboratory Catania, Sicily, Italy

WORK EXPERIENCE

2011, January–July: Research student, Istituto Nazionale Fisica Nucleare Laboratori Nazionali del Sud INFN LNS, Nuclear Physics Laboratory Catania, Sicily, Italy

2012–present: Junior researcher - assistant, PhD Student, University of Zagreb, Faculty of Geotechnical Engineering, Varaždin, Croatia

SKILLS

Technical skills: instrumentation for geophysical measurements, ambient noise and vibration measurements, radioactivity measurements (radon in soil, air and buildings)

Computer skills: Windows, Linux, Microsoft Office, Matlab, Sigma Plot, Surfer, Microsoft Visio, Deepsoil, Strata, Geopsy, SeisImager, Grilla

Research skills: analytical solutions to the problems in engineering seismology and earthquake engineering, programming and developing programs for data analysing and processing for joint

Seismic Site Response Analysis modelling based on geophysical and seismic measurements, statistical analysis and modelling of seismic data

ACTIVITIES

Teaching assistant: Physics 1 and 2 (acad. years: 2012/2013, 2013/2014, 2014/2015, 2015/2016), Soil Dynamics and Earthquake Engineering (acad. years: 2014/2015, 2015/2016, 2016/2017, 2017/2018, 2018/2918), Noise, Vibrations and Light Pollution (acad. years: 2015/2016, 2016/2017, 2017/2018, 2018/2019), Geophysics (acad. years: 2012/2013, 2013/2014, 2017/2018, 2018/2019)

Technical editor: Journal of Environmental Engineering published by Faculty of Geotechnical Engineering, University of Zagreb (2013-present)

Reviewer: Journal of Applied Geophysics (ISSN: 0926-9851), Bulletin of Earthquake Engineering (ISSN: 1573-1456), Environmental Earth Sciences (ISSN: 1866-6299)

Associate on projects:

1) Nano-effects and disturbance influences in solid state ionic materials in the period (2012–2013), 160-0982886-0873

2) Geophysical-geotechnical investigation landfill site investigations in the period 2013–2014 funded by financial support of the University of Zagreb,

3) Assessment of the dynamic soil properties with seismic methods in 2014 funded by financial support of the University of Zagreb,

4) "Čista petica" funded by European Social Fond ESF 2015-2016, HR.3.1.20-0031

5) Analysis of the local site effects on the amplification of seismic ground motion in Croatia" in the period 2016–2017 funded by financial support of the University of Zagreb,

6) Erasmus + 2016–2019 Western Balkans Academic Education Evolution and Professional's Sustainable Training for Spatial Data Infrastructures (BESTSDI).

ADDITIONAL INFORMATION:

Crosbi: https://bib.irb.hr/lista-radova?autor=336630
Google Scholar: https://scholar.google.hr/citations?user=tFi_OTsAAAAJ&hl=hr
Scopus: https://www.scopus.com/authid/detail.uri?authorId=55596104000
ResearchGate: https://www.researchgate.net/profile/Davor_Stanko
Orcid: orcid.org/0000-0003-1829-0862

List of Publications

Scientific papers in CC/SCI journals:

1. Stanko, D., Markušić, S., Strelec, S., Gazdek, M., 2017. Equivalent-linear site response analysis on the site of the historical Trakošćan Castle, Croatia, using HVSR method. Environmental Earth Sciences. 76:642. Doi: 10.1007/s12665-017-6971-4

2. Stanko, D., Markušić, S., Strelec, S., Gazdek, M., 2017. HVSR analysis of seismic site effects and soil-structure resonance in Varaždin city (North Croatia). Soil Dynamics and Earthquake Engineering 92, 666–677. Doi: 10.1016/j.soildyn.2016.10.022

3. Šalić, R., Sandikkaya, M. A., Milutinović, Z., Gülerce, Z., Duni, L., Kovačević, V., Markušić, S., Mihaljević, J., Kuka, N., Kaludjerović, N., Kotur, N., Krmpotić, S., Kuk, K., **Stanko, D**., 2017. Reply to "Comment to BSHAP project strong ground motion database and selection of suitable ground motion models for the Western Balkan Region" by Carlo Cauzzi and Ezio Faccioli. Bulletin of Earthquake Engineering 15, 1349–1353. Doi: 10.1007/s10518-017-0095-9

4. Šalić, R., Sandikkaya, M. A., Milutinović, Z., Gülerce, Z., Duni, L., Kovačević, V., Markušić, S., Mihaljević, J., Kuka, N., Kaludjerović, N., Kotur, N., Krmpotić, S., Kuk, K., **Stanko, D**., 2016. BSHAP project strong ground motion database and selection of suitable ground motion models for the Western Balkan Region. Bulletin of Earthquake Engineering. 15:1319. Doi: 10.1007/s10518-016-9950-3

5. Stanko, D., Markušić, S., Strelec, S., Gazdek, M., 2016. Seismic response and vulnerability of historical Trakošćan Castle, Croatia using HVSR method. Environmental Earth Sciences 75, 1–14. Doi:10.1007/s12665-015-5185-x

6. Strelec, S., **Stanko, D.**, Gazdek, M., 2016. Empirical correlation between the shear-wave velocity and the dynamic probing heavy test: Case study, Varaždin, Croatia. Acta Geotechnica Slovenica 13, 3–15.

7. Studenyak, I. P., Neimet, Y. Y., Rati, Y.Y., **Stanko, D.,** Kranjčec, M., Kokenyesi, S., Daróci, L., Bohdan, R., 2014. Structural and optical properties of annealed and illuminated $(Ag_3AsS_3)_{0.6}(As_2S_3)_{0.4}$ thin films. Optical Materials 37, 718–723. Doi: 10.1016/j.optmat.2014.08.019

8. Torresi, D., **Stanko, D.**, Di Pietro, A., Figuera, P., Fisichella, M., Lattuada, M., Milin, M., Musumarra, A., Pellegriti, M. G., Scuderi, V., Strano, E., Zadro, M., 2013. Nuclear Instruments and Methods in Physics Research. Section A: Accelerators, Spectrometers, Detectors and Associated Equipment 713, 11-18. Doi: 10.1016/j.nima.2013.02.027

9. Zadro, M., Figuera, P., Di Pietro, A., Fisichella, M., Lönnroth, T., Milin, M., Ostashko, V., Pellegriti, M. G., Scuderi, V., **Stanko, D.,** Strano, E., Torresi, D., 2013. Quasielastic backscattering and barrier distributions for the 6,7Li+64Zn systems. Physical review C 87, 054606: 1–10. Doi: 10.1103/PhysRevC.87.054606

Scientific papers in other journals:

1. Gülerce, Z., Šalić, R., Kuka, N., Markušić, S., Mihaljević, J., Kovačević, V., Sandikkaya, A. M., Milutinović, Z., Duni, L., **Stanko, D.**, Kaludjerović, N., Kovačević, S., 2017. Seismic hazard maps for the Western Balkan. Inženjerstvo okoliša (Environmental Engineering) 4 (1), 7–17

Professional papers:

1. Stanko, D., Strelec, S., Gazdek, M., Filipović, A., Kaniški, N., 2015. Assessment of site effects using microtremor measurements in Varaždin city. Inženjerstvo okoliša (Environmental Engineering) 2 (1), 45–54

2. Strelec, S., Grabar, K., Gazdek, M., Špiranec, M., **Stanko, D.,** Jug, J., 2014. Geophysical-geotechnical landfill investigation. Inženjerstvo okoliša (Environmental Engineering) 1 (2), 103–112

3. Strelec, S., Jug, J., **Stanko, D.,** 2014. Determination of project values of the maximum earthquake (Eurocode 8) using a multichannel analysis of surface waves (MASW). Mineral 3, 24–30

Scientific conference papers with international peer-review:

1. Šalić, R., Gülerce, Z., Kuka, N., Markušić, S., Mihaljević, J., Kovačević, V., Sandikkaya, A. M., Milutinović, Z., Duni, L., **Stanko, D.,** Kaluđerović, N., Kovačević, S., Harmonized Seismic Hazard Maps for the Western Balkan Countries., 2018. 16th European Conference on Earthquake Engineering-Conference proceedings. 1–12

2. Stanko, D., Markušić, S., Ivančić, I., Gazdek, M., Gülerce, Z., 2017. Preliminary Estimation of Kappa Parameter in Croatia. IOP Conference Series: Earth and Environmental Science 95, 032014: 1–10. Doi:10.1088/1755-1315/95/3/032014

3. Strelec, S., Gazdek, M., Mesec, J., Jug, J., **Stanko, D.,** 2016. Implementation of in situ and geophysical methods for road landslides investigations // Geotechnical aspects of damages caused by natural phenomena. Sokolić Igor, Zlatović Sonja, editor(s). Zagreb: Croatian Geotechnical Society, 179–184

4. Strelec, S., Jug, J., **Stanko, D.,** Gazdek, M., Anić Vučinić, A., 2016. Geophysical investigations at municipal solid waste landfill Jakuševac. ISWA world congress 2016 uniting ideas for successful waste management. Stanisavljević N., Fellner J., Hossain S., Levis J.W., editor(s). Novi Sad: University of Novi Sad, Faculty of Technical Sciences, 1379–1389

5. Torresi, D., Forneris, J., Grassi, L., Acosta, L., Di Pietro, A., Figuera, P., Fisichella, M., Grilj, V., Jakšić, M., Lattuada, M., Mijatović, T., Milin, M., Prepolec, L., Skukan, N., Soić, N., **Stanko, D.,** Tokić, V., Uroić, M.; Zadro, M.., 2016. Effects of the interstrip gap on the efficiency and response of Double Sided Silicon Strip Detectors. The European Physical Journal Web of Conferences 117, 10009:1–6. Doi: 10.1051/epjconf/201611710009

6. Stanko, D., Markušić, S., Strelec, S., 2015. Estimation of Seismic Site Effects from Ambient Noise Measurements using HVSR Method: Varaždin city, Croatia. International Conference on Earthquake Engineering and Seismology–IZIIS-50 Conference - Conference Proceedings ID315, 1–8.

7. Torresi, D., Forneris, J., Grassi, L., Acosta, L., Di Pietro, A., Figuera, P., Grilj, V., Jakšić, M., Lattuada, M., Mijatović, T., Milin, M., Prepolec, L., Skukan, N., Soić, N., **Stanko, D.,** Tokić, V., Uroić, M., Zadro, M., 2015. The sneaky interstrip gap of double sided silicon strip detector. Nuclear structure and dynamics: AIP Conference Proceedings, 1681, 030003:1–4. Doi: /10.1063/1.4932247

8. Torresi, D., Forneris, J., Grassi, L., Acosta, L., Di Pietro, A., Figuera, P., Grilj, V., Jakšić, M., Lattuada, M., Mijatović, T., Milin, M., Prepolec, L., Skukan, N., Soić, N., **Stanko, D.,** Tokić, V., Uroić, M., Zadro, M., 2015. Study of interstrip gap effects and efficiency for full energy detection of Double Sided Silicon Strip Detectors. Journal of Physics: Conference Series 590, 012029:1–5. Doi: 10.1088/1742-6596/590/1/012029

9. Torresi, D., **Stanko, D.,** Di Pietro, A., Figuera, P., Fisichella, M., Lattuada, M., Milin, M., Musumarra, A., Pellegriti, M. G., Scuderi, V., Strano, E., Zadro, M., 2012. Studies on the response of double sided silicon strip detectors. Nuclear structure and dynamics: AIP Conference Proceedings 1491, 89-92. Doi: 10.1063/1.4764209

Abstracts in Book of abstracts

1. Markušić, S., **Stanko, D.,** Sović, I., Gazdek, M., Korbar, T., 2018. Estimation of near-surface attenuation in the Northwestern External Dinarides. Book of Abstracts of the 36th General Assembly of the European Seismological Commission. D'Amico Sebastiano, Galea Pauline, Bozionelos George, Colica Emanuele, Farrugia Daniela, Agius Matthew R., editor(s). Valletta, Malta: Mistral Service Anna Lo Presti Via Romagnosi, 28 98100 - Messina (Italy), 440-ESC2018-S30-39 (poster, international peer-review, abstract, scientific).

2. Strelec, S., Gazdek, M., Grabar, K., Špiranec, M., **Stanko, D.,** Jug, J., 2014. Geophysical-Geotechnical Landfill Site Investigations. XIII. International Waste Management Symposium Zagreb. Aleksandra Anić Vučinić, editor(s). Zagreb: Faculty of Geotechnical Engineering, 34-35 (lecture, international peer-review, abstract, expert).